

THE UNIVERSITY OF TULSA
THE GRADUATE SCHOOL

WELLBORE EFFECTS
ON
PRESSURE TRANSIENT ANALYSIS

by
Jinjiang Xiao

A dissertation submitted in partial fulfillment of
the requirements for the degree of Doctor of Philosophy
in the Discipline of Petroleum Engineering
The Graduate School
The University of Tulsa

1993

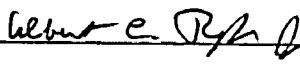
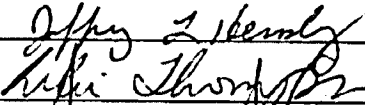
THE UNIVERSITY OF TULSA
THE GRADUATE SCHOOL


WELLBORE EFFECTS
ON
PRESSURE TRANSIENT ANALYSIS


by
Jinjiang Xiao

A DISSERTATION
APPROVED FOR THE DISCIPLINE OF
PETROLEUM ENGINEERING

By Dissertation Committee


_____, Chairperson






ABSTRACT

Xiao, Jinjiang (Doctor of Philosophy in Petroleum Engineering)

Wellbore Effects on Pressure Transient Analysis (198 pp. - Chapter V)

Directed by Dr. Albert C. Reynolds, Jr.

(340 Words)

The knowledge of wellbore effects is essential for the proper interpretation of well testing data. This work considers wellbore effects on closed chamber tests and pressure buildup tests.

An analytical expression is derived for the overall wellbore storage coefficient for a closed chamber test (CCT) in an oil well. This allows the correct wellbore boundary condition to be written which suggests that a version of pseudotime can be used to correlate the CCT solution with the corresponding slug test solution. In many realistic cases, the pseudotime correlation is applicable and thus pressure data from a CCT can be analyzed using several available slug test analysis techniques. The new pseudotime is also applicable to analyze slug test data influenced by a step change in the wellbore storage coefficient.

This work also presents new methods for the analysis of gas-well, closed-chamber tests. It is shown that pseudopressure and pseudotime can be used to correlate gas-well, closed-chamber test results with the analogous liquid, slug-test solutions. This allows data from a gas-well CCT to be analyzed using liquid slug-test analysis procedures. Multirate analysis techniques were found to be applicable to gas-well, closed-chamber tests in terms of pseudopressure and time, not pseudotime.

A drift-flux model is formulated to simulate wellbore phase redistribution and to investigate its effect on pressure buildup data. This model rigorously treats wellbore and reservoir flow interaction and accurately handles the effect of interphase mass transfer through the black-oil approach accounting for a variable bubble-point pressure. The investigation reveals that buildup tests influenced by wellbore phase redistribution can show an increasing or a decreasing wellbore storage coefficient. The variation in the wellbore storage coefficient is affected by both phase segregation and gas compression. If the magnitude of afterflow is small after the end of wellbore phase segregation, pressure buildup data will show an increasing wellbore storage coefficient at the end of the test. If afterflow is still large after complete phase segregation, the gas column will be compressed due to afterflow and the pressure buildup data will show a decreasing wellbore storage coefficient.

ACKNOWLEDGEMENTS

The author wishes to express his sincerest appreciation to Dr. Albert C. Reynolds Jr. for his assistance, guidance and encouragement provided throughout this study. He thanks Dr. Jeff Hensley, Dr. Siamack Shirazi and Dr. Leslie Thompson, members of the Dissertation Committee, for their useful suggestions and comments.

The author is very grateful for the financial support provided by the university of Tulsa and the Tulsa University Reservoir Exploitation Projects (TUPREP). Member companies of TUPREP are acknowledged for their interest in this study.

Thanks are due to Dr. Lifu Chu and all fellow graduate students who helped the author in many aspects of his endeavor. Dr. F. Alhanati deserves special thanks for many stimulating discussions on the difficult aspects of transient two-phase simulation.

This dissertation is dedicated to the author's wife, Jindi, whose love, understanding and patience made this work possible.

TABLE OF CONTENTS

	<u>Page</u>
TITLE PAGE	i
APPROVAL PAGE	ii
ABSTRACT	iii
ACKNOWLEDGEMENTS	v
TABLE OF CONTENTS	vi
LIST OF TABLES	ix
LIST OF FIGURES	x
CHAPTER I INTRODUCTION	1
CHAPTER II ANALYSIS OF CLOSED CHAMBER TESTS	
IN OIL WELLS	7
2.1 Background	7
2.2 Definitions	11
2.3 Review of Theory	14
2.3.1 Slug Test Interpretation Methods	15
2.3.2 CCT Numerical Solutions	16
2.4 New CCT Interpretation Methods	24
2.4.1 CCT Problem Formulation	24
2.4.2 New Pseudotime	25
2.4.3 Practical Computation	27
2.5 Simulator Validation	28
2.5.1 Duplication of Slug Test Solutions	28

2.5.2	Comparison with Simmons and Grader Solution	29
2.5.3	Comparison with Salas and Sageev Solution	29
2.6	Results and Discussion	37
2.6.1	Base Case CCT Analysis	37
2.6.2	Sensitivity Analysis	45
2.6.3	Peres-Onur-Reynolds Methods	69
2.6.4	Step Change in Wellbore Storage Coefficient	75
CHAPTER III	ANALYSIS OF CLOSED CHAMBER TESTS	
	IN GAS WELLS	77
3.1	Background	77
3.2	Theoretical development	81
3.2.1	IBVP for Gas Well CCT	81
3.2.2	Type Curve Matching	85
3.2.3	Multirate Analysis	85
3.3	Results and Discussion	88
3.3.1	Type Curve Matching Analysis	91
3.3.2	Multirate Analysis	107
CHAPTER IV	MODELING WELLBORE PHASE REDISTRIBUTION	
	IN PRESSURE BUILDUP TESTS	113
4.1	Background	114
4.2	Definitions	117
4.3	Governing Equations	122
4.3.1	Material Balance Equations	123
4.3.2	Simplified Momentum Equations	125
4.3.3	Closure Relationship	125
4.3.4	Initial and Boundary Conditions	126
4.4	Numerical Solution Method	129

4.4.1	Finite Difference Equations	129
4.4.2	Calculation Algorithm	138
4.5	Results and Discussion	142
4.5.1	Case A	143
4.5.2	Case B	149
4.5.3	Case C	156
CHAPTER V	CONCLUSIONS	168
	NOMENCLATURE	173
	REFERENCES	179
APPENDIX A	DUHAMEL'S PRINCIPLE FOR VARIABLE BOTTOMHOLE PRESSURE PRODUCTION	187
APPENDIX B	WELLBORE STORAGE COEFFICIENT FOR CCT IN OIL WELLS	193
APPENDIX C	LATE TIME ANALYSIS OF CCT IN OIL WELLS	197

LIST OF TABLES

<u>Table</u>	<u>Title</u>	<u>Page</u>
2.1	Parameters Used for Slug Test Comparison	30
2.2	Comparison with Analytical Slug Test Solutions	31
2.3	Parameters Used for Comparison with Simmons & Grader Solutions	32
2.4	Comparison with Simmons and Grader Solutions	33
2.5	Comparison with Salas and Sageev Solutions	35
2.6	Parameters for Base Case Closed Chamber Test	38
3.1	Gas Physical Properties As Functions of Pressure	89
3.2	Parameters for Base Case Gas Well Closed Chamber Test . . .	90
4.1	Input Parameters for Case A	144
4.2.1	Input Parameters for Case B	150
4.2.2	Physical Properties As Functions of Pressure for Case B	151
4.3	Input Parameters for Case C	159

LIST OF FIGURES

<u>Figure</u>	<u>Title</u>	<u>Page</u>
2.1	Schematic of Closed Chamber Test	17
2.2	Discrete Representation of the Pressure Response of a Closed Chamber Test	19
2.3	BHP and Chamber Gas Pressure for Base Case CCT	39
2.4	Liquid Level As a Function of Time for Base Case CCT	40
2.5	Wellbore Storage Coefficient for Base Case CCT	41
2.6	Comparison of Slug Test and Base Case Closed Chamber Test Solutions	43
2.7	Correlation of Base Case CCT with Analogous Slug Test Solution	44
2.8	Effect of Skin Factor on Closed Chamber Test	46
2.9	Correlation of CCT Solution with Analogous Slug Test Solution, $s = 5$	47
2.10	Correlation of CCT Solution with Analogous Slug Test Solution, $s = 10$	48
2.11	Effect of Skin Factor on Wellbore Storage Coefficient for CCT	49
2.12	Effect of Initial Chamber Gas Pressure on Dimensionless Wellbore Storage Coefficient for Closed Chamber Tests	51
2.13	Use of Pseudotime for Closed Chamber Test, $p_{chi} = 0$ psig, $C_{aDi} = 1126$ and $s = 0$	52
2.14	Use of Pseudotime for Closed Chamber Test, $p_{chi} = 1000$ psig,	

	$C_{aDi} = 1094$ and $s = 0$	53
2.15	Use of Pseudotime for Closed Chamber Test, $p_{chi} = 1000$ psig, $C_{aDi} = 892$ and $s = 0$	54
2.16	Use of Pseudotime for Closed Chamber Test, $p_{chi} = 2000$ psig, $C_{aDi} = 741$ and $s = 0$	55
2.17	Use of Pseudotime for Closed Chamber Test, $p_{chi} = 3000$ psig, $C_{aDi} = 663$ and $s = 0$	56
2.18	Use of Pseudotime for Closed Chamber Test, $p_{chi} = 4000$ psig, $C_{aDi} = 553$ and $s = 0$	57
2.19	Effect of Initial Liquid Level on Dimensionless Wellbore Storage Coefficient for Closed Chamber Tests	59
2.20	Use of Pseudotime for Closed Chamber Test, $L_i = 2500$ ft, $C_{aDi} = 959$ and $s = 0$	60
2.21	Use of Pseudotime for Closed Chamber Test, $L_i = 5000$ ft, $C_{aDi} = 892$ and $s = 0$	61
2.22	Effect of Total Chamber Length on Dimensionless Wellbore Storage Coefficient for Closed Chamber Tests	62
2.23	Use of Pseudotime for Closed Chamber Test, $L_c = 2500$ ft, $C_{aDi} = 728$ and $s = 0$	63
2.24	Use of Pseudotime for Closed Chamber Test, $L_c = 5000$ ft, $C_{aDi} = 888$ and $s = 0$	64
2.25	Use of Pseudotime for Closed Chamber Test, $p_i = 4000$ psig, $C_{aDi} = 995$ and $s = 0$	66
2.26	Effect of p_{chi} and p_i on Dimensionless Wellbore Storage Coefficient for Closed Chamber Tests	67
2.27	Use of Pseudotime for Closed Chamber Test, $p_i = 6000$ psig, $p_{chi} = 1000$ psig, $C_{aDi} = 893$ and $s = 0$	68
2.28	Effect of Liquid Compressibility on CCT ($L_i = 0$ ft)	70

2.29	Effect of Wellbore Friction on Closed Chamber Test ($L_i = 0$ ft) . . .	71
2.30	Use of Pseudotime for Closed Chamber Test, $L_c = 1000$ ft, $C_{aDi} = 458$ and $s = 10$	73
2.31	Comparison of Converted Closed Chamber Test Response with Wellbore Storage and Skin Constant Surface Rate Solution	74
2.32	Use of Pseudotime for Slug Test with Step Change in Wellbore Storage	76
3.1	Comparison of Gas Well CCT with Ramey et al. Slug Test Solution	92
3.2	a_D as a Function of Time and Pressure, Base Case	93
3.3	Effect of Skin Factor on Gas Well CCT ($s = 5$)	94
3.4	Effect of Skin Factor on Gas Well CCT ($s = -2$)	95
3.5	Effect of Skin Factor on a_D	96
3.6	Effect of Initial Chamber Pressure on Gas Well CCT ($p_o = 2000$ psig)	98
3.7	Effect of Initial Chamber Pressure on Gas Well CCT ($p_o = 4000$ psig)	99
3.8	Effect of Wellbore Wellbore Pressure on a_D	100
3.9	Effect of Initial Reservoir Pressure on Gas Well CCT ($p_i = 4000$ psig)	101
3.10	Effect of Initial Reservoir Pressure on Gas Well CCT ($p_i = 2500$ psig)	102
3.11	Effect of Reservoir Initial Pressure on a_D	103
3.12	Effect of Chamber Volume on Gas Well CCT ($V_w = 60$ bbl) . . .	104
3.13	Effect of Chamber Volume on Gas Well CCT ($V_w = 500$ bbl) . . .	105
3.14	Effect of Gas Chamber Volume on a_D	106
3.15	Comparison of Converted Gas Well CCT Response with Wellbore Storage and Skin Constant Surface Rate Solution, Base Case . . .	108

3.16	Comparison of Converted Gas Well CCT Response with Wellbore Storage and Skin Constant Surface Rate Solution, $s = 5$	109
3.17	Comaprison of Convolution Analysis for Gas Well CCT in Terms of Time and Pseudotime, Base Case	111
3.18	Convolution Analysis for Gas Well CCT ($s = 5$)	112
4.1	The Control Volumes and Grids	130
4.2	Type Curve Analysis for Case A, Single Phase Oil Well	145
4.3	Horner Plot of Pressure Buildup Data for Case A	147
4.4	Sandface Flow Rate Ratio as a Function of Shut-in Time, Case A	148
4.5	Type Curve Analysis for Case B, Naturally Flowing Well	152
4.6	Gas Viod Fraction Distribution, Case B	154
4.7	Horner Plot for Case B, Naturally Flowing Well	155
4.8	Sandface Flow Rate Ratio as a Function of Shut-in Time, Case B	157
4.9	Change of Wellbore Storage Coefficient for Case B	158
4.10	Pressure Buildup, Case C	160
4.11	Type Curve Analysis for Case C, Gas-lift Well	162
4.12	Gas Void Fraction Distribution, Case C	164
4.13	Horner Plot of Pressure Buildup data for Case C	165
4.14	Change of Wellbore Storage Coefficient for Case C	166

CHAPTER I

INTRODUCTION

Successful field developments require reliable information about reservoir in-situ conditions such as formation flow capacity, extent of near wellbore damage or stimulation, reservoir average pressure, drainage volume, boundaries and heterogeneities. Much of this information is obtained through geological studies, examination of cores, analysis of logs and interpretation of pressure transient tests.

Pressure transient tests, being the subject of the current study, are conducted by creating and measuring pressure variation with time in wells and subsequently analyzing pressure recordings to estimate rock, fluid and reservoir properties. Therefore, interpretation of pressure transient tests is an inverse problem. As an indispensable part of the package of tools used for reservoir characterization, the importance of pressure transient tests is evidenced by the large number of publications appearing each year.

In petroleum engineering, pressure transient tests are used in a variety of forms^{1,2}. The most natural type is a drawdown test which is performed by simply measuring the wellbore pressure decline with time while the well is producing. Drawdown data are analyzed using semilog analysis and type-curve matching techniques. Successful interpretation of the test will yield formation flow capacity and skin factor. The reservoir drainage volume can be also determined if the test is run for a sufficiently long period of time for flow to reach pseudosteady state. In this circumstance, drawdown tests are also called "reservoir limit tests". Depending on the variation of well production rates, drawdown tests can be classified into either constant rate drawdown tests or variable rate drawdown tests.

After the well has been produced for a period of time, a pressure buildup test can be conducted by closing the well and subsequently recording the wellbore pressure responses. Buildup data are analyzed with Horner analysis technique or by type-curve matching with drawdown type curves. Interpretation of buildup test data usually yields flow capacity, skin factor and reservoir average pressure. A buildup test can also be treated as a variable rate drawdown test.

A slug test is created by imposing an instantaneous pressure increase or drop on the formation sandface. The wellbore pressure recovery towards equilibrium can be analyzed to determine reservoir properties. In the petroleum industry, a slug test corresponds to the flowing period of a drillstem test (DST). Traditionally, analysis of slug test data is carried out through type curve matching techniques. When a slug test is conducted with a gas cushion, the test becomes a closed-chamber test (CCT). At present, the analysis of data from closed-chamber tests is usually done by using numerical simulators in the history-matching mode.

Other commonly used pressure transient tests include, but are not limited to, injection/falloff tests and interference tests. It should be pointed that different types of tests may be interrelated. Moreover, conceptually, all pressure transient tests are the same in a sense that we attempt to obtain reservoir flow properties by monitoring and analyzing output signals (pressure or flow rate) generated by a reservoir as it responds to input signals (changes in flow rate or pressure). As a matter of fact, if flow rate and pressure measurements are all done at the formation sandface, deconvolution techniques can be applied to convert all types of tests into a unit rate pressure drawdown test.

Like other inverse problems, interpretation of pressure transient test data sometimes suffers from the problem of non-uniqueness, meaning that one could obtain multiple combinations of parameters which may yield the same pressure responses as those recorded during the tests. The process of interpretation becomes

even more complicated in view of the existence of various possibilities in reservoir type (homogeneous versus heterogeneous), well completion practice (fully or partially penetrating) and the type of fluids flowing in the reservoirs (oil, gas or multiphase). Therefore, the first step in the interpretation of pressure transient tests is to identify reservoir models.

Another major complication involved in well test interpretation is the wellbore effect. Since the objective of well testing is to obtain formation properties, naturally, it is desirable to know the exact input signals applied to the reservoir and to isolate the output signals which correspond solely to the reservoir responses. Realistically, however, well test signals are given and measured through the wellbore, not inside the reservoir, and consequently, those signals are influenced by what happens in the wellbore. Consider the constant surface rate drawdown test as an example. The test begins when the surface valve is opened. A constant surface rate is maintained as the test proceeds. The sandface flow rate does not become a constant value equal to the surface rate right after the test begins, but rather, it is initially zero and gradually increases with time. What happens in the wellbore is that during the early time of the test, fluids produced at the surface mostly come from the wellbore due to wellbore fluid expansion. This wellbore phenomenon is called wellbore unloading. The time for the sandface rate to reach the surface rate will depend on the wellbore characteristic and fluid properties. Similarly, a buildup test is also influenced by the wellbore storage effect, called afterflow, if the well is shut-in at the surface instead of at the formation sandface. During the test, the sandface flow does not cease instantaneously, but rather its rate gradually decreases with time due to wellbore fluid compression. Early time pressure measurements during either drawdown or buildup tests show wellbore and wellbore fluid properties, not the reservoir characteristics.

Recognizing the effect of wellbore storage is of vital importance toward the success of any well test interpretation. Failure to properly account for the effect of

wellbore storage could lead to no interpretation or, to say the least, misinterpretation of well-test data. Traditionally, well-test interpretation methods are developed based on theories that assume sandface measurements of flow rate and pressure. For many years, there has been interest in combining reservoir flow theory and wellbore flow mechanics to yield interpretation methods which properly account for wellbore storage effects. At present, excellent analytical models exist for cases where the wellbore storage coefficient remains constant or changes from one constant to another constant. However, multiphase flow in the wellbore creates a variable wellbore storage coefficient and our current treatment in this area is still not satisfactory. The difficulty persists largely due to the fact that multiphase wellbore flow is of nonlinear nature and application of our mathematical tools produces limited success.

The current study is undertaken in order to address the frequent occurrence of wellbore multiphase flow and the need to develop better well testing interpretation methods. Here, we consider wellbore storage effects in closed-chamber tests as well as in pressure buildup tests in which multiphase flow exists in the wellbore prior to the surface shut-in. Specifically, the current study is intended to accomplish the following objectives: (1) investigate the effect of a gas cushion in oil-well closed-chamber tests; (2) develop better interpretation methods for gas-well closed-chamber tests; and finally, (3) develop computer simulators coupling wellbore multiphase flow with reservoir flow and investigate the effect of wellbore multiphase transient flow on pressure buildup data.

This dissertation is organized in keeping with the three objectives stated above. *Chapter II* deals with closed-chamber tests in oil wells. Mathematically, we derive an analytical expression for the effective wellbore storage coefficient for a closed-chamber test and show that this storage coefficient is a combination of wellbore storage due a rising liquid level and wellbore storage due to the compression of

the gas cushion. As opposed to conventional slug tests where the wellbore storage coefficient is constant, closed-chamber tests have a decreasing wellbore storage coefficient because of the decrease in gas compressive wellbore storage. Nevertheless, it is also shown that conventional slug tests are a special type of closed-chamber tests when the chamber volume becomes infinite, and with a new form of pseudotime, the pressure response of a closed-chamber test can be converted to the response of an equivalent slug test. The proposed correlation is found to be valid for a sufficiently long period of time such that slug test analysis techniques can be used to analyze data from closed-chamber tests. Sensitivity analysis is also performed to investigate effects of various reservoir and operational parameters on the suggested correlation.

Chapter III considers closed-chamber tests in gas wells. Mathematical equations for gas-well, closed-chamber tests are first derived. The governing partial differential equations are then solved numerically using finite difference methods. When reservoir and operational parameters are specified, the numerical simulator is used to generate pressure responses for a gas-well, closed-chamber test. With results from the simulator, it is demonstrated that the pressure response of a gas-well, closed-chamber test can be correlated with the pressure response of a corresponding liquid slug test. This correlation is based on variable transformations using pseudopressure and pseudotime. The proposed correlation works well for all the cases investigated. A gas-well, closed-chamber test is a variable rate problem. Convolution analysis techniques are shown to be applicable in terms of pseudopressure and time, not pseudotime.

Chapter IV focuses on the investigation of wellbore phase redistribution on pressure buildup tests. Based on fluid mechanics principles and the drift-flux model, we derive equations governing the wellbore phase segregation process. During well production, gas comes out of solution and becomes free gas due to decreases in wellbore pressure. During pressure buildup tests, some of this free gas may segregate

and flow to the top of the wellbore, whereas some of this free gas may redissolve into liquid phase due to increases in wellbore pressure. To accurately model phase segregation, the black oil approach is used to account for the interphase mass transfer. Furthermore, since fluid composition changes along the wellbore due to the slippage between gas and liquid, it was found to be necessary to incorporate the variable bubble-point pressure concept to evaluate fluid physical properties. Other characteristics of the model include the use of a simplified momentum equation which only considers equilibrium between the pressure force and the gravity force. This is justified by the fact that gravity is the driving force for wellbore phase segregation. The formulated model is solved numerically using a simulator based on finite difference methods. Results from the simulator help to bring us better understanding of the effect of wellbore phase segregation on buildup tests.

Chapter V summarizes conclusions reached as a result of this study and discusses areas in which additional investigation is needed.

CHAPTER II

ANALYSIS OF CLOSED CHAMBER TESTS IN OIL WELLS

In this chapter, an analytical expression is derived for the wellbore storage coefficient for closed chamber tests (CCT) in oil wells. A relationship between closed chamber tests and conventional slug tests is established and discussed. New analysis methods for closed chamber tests are presented.

2.1 Background

Drillstem testing is well established as a primary technique for evaluating the commercial viability of newly discovered (virgin) reservoirs. A successful drillstem test (DST) gives a measurement of flow rates, an estimate of static reservoir pressure and pressure-time data corresponding to a short pressure transient test. Successful analysis of DST pressure data yields an estimate of the flow capacity, kh , and the skin factor, s . The flowing period of a DST corresponds to a slug test.

Although slug tests were first considered in the field of groundwater hydrology, the industry-standard interpretation methods are based on the work of Ramey et al.³. Considering wellbore storage and skin effects, Ramey et al.³ derived analytical solutions for slug tests for radial flow in a homogeneous reservoir, and developed type curves with CDe^{2s} as a correlating factor. These type curves later became the industry standard for analyzing data from slug tests.

Recently, Peres et al.⁴ discovered a general relationship between the slug test solution and the solution for the classical wellbore storage and skin constant surface

rate production problem. This general relationship enabled them to develop new procedures to analyze slug tests. They showed that pressure data from slug tests can be conveniently converted to pressure data of equivalent constant surface rate production tests. Slug tests, therefore, can be analyzed using existing type curves for the classical wellbore storage and skin constant surface rate production problem, and slug test type curves are no longer needed.

Closed chamber drillstem tests were first introduced to petroleum industry by Alexander⁵ as an improvement to conventional drillstem tests; the objective was to reduce operational and safety problems. As in a conventional drillstem test, a closed chamber DST is conducted to gain information on well potential and formation fluid type. The only major difference between a conventional DST and a closed chamber DST is that in a closed chamber DST, the well is closed in at the surface.

Erdle et al.⁶ conducted an extensive review of closed chamber drillstem testing and concluded that the advantages of closed chamber drillstem testing over conventional drillstem testing are improved safety, reduced test time and better test engineering at the wellsite.

Unfortunately, the mathematical problem for a closed chamber DST is more complicated than for a conventional DST because the former has a nonlinear boundary condition. To the best of our knowledge, no analytical solution to the closed chamber DST problem has been presented in the literature. Quantitative data analysis of a closed chamber DST was not available until recently.

Saldana and Ramey⁷ presented detailed studies for closed chamber drillstem testing. A momentum balance including frictional and inertial effects was applied to the rising liquid level within the wellbore. This resulted in a nonlinear wellbore equation which was then coupled with the reservoir diffusivity equation through the

wellbore storage coefficient. The solution was obtained numerically using a finite difference scheme.

A new and different approach was proposed by Simmons and Grader⁸ for closed chamber tests. Their method generates the pressure response of a closed chamber test using a numerical method based on superposition of the cumulative rate of the constant pressure production solution of the radial diffusivity equation. Sensitivity studies were conducted for various tool and reservoir parameters.

In the work of Simmons and Grader⁸, wellbore friction, liquid compression and inertial effects are neglected. As a follow-up study, Salas and Sageev⁹ adopted the same approach as developed by Simmons and Grader⁸, but included liquid compression and wellbore friction into their analysis. They found that the effects of wellbore friction and liquid compression can be significant. Parametric studies were also performed to analyze the influences of different test tools and reservoir parameters on closed chamber tests.

An implicit numerical model has been developed for closed chamber tests by Mfonfu and Grader¹⁰. The wellbore flow and reservoir flow are combined through the use of Bernoulli's law. To regenerate field test data, variable skin factors were assumed. Refs. 8-10 discussed methods to analyze field test data by using their simulators in a history-matching mode.

Petak et al.¹¹ presented another approach for closed chamber tests. In their work, a r - θ - z reservoir simulator was linked to the wellbore flow by using a wellbore storage term which is calculated at each time step by performing a mass balance on the wellbore fluids. In their study, however, frictional and inertial effects are neglected.

In recent years, there has been a great interest in the interpretation of pressure data from underbalanced perforation and backsurge perforation cleaning. When underbalanced perforation is used, the reservoir sandface is suddenly exposed

to a relatively low pressure and reservoir fluid may be produced at extremely high flow rates. Drilling fluid contamination around the wellbore, and gun debris and crushed rock in the perforation channels are washed out. As a result, an improved productivity is achieved. Although there are differences in operation, underbalanced perforation, backsurge perforation cleaning and closed chamber DST are the same from the transient well testing point of view. In this work, therefore, the term “closed chamber test” is generally used to refer to all of them.

During closed chamber tests, the sandface flow rate continuously declines as the bottomhole pressure increases as a result of the increase of the liquid level in the wellbore and the chamber gas pressure. If the sandface flow rate is known, variable rate well test techniques can be used to interpret pressure data to estimate the reservoir flow capacity and skin factor. Tariq and Ayestaran¹² presented a convolution method for closed chamber tests. Their method requires that flow rates are measured from MWP (Measurement While Perforating) tools or calculated from the time derivative of the measured chamber gas pressure. They used their method to analyze pressure data from two field surge perforation tests. Simmons¹³ proposed a similar interpretation method.

By viewing a closed chamber test as a short, high rate drawdown, Soliman et al.¹⁴ derived an approximate interpretation method applicable to tests with a small chamber volume. In this method, a log-log plot of pressure change (from original reservoir pressure) versus total test time yields a straight line with a slope of -1.0 during late time radial flow in a homogeneous reservoir. The reservoir flow capacity can then be calculated from any point on that straight line. The skin factor is determined by matching with type curves generated from the calculated flow capacity. This method requires an estimate of the initial reservoir pressure.

Garrett et al.¹⁵ applied interpretation techniques presented by Simmons¹³ and Soliman et al.¹⁴ to field underbalanced perforating pressure data. They also

modified the Soliman et al.¹⁴ technique, and presented a Cartesian straight line method which can be used to obtain not only the reservoir flow capacity, but also the reservoir initial pressure.

Another interpretation method, ImpulseTM Testing, which also utilizes the concept of short producing time, was developed by Ayoub et al.¹⁶. (The ideas for Impulse Test analysis are similar to those presented by Cinco-Ley et al.¹⁷.) When this technique is applied to closed chamber tests, the product of the pressure change and the elapsed test time is plotted versus the elapsed time in a log-log scale, and matched with the classical wellbore storage and skin pressure derivative type curves. From type-curve matching, flow regimes are identified and reservoir parameters are determined. As in the case of Soliman et al.¹⁴, this method also requires an estimate of the initial reservoir pressure. Impulse Testing method has been applied to several sets of field underbalanced perforating pressure data¹⁸.

Despite the contributions mentioned above, the successful interpretation of pressure data from closed chamber tests is still difficult. The objective of this chapter is to present new methodology which will improve the analysis of CCT data.

2.2 Definitions

In this section, definitions of the dimensionless variables used in this chapter are summarized. All definitions are presented in oil field units. Throughout, p_i denotes the initial reservoir pressure, whereas at the wellbore, the pressure is instantaneously set to p_o in a slug, drillstem or closed chamber test.

Dimensionless time, dimensionless radial distance and dimensionless wellbore storage coefficient are defined, respectively, by

$$t_D = \frac{2.637 \times 10^{-4} kt}{\phi \mu c_t r_w^2}, \quad (2.1)$$

$$r_D = \frac{r}{r_w}, \quad (2.2)$$

and

$$C_D = \frac{5.615C}{2\pi\phi c_l h r_w^2}, \quad (2.3)$$

where C denotes the wellbore storage coefficient in RB/psi, corresponding to the change of liquid level, the compression of a fluid in the wellbore or the combination effects of both a changing liquid level and fluid compression. For a changing liquid level, the wellbore storage coefficient is given by

$$C_l = \frac{144\pi r_p^2}{(5.615\rho g \sin\theta)/g_c}, \quad (2.4)$$

where r_p is the radius of the wellstring, ρ is the density of the fluid being produced into the wellbore and θ represents the inclination of the wellstring from horizontal direction. In a closed chamber test, the chamber gas is compressed as the liquid level rises in the wellbore. The wellbore storage coefficient due to gas compression is defined as

$$C_g = V_g c_g, \quad (2.5)$$

where V_g is the wellbore volume in RB occupied by the chamber gas and c_g is the isothermal gas compressibility. In a CCT, we show later that the effective or overall wellbore storage coefficient represents the combined effects of a rising liquid level and the compressive storage due to the compression of the gas cushion. Throughout, this effective wellbore storage coefficient is denoted by C_a (RB/psi) and C_{aD} denotes the dimensionless analogue of C_a .

In this chapter, we consider several dimensionless pressure solutions. Throughout, p_D denotes the dimensionless pressure for slug tests and closed chamber tests at any point of the reservoir, p_{wD} represents the corresponding dimensionless wellbore pressure, p_{cD} denotes the dimensionless reservoir pressure for the classical

wellbore storage and skin constant surface rate problem and p_{wcD} represents the corresponding dimensionless wellbore pressure. We define p_D and p_{wD} , respectively, by

$$p_D = \frac{p_i - p(r, t)}{p_i - p_o}, \quad (2.6)$$

and

$$p_{wD} = \frac{p_i - p_{wf}(t)}{p_i - p_o}, \quad (2.7)$$

where $p(r, t)$ and $p_{wf}(t)$, respectively, denote the pressure at any point of the reservoir at time t and the wellbore pressure in slug or closed chamber tests.

For production at a constant surface rate q , in STB/D, the dimensionless pressure and dimensionless wellbore pressure are defined by

$$p_{cD} = \frac{kh[p_i - p(r, t)]}{141.2qB\mu}, \quad (2.8)$$

and

$$p_{wcD} = \frac{kh[p_i - p_{wf}(t)]}{141.2qB\mu}, \quad (2.9)$$

where $p(r, t)$ and the $p_{wf}(t)$, respectively, denote the corresponding pressures in the reservoir and at the wellbore.

Based on the concept of an infinitesimally thin skin, the skin factor is defined by

$$s = \frac{kh}{141.2q_{sf}(t)\mu} \Delta p_{skin}, \quad (2.10)$$

where q_{sf} denotes the sandface flow rate, in RB/D, and Δp_{skin} denotes the additional pressure drop which occurs due to formation damage or improvement around the wellbore.

In the present study, pressure responses during closed chamber tests are generated using a computer simulator based on the superposition of the cumulative

production solution for the constant bottomhole pressure production problem. The dimensionless instantaneous sandface flow rate for a well produced at a constant bottomhole pressure, p_{wf} , is defined by

$$q_D = \frac{141.2q_{sf}(t)\mu}{kh(p_i - p_{wf})}. \quad (2.11)$$

The dimensionless cumulative production is defined as

$$Q_D = \frac{5.615Q_{sf}}{2\pi\phi hc_t r_w^2 (p_i - p_{wf})}, \quad (2.12)$$

where Q_{sf} denotes the dimensional sandface cumulative production, in RB, for a well which produces at a constant bottomhole pressure. $Q_{sf}(t)$ and $q_{sf}(t)$ are related by

$$Q_{sf}(t) = \int_0^t q_{sf}(\tau) d\tau. \quad (2.13)$$

2.3 Review of Theory

In this section, we briefly review slug test interpretation methods and present an outline of the numerical procedure utilized to generate pressure responses for a closed chamber test. We consider slug tests and closed chamber tests conducted in a fully-penetrating well located in an infinite, homogeneous and isotropic reservoir of uniform thickness. Initially, the pressure is constant throughout the reservoir and equal to p_i , whereas at the wellbore, the pressure is instantaneously set to p_o . In addition, it is assumed that in slug tests, friction and inertial effects in the wellbore can be neglected, and critical flow is not present. We also assume that the wellstring has a constant inner diameter and a constant inclination angle.

2.3.1 Slug Test Interpretation Methods

Under the stated assumptions and using the dimensionless variable defined previously, the slug test initial boundary value problem (IBVP) can be stated as

$$\frac{1}{r_D} \frac{\partial}{\partial r_D} \left(r_D \frac{\partial p_D}{\partial r_D} \right) = \frac{\partial p_D}{\partial t_D}, \quad (2.14.1)$$

$$p_D(r_D, 0) = 0; \quad 1 < r_D < \infty, \quad (2.14.2)$$

$$p_{wD}(0) = 1, \quad (2.14.3)$$

$$\lim_{r_D \rightarrow \infty} p_D(r_D, t_D) = 0; \quad t_D > 0, \quad (2.14.4)$$

$$p_{wD} = \left[p_D - s \left(r_D \frac{\partial p_D}{\partial r_D} \right) \right]_{r_D=1}, \quad (2.14.5)$$

and

$$\left(r_D \frac{\partial p_D}{\partial r_D} \right)_{r_D=1} = C_D \frac{\partial p_{wD}}{\partial t_D}. \quad (2.14.6)$$

In Eq. 2.14.6, C_D is the dimensionless wellbore storage coefficient during slug tests due to a rising liquid level. For a slug test conducted in a wellstring with a constant inner diameter and a constant inclination angle, C_D is considered to be constant. Thus, the IBVP for a slug tests is linear, and can be solved analytically. Ramey and Agarwal¹⁹ derived solutions to Eqs. 2.14.1 through 2.14.6 using Laplace transform techniques.

Using the solutions derived by Ramey and Agarwal¹⁹, Ramey et al.³ developed slug test type curves in which p_{wD} is plotted versus t_D/C_D with $C_D e^{2s}$ as the correlating parameter. For more than a decade, these type curves have provided the standard technique for interpreting slug test pressure data.

Recently, Peres et al.⁴ discovered a general relationship between the slug test solution and the solution for the classical wellbore storage and skin constant surface

rate production problem. This relationship is valid for any well/reservoir geometry and holds at any position in the reservoir. At the wellbore, this relationship is described by

$$p_{wcD}(t_D, C_D, s) = \frac{I(p_{wD})}{C_D}, \quad (2.15)$$

and

$$p'_{wcD} = \frac{t_D}{C_D} p_{wD}. \quad (2.16)$$

In Eq. 2.15, $I(p_{wD})$ denotes the slug test pressure integral, given by

$$I(p_{wD}) = \int_0^{t_D} p_{wD}(\tau, C_D, s) d\tau. \quad (2.17)$$

In Eq. 2.16, p'_{wcD} denotes the logarithmic time derivative of the constant surface rate dimensionless wellbore pressure, i.e., $p'_{wcD} = dp_{wcD}/d \ln t_D$. Eq. 2.15 shows that a simple integration of the slug test pressure data over time will generate the equivalent pressure data that would be obtained if the well was produced at a constant surface flow rate. Moreover, as indicated in Eq. 2.16, the multiplication of the slug test data by time yields the equivalent constant surface rate pressure derivative data, without applying any numerical differentiation technique. Peres et al.⁴ concluded that slug test pressure data can be analyzed using type curves constructed for the constant surface rate production problem, and type curves developed specifically for slug tests are no longer needed.

2.3.2 CCT Numerical Solutions

The configuration of a closed chamber test is schematically shown in Fig. 2.1. The two primary differences between a closed chamber test and a slug test are as follows: (i) in a CCT the well is always closed somewhere along the wellbore when the test is being conducted; and (ii) in a CCT, part or all of the wellbore cushion is composed of gas, thus, the effective wellbore storage coefficient (which is

a combination of storage due to a rising liquid level and gas compressive storage) is a strong function of pressure and may not be considered as a constant. The later difference means that the IBVP for a CCT is nonlinear. To the best of our knowledge, no analytical solution for the CCT IBVP has been presented in the literature.

In the present work, we use the numerical method proposed by Simmons and Grader⁸ to generate the pressure responses during closed chamber tests. The numerical method developed by Simmons and Grader⁸ is based on the superposition of the constant bottomhole pressure production solution of the radial diffusivity equation. The superposition principle, derived in *Appendix A*, is given by

$$Q_{vD}(t_D) = \int_0^{t_D} Q'_{cD}(t_D - \tau) p_{wvD}(\tau) d\tau, \quad (2.18)$$

where Q_{vD} and Q_{cD} , respectively, denote the dimensionless cumulative rate for variable and constant bottomhole pressure production problems, and p_{wvD} denotes the variable dimensionless bottomhole pressure.

A closed chamber test can be viewed as a test where the well is producing at a sequence of constant bottomhole pressures, as depicted in Fig. 2.2, and then Eq. 2.18 can be approximated by

$$Q_{sf}(t_N) = \beta(p_i - p_o)Q_{cD}(t_D) - \beta \sum_{j=1}^{N-1} (p_j - p_{j-1})Q_{cD}(t_D - t_{D,j}), \quad (2.19)$$

where $\beta = 2\pi\phi h c_l r_w^2 / 5.615$ and $p_j = p_{wv}(t_j)$. For the well/reservoir geometry under consideration, when the well produces at a constant bottomhole pressure, the Laplace transform of the dimensionless cumulative rate is given by²⁰

$$\bar{Q}_{cD}(u) = \frac{\sqrt{u}K_1(\sqrt{u})}{u^2[K_0(\sqrt{u}) + s\sqrt{u}K_1(\sqrt{u})]}, \quad (2.20)$$

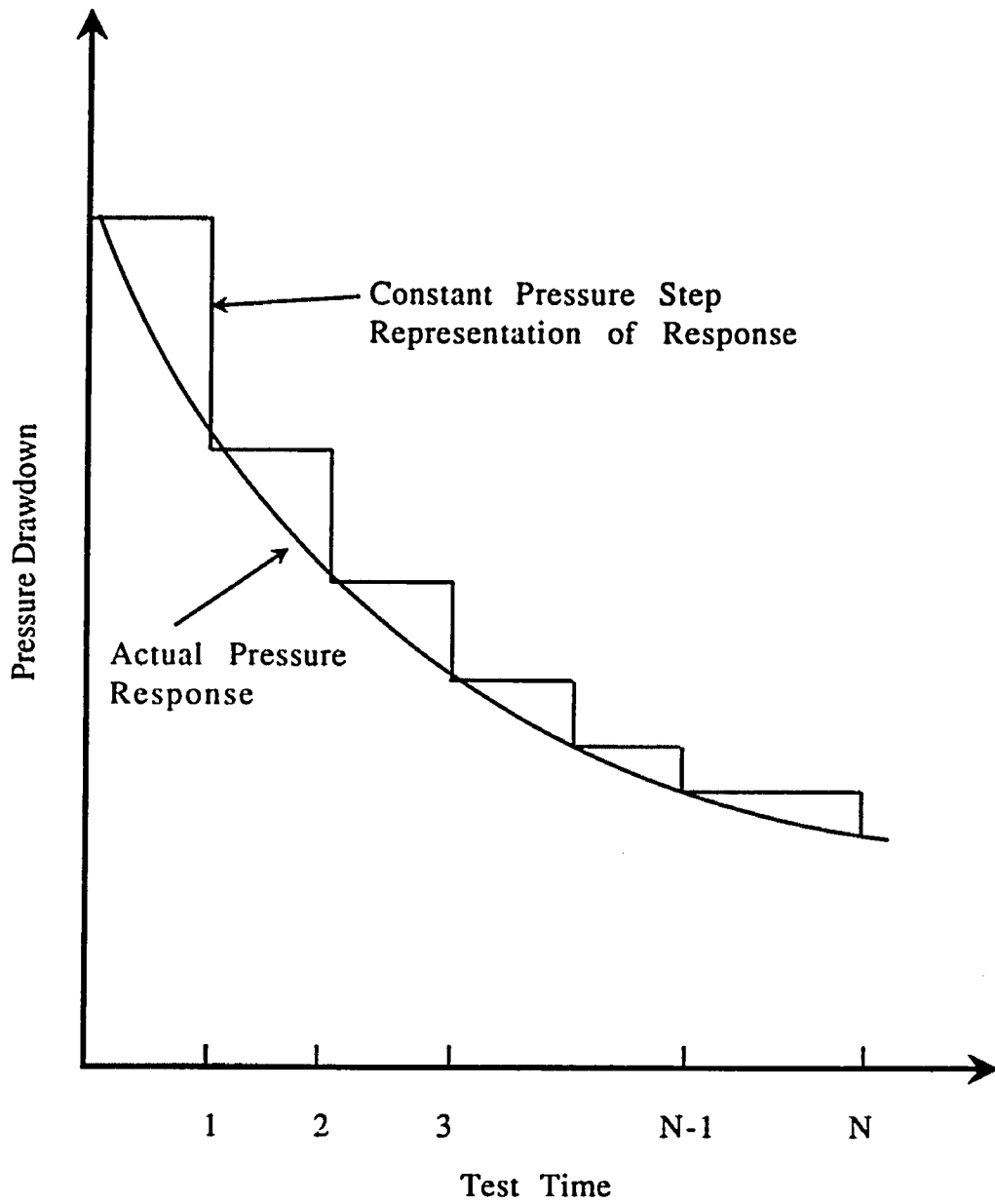


Fig. 2.2 - Discrete Representation of the Pressure Response of a Closed Chamber Test

where u is the Laplace transform variable, and K_0 and K_1 are modified Bessel functions of the second kind, zero and first order respectively. The Stehfest Algorithm²¹ is applied to Eq. 2.20 to obtain the cumulative rate in the real time domain.

Eq. 2.19 gives the cumulative production at time t_N . Then, the liquid level in the wellbore at this time can be calculated as

$$X = L_i + \frac{5.615Q_{sf}}{A_{ch}}, \quad (2.21)$$

where L_i is the initial height of the liquid in the wellbore (drillstring) and $A_{ch} = \pi r_p^2$ is the cross sectional area of the drillpipe. In Eq. 2.21, we implicitly assume that the liquid in the wellbore is incompressible. Assuming that the chamber gas behaves as an ideal gas and the temperature and pressure gradients in the gas column are negligible, the chamber gas pressure can be obtained from

$$p_{ch} = \frac{p_{chi}[L_c - L_i]}{[L_c - X]}, \quad (2.22)$$

where L_c is the length of the chamber and p_{chi} is the initial pressure in the gas cushion. The bottomhole pressure is the summation of the chamber gas pressure and the hydrostatic pressure caused by the liquid column. Therefore, at any time t_N , the bottomhole pressure is given by

$$p_{wf} = p_{ch} + \frac{\rho g}{144g_c} X. \quad (2.23)$$

Starting at $t = 0$ and $[p_{wf}]_{t=0} = p_o$, we can use the procedure outlined above to generate pressure responses for a closed chamber test with a given set of tool and reservoir parameters. The specific steps of the solution are as follows:

1. Choose the maximum test duration that one wants to investigate, t_{max} , and the uniform time step, Δt . Calculate the dimensionless time step, Δt_D .

2. Invert $\bar{Q}_{cD}(u)$ in Eq. 2.20 for $t_D = i\Delta t_D$, for $i = 1, 2, \dots, M = t_{max}/\Delta t$ and store values for later use.
3. Begin calculation at $N = 1$. Assume that from t_{N-1} to t_N the wellbore pressure remains constant and calculate the cumulative production at t_N from Eq. 2.19.
4. Calculate liquid level at t_N from Eq. 2.21.
5. Calculate the chamber gas pressure at t_N from Eq. 2.22.
6. Calculate the wellbore pressure at t_N from Eq. 2.23.
7. Update N and repeat steps from 3 through 6 until $N = M$.

Ideally, one may want to use variable time steps in the numerical simulator, but in order to speed-up the calculation a uniform time step is more desirable such that inversion of $\bar{Q}_{cD}(u)$ for $t_D = i\Delta t_D$ ($i = 1, 2, \dots, M$) can be carried out outside the pressure calculation loop. To insure numerical stability, a small time step is usually required. Numerical experiments indicate that the size of the time step depends on the length of the chamber. For $L_c = 1000$ ft, $\Delta t = 0.01$ second can be used, while for $L_c = 10,000$ ft, $\Delta t = 2$ seconds can be used. In principle, the time step is chosen such that the pressure change in each time interval is relatively small.

In the current study, we also implement the methods of Salas and Sageev⁹ to take into account the effects of the wellbore friction and liquid compression. Salas and Sageev⁹ developed methods for three calculation modes: (1) with frictional but without compressional effects; (2) without frictional but with compressional effects; and (3) with both frictional and compressional effects. To simplify the numerical calculation, we consider the effects of wellbore friction and liquid compression separately.

Numerical procedures for closed chamber tests including the wellbore liquid frictional effect is considered first. The cumulative production is calculated in exactly the same way as previously presented. To calculate the frictional pressure drop, the velocity of the liquid column needs to be determined. The average liquid flow rate during each time step is given by

$$q_{sf} = \frac{Q_{sf}(t_N) - Q_{sf}(t_{N-1})}{\Delta t / 86400}, \quad (2.24)$$

where q_{sf} is in RB/D and Δt is in seconds. From Eq. 2.24, the average liquid velocity in the drillstring can be obtained

$$v_l = \frac{5.615q_{sf}}{86400A_{ch}}, \quad (2.25)$$

where v_l is in ft/s. Subsequently, the frictional pressure drop along the liquid column can be evaluated

$$\Delta p_f = \frac{1}{144} \frac{f \rho v_l^2}{2d_p g_c} X, \quad (2.26)$$

where f is friction factor calculated from the liquid Reynolds number and the roughness of the drillpipe and d_p is the diameter of the drillpipe. When the wellbore friction is considered in the CCT numerical model, the wellbore pressure calculation will become

$$p_{wf} = p_{ch} + \frac{\rho g}{144 g_c} X + \frac{1}{144} \frac{f \rho v_l^2}{2d_p g_c} X. \quad (2.27)$$

With a minor modification to the calculation procedures proposed by Simmons and Grader⁸, frictional pressure drop can be included in the calculation of CCT pressure responses. The modification is that during each time step we calculate the liquid upward moving velocity and add the frictional pressure drop along the liquid column to the wellbore pressure calculation, as given by Eq. 2.27.

Calculation procedures considering the effect of liquid compression is outlined below. The hydrostatic pressure drop along the liquid column at time t_N is given by

$$\Delta p = \frac{5.615\rho Q_{sf} g}{144A_{ch} g_c}. \quad (2.28)$$

Note that Eq. 2.28 is valid regardless of the compressibility of the liquid. The chamber gas pressure depends on the liquid level as indicated by Eq. 2.22. On the other hand, the length of the liquid column, which is a function of the liquid compressibility, also depends on the chamber gas pressure. Salas and Sageev⁹ show that

$$X = \frac{144 g_c}{c_l \rho g} \ln \left[1 + \frac{c_l \Delta p}{1 + c_l (p_{ch} - p_i)} \right]. \quad (2.29)$$

Consequently, at each time step, an iteration process is needed to determine the liquid level and the chamber gas pressure in order to calculate the wellbore pressure. Specifically, for each time step, we resort to the following calculation procedure:

1. Calculate the cumulative production using the method outlined for the case where the effect of liquid compression is not considered;
2. Calculate the hydrostatic pressure drop along the liquid column using Eq. 2.28;
3. Solve Eqs. 2.22 and 2.29 to obtain X and p_{ch} . These two equations are solved iteratively. A good initial guess for X is obtained from Eq. 2.21;
4. Calculate the wellbore pressure from

$$p_{wf} = p_{ch} + \Delta p. \quad (2.30)$$

The calculation procedures proposed by Simmons and Grader⁸ and Salas and Sageev⁹ are used to generate pressure responses for closed chamber tests. Generated

pressure responses are subsequently used to verify our new closed chamber test interpretation methods.

2.4 New CCT Interpretation Methods

In this section, a new formulation of the CCT problem is presented. This suggests a new pseudotime for correlating the CCT solution with the corresponding slug test solution. This correlation suggests that slug test analysis techniques can be used to analyze pressure data from a CCT test provided that CCT data are considered as a function of the new pseudotime.

2.4.1 CCT Problem Formulation

Under the assumptions stated previously, Eqs. 2.14.1 through 2.14.5 also apply to a CCT. The inner boundary condition, Eq. 2.14.6, however, is no longer appropriate for a CCT since the wellbore storage coefficient attributed to gas compression has to be taken into account.

As one of the principle theoretical contributions of this work, we show in *Appendix B* that the effective wellbore storage coefficient for a CCT is given by

$$C_a = \frac{C_g C_l}{C_g + C_l}, \quad (2.31)$$

where C_l and C_g , respectively, denote the wellbore storage coefficients due to a rising liquid level and gas compression, given by Eq. 2.4 and Eq. 2.5 respectively. Eq. 2.31 can be written in a dimensionless form as

$$C_{aD} = \frac{C_{gD} C_{lD}}{C_{gD} + C_{lD}}, \quad (2.32)$$

Eqs. 2.31 and 2.32 indicate clearly that both the rising liquid level and gas compression influence the test simultaneously. C_a is a function of time because of the

time-dependence of C_g caused by the change of gas volume and gas compressibility during the test; however C_l can be considered to be a constant.

It is worth pointing out that C_a computed from Eq. 2.31 will be equal to C_l , if C_g becomes infinite. In this case, a closed chamber test becomes a slug test. This observation implies that conventional slug tests are a special form of a closed chamber test where the chamber volume approaches infinity.

It is also shown in *Appendix B* that the proper inner boundary condition for a CCT is given by

$$\left(r_D \frac{\partial p_D}{\partial r_D} \right)_{r_D=1} = C_{aD} \frac{\partial p_{wD}}{\partial t_D}. \quad (2.33)$$

Although Eq. 2.33 has the same form as Eq. 2.14.6, the two equations differ significantly. In Eq. 2.33, C_{aD} is a function of p_{wD} so the inner boundary condition is non-linear, whereas, in Eq. 2.14.6, C_D is constant and the problem is linear.

2.4.2 New Pseudotime

Since its introduction by Agarwal²², pseudotime has been widely studied, accepted and applied to improve the analysis of gas well buildup tests. As suggested by theoretical arguments of Finjord²³, the work of Reynolds et al.²⁴ shows that pseudotime based on values of the gas compressibility-viscosity product should not be applied to analyze gas well drawdown data by semilog methods, even though the application of pseudotime will allow one to correlate the gas solution with the liquid solution during wellbore storage dominated flow. Aanonsen²⁵ has also provided theoretical arguments on why Agarwal's pseudotime can be applied to buildup data, but may not be applicable to drawdown data.

We define the new dimensionless pseudotime for CCT analysis as

$$t_{aD} = \int_0^{t_D} \frac{C_{aDi}}{C_{aD}} dt'_D, \quad (2.34)$$

where C_{aDi} is the dimensionless effective wellbore storage coefficient at the beginning of a closed chamber test. Using Eq. 2.34, it follows that we can rewrite Eq. 2.33 to obtain the following linearized inner boundary condition for closed chamber tests:

$$\left(r_D \frac{\partial p_D}{\partial r_D} \right)_{r_D=1} = C_{aDi} \frac{\partial p_{wD}}{\partial t_{aD}}. \quad (2.35)$$

A comparison of Eqs. 2.14.6 and 2.35 suggests that the dimensionless pressure solution for a CCT, considered as a function of pseudotime, t_{aD} , may be equal to an equivalent slug test solution considered as a function of time, t_D , where the equivalent slug test solution is the one with a constant wellbore storage coefficient equal to the initial effective wellbore storage coefficient of the closed chamber test, C_{aDi} . If the conjectured correlation applies, it follows that the pressure transient interpretation methods developed for slug tests can be easily applied to closed chamber tests.

Although the change of variables defined by Eq. 2.34 completely linearizes the inner boundary condition of our problem, corresponding changes have to be made to the original flow equation. Specifically, in terms of pseudotime, Eq. 2.14.1 is equivalent to

$$\frac{1}{r_D} \frac{\partial}{\partial r_D} \left(r_D \frac{\partial p_D}{\partial r_D} \right) = \frac{C_{aDi}}{C_{aD}} \frac{\partial p_D}{\partial t_{aD}}. \quad (2.36)$$

Eq. 2.36 is nonlinear. Therefore, the use of pseudotime has transferred the inherent non-linearity of our problem from the inner boundary condition to the original flow equation. From Eq. 2.36, we conjecture that the applicability of pseudotime to correlate the CCT solution with the slug test solution with $C_D = C_{aDi}$ will depend on how much and how quickly C_{aDi}/C_{aD} varies from unity. Investigation of the applicability of the pseudotime concept to closed chamber tests is given in a later section.

2.4.3 Practical Computation

The theoretical discussion of the preceding sections suggests that we can use analysis methods developed for slug tests to analyze CCT pressure data provided we consider the CCT data as a function of pseudotime. In order to apply this analysis procedure, we must be able to generate the dimensional form of pseudotime directly from field data.

The dimensional form of our new pseudotime is given by

$$t_a = \int_0^t \frac{C_{ai}}{C_a} dt'. \quad (2.37)$$

Numerical integration techniques can be used to obtain pseudotime from Eq. 2.37 provided C_a (see Eq. 2.31) can be computed. The wellbore storage coefficient due to a rising liquid level, C_l , is given by Eq. 2.4 and can be calculated directly provided we know the angle of the inclination of the wellbore, the inner diameter of the chamber and the liquid density. With the assumption that the chamber gas behaves as an ideal gas so that $(p_{ch}V_g)$ is constant, Eq. 2.5 will be equivalent to

$$C_g = \frac{p_{chi}(L_c - L_i)A_{ch}}{5.615p_{ch}^2}. \quad (2.38)$$

Thus, the measured chamber gas pressure during a CCT can be used to compute C_g . It follows that Eq. 2.31 can be used to compute C_a as a function of time and hence, Eq. 2.37 can be used to generate pseudotime.

As shown later, a version of pseudotime similar to the one of Eq. 2.37 can also be used to account for a changing wellbore storage coefficient due to the change in the wellstring diameter or inclination angle.

2.5 Simulator Validation

In subsection 2.3.2, CCT numerical solution methods proposed by Simmons and Grader⁸ and Salas and Sageev⁹ were reviewed. In this section, implementation of these numerical solution methods is verified by comparing pressure responses generated by computer simulators with solutions found in the literature.

2.5.1 Duplication of Slug Test Solutions

The slug test analytical solution derived by Ramey and Agarwal¹⁹ is given by

$$\bar{p}_{wD} = C_D \frac{K_0(\sqrt{u}) + s\sqrt{u}K_1(\sqrt{u})}{\sqrt{u}K_1(\sqrt{u}) + C_D u [K_0(\sqrt{u}) + s\sqrt{u}K_1(\sqrt{u})]}. \quad (2.39)$$

When the dimensionless wellbore storage coefficient and the skin factor are specified, the Stehfest algorithm²¹ is used to invert Eq. 2.39 to obtain the dimensionless wellbore pressure at a given dimensionless time.

It has been previously pointed out that conventional slug tests are special cases of closed chamber tests. This can be understood from another point of view. If in a closed chamber test a constant chamber gas pressure can be maintained, no chamber gas compression will occur, and consequently, the closed chamber test is equivalent to the conventional slug test. This suggests a method to verify our numerical simulator.

Parameters given in Table 2.1 are used in our simulator. Note that the total chamber length, initial liquid height and initial chamber gas pressure are not listed in this table because the dimensionless wellbore pressure generated by the simulator is independent of these parameters so long as the chamber gas pressure is held as a constant in running the simulator. With these parameters, the dimensionless wellbore storage coefficient due to a rising liquid level was found to be 1127. Using $C_D = 1127$ and $s = 0$, analytical dimensionless wellbore pressures are obtained by

inverting Eq. 2.39. Numerical and analytical solutions are listed in Table 2.2. Note that good agreement was obtained between the two solutions for four log-cycles of dimensionless time.

2.5.2 Comparison with Simmons and Grader Solutions

Simmons and Grader⁸ presented results for a base case closed chamber test and also conducted sensitivity analysis for various tool and reservoir parameters. Table 2.3 lists the parameters for the base case closed chamber test used by Simmons and Grader⁸. In their numerical model, the chamber gas was treated as a real gas and, thus, the gas compressibility factor was allowed to change as a function of pressure and temperature. However, they found out that the effect of assuming that the chamber gas is an ideal gas is not significant. Our simulator was run with the parameters listed in Table 2.3 without considering the change of gas compressibility factor. Results are compared in Table 2.4.

From Table 2.4, we see that the two solutions agree very well except for the period of 15-20 seconds. This may be attributed to the effect of the change of gas Z-factor, but the deviation between the two solutions is within 5%.

2.5.3 Comparison with Salas and Sageev Solutions

We also compare our solutions with the those obtained by Salas and Sageev⁹ when the effect of liquid compression is considered. It is assumed that the initial liquid height $L_i = 0$ ft and liquid compressibility $c_l = 1 \times 10^{-6}$. All other parameters are exactly the same as those given in Table 2.3. Our simulator solutions are compared with the solutions given by Salas and Sageev⁹ in Table 2.5. The two solutions give similar results. Again, except during a short period of time, the deviation between the two solutions is small and may be attributed to the ideal-gas assumption we made in our model.

Table 2.1
Parameters Used for Slug Test Comparison

Parameter	Value	Unit
Initial Reservoir Pressure	5000.0	psig
Fluid Gravity	25.0	API
Fluid Viscosity	1.25	cp
Formation Porosity	0.27	-
Formation Permeability	100.0	md
Skin Factor	0.0	-
Total System Compressibility	0.00001	1/psi
Reservoir Thickness	25.0	ft
Well Diameter	10.0	in.
Chamber ID	2.441	in.
Initial Wellbore Storage Coefficient	1127.0	-

Table 2.2
Comparison with Analytical Slug Test Solutions

t_D	P_{wD} (Numerical)	P_{wD} (Analytical)
10.0	0.993430	0.993461
20.0	0.989107	0.989145
30.0	0.985240	0.985286
40.0	0.981632	0.981685
50.0	0.978201	0.978260
60.0	0.974903	0.974969
70.0	0.971712	0.971783
80.0	0.968608	0.968685
90.0	0.965579	0.965662
100.0	0.962616	0.962703
200.0	0.935430	0.935561
300.0	0.911064	0.911231
400.0	0.888508	0.888706
500.0	0.867314	0.867540
600.0	0.847228	0.847478
700.0	0.828082	0.828355
800.0	0.809759	0.810052
900.0	0.792170	0.792481
1000.0	0.775245	0.775573
2000.0	0.633533	0.633967
3000.0	0.526575	0.527043
4000.0	0.442757	0.443227
5000.0	0.375714	0.376179
6000.0	0.321339	0.321801
7000.0	0.276774	0.277235
8000.0	0.239933	0.240397
9000.0	0.209256	0.209722
10000.0	0.183546	0.184011
20000.0	0.064649	0.064837
30000.0	0.032962	0.032864
40000.0	0.021090	0.020935
50000.0	0.015361	0.015252
60000.0	0.012067	0.012019
70000.0	0.009938	0.009937
80000.0	0.008451	0.008478
90000.0	0.007351	0.007395
100000.0	0.006506	0.006556

Table 2.3
Parameters Used for Comparison with Simmons & Grader Solutions

Parameter	Value	Unit
Initial Reservoir Pressure	5000.0	psig
Fluid Gravity	25.0	API
Fluid Viscosity	1.25	cp
Formation Porosity	0.27	-
Formation Permeability	100.0	md
Skin Factor	0.0	-
Total System Compressibility	0.00001	1/psi
Reservoir Thickness	25.0	ft
Well Diameter	10.0	in.
Initial Fluid Height	100.0	ft
Chamber ID	2.441	in.
Total Chamber Length	1000.	ft
Initial Chamber Gas Pressure	30.0	psig
Initial Wellbore Storage Coefficient	999.8	-

Table 2.4
Comparison with Simmons and Grader Solutions

time (sec.)	P_{wf} (psia)	S-G P_{wf} (psia)	time (sec.)	P_{wf} (psia)	S-G P_{wf} (psia)
1.000	127.13	127.11	26.00	4019.27	4023.00
2.000	156.83	156.78	27.00	4086.91	4090.22
3.000	184.12	184.05	28.00	4144.87	4147.84
4.000	210.36	210.25	29.00	4195.28	4197.95
5.000	236.17	236.02	30.00	4239.64	4242.06
6.000	261.99	261.79	31.00	4279.04	4281.25
7.000	288.21	287.94	32.00	4314.35	4316.37
8.000	315.25	314.87	33.00	4346.19	4348.05
9.000	343.59	343.09	34.00	4375.10	4376.81
10.00	373.92	373.24	35.00	4401.46	4403.05
11.00	407.22	406.27	36.00	4425.64	4427.10
12.00	444.96	443.61	37.00	4447.88	4449.25
13.00	489.61	487.62	38.00	4468.44	4469.72
14.00	545.51	542.43	39.00	4487.50	4488.69
15.00	621.08	615.96	40.00	4505.22	4506.34
16.00	734.56	725.16	41.00	4521.75	4522.80
17.00	931.26	911.59	42.00	4537.21	4538.20
18.00	1333.31	1287.28	43.00	4551.70	4552.63
19.00	2120.57	2055.68	44.00	4565.31	4566.19
20.00	2891.78	2879.14	45.00	4578.12	4578.95
21.00	3308.51	3312.87	46.00	4590.20	4590.99
22.00	3551.17	3557.09	47.00	4601.62	4602.36
23.00	3716.76	3722.23	48.00	4612.42	4613.13
24.00	3840.75	3845.56	49.00	4622.66	4623.33
25.00	3938.84	3943.06	50.00	4632.38	4633.02

Table 2.4 (cont'd)

time (sec.)	P_{wf} (psia)	S-G P_{wf} (psia)	time (sec.)	P_{wf} (psia)	S-G P_{wf} (psia)
51.00	4641.62	4642.23	76.00	4781.48	4781.71
52.00	4650.42	4651.00	77.00	4784.91	4785.13
53.00	4658.81	4659.36	78.00	4788.24	4788.45
54.00	4666.81	4667.34	79.00	4791.47	4791.68
55.00	4674.45	4674.96	80.00	4794.61	4794.81
56.00	4681.76	4682.25	81.00	4797.67	4797.86
57.00	4688.76	4689.22	82.00	4800.64	4800.83
58.00	4695.46	4695.91	83.00	4803.53	4803.71
59.00	4701.89	4702.32	84.00	4806.34	4806.52
60.00	4708.07	4708.48	85.00	4809.08	4809.25
61.00	4714.00	4714.40	86.00	4811.74	4811.91
62.00	4719.71	4720.08	87.00	4814.34	4814.51
63.00	4725.19	4725.56	88.00	4816.87	4817.03
64.00	4730.48	4730.83	89.00	4819.34	4819.50
65.00	4735.58	4735.91	90.00	4821.75	4821.90
66.00	4740.49	4740.82	91.00	4824.10	4824.24
67.00	4745.23	4745.55	92.00	4826.39	4826.53
68.00	4749.81	4750.11	93.00	4828.63	4828.76
69.00	4754.24	4754.53	94.00	4830.81	4830.94
70.00	4758.51	4758.80	95.00	4832.94	4833.07
71.00	4762.65	4762.93	96.00	4835.03	4835.15
72.00	4766.66	4766.92	97.00	4837.06	4837.19
73.00	4770.54	4770.79	98.00	4839.05	4839.18
74.00	4774.30	4774.54	99.00	4841.00	4841.12
75.00	4777.94	4778.18	100.00	4842.90	4843.02

Table 2.5
Comparison with Salas and Sageev Solutions

time (sec.)	P_{wf} (psia)	S-S P_{wf} (psia)	time (sec.)	P_{wf} (psia)	S-S P_{wf} (psia)
1.000	87.73	87.69	23.00	3083.47	3110.79
2.000	117.13	117.06	24.00	3386.93	3410.80
3.000	144.01	143.91	25.00	3584.75	3601.05
4.000	169.68	169.55	26.00	3728.00	3740.95
5.000	194.74	194.56	27.00	3838.92	3850.56
6.000	219.55	219.32	28.00	3928.66	3939.98
7.000	244.41	244.13	29.00	4003.43	4011.74
8.000	269.61	269.25	30.00	4067.10	4074.60
9.000	295.44	294.97	31.00	4122.22	4129.56
10.00	322.26	321.67	32.00	4170.56	4178.25
11.00	350.55	349.83	33.10	4217.43	4220.78
12.00	380.95	380.05	34.00	4251.70	4257.87
13.00	414.37	413.15	35.10	4289.51	4294.17
14.00	452.22	450.58	36.00	4317.55	4322.41
15.00	496.76	494.48	37.20	4351.51	4354.56
16.00	551.85	548.55	38.00	4372.25	4375.42
17.00	624.61	619.43	39.00	4396.32	4403.23
18.00	729.50	720.79	40.00	4418.55	4424.58
19.00	898.97	883.07	41.00	4443.10	4445.03
20.00	1210.98	1180.74	42.00	4458.33	4464.65
21.00	1803.28	1764.72	43.00	4476.21	4484.56
22.00	2562.09	2570.56	44.00	4492.93	4499.46

Table 2.5 (cont'd)

time (sec.)	P_{wf} (psia)	S-S P_{wf} (psia)	time (sec.)	P_{wf} (psia)	S-S P_{wf} (psia)
44.90	4505.55	4511.49	67.00	4708.06	4711.04
46.10	4524.75	4529.90	67.90	4712.88	4715.77
47.10	4538.54	4540.73	68.80	4717.04	4720.38
49.10	4563.84	4564.59	69.70	4722.08	4723.37
50.20	4576.61	4579.36	70.20	4724.53	4725.38
50.10	4586.52	4595.88	71.80	4731.66	4733.81
52.40	4600.04	4596.88	72.80	4736.21	4742.03
53.40	4609.87	4611.81	74.80	4744.89	4745.36
54.10	4616.47	4620.12	76.70	4753.04	4753.90
55.10	4625.52	4629.03	77.30	4755.00	4756.45
56.00	4633.32	4637.85	77.90	4757.70	4759.34
57.40	4644.79	4647.54	79.30	4762.56	4768.78
58.00	4649.53	4652.39	84.70	4781.22	4771.64
59.20	4658.62	4661.29	85.00	4782.16	4778.98
60.20	4665.85	4667.63	86.00	4785.23	4788.12
61.00	4671.42	4673.51	87.10	4788.52	4797.78
62.30	4680.09	4682.39	97.00	4814.33	4805.95
63.30	4686.47	4689.23	98.20	4817.06	4810.06
64.00	4690.78	4694.34	99.20	4819.28	4815.83
65.30	4697.92	4699.60	99.70	4820.37	4818.93
66.60	4705.31	4706.50	100.20	4821.02	4819.90

2.6 Results and Discussions

In this section, we illustrate the application of new interpretation methods for closed chamber tests, using pressure data generated by computer simulators. In exploring the applicability of the pseudotime correlation for closed chamber tests, We consider a base case closed chamber test and then conduct sensitivity analysis to evaluate the influence of each parameter on the performance of our new interpretation methods.

2.6.1 Base Case Closed Chamber Test Analysis

Parameters for the base case closed chamber test are presented in Table 2.6. Results for the base case closed chamber test are given in Figs. 2.3-2.7.

Fig. 2.3 is a Cartesian plot of the bottomhole pressure and the gas chamber pressure versus test time in seconds. As shown, both pressures increase rather rapidly until about 600 seconds and thereafter, both pressures increase only slightly. Similarly, the liquid level, shown in Fig. 2.4, rises rapidly at early times (increasing to approximately 7000 feet within the first 600 seconds) and then increases much more slowly (the total liquid level at 1800 seconds is still less than 8000 feet).

A CCT is characterized by the changing wellbore storage coefficient where the change in the wellbore storage coefficient is governed by the change in the volume and compressibility of the chamber gas. Fig. 2.5 is a log-log plot of the dimensionless wellbore storage coefficients versus dimensionless time. As suggested in this figure, the wellbore storage coefficient due to gas compression changes significantly during the test and finally becomes approximately constant as the flow becomes very small and the change in bottomhole pressure becomes small. On the other hand, the wellbore storage coefficient due to rising liquid level remains constant during the test. For $t_D \leq 1000$ (approximately $t \leq 100$ seconds), the combined wellbore storage coefficient is dominated by the wellbore storage due to the rising liquid

Table 2.6
Parameters for Base Case Closed Chamber Test

Parameter	Value	Unit
Initial Reservoir Pressure	5000.0	psig
Fluid Gravity	25.0	API
Fluid Viscosity	1.25	cp
Formation Porosity	0.27	–
Formation Permeability	100.0	md
Skin Factor	0.0	–
Total System Compressibility	0.00001	1/psi
Reservoir Thickness	25.0	ft
Well Diameter	10.0	in.
Initial Fluid Height	100.0	ft
Chamber ID	2.441	in.
Total Chamber Length	10,000.0	ft
Initial Chamber Gas Pressure	500.0	psig
Initial Wellbore Storage Coefficient	994.0	–

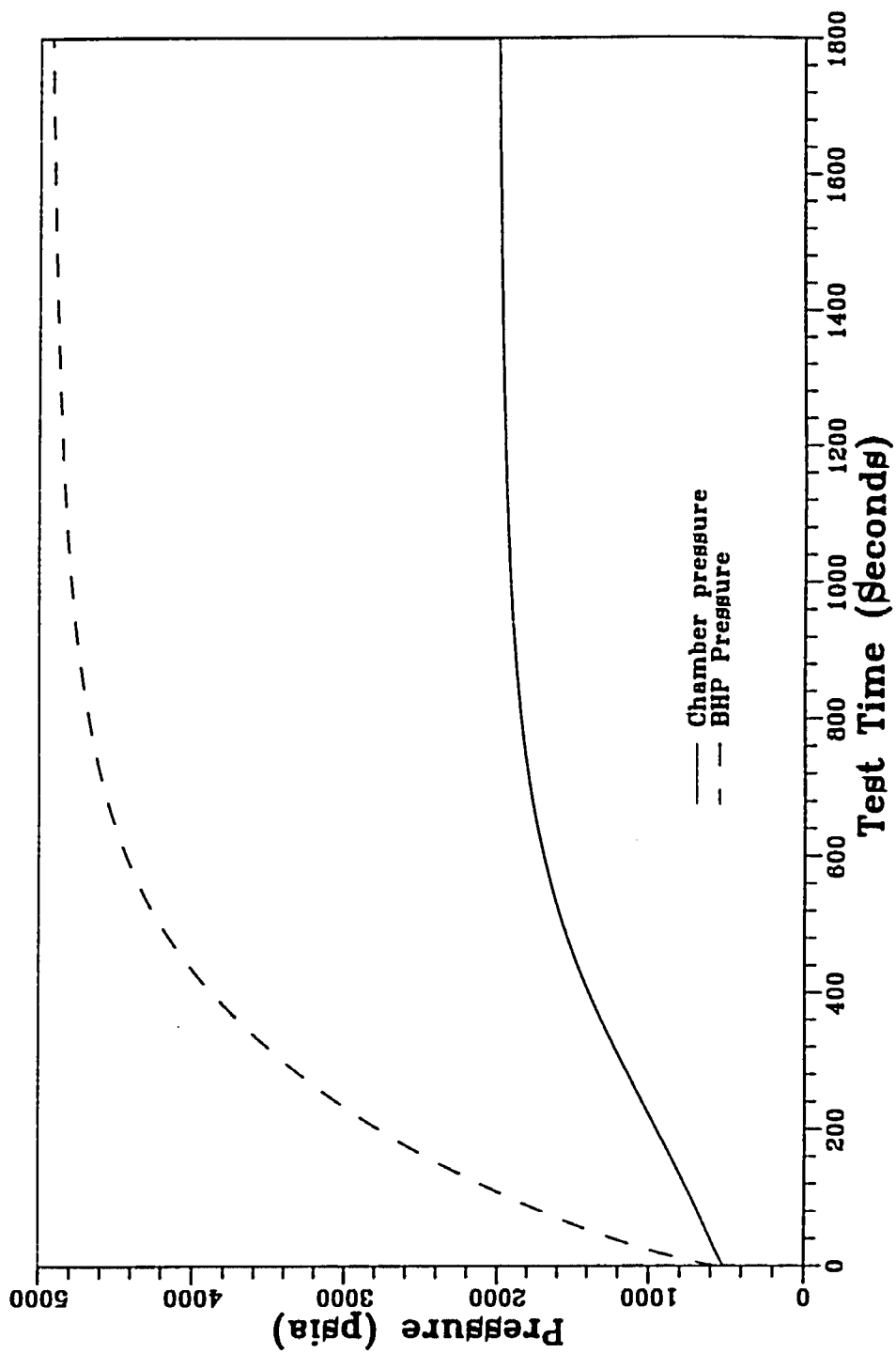


Fig. 2.3 - BHP and Chamber Gas Pressure for Base Case CCT

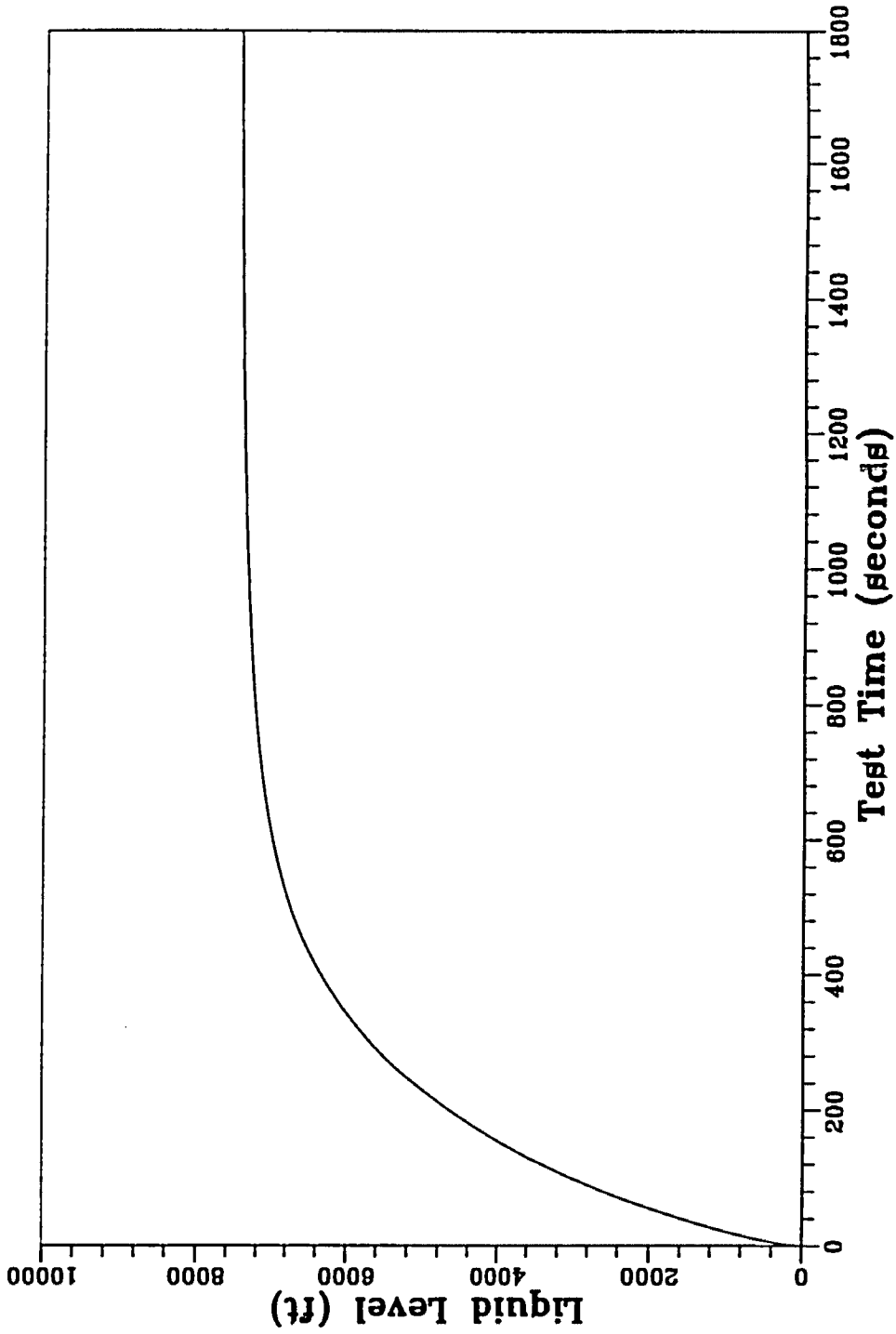


Fig. 2.4 - Liquid Level As A Function of Time for Base Case CCT

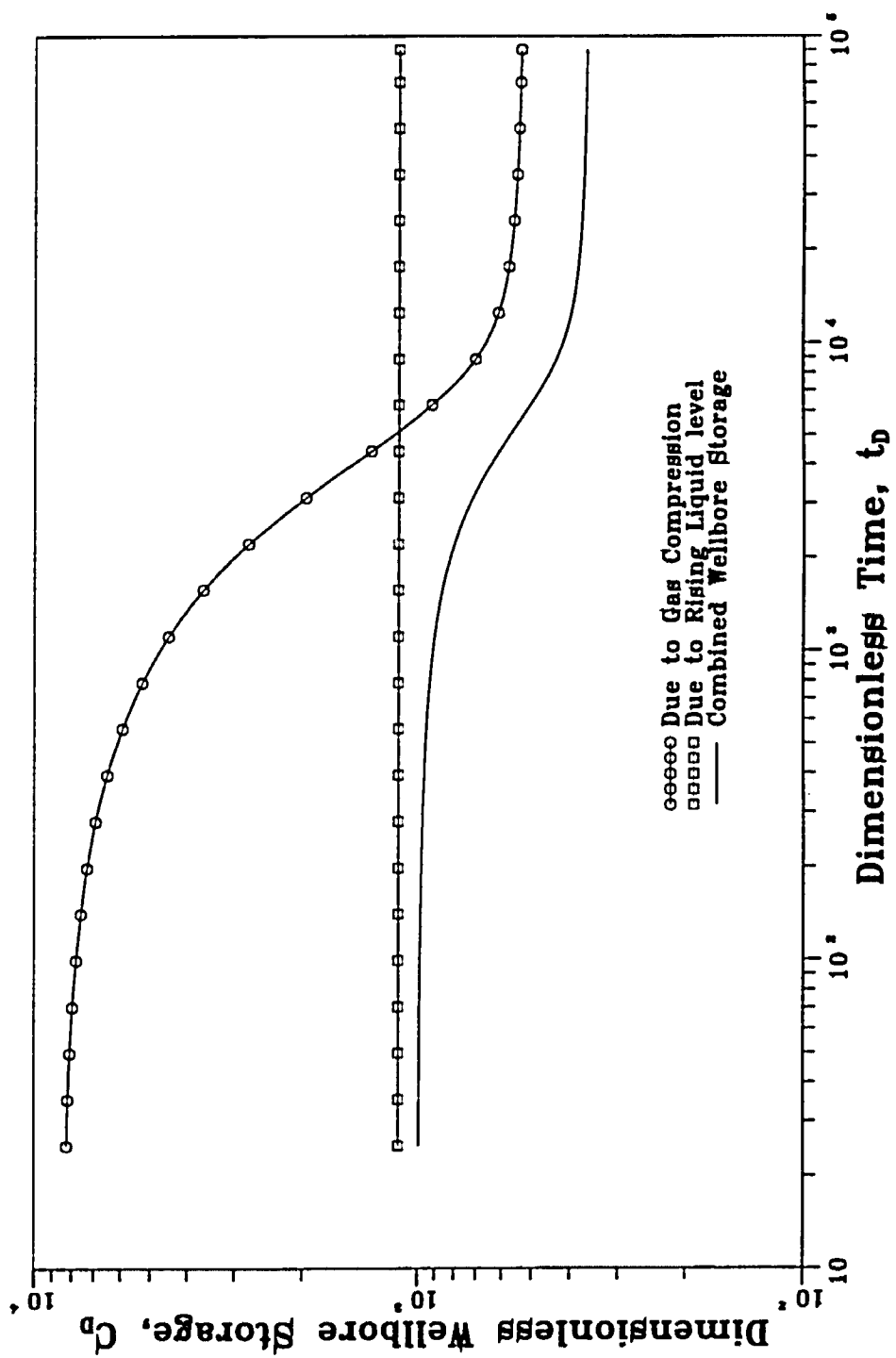


Fig. 2.5 - Wellbore Storage Coefficient for Base Case CCT

level and remains almost equal to its initial value of $C_{aD} = 994$. During the intermediate flow period the combined wellbore storage is controlled by both rising liquid level and gas compression. However, as the bottomhole pressure approaches the static reservoir pressure, the combined wellbore storage coefficient tends to approach another constant value, $C_{aD} = 362$.

The variation in the wellbore storage coefficient during a CCT is normally large enough to cause the pressure response to differ significantly from that of a slug test. Two of the solutions in Fig. 2.6 represent slug test solutions with constant wellbore storage coefficients equal to the initial ($C_{aD} = 994$) and final ($C_{aD} = 362$) wellbore storage coefficients attained during the CCT. The CCT response in Fig. 2.6 is plotted as a solid line and, for $t_D > 2 \times 10^3$, does not correlate with either of the slug test responses, but falls in between the two slug test solutions. This implies that parameters obtained may not be reliable if one analyzes the CCT data using the slug test analysis methods such as those presented in Refs. 3 and 4.

Fig. 2.7 illustrates the applicability of pseudotime for the base case CCT. In Fig. 2.7, the dashed line represents a plot of the slug test solution (with a constant wellbore storage coefficient equal to the initial wellbore storage coefficient of the CCT) versus t_D , and the solid line is the pressure response for the CCT plotted versus t_D . Also shown in Fig. 2.7 is a plot of the CCT p_{wD} versus t_{aD} (Eq. 2.34). As shown, when plotted versus dimensionless pseudotime, the CCT dimensionless pressure solution correlates almost perfectly with the slug test solution for $t_D \leq 10^4$ ($t_D/C_{aDi} \leq 10$, $p_{wD} \geq 0.15$). Therefore, the base case CCT pressure data corresponding to $t_D \leq 10^4$ ($t_D/C_{aDi} \leq 10$) can be analyzed using methods developed for slug tests. Clearly there are enough data corresponding to this range to perform a preliminary analysis to obtain estimates of reservoir parameters. These estimates could be verified or refined by using a numerical method in a history-matching mode. Also note that at $t_D = 10^4$, $p_i - p_{wf} \approx 0.15(p_i - p_o)$ so by the time the

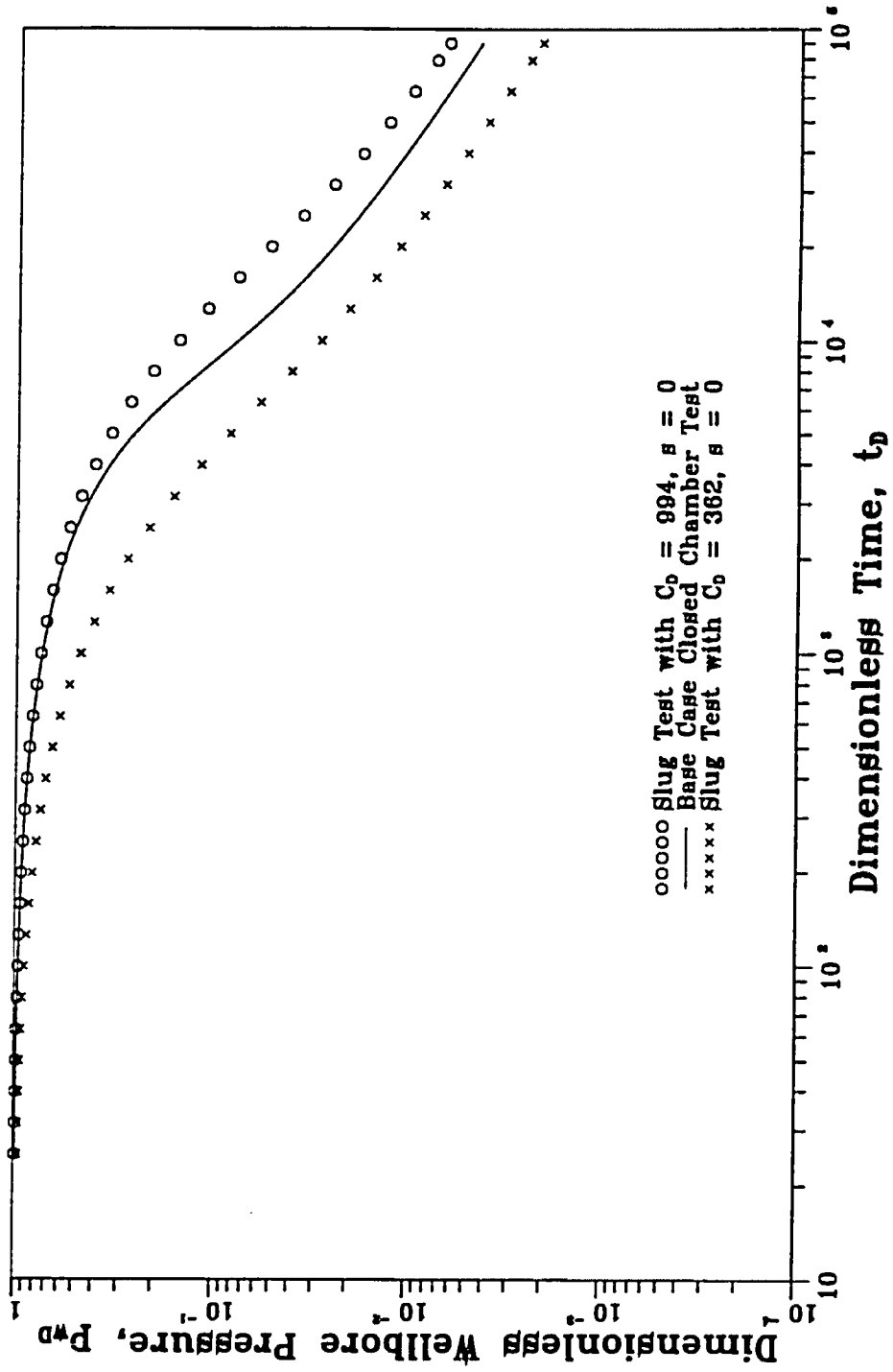


Fig. 2.6 - Comparison of Slug Test and Base Case Closed Chamber Test Solutions

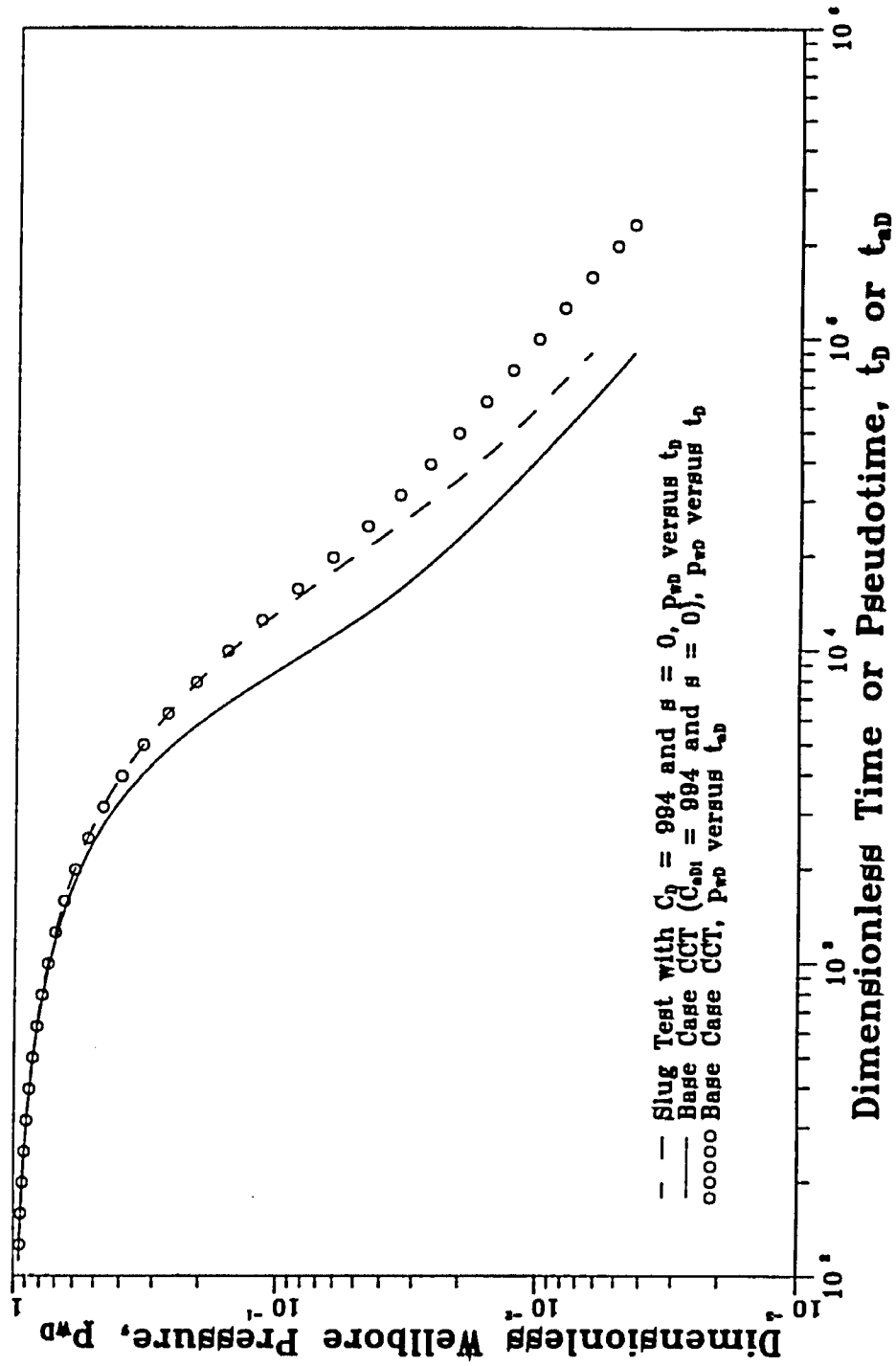


Fig. 2.7 - Correlation of Base Case CCT with Analogous Slug Test Solution

pseudotime correlation begins to become less accurate, we have recovered most of the pressure drop imposed initially at the wellbore.

2.6.2 Sensitivity Analysis

In this subsection, we consider effects of various reservoir and operational parameters on the performance of the proposed new CCT interpretation method.

Effect of Skin Factor: For the base case CCT, we have used $s = 0$. In Fig. 2.8, pressure responses from closed chamber tests with $s = 5$ and $s = 10$ are compared with the base case. (Except for the variation in the skin factor, all other parameters used to generate the results of Figs. 2.8-2.11 are the same as those given for the base case, Table 2.6.) As expected, the results of Fig. 2.8 indicate that increasing the skin factor results in a slower pressure recovery, thus, at a given value of time, a larger value of skin factor results in a larger value of p_{wD} .

The application of pseudotime for the $s = 5$ case is shown in Fig. 2.9. Comparing the results of Fig. 2.9 with the base case results of Fig. 2.7, we see that the CCT solution plotted versus pseudotime correlates with the corresponding slug test solution (C_D for slug test equal to the initial combined wellbore storage coefficient for CCT and same s value) for a longer period of time for the $s = 5$ case than for the $s = 0$ case. The application of pseudotime for the $s = 10$ case is shown in Fig. 2.10. We see that the correlation applies for a significantly longer period of time for the $s = 10$ case than for the $s = 0$ and $s = 5$ cases.

As discussed previously, the introduction of pseudotime transfers the non-linearity of the CCT problem from its inner boundary condition to the original flow equation and the variation in C_{aDi}/C_{aD} from unity is the controlling factor that determines the length of the time period during which the CCT solution considered as a function of pseudotime can be correlated with the analogous slug test solution. Fig. 2.11 presents semilog plots of C_{aDi}/C_{aD} versus t_D for $s = 0, 5$ and 10 . The

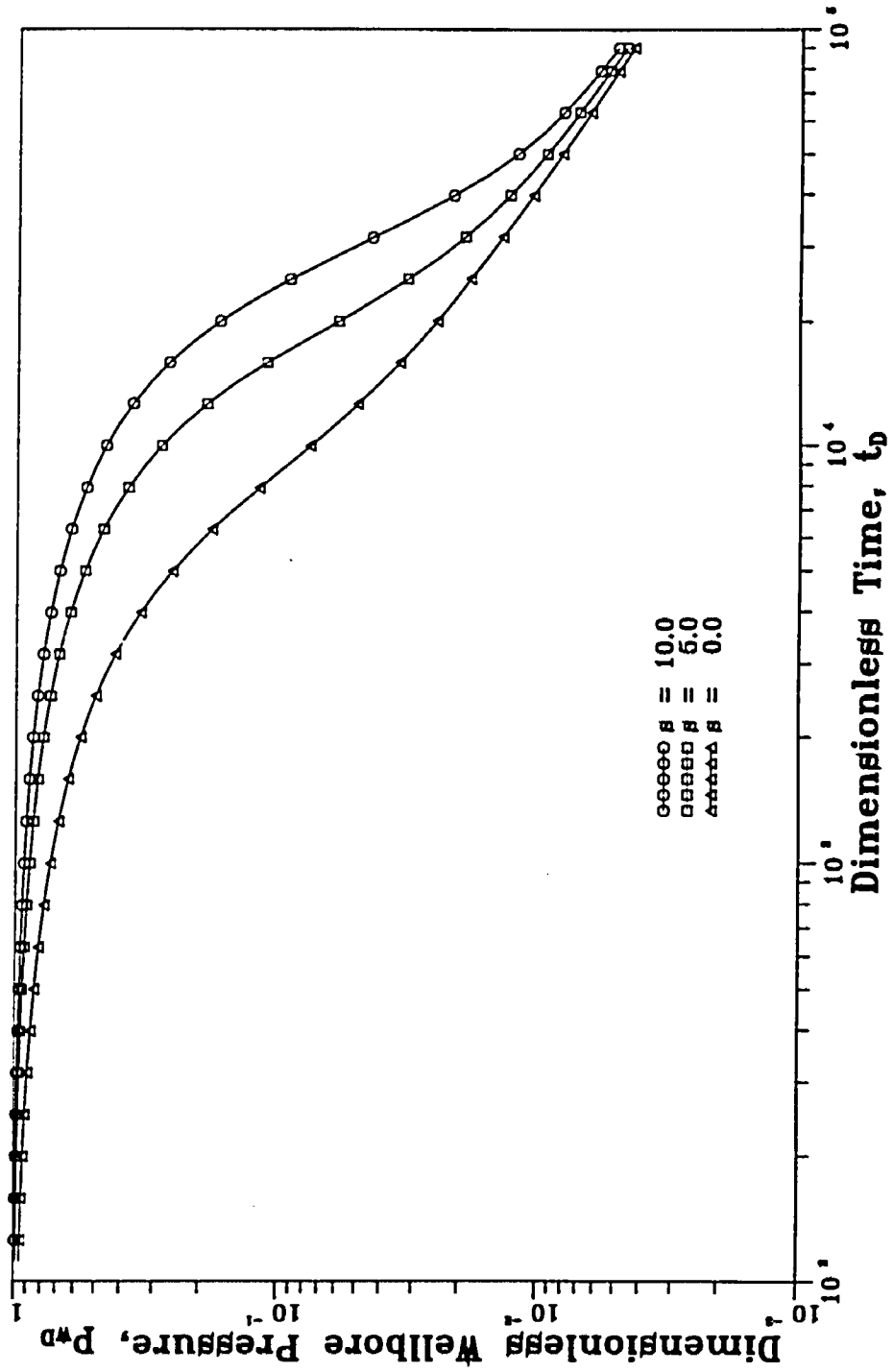


Fig. 2.8 - Effect of Skin Factor on Closed Chamber Test

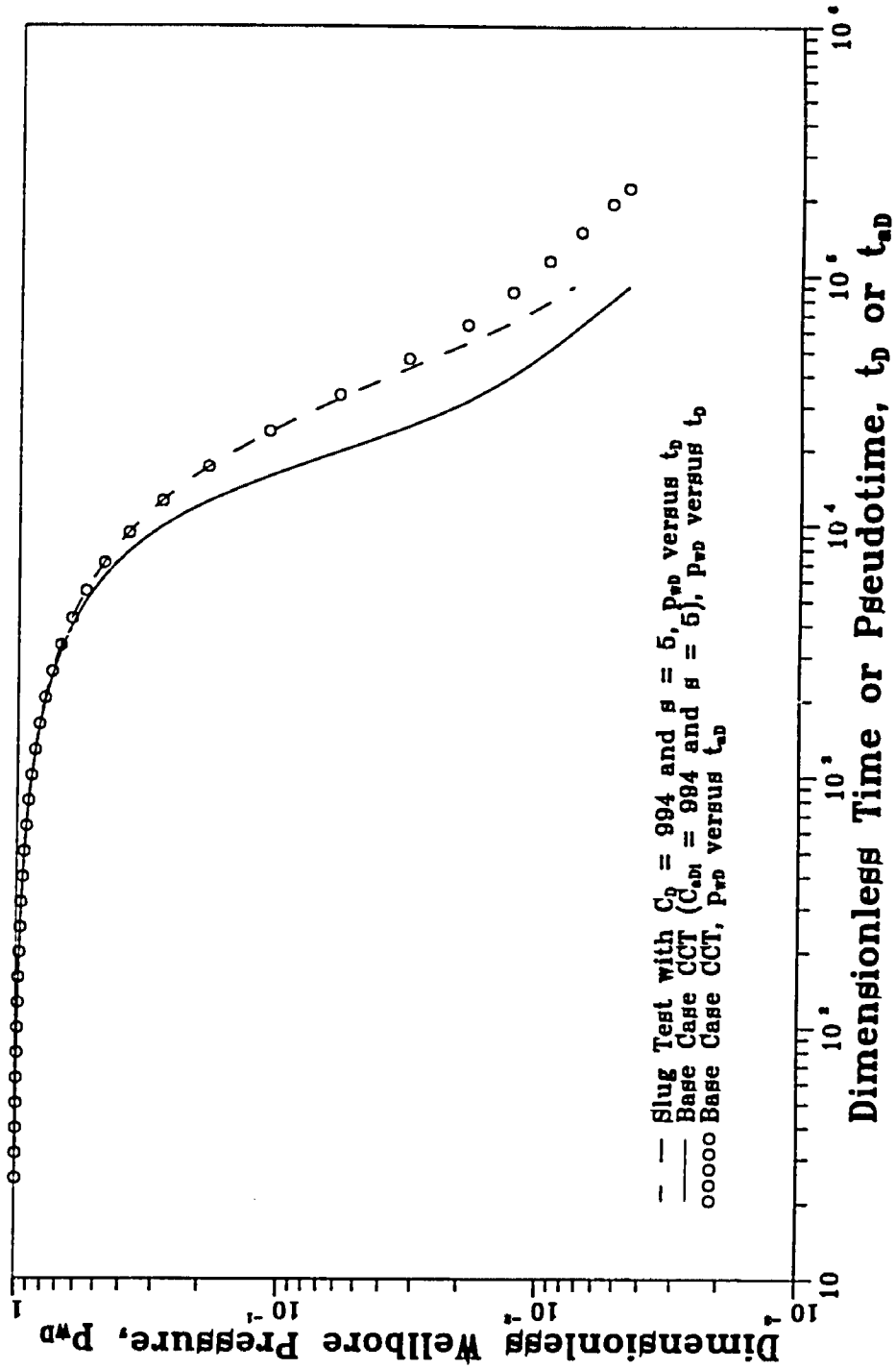


Fig. 2.9 - Correlation of CCT Solution with Analogous Slug Test Solution, $\beta = 5$

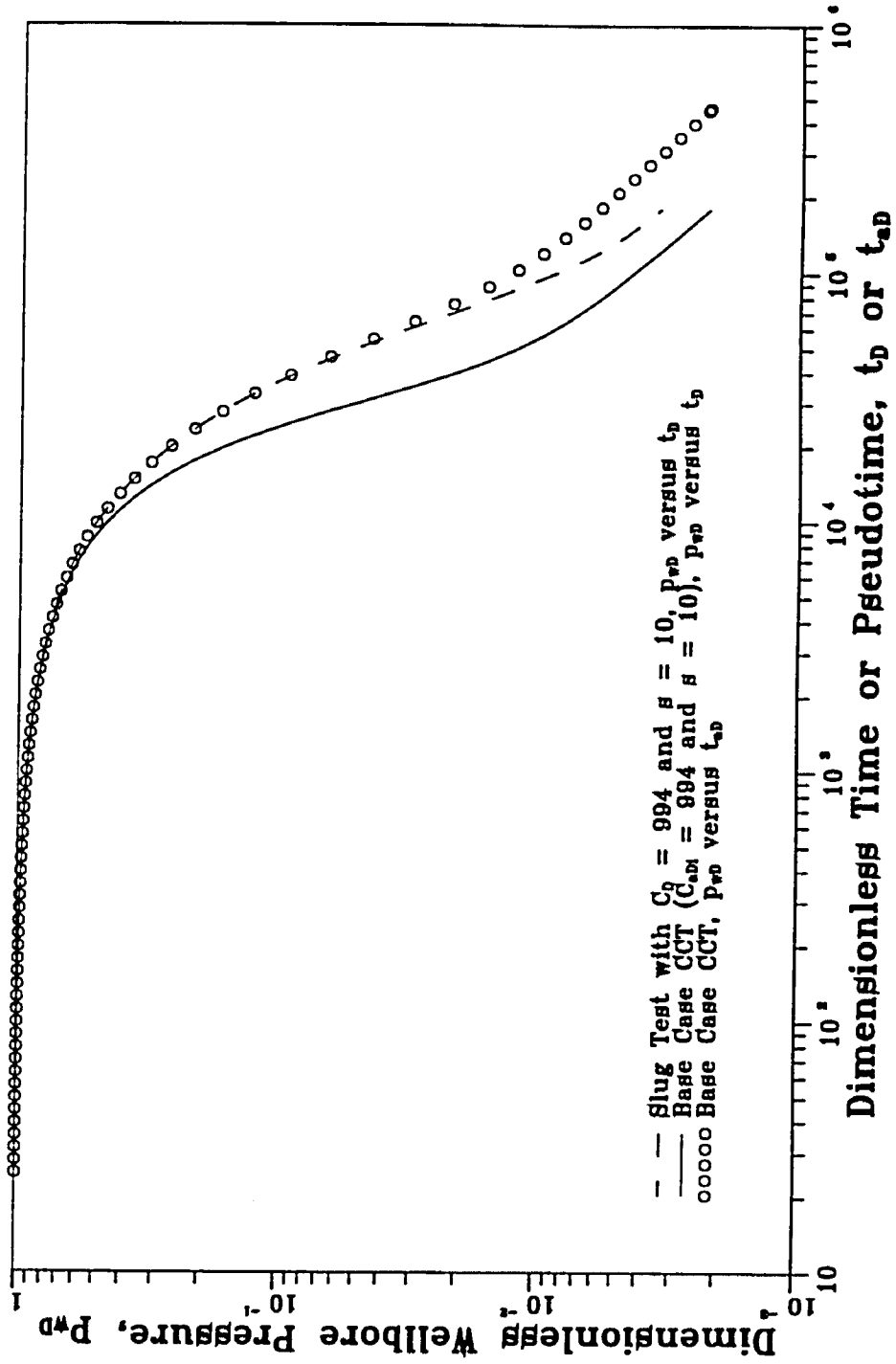


Fig. 2.10 - Correlation of CCT Solution with Slug Test Solution, $\beta = 10$

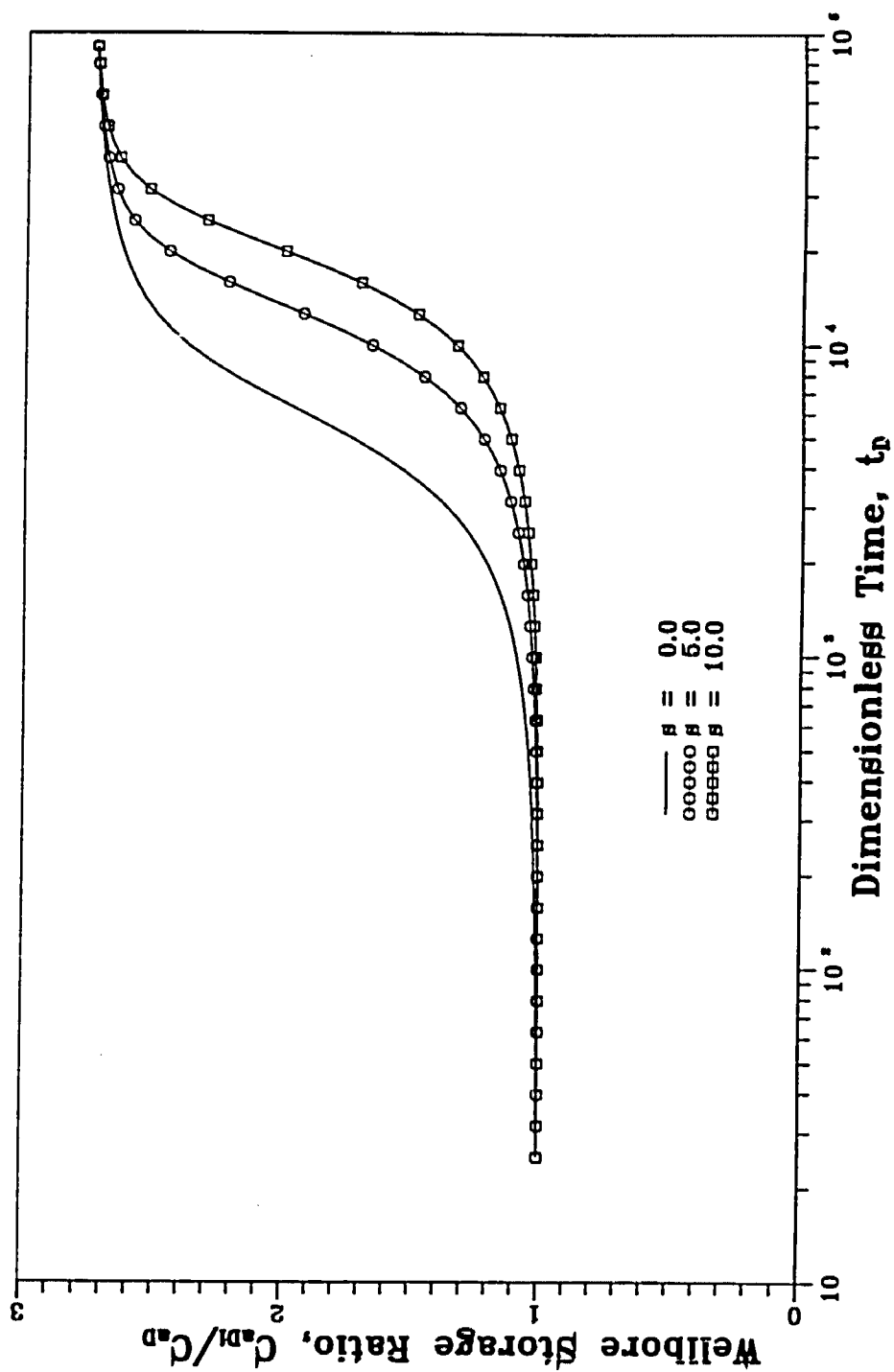


Fig. 2.11 - Effect of Skin Factor on Wellbore Storage Coefficient for CCT

results indicate that as the skin factor increases, the increase in C_{aDi}/C_{aD} not only is delayed but also becomes more gradual (note that the time scale in Fig. 2.11 is a log scale). Therefore, we expect that pseudotime can be applied for a longer period of time for the case with a larger skin factor. This explanation is confirmed by the results shown in Figs. 2.7, 2.9 and 2.10.

Effect of Initial Chamber Gas Pressure: In a CCT, to effectively wash out drilling mud around the wellbore and debris in the perforation channels, it is desirable to impose a higher pressure differential on the sandface of a formation being tested. On the other hand, to avoid casing collapses, formation failure and severe sand production, a lower pressure differential is often required. Therefore, an optimum initial chamber gas pressure in a CCT is chosen to carefully balance the two opposing factors.

Here, a parametric study is conducted to investigate the effect of the initial chamber gas pressure on the CCT dimensionless pressure solutions. Pressure responses are generated for a wide range of initial gas chamber pressures, specifically, for $p_{chi} = 0, 100, 1000, 2000, 3000,$ and 4000 (psig). Different initial chamber gas pressures give different values of the initial combined wellbore storage coefficient, C_{aDi} ; in all cases, we compare the CCT solution with the slug test solution that has a constant wellbore storage coefficient equal to the initial wellbore storage coefficient of the corresponding CCT problem. Except for the variation in p_{chi} and C_{aDi} , all parameters used in the results presented here are the same as those in the base case. Results are given in Figs. 2.12 - 2.18.

The effect of the initial chamber gas pressure on the change in C_{aDi}/C_{aD} is shown in Fig. 2.12. Note that for $t_D < 8 \times 10^3$, C_{aDi}/C_{aD} increases only slightly for all cases considered. When, $t_D > 8 \times 10^3$, a higher initial gas chamber pressures gives a smaller magnitude change in the combined wellbore storage coefficient relative to its initial value. Hence, in terms of correlating a CCT solution with the

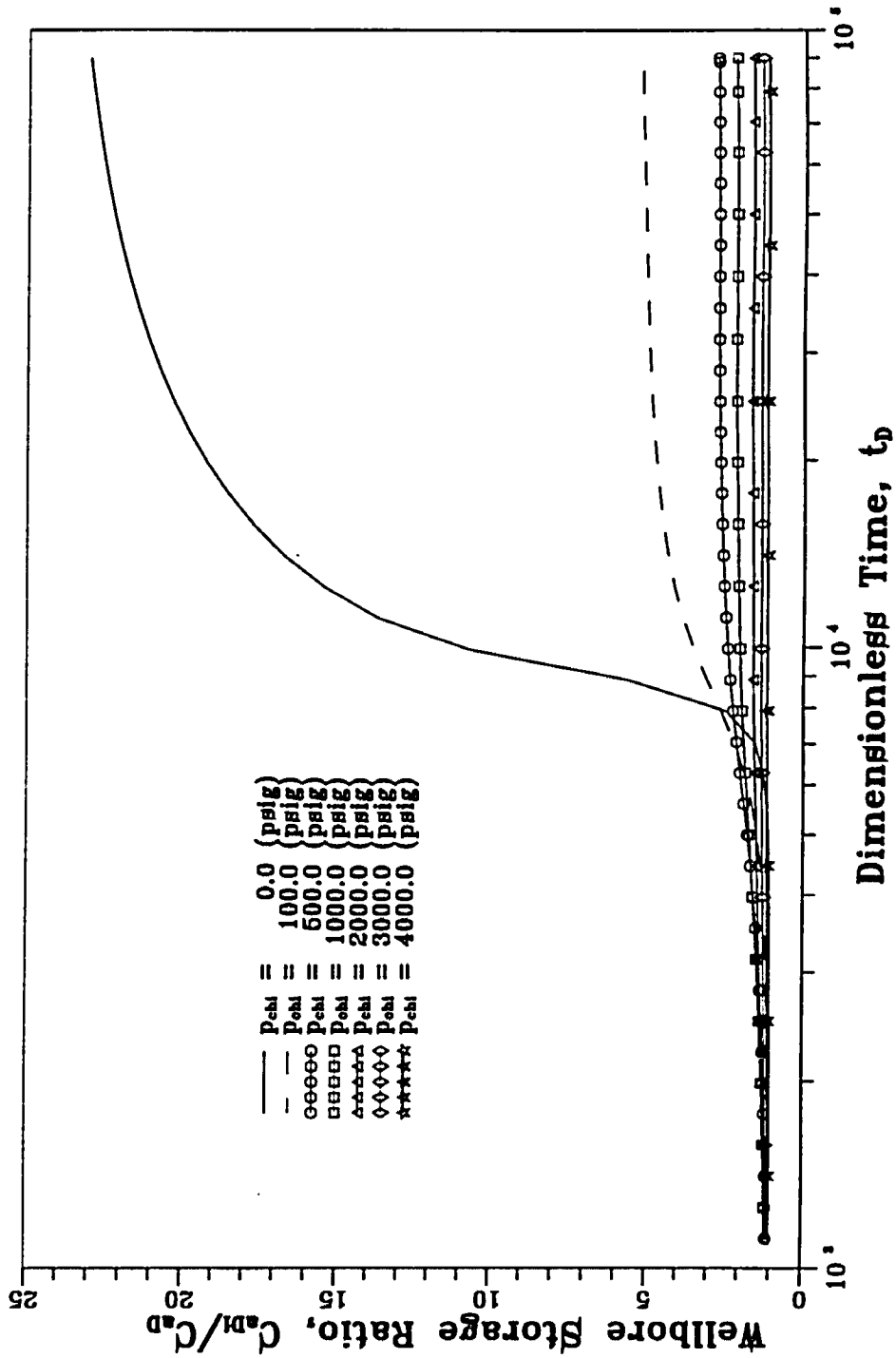
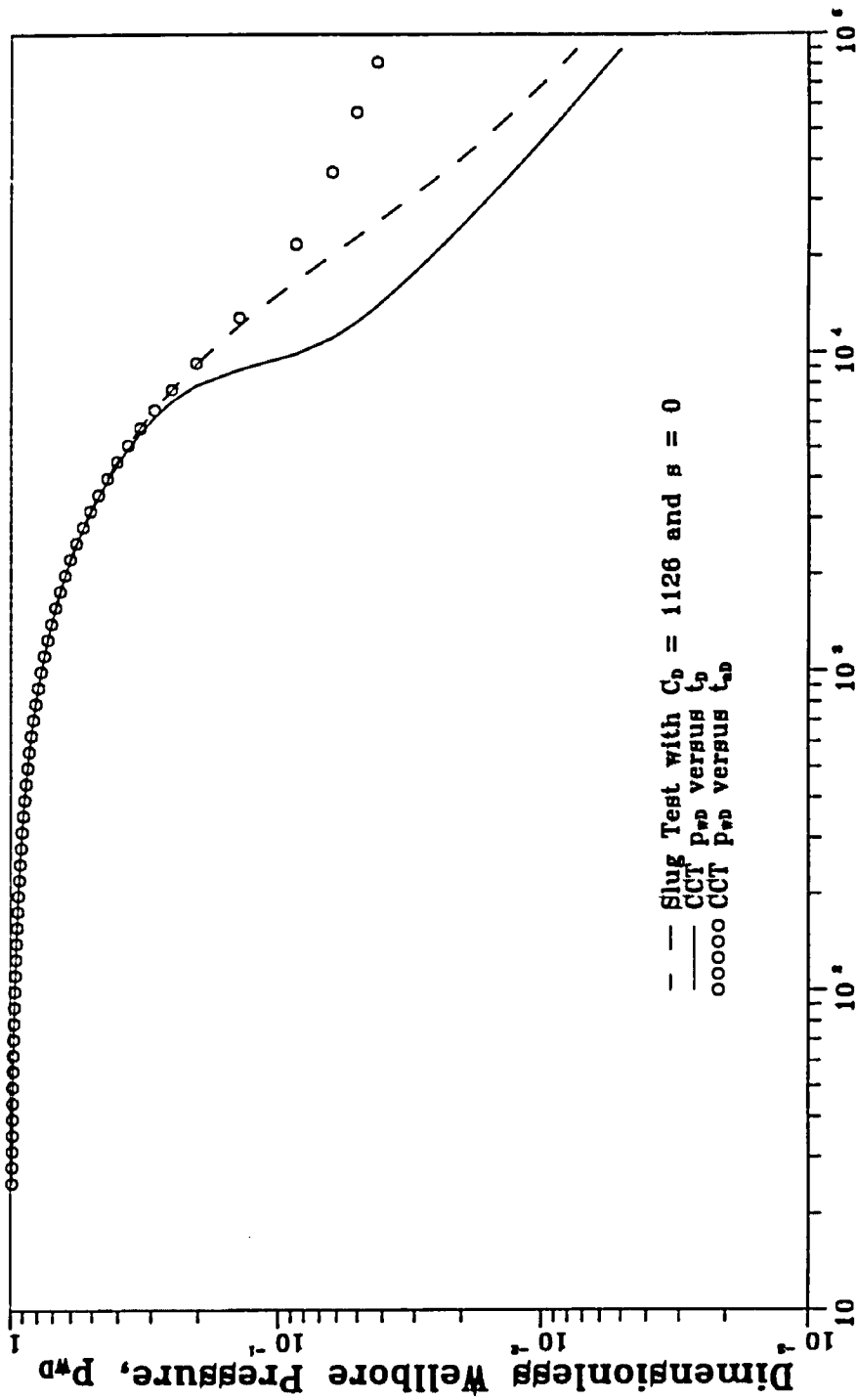


Fig. 2.12 - Effect of Initial Chamber Gas Pressure on Dimensionless Wellbore Storage Coefficient for Closed Chamber Tests



Dimensionless Time or Pseudotime, t_D or t_{aD}

Fig. 2.13 - Use of Pseudotime for Closed Chamber Test,
 $P_{chl} = 0.0$ psig, $C_{aD1} = 1126$ and $\beta = 0$

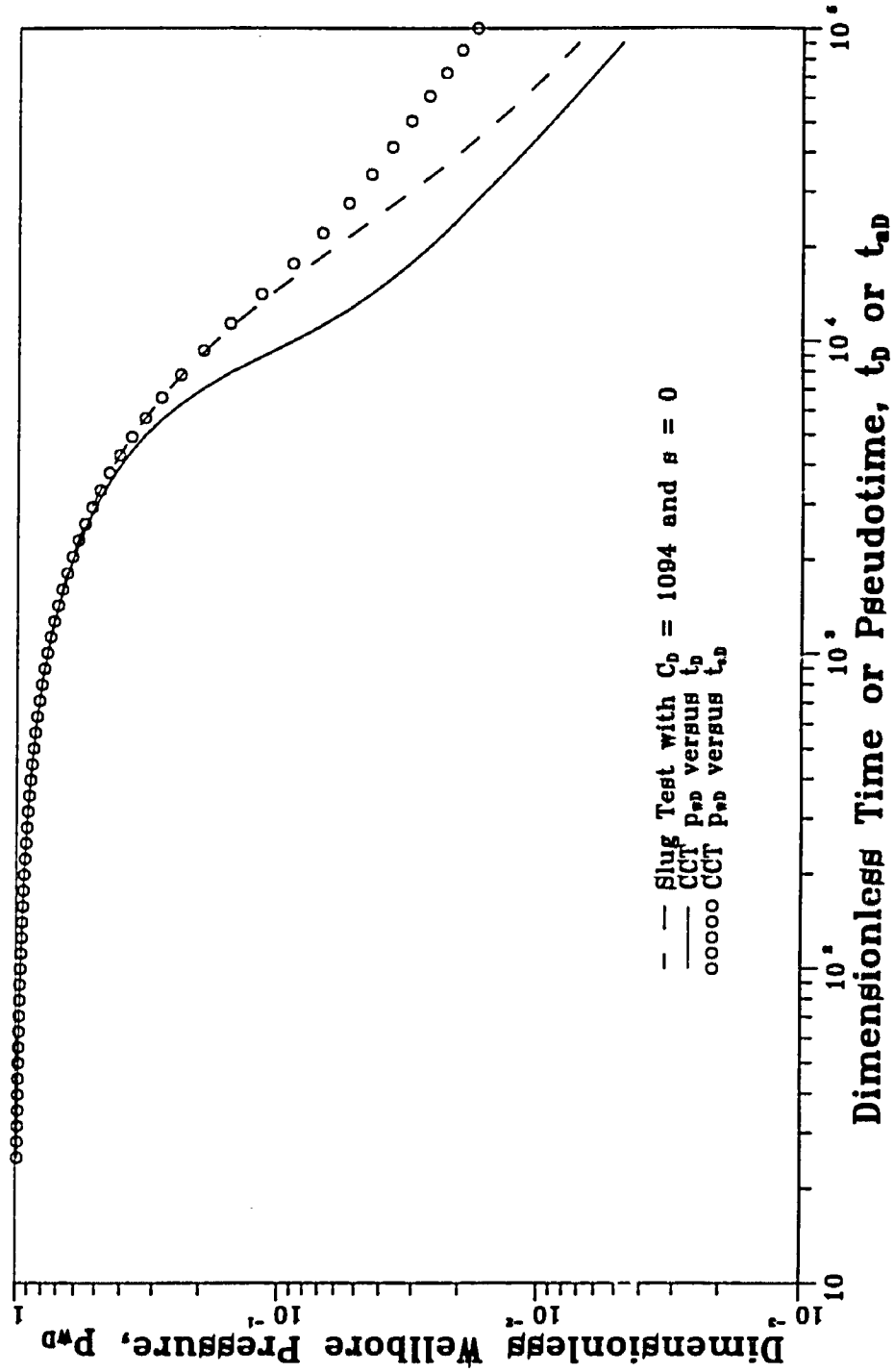


Fig. 2.14 - Use of Pseudotime for Closed Chamber Test, $P_{chl} = 100.0$ psig, $C_{D1} = 1094$ and $s = 0$

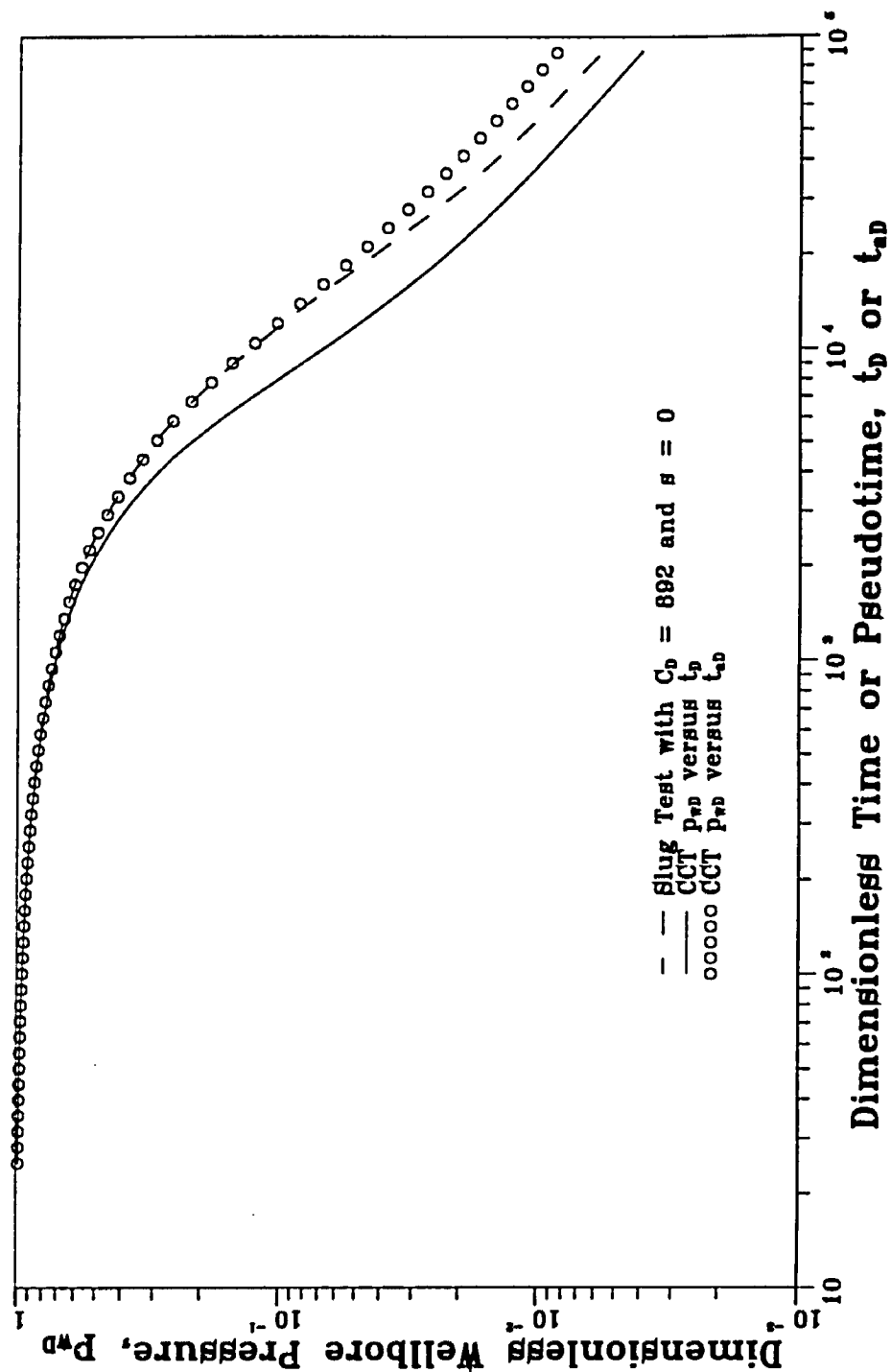


Fig. 2.15 - Use of Pseudotime for Closed Chamber Test,
 $P_{eal} = 1000.0$ psig, $C_{Df} = 892$ and $\beta = 0$

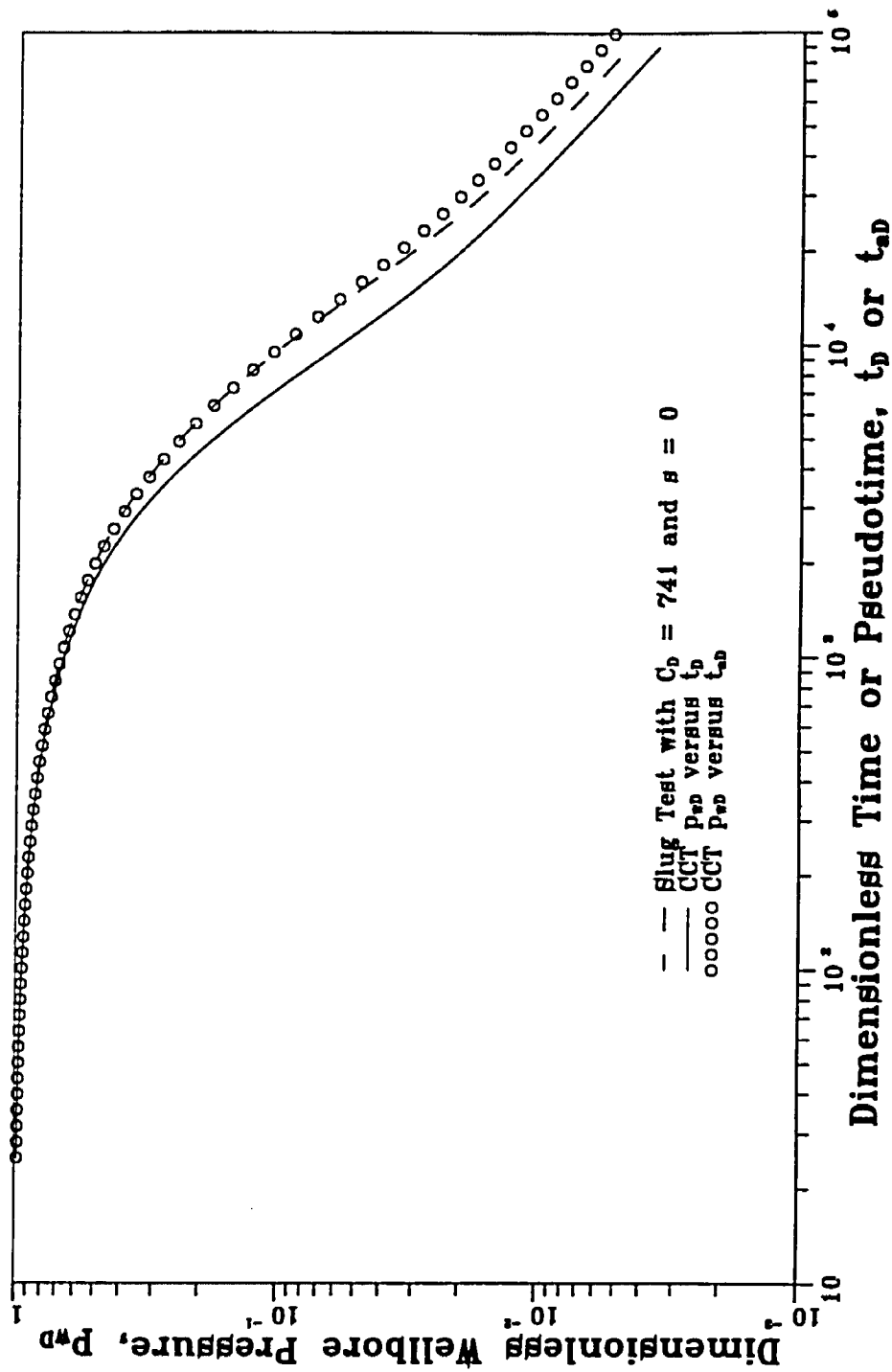


Fig. 2.16 - Use of Pseudotime for Closed Chamber Test, $P_{chl} = 2000.0$ psig, $C_{D1} = 741$ and $\beta = 0$

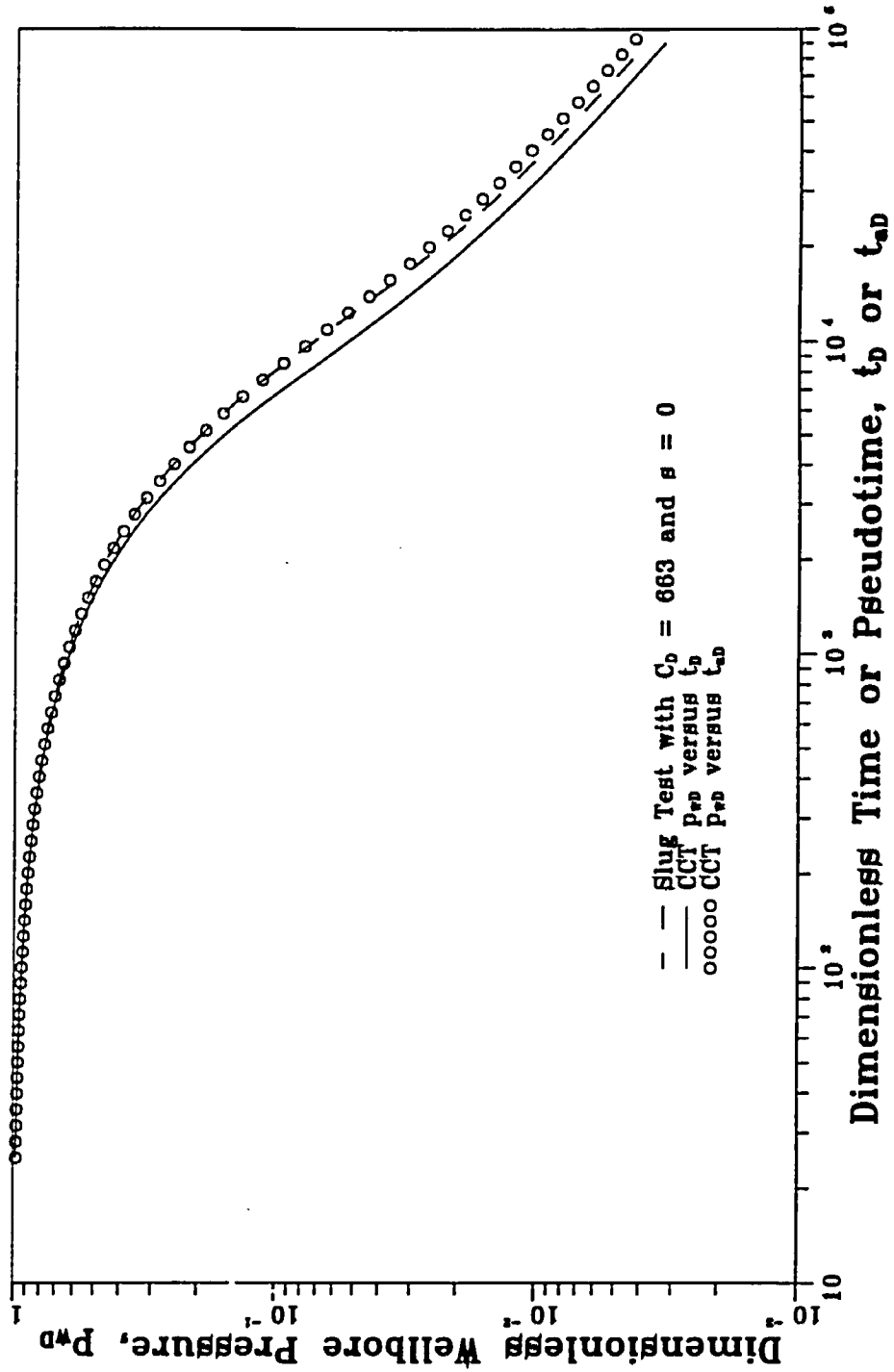


Fig. 2.17 - Use of Pseudotime for Closed Chamber Test,
 $P_{ch1} = 3000.0$ psig, $C_{aD1} = 663$ and $s = 0$

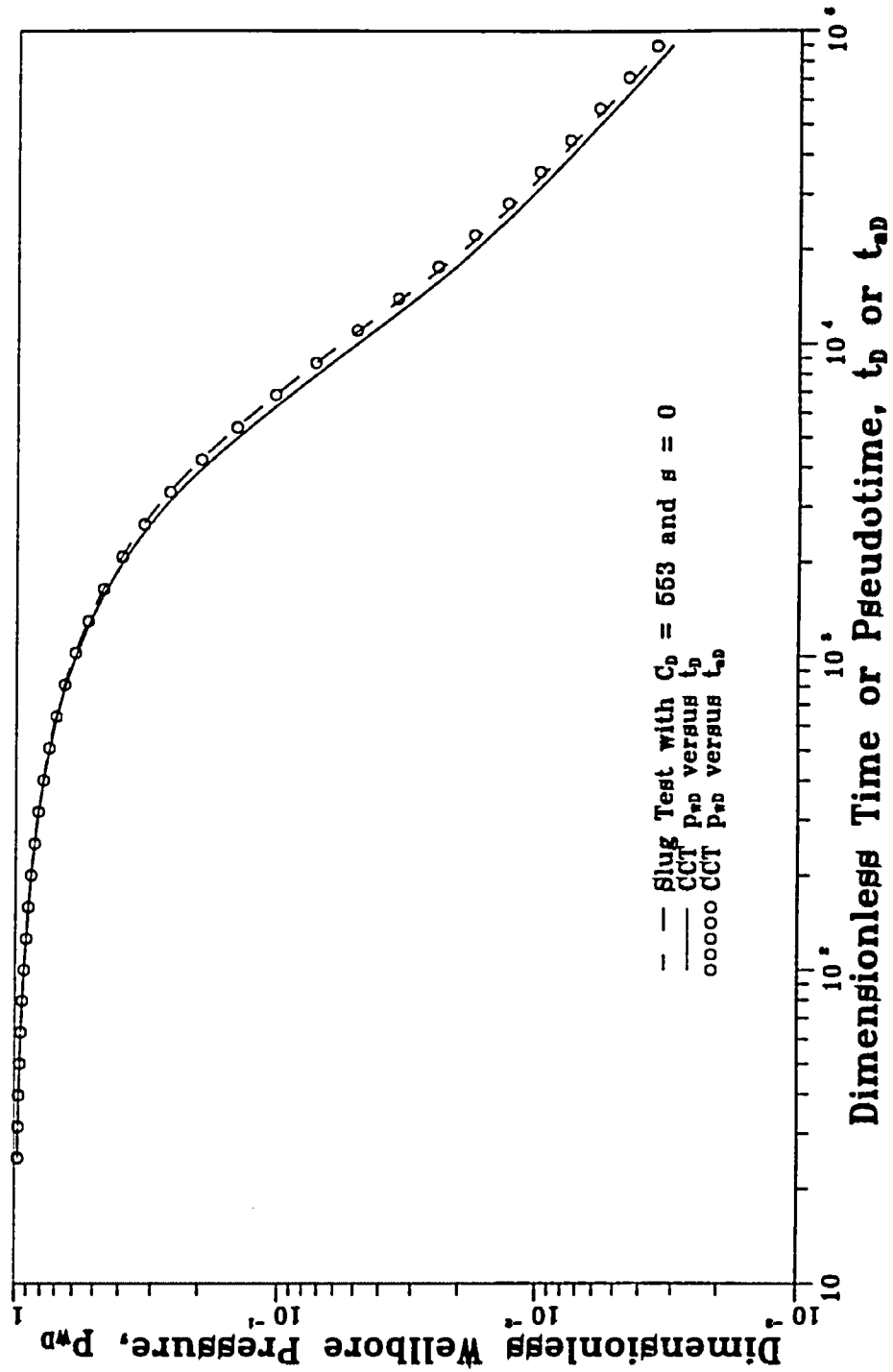


Fig. 2.18 - Use of Pseudotime for Closed Chamber Test, $P_{chl} = 4000.0$ psig, $C_{vD1} = 553$ and $s = 0$

corresponding slug test solution, we expect that pseudotime will work more effectively as the initial chamber gas pressure is increased. Figs. 2.13-2.18 illustrate this conclusion. For the $p_{chi} = 0$ (psig) case the pseudotime correlates the CCT solution with the slug test solution for all $p_{wD} \geq 0.22$, whereas for the $p_{chi} = 2000$ (psig) case, the correlation applies for all $p_{wD} \geq 0.08$. Results indicate that the difference between the CCT solution, considered as a function of t_{aD} , the corresponding slug test solution decreases as p_{chi} increases from 0 (psig) to 4000 (psig). For the $p_{chi} = 4000$ (psig) case, the CCT solution as a function of pseudotime is graphically indistinguishable from the corresponding slug test solution for all $p_{wD} \geq 0.002$.

Effect of Initial Liquid Level: The differential pressure imposed on the sandface is controlled by the initial chamber gas pressure and the initial liquid level. Here, we consider the effect of the initial liquid level on the CCT dimensionless solutions by allowing the initial liquid level to change from $L_i = 100$ ft in the base case to $L_i = 2500$ and 5000 ft. Fig. 2.19 presents changes of C_{aDi}/C_{aD} versus t_D for cases with $L_i = 100, 2500$ and 5000 ft. Figs. 2.20 and 2.21 illustrate the application of pseudotime for cases with $L_i = 2500$ (ft) and $L_i = 5000$ (ft), respectively.

Results in Figs. 2.19-2.21 indicate that increasing the initial liquid level results in a higher magnitude change in C_{aDi}/C_{aD} , but the difference in C_{aDi}/C_{aD} caused by the different initial liquid level is small, and more importantly, the influence of the initial liquid level on the length of time interval on which the pseudotime correlation applies is insignificant.

Effect of Total Chamber Length: Safety concerns and reservoir formation depth dictate the total chamber length to be used in conducting a CCT. To evaluate the effect of total chamber length, we consider two cases with the chamber length of 5000 ft and 2500 ft, respectively. Results are presented in Figs. 2.22, 2.23 and 2.24.

As the length (volume) of the chamber becomes infinite, the change in the chamber gas pressure with production is negligible. In this case, C_{aDi}/C_{aD} will

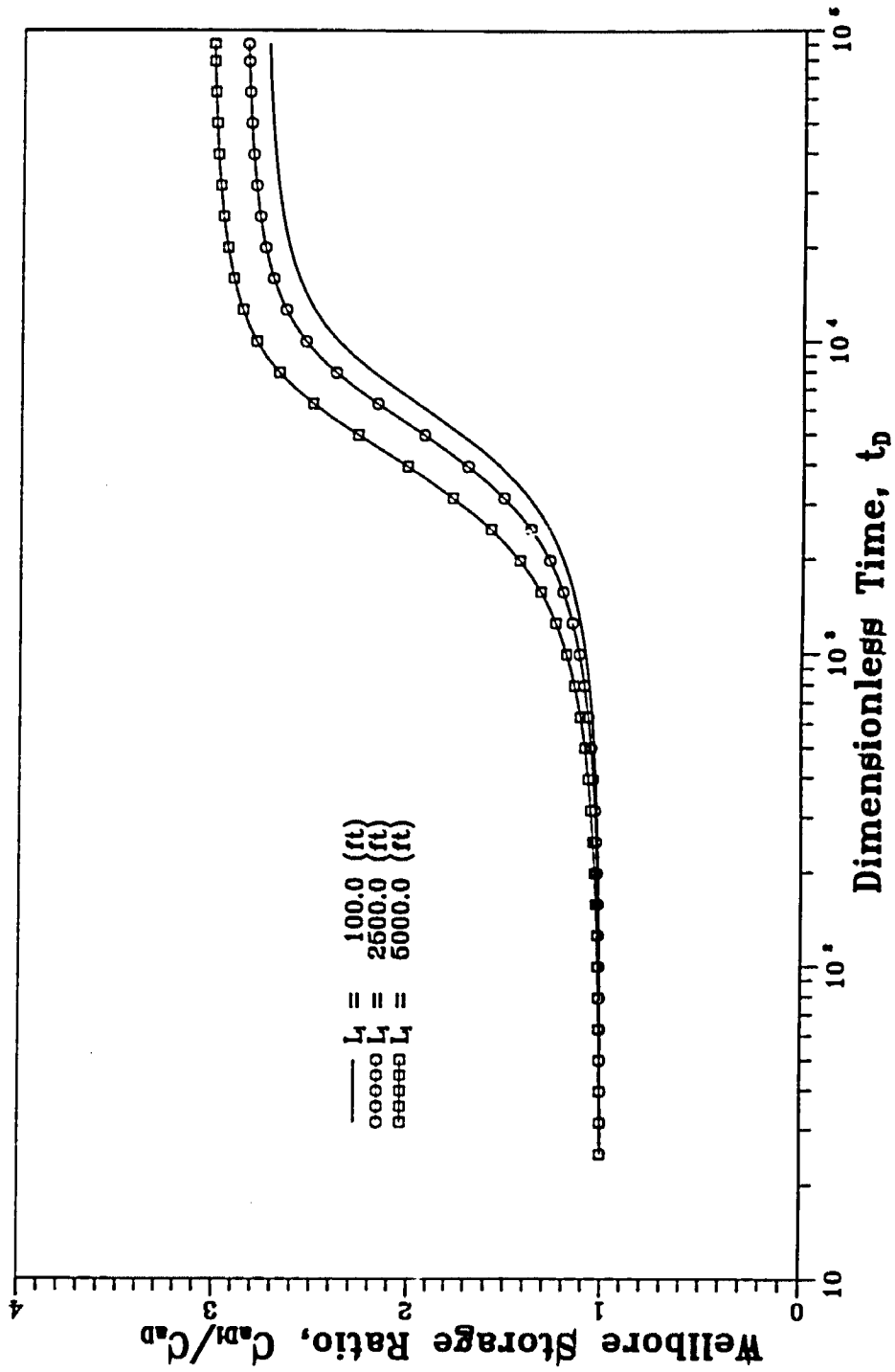


Fig. 2.19 - Effect of Initial Liquid Level on Dimensionless Wellbore Storage Coefficient for Closed Chamber Tests

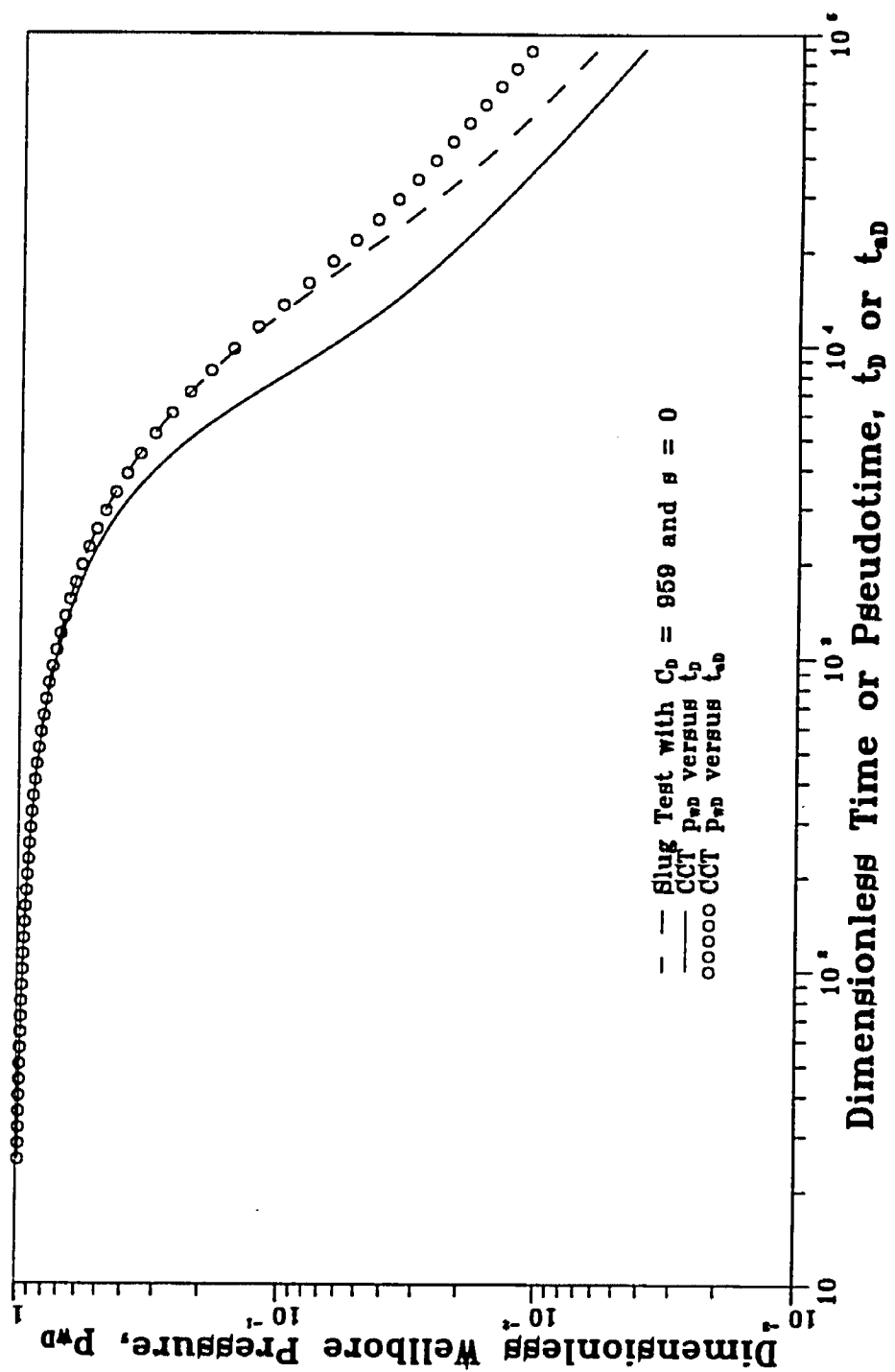


Fig. 2.20 - Use of Pseudotime for Closed Chamber Test,
 $L_1 = 2500.0$ ft, $C_{a1} = 959$ and $\beta = 0$

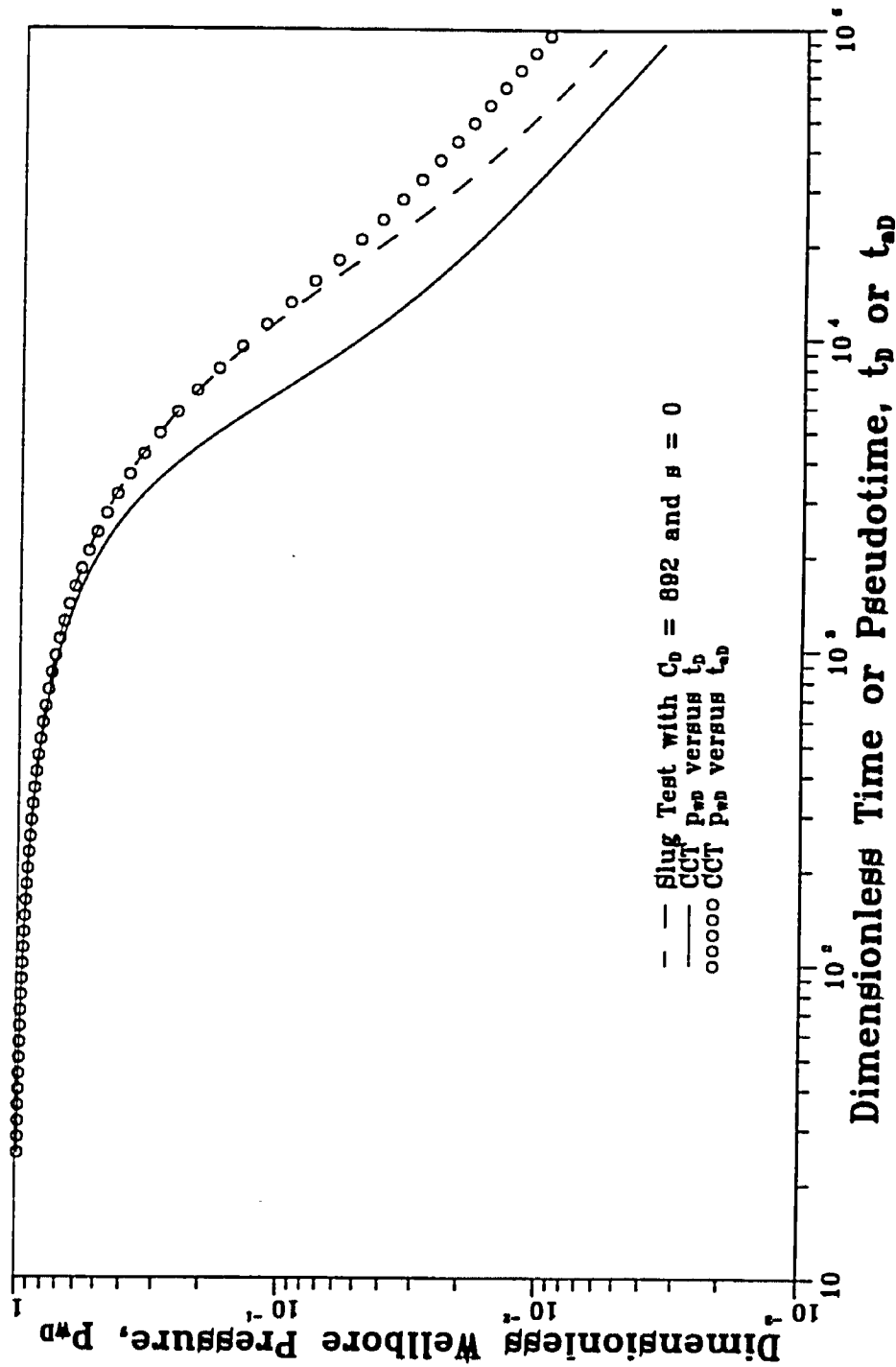


Fig. 2.21 - Use of Pseudotime for Closed Chamber Test,
 $L_1 = 5000.0$ ft, $C_{aD1} = 892$ and $\beta = 0$

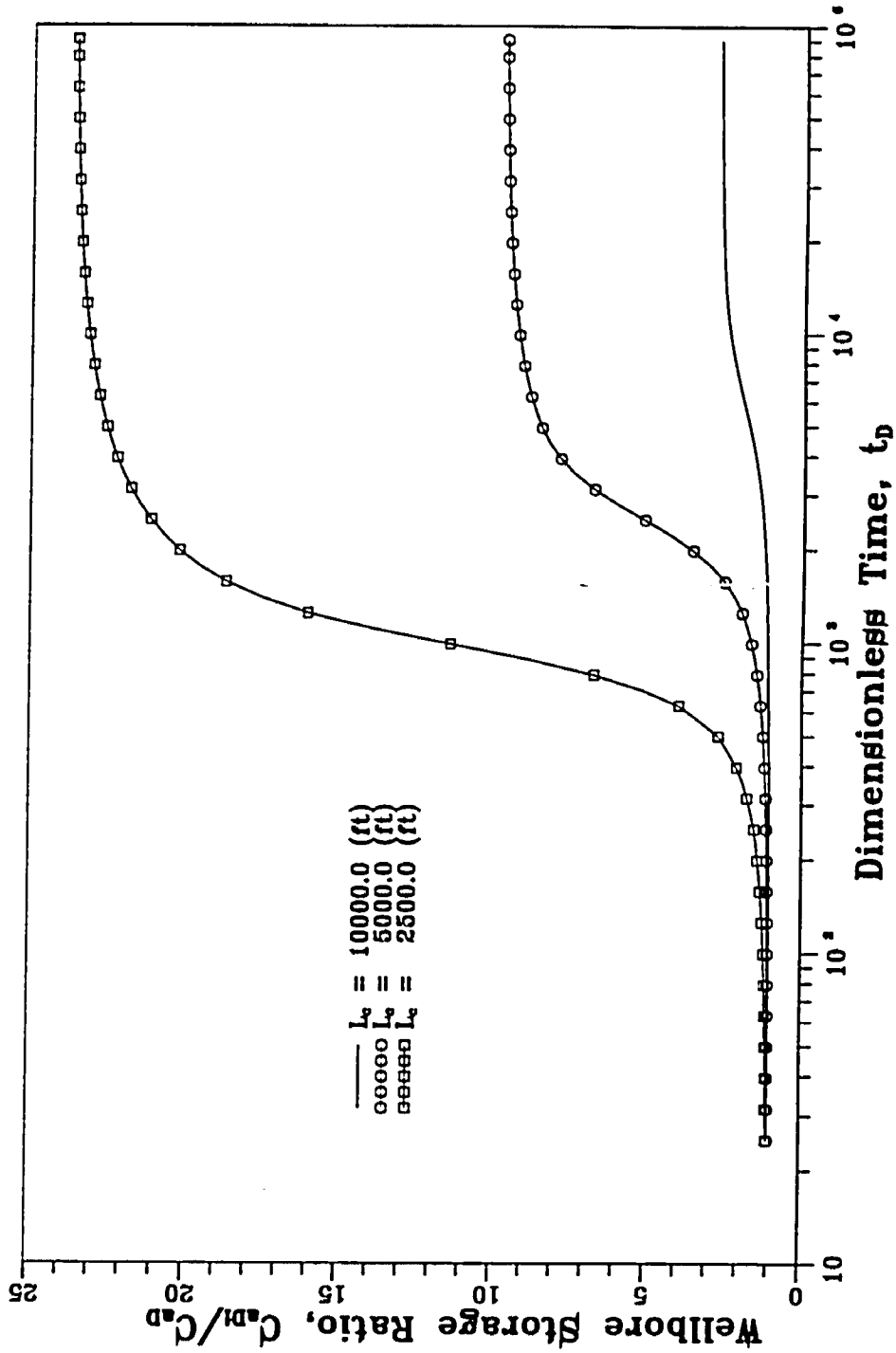


Fig. 2.22 - Effect of Total Chamber Length on Dimensionless Wellbore Storage Coefficient for Closed Chamber Tests

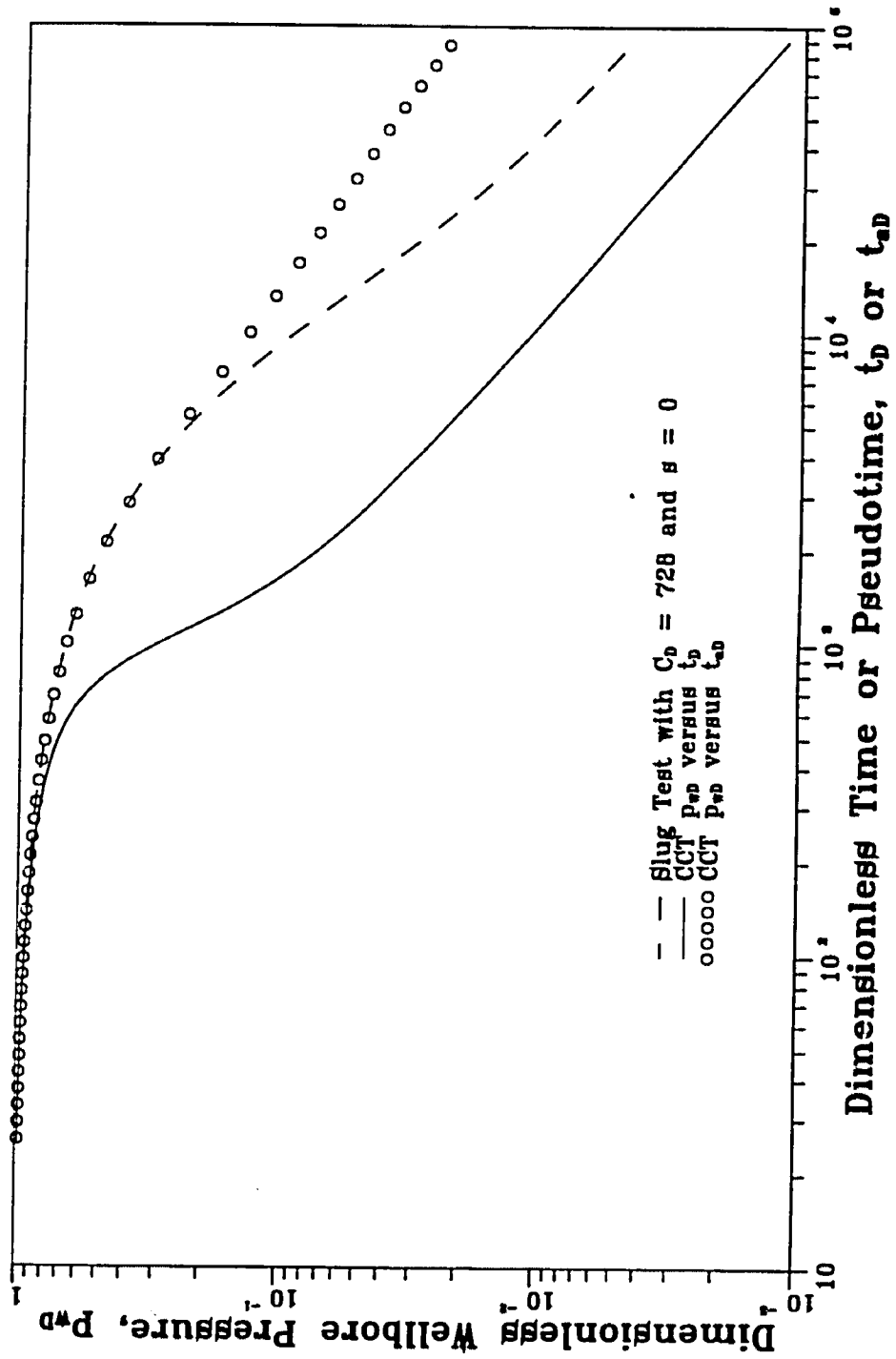
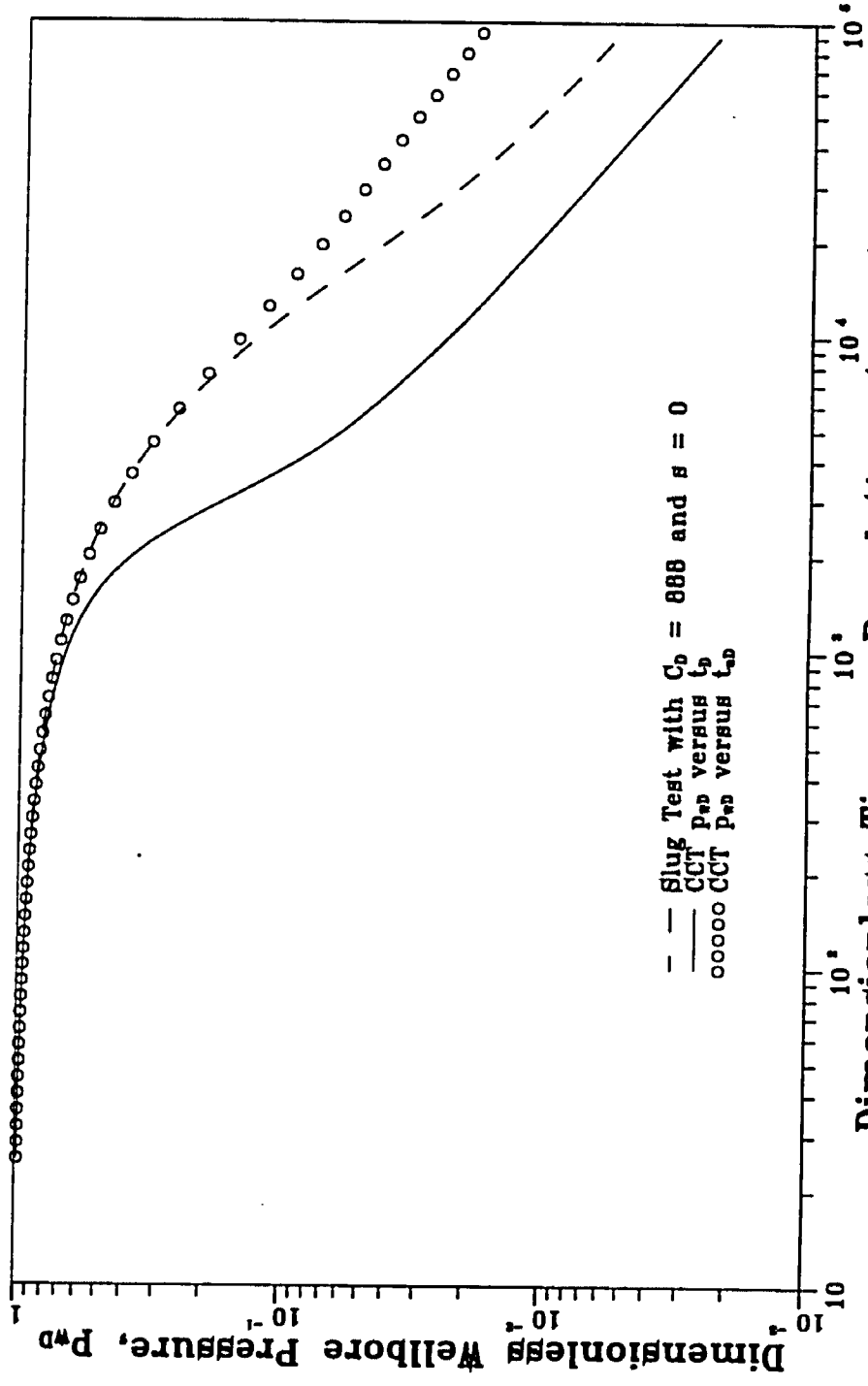


Fig. 2.23 - Use of Pseudotime for Closed Chamber Test, $L_c = 2500.0$ ft, $C_{ch} = 728$ and $s = 0$



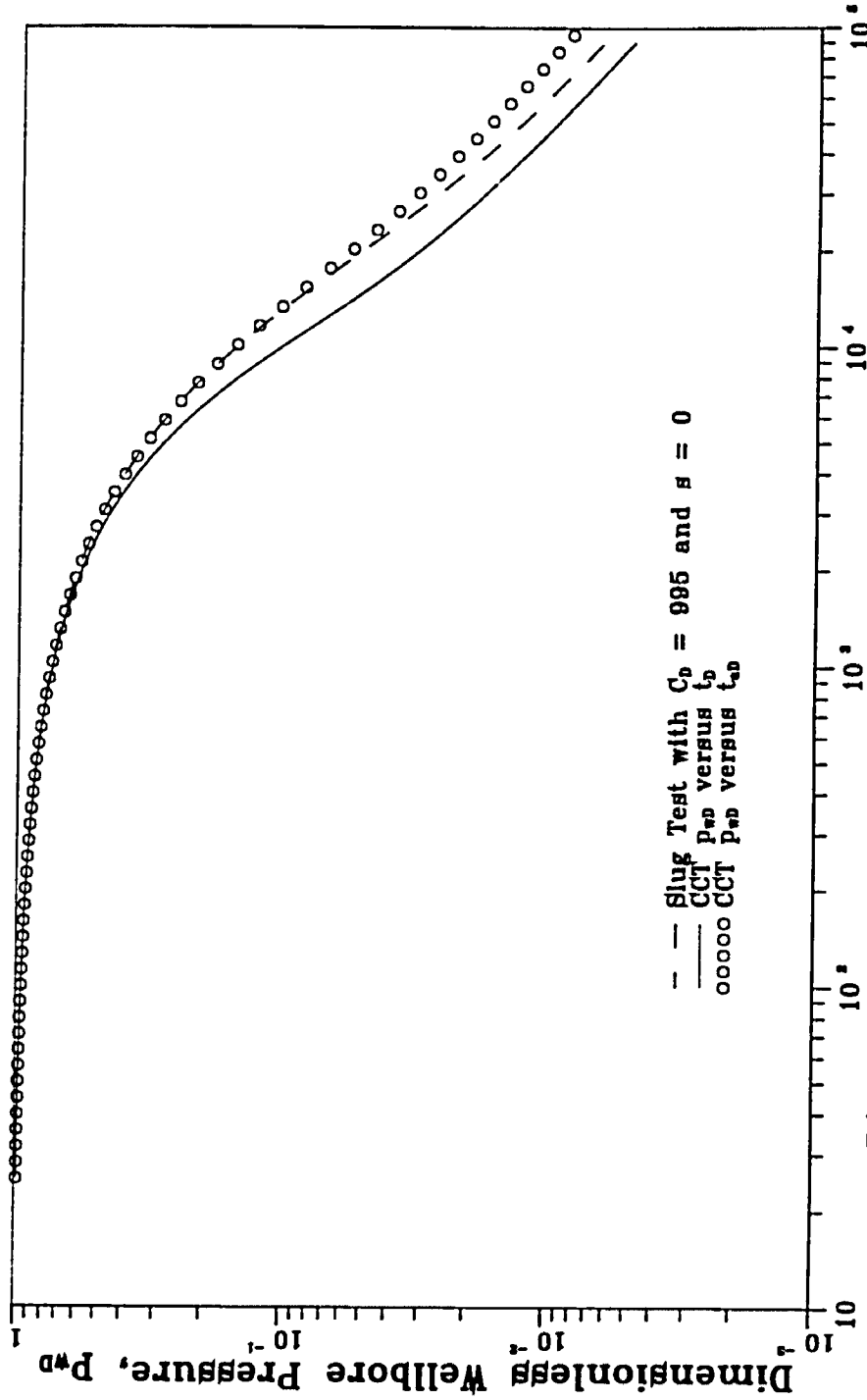
Dimensionless Time or Pseudotime, t_D or t_{Dp}

Fig. 2.24 - Use of Pseudotime for Closed Chamber Test,
 $L_c = 5000.0$ ft, $C_{AD} = 888$ and $s = 0$

remain approximately equal to one and the closed chamber test will degenerate to the corresponding slug test solution. Hence, we expect that a longer total chamber length will cause the CCT p_{wD} solution plotted versus t_{aD} to correlate for a longer period of time with the corresponding slug test p_{wD} plotted versus t_D . As an example, comparing the results of Fig. 2.23 ($L_c = 2500$ ft) with those of Fig. 2.7 ($L_c = 10,000$ ft), we see that the CCT solution in terms of pseudotime correlates better with the corresponding slug test solution for the case where the chamber length is longer (Fig. 2.7).

Effect of Initial Reservoir Pressure: Decreasing the initial reservoir pressure while keeping all other tool and reservoir parameters fixed results in a lower magnitude change in the combined wellbore storage coefficient. Thus, it is anticipated that pseudotime can be used to correlate a CCT solution with the corresponding slug test solution more effectively as the initial reservoir pressure is decreased provided all other parameters remain unchanged. This argument is illustrated by the results of Fig. 2.25 where the initial reservoir pressure is 4000 (psig) as compared with the base case value of 5000 (psig). As a matter of fact, if the initial reservoir pressure is reduced to 2500 (psig), then the pressure response for a CCT was found to be quite close to the corresponding slug test even without applying pseudotime.

At this point, it may be appropriate to reiterate that the proposed correlation between the CCT solution and the corresponding slug test solution is controlled by the variation of C_{aDi}/C_{aD} from unity, not by the pressure differential initially imposed on the sandface, $p_i - p_o$, as one might speculate. This notion is further illustrated with examples given in Figs. 2.26 and 2.27. Here, two cases with the same pressure differential ($p_i - p_{chi} = 5000$ psi) are considered; one case has $p_i = 5000$ psig and $p_{chi} = 0.0$ psig, and the other case has $p_i = 6000$ psig and $p_{chi} = 1000$ psig. Fig. 2.26 reveals the dramatic difference in C_{aDi}/C_{aD} between the two cases. This difference inevitably affects the application of pseudotime, as one can see from Figs. 2.13 and 2.27.



Dimensionless Time or Pseudotime, t_D or t_{Dp}

Fig. 2.25 - Use of Pseudotime for Closed Chamber Test,
 $P_1 = 4000.0$ psig, $C_{D1} = 995$ and $\beta = 0$

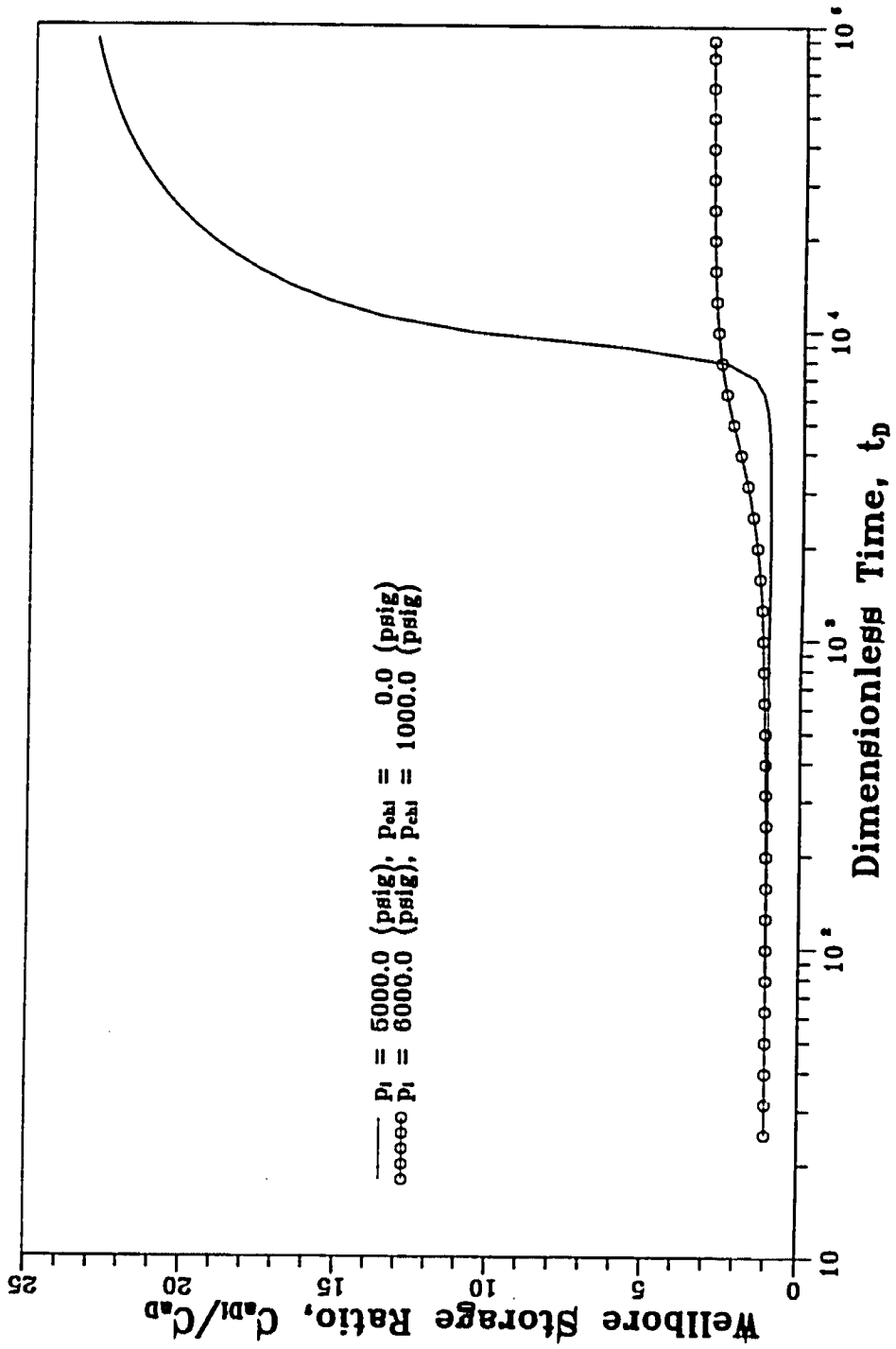
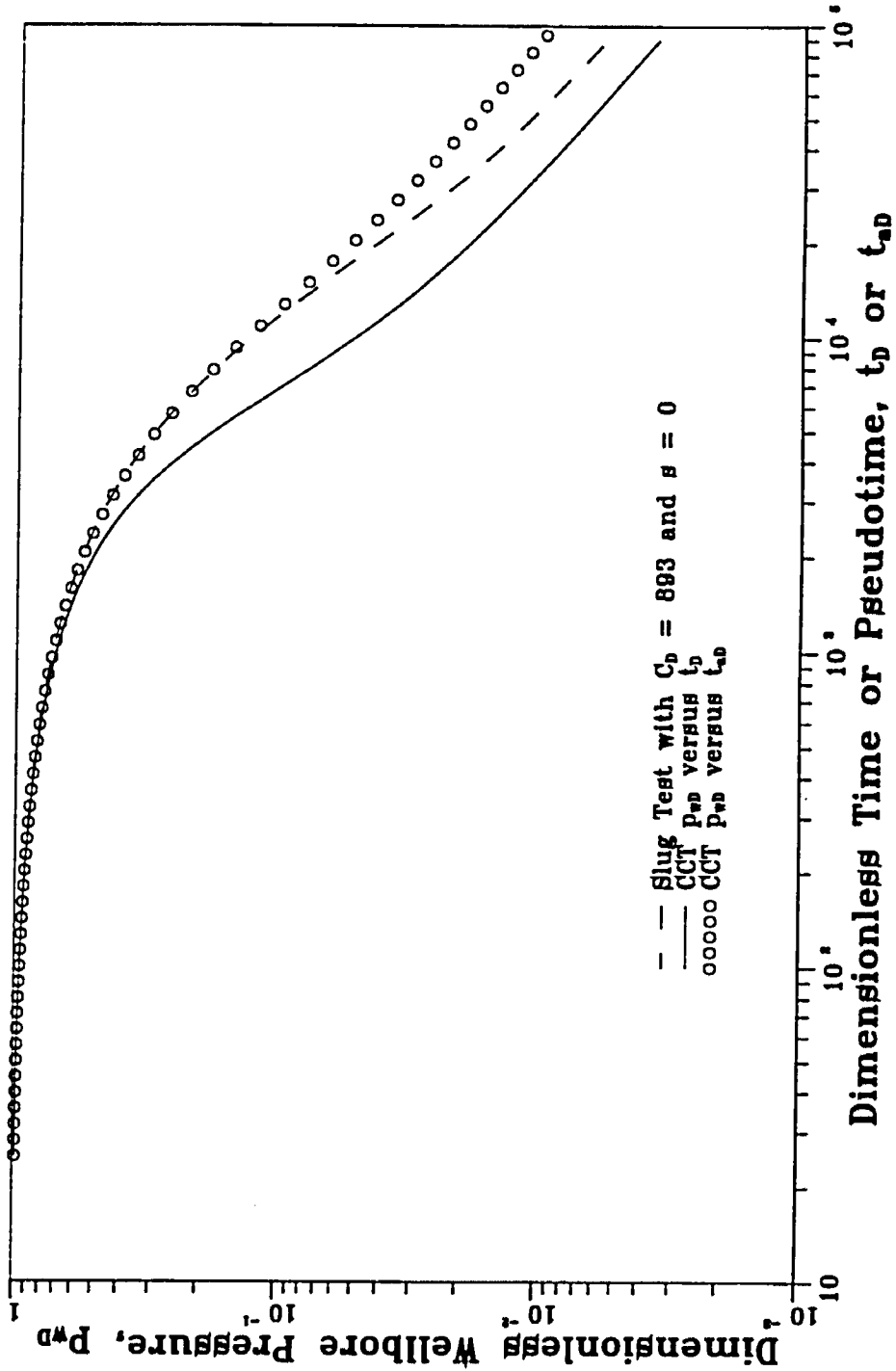


Fig. 2.26 - Effect of p_{eh} and P_i on Dimensionless Wellbore Storage Coefficient for Closed Chamber Tests



Dimensionless Time or Pseudotime, t_D or t_{Dp}
 Fig. 2.27 - Use of Pseudotime for Closed Chamber Test, $p_i = 6000.0$ psig,
 $P_{chl} = 1000.0$ psig, $C_{rD1} = 893$ and $\beta = 0$

Effect of Liquid Compression and Wellbore Friction: So far, we have neglected the effects of liquid compression and wellbore friction to a CCT. To investigate these effects, the numerical method proposed by Salas and Sageev⁹ is implemented. Also, we change L_i from 100 ft of the base case to zero, since Salas and Sageev⁹ assume zero initial liquid level when deriving their numerical solution method. When wellbore friction is considered, we use a value of 0.00025 for the absolute roughness of the drillpipe.

Fig. 2.28 illustrates the effect of liquid compression for cases with $s = 0$ and $s = 5$. The results of Fig. 2.28 indicate that effect of liquid compression on the CCT solution is small. Fig. 2.29 shows the effect of wellbore friction on the pressure response for cases with $s = 2$ and $s = 10$. Like the effect of liquid compression, the effect of wellbore friction is also small. Results of Figs. 2.28 and 2.29 indicate that, at least for the cases we studied, pseudotime can be used without introducing significant errors by neglecting the effects of liquid compression and wellbore friction.

2.6.3 Peres-Onur-Reynolds Methods

Results indicate that pseudotime can be used to correlate a closed chamber test solution with the slug test solution for a significant period of time. This suggests that the Peres et al.⁴ procedures, thereafter referred to as the POR method can be applied to analyze CCT data.

The basic POR method relies on converting slug test data to equivalent data that would be obtained for the corresponding wellbore storage and skin constant surface rate production problem. The equivalent data can then analyzed using type curves developed for the wellbore storage and skin constant surface rate production problem. To use POR method for CCT data, one must first calculate the integral of the CCT dimensionless pressure solution by

$$I(p_{wD}) = \int_0^{t_{aD}} p_{wD}(\tau, C_{aD}, s) d\tau. \quad (2.40)$$

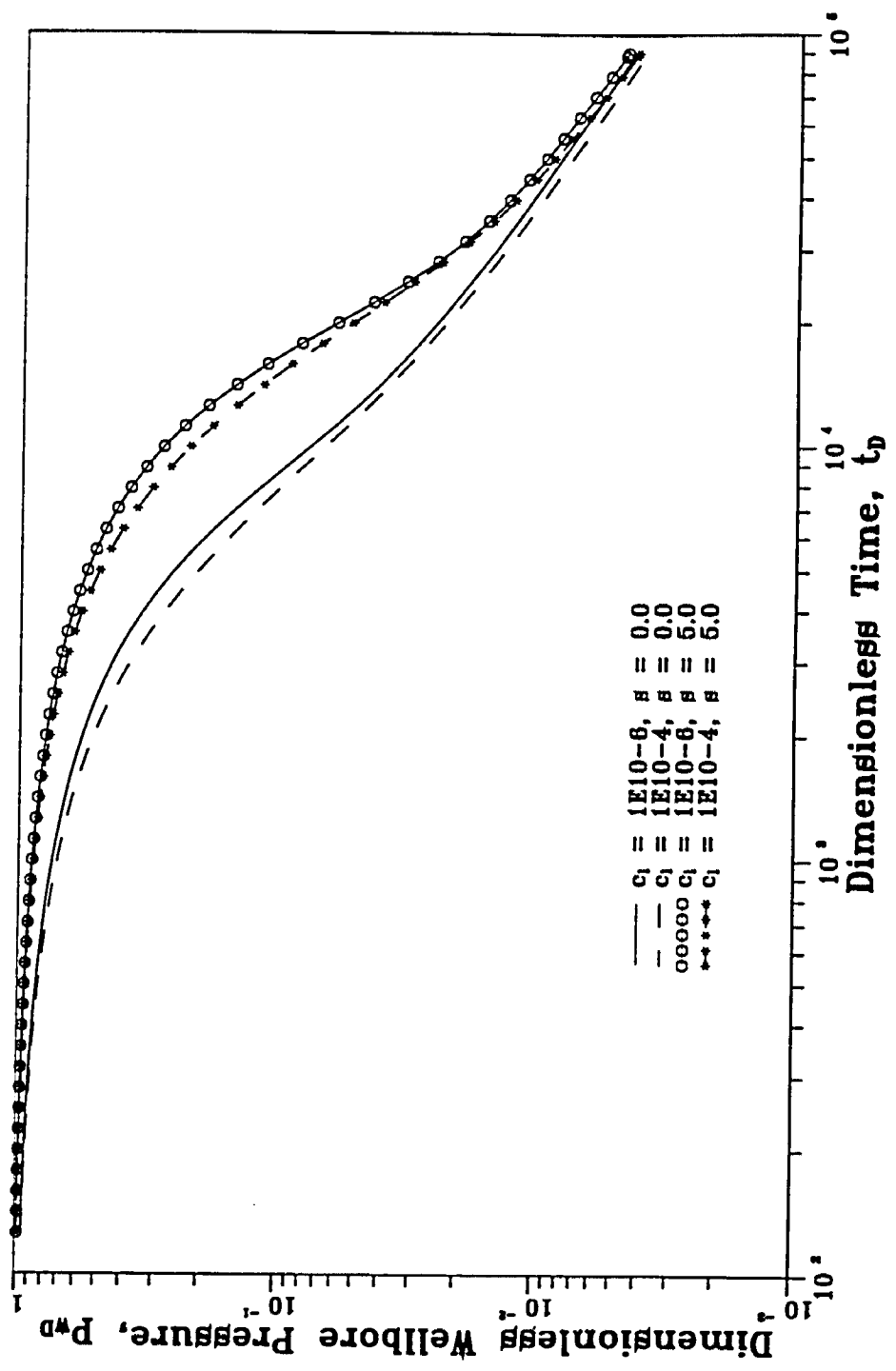


Fig. 2.2B - Effect of Liquid Compressibility on CCT ($L_1 = 0.0$ ft)

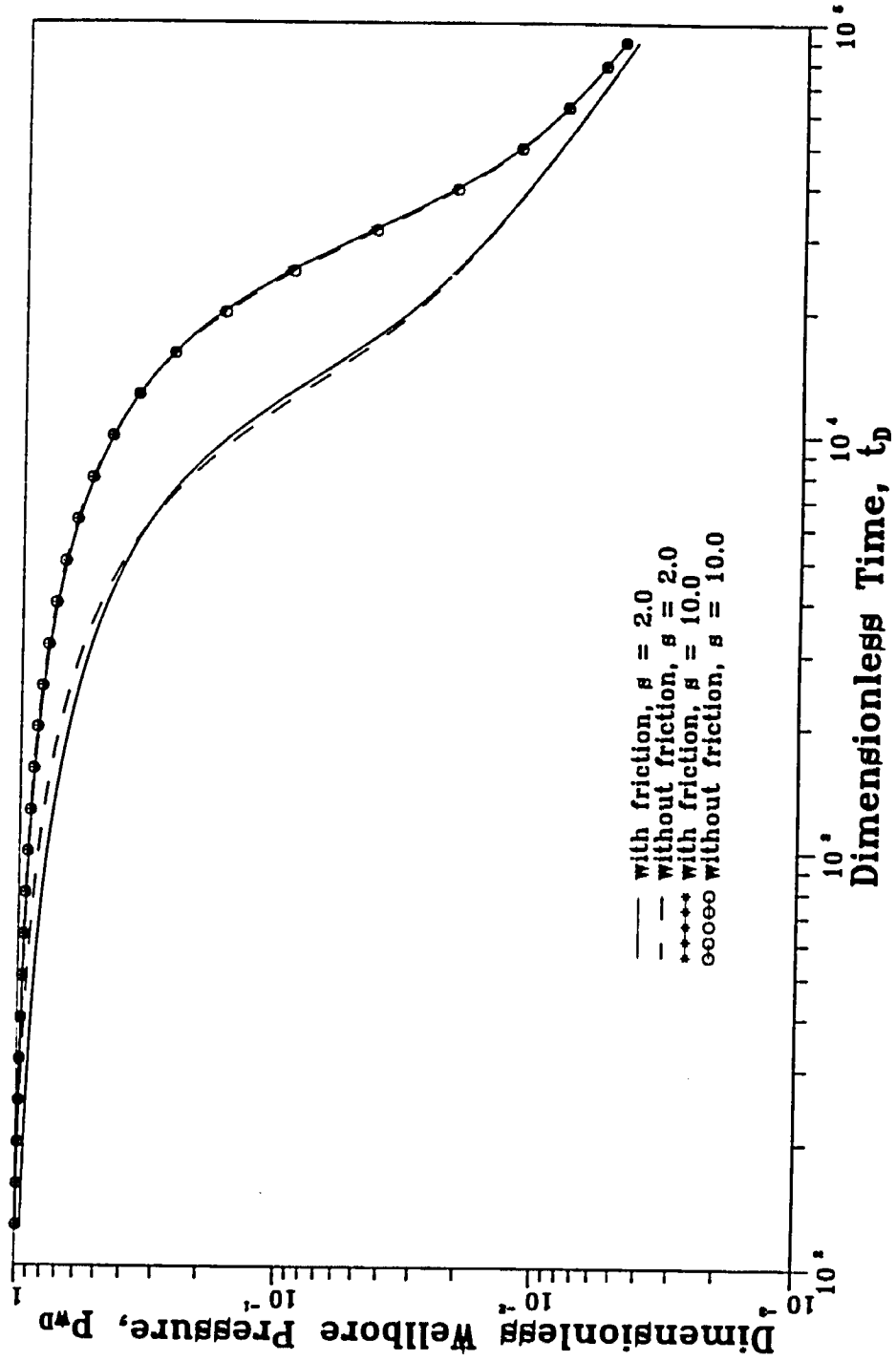


Fig. 2.29 - Effect of Wellbore Friction on Closed Chamber Test ($L_1 = 0$ ft)

Then, the equivalent dimensionless pressure and its logarithmic derivative of the constant surface rate production problem are calculated by

$$p_{wcD}(t_{aD}, C_{aDi}, s) = \frac{I(p_{wD})}{C_{aDi}}, \quad (2.41)$$

and

$$p'_{wcD} = \frac{t_{aD}}{C_{aDi}} p_{wD}, \quad (2.42)$$

respectively.

To illustrate the applicability of the POR method, we present a case where the chamber length is $L_c = 1000$ ft; initial reservoir pressure is $p_i = 3500$ psig; initial chamber gas pressure is $p_{chi} = 500$ psig and the skin factor is $s = 10$. The results of Fig. 2.30 indicate that the CCT solution plotted versus pseudotime can be correlated with the corresponding slug test solution for $t_{aD}/C_{aDi} < 20$. Thus, we expect the POR method should apply during this period of time. Fig. 2.31 shows three sets of results. Here, p_{wcD} and p'_{wcD} , respectively, represent the dimensionless pressure solution and its logarithmic derivative for the classical wellbore storage and skin problem for $C_D = C_{aDi} = 458$ and $s = 10$. The second set of results shown is the converted data obtained from the POR method using dimensionless time. The third set of results represent plots of converted data using dimensionless pseudotime; see Eqs. 2.41 and 2.42. The results indicate that by introducing pseudotime into the POR method we can analyze CCT data using the classical wellbore storage and skin type curves. Note that even though the difference between the classical wellbore and skin solution and the CCT solution (as a function of pseudotime) increases as t_{aD}/C_{aDi} increases above 20, the correlation persists for a sufficiently long period of time so that we should be able to apply regression analysis procedures to obtain parameter estimates. If necessary, one could then use the numerical solution procedure discussed here and presented originally in Refs. 8-10 to verify and refine the estimates.

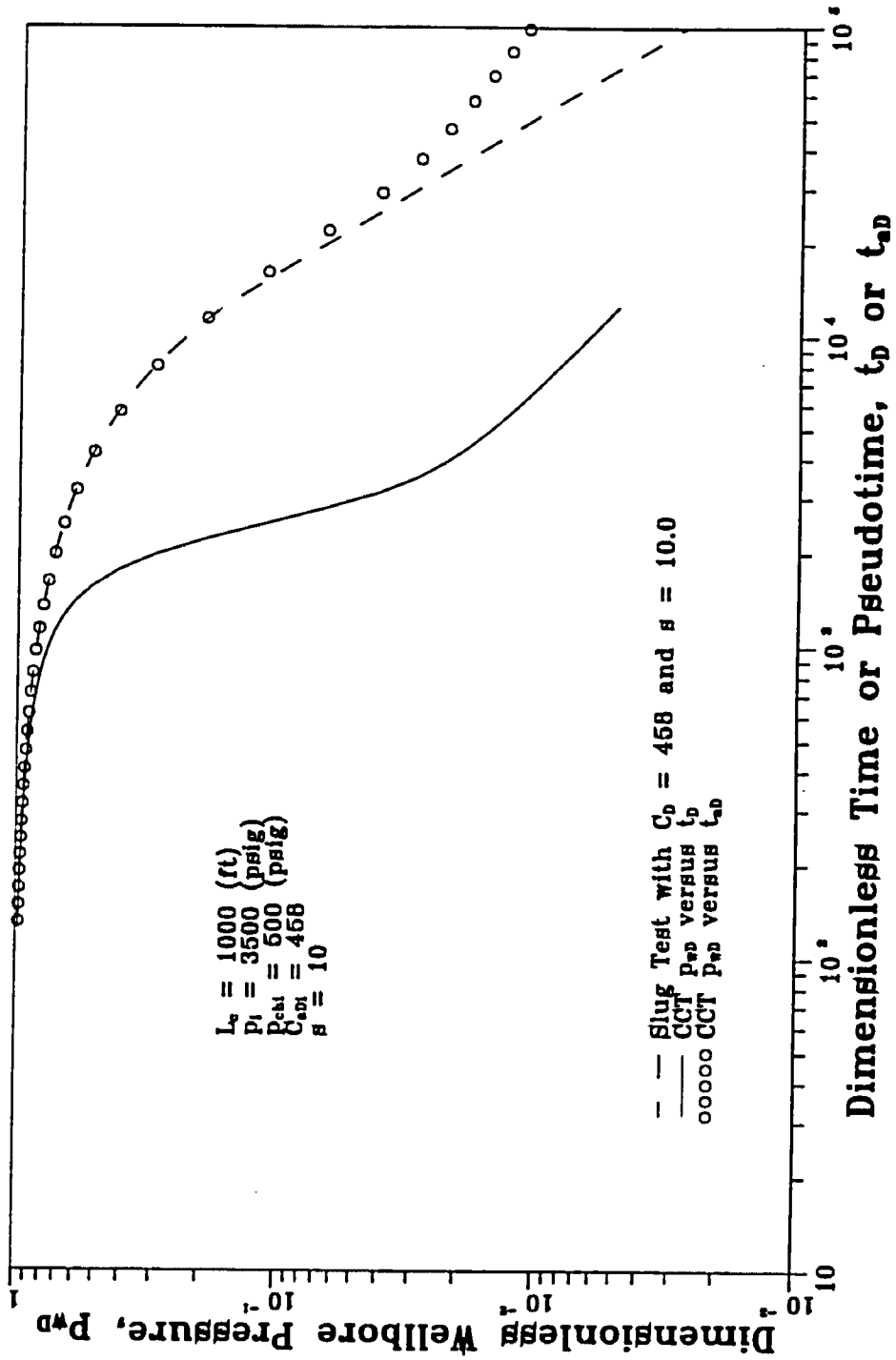


Fig. 2.30 - Use of Pseudotime for Closed Chamber Test, $L_c = 1000.0$ ft, $C_{aD1} = 458$ and $s = 10.0$

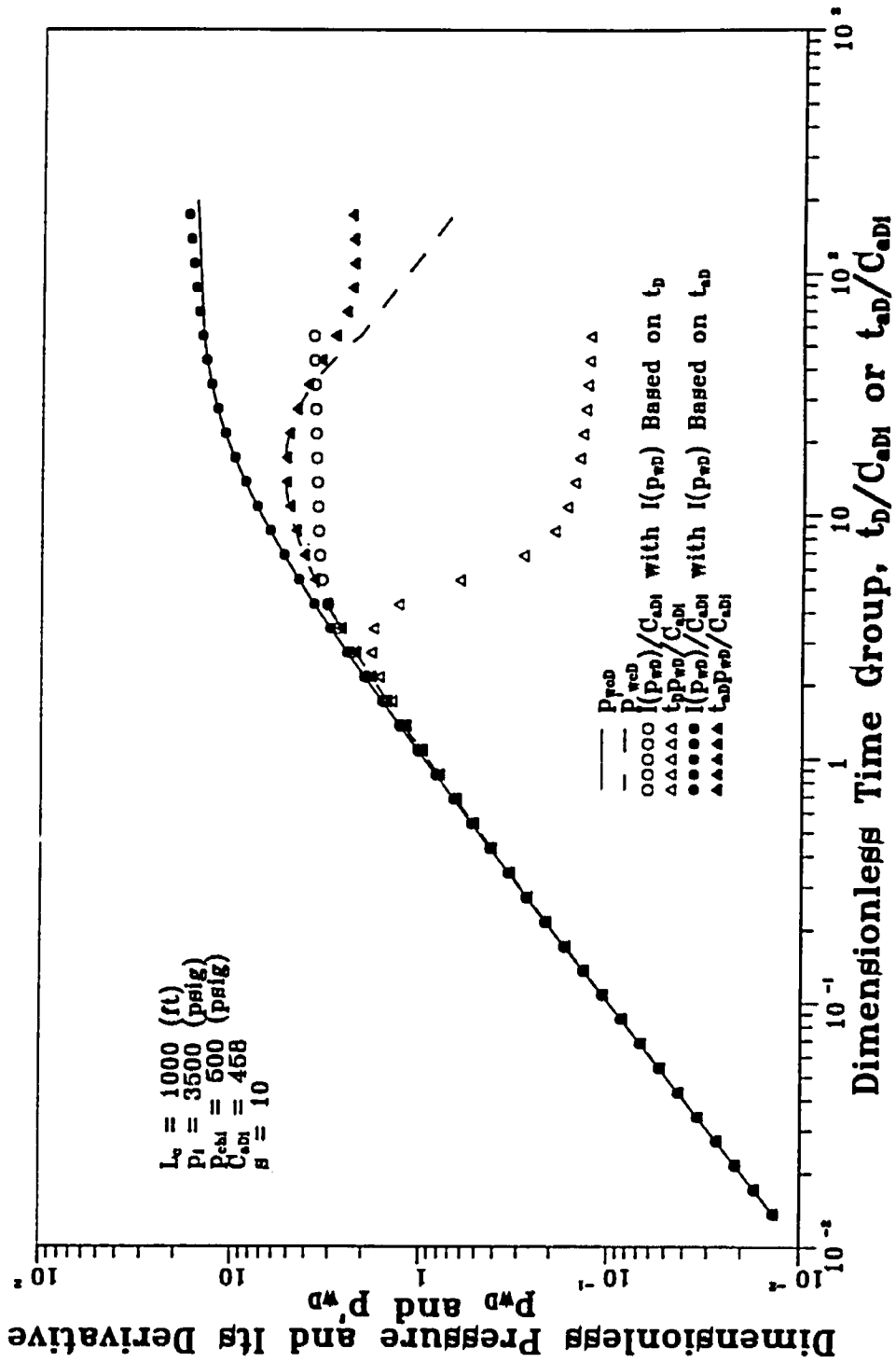


Fig. 2.31 - Comparison of Converted Closed Chamber Test Response with Wellbore Storage and Skin Constant Surface Rate Solution

In Fig. 2.31, the plot of converted derivative data using dimensionless time seems to approach a constant at late time. Consequently, one may attempt to analyze CCT late-time data using the conventional semilog analysis technique. In *Appendix C*, we show that the converted derivative data using dimensionless time indeed becomes constant at late time. However, this constant is no longer $1/2$. Therefore, if used, the conventional semilog analysis technique will yield incorrect parameter values.

2.6.4 Step Change in Wellbore Storage Coefficient

In slug tests, as the liquid level rises from drill collar into drill pipe, there is usually a change in the inner diameter of the wellstring, and this translates into a step change in the wellbore storage coefficient. Correa and Ramey²⁶ developed an analytical solution for this problem. In Fig. 2.32, we consider a slug test with a step change in the dimensionless wellbore storage coefficient from $C_D = 500$ to $C_D = 1000$ at $t_D = 1000$. As shown in Fig. 2.32, pseudotime almost completely correlates the solution for a step-change in the wellbore storage coefficient with the corresponding solution for a constant wellbore storage coefficient. Clearly, standard slug test analysis techniques can be applied to analyze field data corresponding to the changing storage case provided results are considered in terms of pseudotime.

A conventional DST buildup test also involves a step change in wellbore storage coefficient. However, during a conventional DST buildup test, the wellbore storage coefficient usually changes two orders of magnitude when the well is shut-in, and this change is so large that pseudotime becomes ineffective.

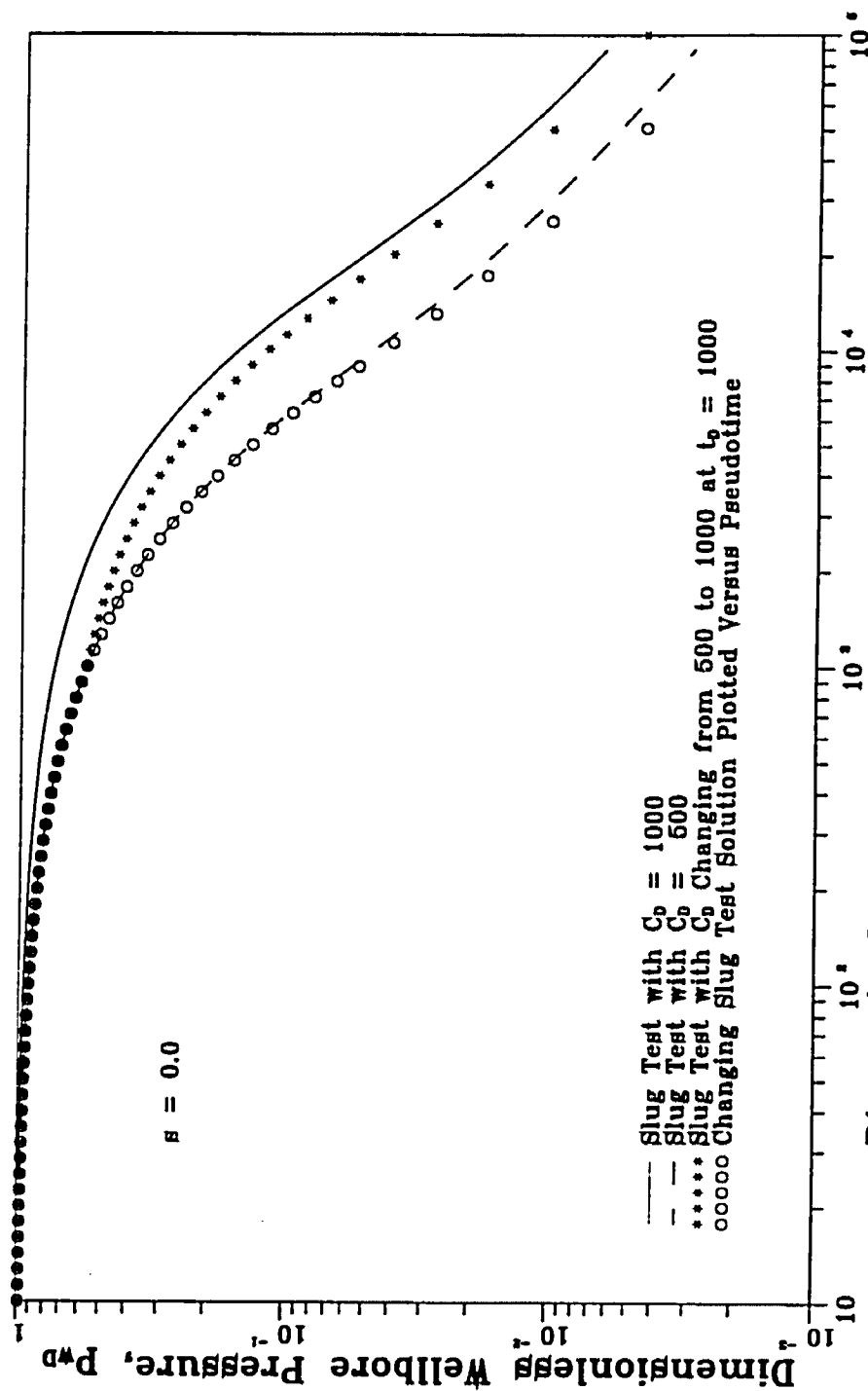


Fig. 2.32 - Use of Pseudotime for Slug Test with Step Change in Wellbore Storage

CHAPTER III

ANALYSIS OF CLOSED CHAMBER TESTS IN GAS WELLS

This chapter discusses analysis of gas-well closed chamber tests. As an introduction, the first part of this chapter reviews theories associated with gas well testing. We then present the real gas radial flow equation and appropriate initial and boundary conditions for gas-well closed chamber tests. The initial and boundary value problem (IBVP) for a gas-well closed chamber test is non-linear, and partial linearization can be achieved through the use of real gas pseudopressure and pseudotime functions. The IBVP for a gas-well closed chamber test in terms of pseudo functions is shown to be analogous to that of a conventional liquid slug test. This leads to the developments of new analysis techniques for gas-well closed chamber tests. The applicability of the proposed new methods are demonstrated by analyzing synthetic data generated from a finite difference numerical simulator developed for the gas-well closed chamber test problem. This chapter also describes how multirate analysis techniques can correctly be used to interpretate gas-well closed chamber test data.

3.1 Background

Fundamental equations describing fluid flow through porous media are obtained by combining conservations of mass, Darcy's law and equations of states. These fundamental equations form the basis of pressure transient theory.

Flow equations are generally nonlinear, which hinders direct analytical solutions. Fortunately, the flow equation for a slightly compressible liquid can be

linearized assuming constant liquid compressibility and viscosity and constant rock properties (k and ϕ). Combining the linearized flow equation with different boundary conditions, a great number of analytical solutions^{2,27,28} have been obtained. These analytical solutions form the foundation for transient analysis of oil wells.

Unlike the flow of a slightly compressible liquid, however, the equation describing isothermal flow of real gases through porous media is not easily linearized. Assumptions made to linearize the liquid flow equation are no longer valid in the case of gas flow because the density ρ and viscosity μ of real gases are strong functions of pressure^{27,29}. The nonlinearity of the gas flow equation has been recognized as a serious problem in analyzing gas well test data.

Al-Hussainy et al.³⁰ proposed to use the Kirchhoff transformation to linearize the flow equation for gases. This transformation converts the pressure to pseudopressure and, when introduced into the equation, it partially eliminates the nonlinearity of the original flow equation. A complete linearization is not achieved because the diffusivity term still involves pressure dependent terms, μ and c . However, nonlinearity of the flow equation becomes much weaker in terms of pseudopressure and, equally important is that use of pseudopressure completely linearizes the inner boundary condition when wellbore storage effect is not present. The governing equation for the flow of gases in terms of pseudopressure is of the same form as the flow equation for a slightly compressible liquid in terms of pressure. Therefore, analytical solutions derived for flow of a slightly compressible liquid can directly be applied to gas flow problems.

Before the introduction of real gas pseudopressure, gas well testing problems were solved by means of the pressure-squared approach. This approach is valid in conditions where $p/\mu z$ can approximately be treated as a linear function of pressure²⁷. This occurs at either very low or very high pressure. The pressure-squared method should now be considered obsolete²⁷ because the pseudopressure

- -

approach is more general and the required computational work is straight forward when a computer is used.

Agarwal²² studied drawdown and buildup tests for vertically fractured gas wells. He found that analyzing the drawdown data with pseudopressure and time gives fracture lengths which are in agreement with their respective input values. However, he obtained poor agreement with pseudopressure and time to analyze buildup data. Much better results were obtained when buildup data were analyzed using pseudopressure and pseudotime. Agarwal then recommend the use of pseudotime in analyzing gas well buildup data.

The work by Agarwal²² represents a step forward in efforts to further linearize the flow equation of real gases. Nevertheless, pseudotime defined by Agarwal²² is not a pure time transformation because μc is a function of both r and t through pressure. Lee and Holditch³¹ formulated the correction terms that appear in the flow equation when pseudotime is used. They used the buildup period of a gas-well closed-chamber drillstem test as a field example to illustrate that pseudotime is necessary for type curve matching to be accurate.

Finjord²³ gives an analytical study of the pseudotime transformation, and shows that for drawdown in an infinite reservoir the correction terms will not be small. Therefore, drawdown analysis with pseudotime could result in large errors. This conclusion does not contradict the results from Agarwal²² and Lee and Holditch³¹ since the work by Finjord²³ is done by assuming no wellbore storage effect. When wellbore storage is present the inner boundary condition in terms of pseudopressure and time is nonlinear, whereas in terms of pseudopressure and pseudotime the inner boundary condition is completely linear³¹. On the other hand, if there is no wellbore storage effect the inner boundary condition is linear in terms of pseudopressure and time, whereas in terms of pseudopressure and pseudotime the inner boundary condition contains a correction term.

Reynolds et al.²⁴ and Spivey and Lee³² carried out computational studies for gas well drawdown and buildup tests. The results from Refs. 24 and 32 can be summarized: in the absence of wellbore storage, gas well tests should be analyzed with pseudopressure and time; when drawdown and buildup data are influenced by wellbore storage and the analysis of data is to be done with type-curves, both pseudopressure and pseudotime should be used.

In *Chapter II*, closed chamber tests in oil wells have been considered. Closed chamber tests can also be used in gas wells. Moreover, as reported by Reid³³, for low permeability gas reservoirs, closed-chamber drillstem tests are more suitable than conventional drillstem tests. In this chapter, we focus on the flowing period of closed-chamber drillstem tests in gas wells. We use a one-dimensional numerical reservoir simulator to generate synthetic data for a gas-well, closed-chamber test (CCT). With simulator results, it is demonstrated that pseudopressure and pseudotime can be used to correlate data from a gas-well CCT with the corresponding liquid slug test solution. This correlation is usually valid for a sufficient period of time to render analysis tractable and, therefore, slug test type curves can be used to analyze gas-well CCT data. We also show that data can be analyzed by using wellbore storage and skin pressure and pressure derivative type curves by applying the method of Peres et al.⁴ to the pseudopressure versus pseudotime data.

We also conducted parametric studies to investigate the effect of various parameters on the pseudopressure/pseudotime correlation. Our results show that the correlation improves as the skin factor increases, initial wellbore pressure increases, initial reservoir pressure decreases or chamber volume increases.

A gas-well, closed-chamber test problem is a variable rate problem. We show that multirate analysis techniques can be applied to gas-well, closed-chamber tests by analyzing data in terms of pseudopressure and time, not pseudotime.

3.2 Theoretical Development

We consider a gas-well, closed-chamber test conducted in a completely-penetrating well located in an infinite, homogeneous, isotropic cylindrical reservoir of uniform thickness. Initially, the pressure is constant throughout the reservoir and equal to p_i whereas, at the wellbore, the pressure is instantaneously set to p_o at time zero. For simplification, we neglect temperature effects. In addition, it is assumed that friction and inertial effects in the wellbore can be neglected, and critical flow does not occur. We also assume that rock compressibility is negligible compared to gas compressibility.

3.2.1 IBVP for Gas-Well CCT

Under the stated assumptions, the initial boundary value problem (IBVP) for a gas-well CCT can be stated as follows:

$$1.127 \times 10^{-3} \frac{1}{r} \frac{\partial}{\partial r} \left[\frac{p}{\mu_g z} r \frac{\partial p}{\partial r} \right] = \frac{1}{5.615} \frac{\phi c_g}{k} \frac{p}{z} \frac{\partial p}{\partial t}, \quad (3.1.1)$$

$$\lim_{r \rightarrow \infty} p(r, t) = p_i, \quad (3.1.2)$$

$$p(r, 0) = p_i, \quad r > r_w, \quad (3.1.3)$$

$$p_{wf}(0) = p_o, \quad (3.1.4)$$

and

$$1.127 \times 10^{-3} (2\pi) \frac{k}{\mu_g} h \left(r \frac{\partial p}{\partial r} \right)_{r=r_w} = C \frac{\mu_{gi} c_{gw}}{(\mu_g c_g)_o} \frac{\partial p_{wf}}{\partial t}, \quad (3.1.5)$$

where μ_{gi} is the gas viscosity at p_i , c_{gw} is the gas compressibility at p_{wf} , and $(\mu_g c_g)_o$ is the gas viscosity and isothermal compressibility product at p_o . In Eq. 3.1.5, C is the wellbore storage coefficient, defined as

$$C = V_w c_{go} \frac{\mu_{go}}{\mu_{gi}}, \quad (3.2)$$

where, V_w is the wellbore volume in bbl and μ_{go} is the gas viscosity at p_o . Note that the right hand side of Eq. 3.1.5 can actually be reduced to $V_w c_{gw} (\partial p_{wf} / \partial t)$, but, as seen later, it is convenient to use the form given in Eq. 3.1.5 and the definition of C given in Eq. 3.2.

The real gas pseudopressure defined by Al-Hussainy et al.³⁰ is normalized by choosing variables at the initial reservoir pressure, i.e., we define real gas pseudopressure as

$$m(p) = \int_{p_r}^p \frac{(2p' / \mu_g z)}{(2p / \mu_g z)_i} dp, \quad (3.3)$$

where p_r is a base pressure or reference pressure. In terms of $m(p)$, the IBVP of Eqs. 3.1.1-3.1.5 can be written as

$$1.127 \times 10^{-3} \frac{1}{r} \frac{\partial}{\partial r} \left[r \frac{\partial m}{\partial r} \right] = \frac{1}{5.615} \frac{\phi c_g \mu_g}{k} \frac{\partial m}{\partial t}, \quad (3.4.1)$$

$$\lim_{r \rightarrow \infty} m(r, t) = m(p_i), \quad (3.4.2)$$

$$m(r, 0) = m(p_i), \quad r > r_w, \quad (3.4.3)$$

$$m(p_{wf}) = m(p_o), \quad t = 0, \quad (3.4.4)$$

and

$$1.127 \times 10^{-3} (2\pi) \frac{k}{\mu_g} h \left(r \frac{\partial m}{\partial r} \right)_{r=r_w} = C \frac{\mu_{gi} c_{gw}}{(\mu_g c_g)_o} \frac{\partial m(p_{wf})}{\partial t}. \quad (3.4.5)$$

We define dimensionless pseudopressure, dimensionless wellbore pseudopressure, dimensionless time, dimensionless radial distance and the dimensionless wellbore storage coefficient, respectively, as

$$m_D = \frac{m(p_i) - m(p)}{m(p_i) - m(p_o)}, \quad (3.5.1)$$

$$m_{wD} = \frac{m(p_i) - m(p_{wf})}{m(p_i) - m(p_o)}, \quad (3.5.2)$$

$$t_D = \frac{0.006328kt}{\phi(\mu_g c_g)_i r_w^2}, \quad (3.6)$$

(where t is in days)

$$r_D = \frac{r}{r_w}, \quad (3.7)$$

and

$$C_D = \frac{5.615C}{2\pi\phi c_g i h r_w^2}. \quad (3.8)$$

In Eq. 3.6, $(\mu_g c_g)_i$ is the compressibility-viscosity product evaluated at p_i . In dimensionless form, the IBVP of Eqs. 3.4.1-3.4.5 is given by

$$\frac{1}{r_D} \frac{\partial}{\partial r_D} \left(r_D \frac{\partial m_D}{\partial r_D} \right) = \frac{(\mu_g c_g)}{(\mu_g c_g)_i} \frac{\partial m_D}{\partial t_D}, \quad (3.9.1)$$

$$\lim_{r_D \rightarrow \infty} m_D(r_D, t_D) = 0, \quad (3.9.2)$$

$$m_D(r_D, 0) = 0, \quad r_D > 1, \quad (3.9.3)$$

$$m_{wD}(0) = 1, \quad (3.9.4)$$

and

$$\left(r_D \frac{\partial m_D}{\partial r_D} \right)_{r_D=1} = \frac{(\mu_g c_g)_w}{(\mu_g c_g)_o} C_D \frac{\partial m_{wD}}{\partial t_D}. \quad (3.9.5)$$

In Eq. 3.9.5, $(\mu_g c_g)_w$ denotes the compressibility-viscosity product evaluated at p_{wf} .

The inner boundary condition given by Eq. 3.9.5 is non-linear because $(\mu_g c_g)_w$ is a function of the wellbore pressure, p_{wf} . To linearize Eq. 3.9.5, we define dimensionless pseudotime as

$$t_{aD} = \int_0^{t_D} \frac{(\mu_g c_g)_o}{(\mu_g c_g)_w} d\tau. \quad (3.10)$$

Note that the definition defined by Eq. 3.10 for pseudotime differs from the one proposed by Agarwal²². Since $\mu_g c_g$ used in Eq. 3.10 is always evaluated at the wellbore, the pseudotime transformation defined in this study is a pure time transformation. As a result, correction terms obtained by Lee and Holditch³¹ will not appear in the flow equation. A similar definition for pseudotime has been used by Weir and Kissling³⁴.

In terms of dimensionless pseudopressure and pseudotime, the IBVP can be written as

$$\frac{1}{r_D} \frac{\partial}{\partial r_D} \left(r_D \frac{\partial m_D}{\partial r_D} \right) = a_D \frac{\partial m_D}{\partial t_{aD}}, \quad (3.11.1)$$

$$\lim_{r_D \rightarrow \infty} m_D(r_D, t_{aD}) = 0, \quad (3.11.2)$$

$$m_D(r_D, 0) = 0, \quad r_D > 1, \quad (3.11.3)$$

$$m_{wD}(0) = 1, \quad (3.11.4)$$

and

$$\left(r_D \frac{\partial m_D}{\partial r_D} \right)_{r_D=1} = C_D \frac{\partial m_{wD}}{\partial t_{aD}}, \quad (3.11.5)$$

where in Eq. 3.11.1, a_D is given by

$$a_D = \frac{(\mu_g c_g)_o (\mu_g c_g)_i}{(\mu_g c_g)_w (\mu_g c_g)_o}. \quad (3.11.6)$$

In the derivation of Eqs. 3.11.1-3.11.5, no skin effect has been considered. To include the effect of a skin factor, an additional boundary condition is required. Applying the concept of an infinitesimally thin skin, we have

$$m_{wD} = \left[m_D - s \left(r_D \frac{\partial m_D}{\partial r_D} \right) \right]_{r_D=1}. \quad (3.11.7)$$

3.2.2 Type Curve Matching

Eqs. 3.11.1-3.11.7 for gas-well, closed-chamber tests reduce to the standard equations for the liquid, slug-test case if a_D is equal to 1. Note that a_D is a function of time, as well as position, and, for any $r_D > 1$, a_D has the minimum value of $a_D = 1.0$ at $t_D = 0.0$ and the maximum value of $a_D = (\mu_g c_g)_o / (\mu_g c_g)_i$ as $t_D \rightarrow \infty$. Intuitively, we expect that one can correlate data from a gas-well CCT with the corresponding slightly compressible liquid slug-test solution when the deviation of a_D from unity is small. This implies that data from gas-well, closed-chamber tests can be analyzed using methods developed for slug tests after one transforms pressure versus time data into pseudopressure versus pseudotime data.

In order to use wellbore storage and skin pressure and pressure derivative type curves, further data transformation is necessary. Following Peres et al.⁴, the relevant equations are

$$p_{wcD}(t_{aD}, C_D, s) = \frac{I(m_{wD})}{C_D}, \quad (3.12)$$

and

$$p'_{wcD} = \frac{t_{aD}}{C_D} m_{wD}, \quad (3.13)$$

where p_{wcD} denotes the solution for the classical wellbore storage and skin problem presented by Agarwal, Al-Hussainy and Ramey³⁵. In Eq. 3.12, $I(m_{wD})$ is given by

$$I(m_{wD}) = \int_0^{t_{aD}} m_{wD}(\tau, C_D, s) d\tau. \quad (3.14)$$

3.2.3 Multirate Analysis

From Darcy's law, we have

$$1.127 \times 10^{-3} (2\pi) \frac{k}{\mu_g} h \left(r \frac{\partial p}{\partial r} \right)_{r=r_w} = q, \quad (3.15)$$

where q , in RB/D, is the sandface, volumetric flow rate. According to Eq. 3.1.5, q can be approximated by

$$q = V_w c_{gw} \frac{dp_{wf}}{dt}. \quad (3.16)$$

We let Q denote the equivalent sandface, volumetric flow rate in RB/D at p_i , i.e., converted to initial pressure. Then, we have

$$Q = q \frac{(p/z)_w}{(p/z)_i}. \quad (3.17)$$

We let Q_D denote the dimensionless, converted, sandface flow rate defined by

$$Q_D = \frac{141.2Q\mu g_i}{kh[m(p_i) - m(p_o)]}. \quad (3.18)$$

With our definitions of dimensionless variables, the inner boundary condition given by Eq. 3.15 becomes

$$\left(r_D \frac{\partial m_D}{\partial r_D} \right)_{r_D=1} = -Q_D. \quad (3.19)$$

The computational study by Reynolds et al.²⁴ and the theoretical work of Finjord²³ and Aanonsen²⁵ indicate that we should not use pseudotime to analyze gas well drawdown tests except during the wellbore storage dominated flow period. Specifically, these works show that when wellbore storage effects become negligible, a semilog plot of m_{wD} versus t_D will give a semilog slope almost exactly equal to the ideal 1.151 value, whereas a semilog plot of m_{wD} versus t_{aD} will have a slope which can be significantly higher than 1.151. Thus, if we wish to use multirate analysis to account for the variable sandface flow rate, we should apply Duhamel's principle in terms of t_D rather than t_{aD} . Then, an approximate Duhamel's principle for a gas-well, closed chamber test can be written as

$$m_{wD}(t_D) = \int_0^{t_D} Q_D(\tau) p_{wcD}^*(t_D - \tau) d\tau + sQ_D(t_D), \quad (3.20)$$

where p_{wcD}^* is the derivative of the dimensionless wellbore pressure solution for the constant sandface rate problem. For the standard radial flow problem, when $t_D \geq 100$, p_{wcD}^* is given by

$$p_{wcD}^* = \frac{1}{2} \ln\left(\frac{4t_D}{e^\gamma}\right), \quad (3.21)$$

where $\gamma = 0.57722$ is Euler's constant.

In gas-well, closed-chamber tests, even though the sandface flow rate continuously declines, we approximate the flow rate profile as a series of discrete constant rates, i.e., from t_{0D} to t_{1D} the flow rate is assumed to be Q_{1D} , from t_{1D} to t_{2D} the flow rate is assumed to be Q_{2D} , and so on. Using the approximate flow rate profile, Duhamel's principle can be written as

$$m_{wD}(t_D) = \sum_{i=1}^n [Q_{iD} - Q_{(i-1)D}] p_{wcD}^*[t_D - t_{(i-1)D}] + sQ_{nD}. \quad (3.22)$$

Note that in deriving Eq. 3.22, we have used $p_{wcD}^*(0) = 0$ and defined Q_{0D} to be equal to zero. Using the definitions for dimensionless variables and Eq. 3.21 in Eq. 3.22, we obtain

$$\frac{m(p_i) - m(p_{wf})}{Q_n} = m' \sum_{i=1}^n \left[\frac{(Q_i - Q_{i-1})}{Q_n} \log(t - t_{i-1}) \right] + b', \quad (3.23.1)$$

where

$$m' = \frac{162.6\mu_g i}{kh}, \quad (3.23.2)$$

and

$$b' = m' \left[\log\left(\frac{k}{\phi(\mu_g c_g)_i r_w^2}\right) - 3.2275 + 0.86859s \right]. \quad (3.23.3)$$

In Eq. 3.23.1, t is in hours. Eq. 3.23.1, which was first presented by Odeh and Jones³⁶, is the working equation for multirate test analysis. Eq. 3.23.1 suggests that a plot of rate-normalized pseudopressure drop versus the multirate time function, i.e.,

$$\frac{m(p_i) - m(p_{wf})}{Q_n} \quad \text{vs} \quad \sum_{i=1}^n \left[\frac{(Q_i - Q_{i-1})}{Q_n} \log(t - t_{i-1}) \right]$$

will be a straight line with slope m' and intercept b' . The formation flow capacity and skin factor can be obtained from the values of m' and b' by the obvious rearrangement of Eqs. 3.23.2 and 3.23.3.

In applying the convolution method, the sandface flow rate must be obtained either from direct measurement or calculation using Eqs. 3.16 and 3.17.

3.3 Results and Discussion

An implicit one-dimensional, radial flow, finite-difference model was used to simulate a gas-well, closed-chamber test. In the simulator, the skin factor is modeled as an inner zone of altered permeability, using Hawkins³⁷ formula.

Gas physical properties input into the simulator are presented in Table 3.1. These properties were used by Fraim and Wattenbarger³⁸ in gas reservoir decline curve analysis. We begin with a base case gas-well CCT and then present results obtained from the sensitivity study. Parameters for the base case are listed in Table 3.2. The fluid properties of Table 3.1 are used only to give a concrete example and do not affect the general conclusions presented.

Throughout, the dimensionless wellbore pressure for either the CCT solution or the corresponding slug test solution is defined by

$$p_{wD} = \frac{p_i - p_{wf}}{p_i - p_o} \quad (3.24)$$

Table 3.1
Gas Physical Properties As Functions of Pressure

Pressure (psia)	$\mu_g(p)$ (cp)	$z(p)$ (-)	$c_g(p)$ (psi ⁻¹)
514.7	0.1272	0.9693	2.2870E-03
1014.7	0.1373	0.9388	1.0500E-03
1514.7	0.1479	0.9184	0.6743E-03
2014.7	0.1570	0.9102	0.5299E-03
2514.7	0.1676	0.9105	0.3890E-03
3014.7	0.1786	0.9198	0.3046E-03
3514.7	0.1899	0.9364	0.2433E-03
4014.7	0.2018	0.9590	0.1978E-03
4514.7	0.2136	0.9861	0.1635E-03
5014.7	0.2258	1.0165	0.1372E-03

Table 3.2
Parameters for Base Case Gas Well Closed Chamber Test

Parameter	Value	Unit
Initial Reservoir Pressure	5000.0	psig
Formation Porosity	0.075	-
Formation Permeability	1.0	md
Skin Factor	0.0	-
Reservoir Thickness	25.0	ft
Well Radius	0.25	ft
Chamber Volume	130.0	bbl
Initial Chamber Gas Pressure	500.0	psig
Initial Wellbore Storage Coefficient	9309.0	-

3.3.1 Type Curve Matching Analysis

Fig. 3.1 presents a comparison of the base case gas-well, closed-chamber test results with the analogous liquid slug-test solution. In Fig. 3.1, the solid line represents the Ramey, Agarwal and Martin³ slug-test solution (with the dimensionless wellbore storage coefficient and skin factor equal to the corresponding gas-well CCT dimensionless wellbore storage coefficient and skin factor), the dashed line represents the CCT dimensionless wellbore pressure plotted versus dimensionless time, and the plot designated by circles represents the CCT dimensionless wellbore pseudopressure plotted versus dimensionless pseudotime. The same notation applies to all subsequent plots which compare the CCT and slug-test solutions. As shown in Fig. 3.1, gas-well, closed-chamber test data plotted as dimensionless pseudopressure versus dimensionless pseudotime correlate well with the analogous liquid slug-test solution. However, this correlation becomes less accurate as dimensionless time increases. Also shown in Fig. 3.1 is a plot of $m_w D$ versus t_D . This plot differs significantly from the liquid, slug-test solutions, indicating that to correlate the gas-well CCT data with the liquid slug-test solution, one has to use pseudopressure and pseudotime.

Fig. 3.2 shows a_D as a function of time for three locations within the reservoir. As expected, a_D for all three locations has a minimum value of $a_D = 1.0$ at $t_D = 0.0$, and at late times, a_D reaches the maximum value of $(\mu_g c_g)_o / (\mu_g c_g)_i \approx 9.39$.

Effect of Skin Factor: For the results considered in this subsection, only the skin factor is varied and all other parameters are the same as in the base case. Figs. 3.3 and 3.4 present results for $s = 5$ and $s = -2$, respectively. Results of Figs. 3.1, 3.3 and 3.4 illustrate our conclusion that the proposed correlation is improved as the skin factor increases. The effect of the skin factor on the variation of a_D for a fixed point in the reservoir ($r_D = 15.22$) is shown in Fig. 3.5. As illustrated in this

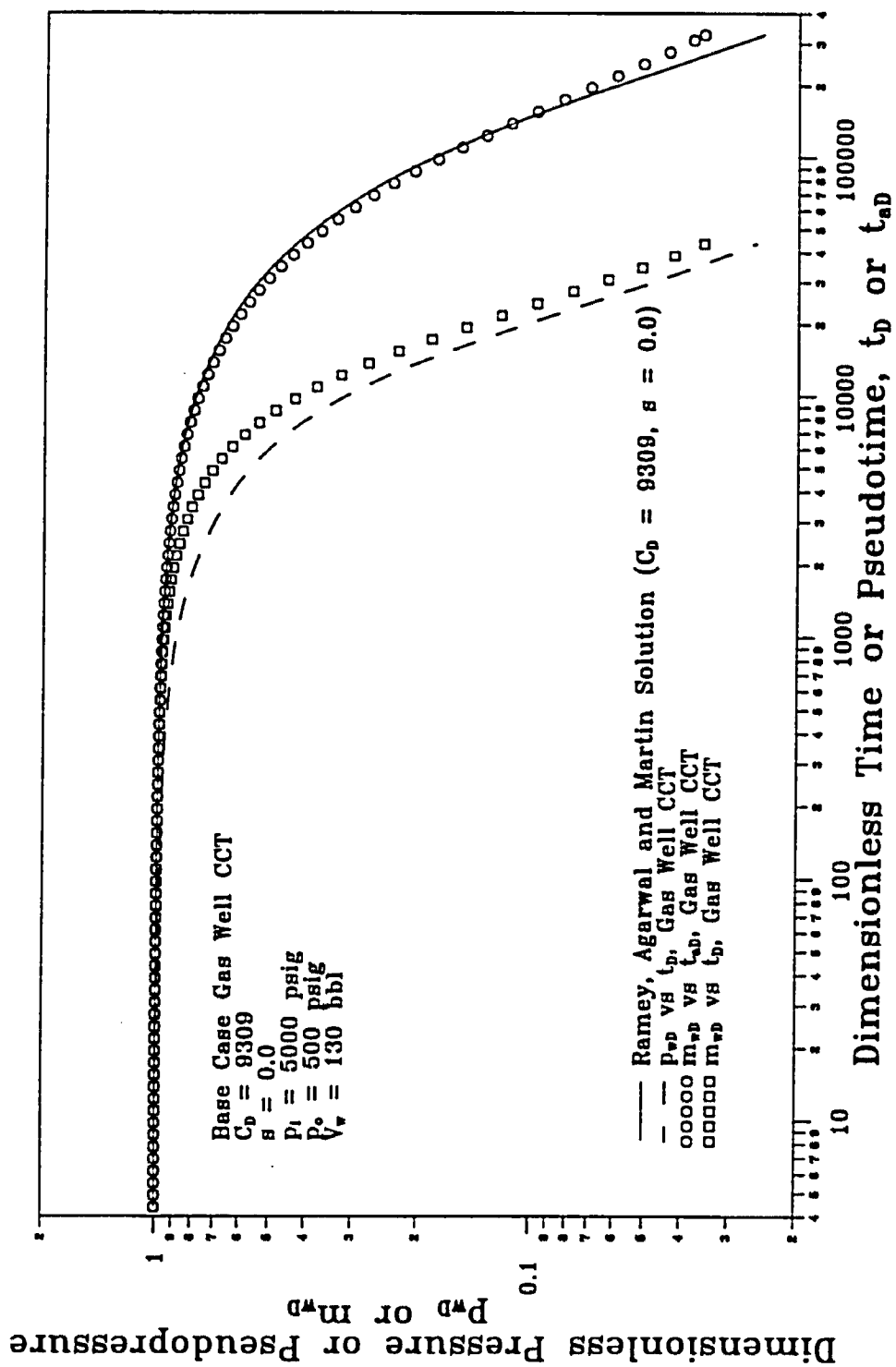


Fig. 3.1 - Comparison of Gas Well CCT with Ramey et al. Slug Test Solution

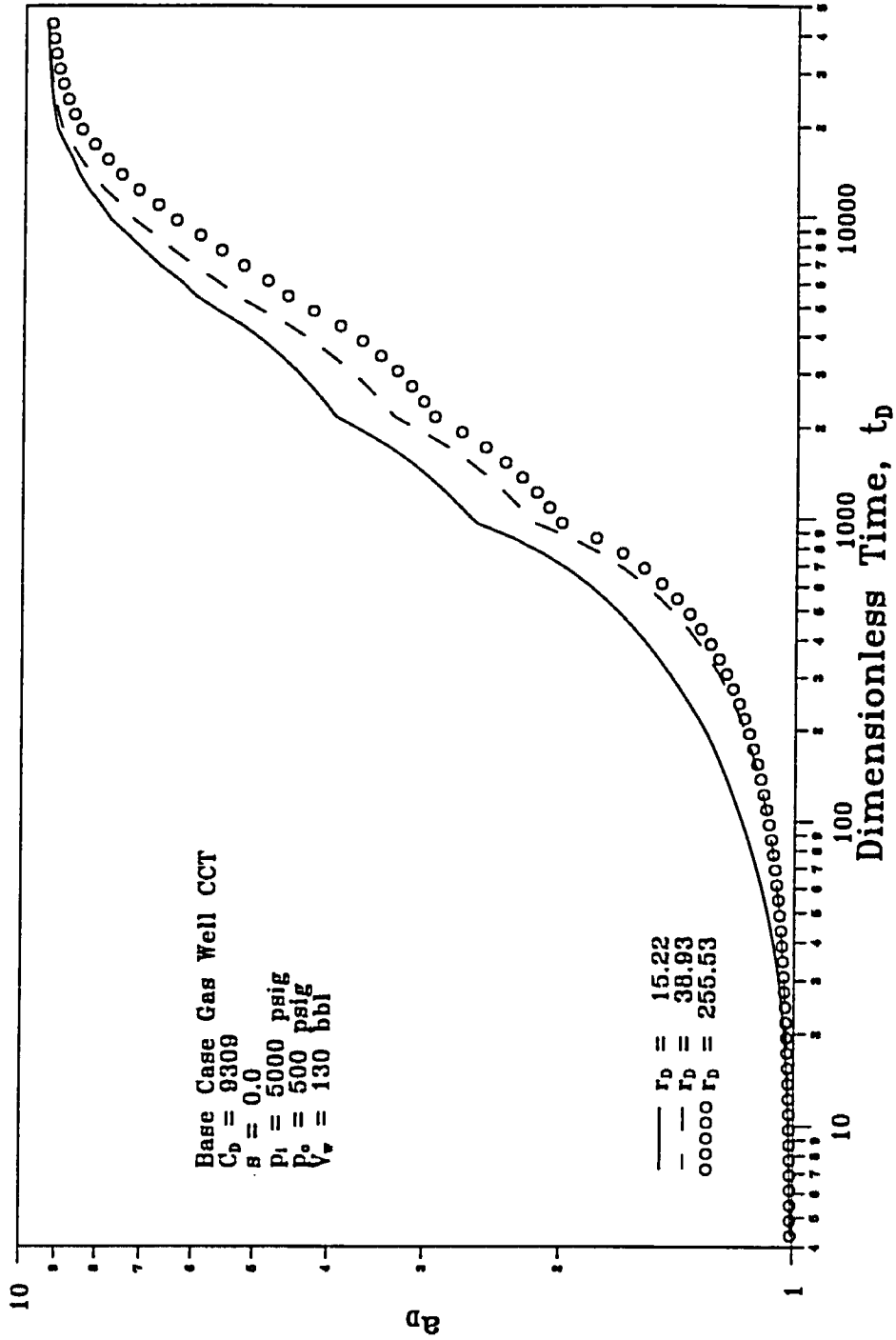


Fig. 3.2 - a_D As a Function of Time and Position, Base Case

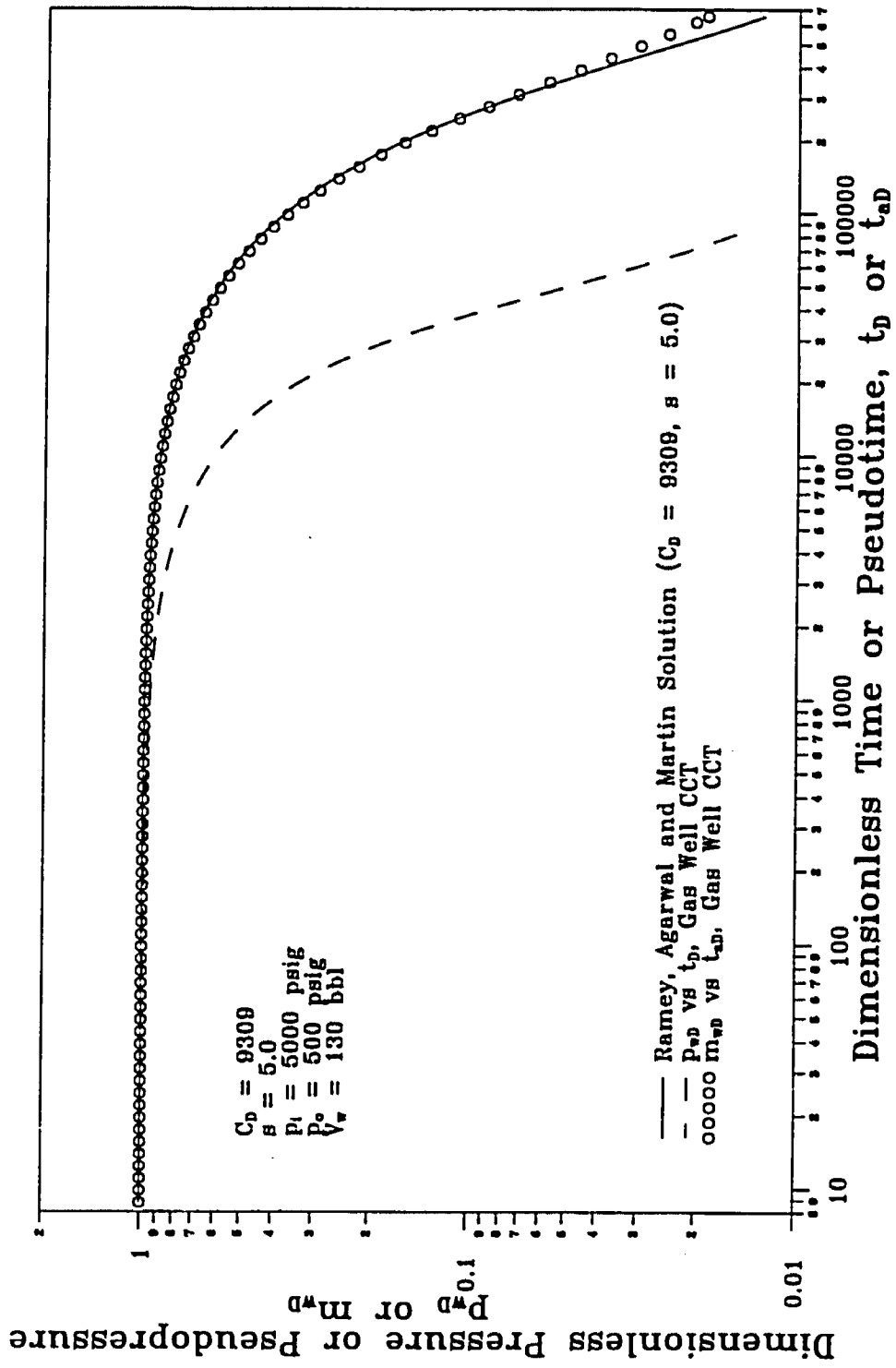


Fig. 3.3 - Effect of Skin Factor on Gas Well CCT ($s = 5.0$)

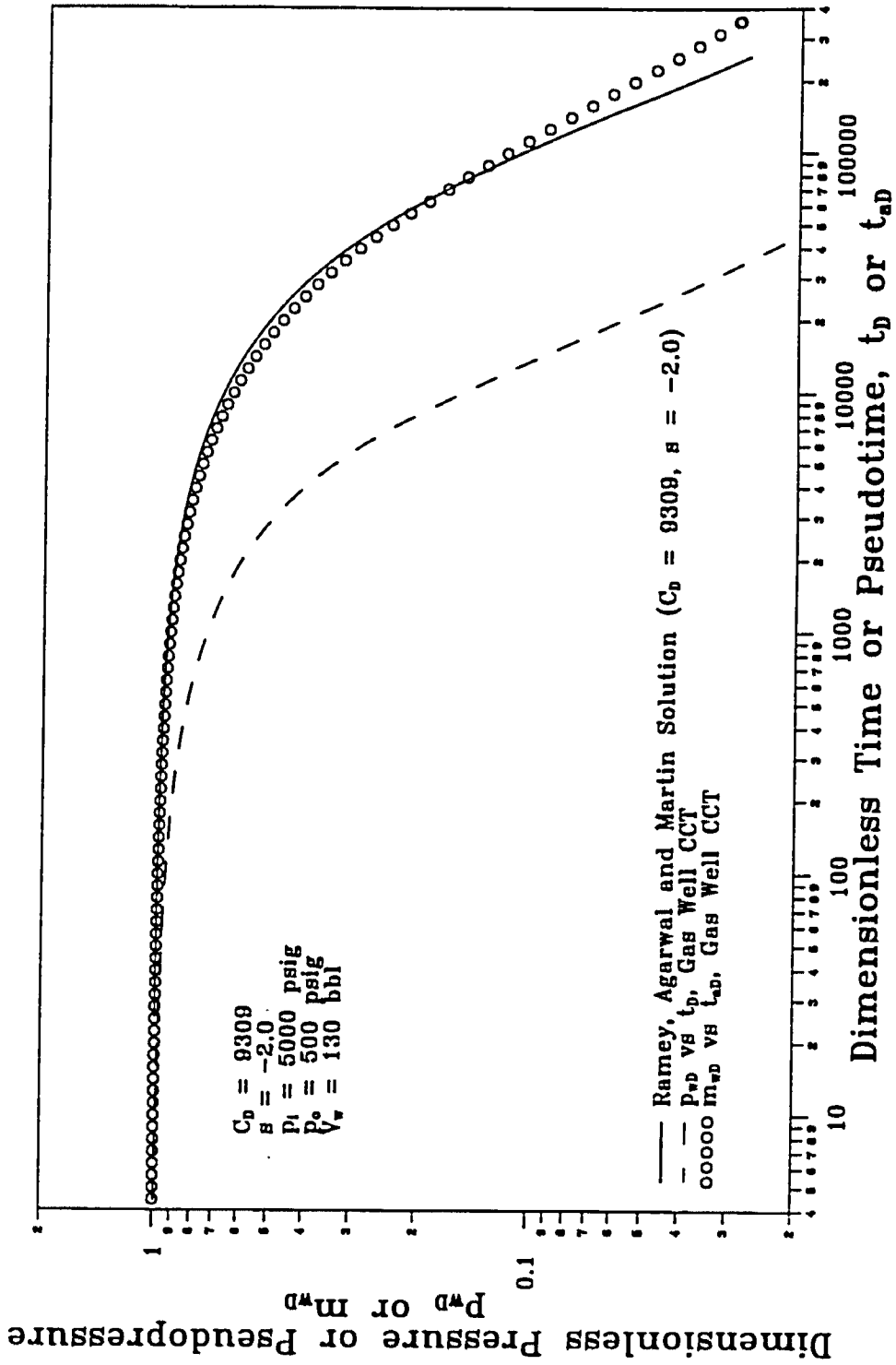


Fig. 3.4 - Effect of Skin Factor on Gas Well CCT ($\beta = -2.0$)

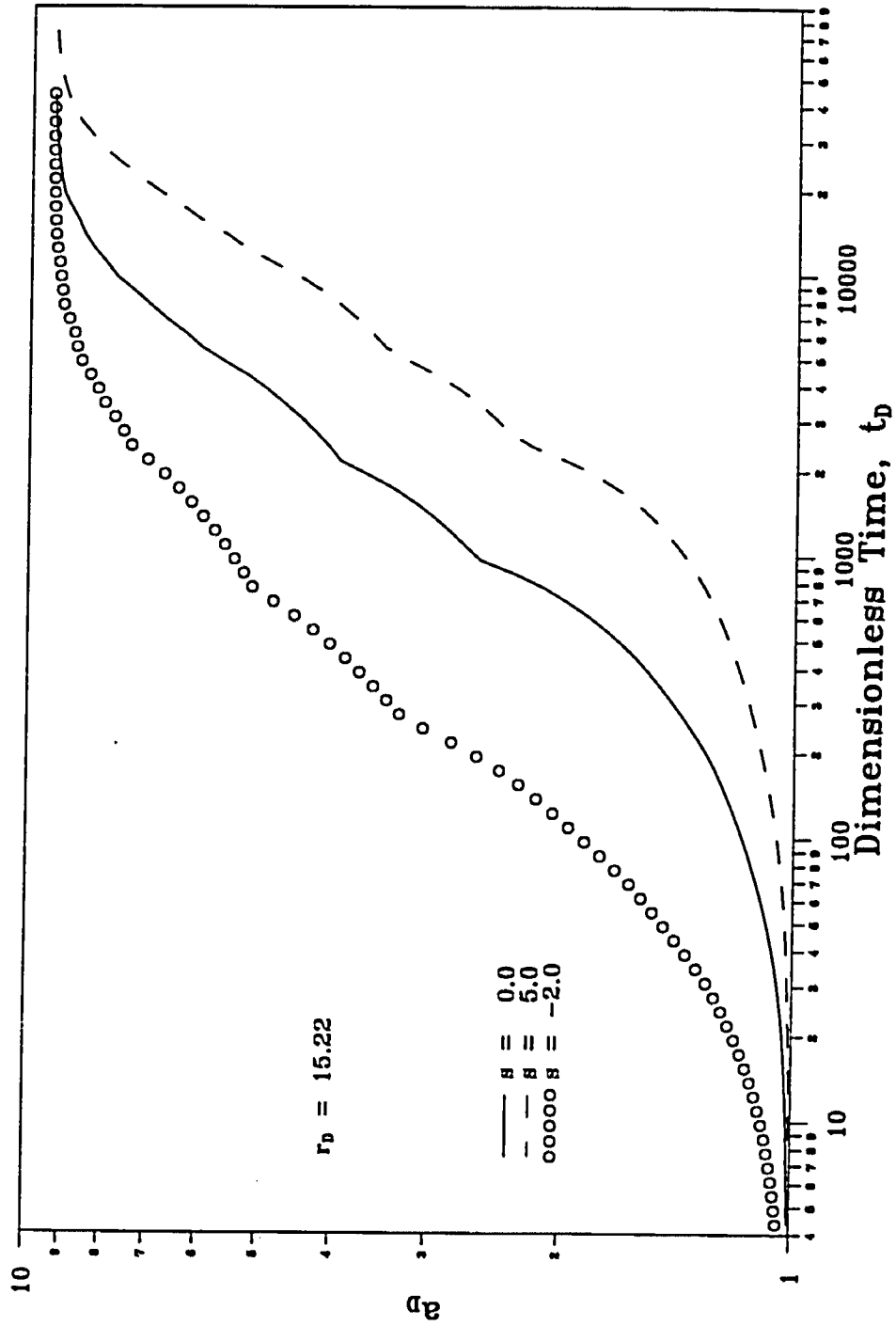


Fig. 3.5 - Effect of Skin Factor on a_D

figure, a case with a larger skin factor has a lower a_D value for a given time. Thus, intuitively, one would expect that the correlation will work for a longer period of time for cases with a higher skin factor.

Effect of Initial Wellbore Pressure: Figs. 3.6 and 3.7 present results for cases with $p_o = 2000$ psig and $p_o = 4000$ psig, respectively. These plots demonstrate that as one increases the initial wellbore pressure, the correlation between the gas-well, closed-chamber test data and liquid slug test solutions becomes better. The variations of a_D at $r_D = 15.22$ for cases with $p_o = 500, 2000$ and 4000 psig are compared in Fig. 3.8. As one increases the wellbore initial pressure, the change in a_D becomes small, and thus, one expects that the correlation will work better for a case with a higher wellbore initial pressure than for a case with a lower wellbore initial pressure.

Effect of Initial Reservoir Pressure: The base case initial reservoir pressure $p_i = 5000$ psig was reduced to $p_i = 4000$ psig and $p_i = 2500$ psig. The results are shown in Figs. 3.9 and 3.10, respectively. Unlike the effect of p_o , as the initial reservoir pressure decreases, the proposed correlation works for a longer period of time and for larger values of p_{wf} . This can also be explained from the variations in a_D , as indicated in Fig. 3.11.

Effect of Chamber Volume: The proposed correlation is also affected by the size of the chamber volume. This is shown in Figs. 3.12 and 3.13. These plots illustrate that the correlation becomes better if a larger chamber is used in conducting the test. The effect of chamber volume on a_D is illustrated in Fig. 3.14. As the chamber volume increases, the increase in a_D is delayed and also occurs more gradually. Hence, intuitively, we expect that a larger chamber will make the correlation work better. Naturally, a longer period of time is needed for the wellbore pressure to buildup when a larger chamber is used.

Above, we conjectured that the correlation of the pseudopressure-pseudotime plot of the CCT solution with the corresponding slug test solution improves as the

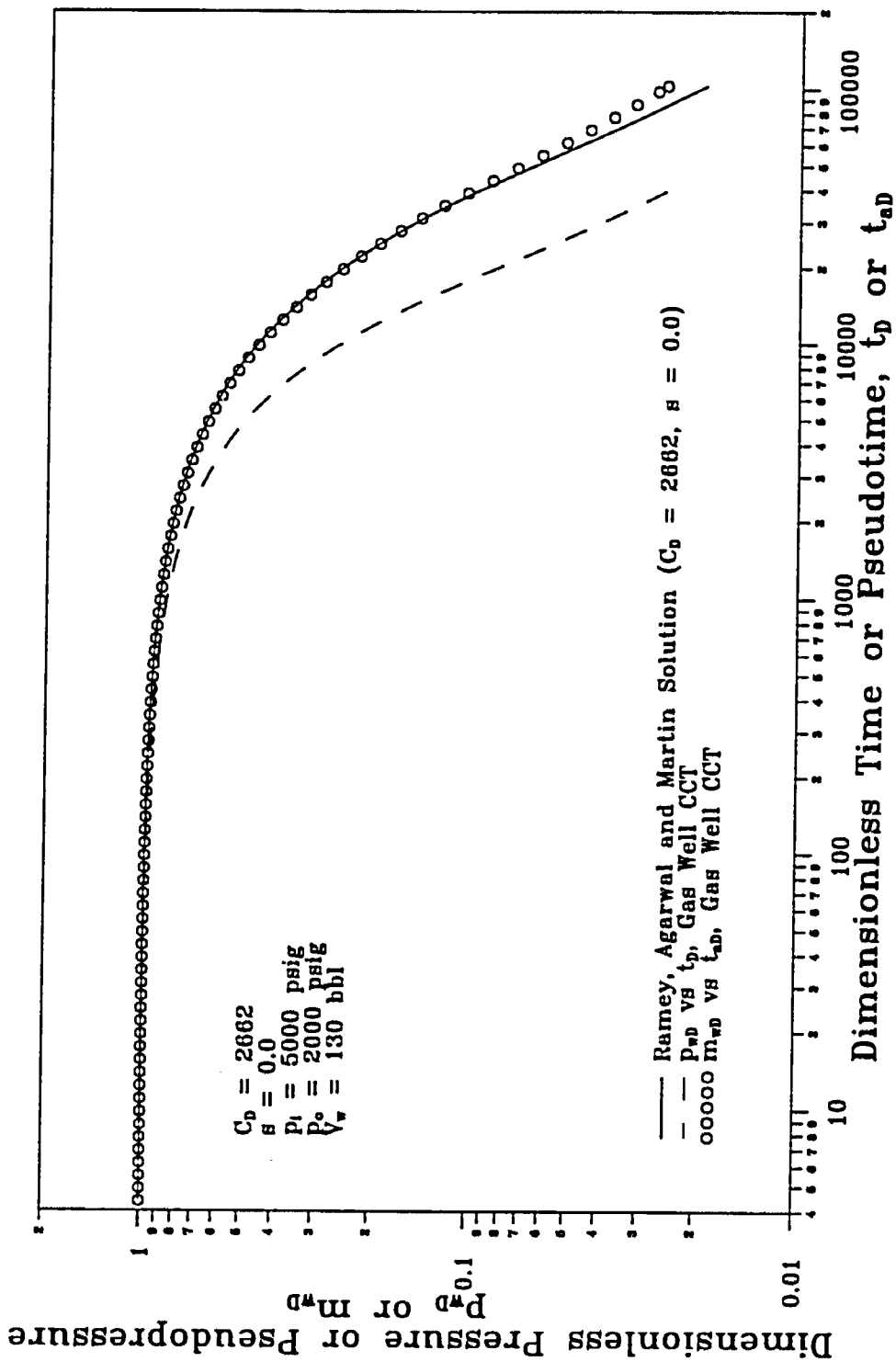


Fig. 3.6 - Effect of Initial Chamber Pressure on Gas Well CCT ($p_o=2000$ psig)

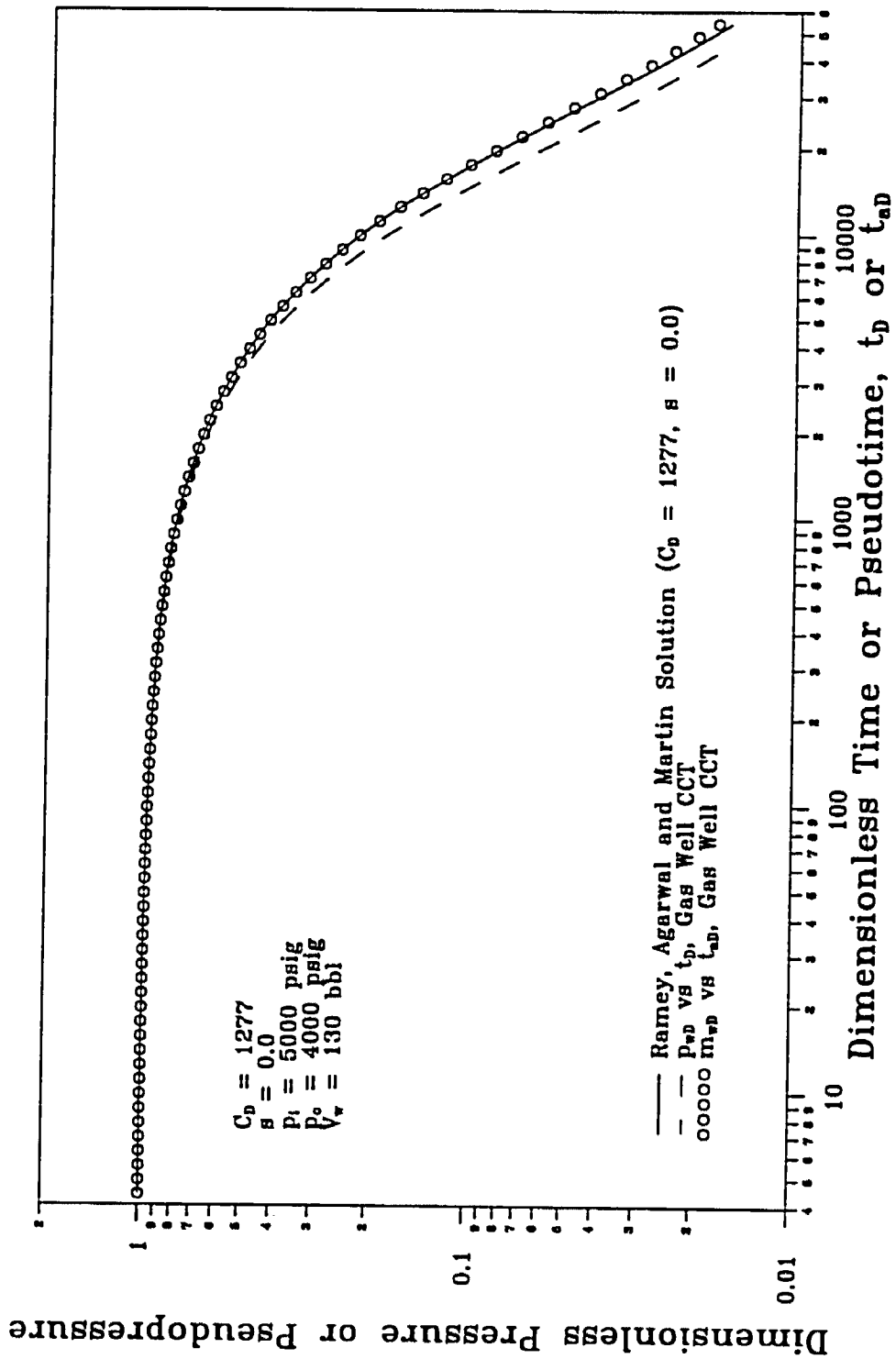


Fig. 3.7 - Effect of Initial Chamber Pressure on Gas Well CCT ($p_o=4000$ psig)

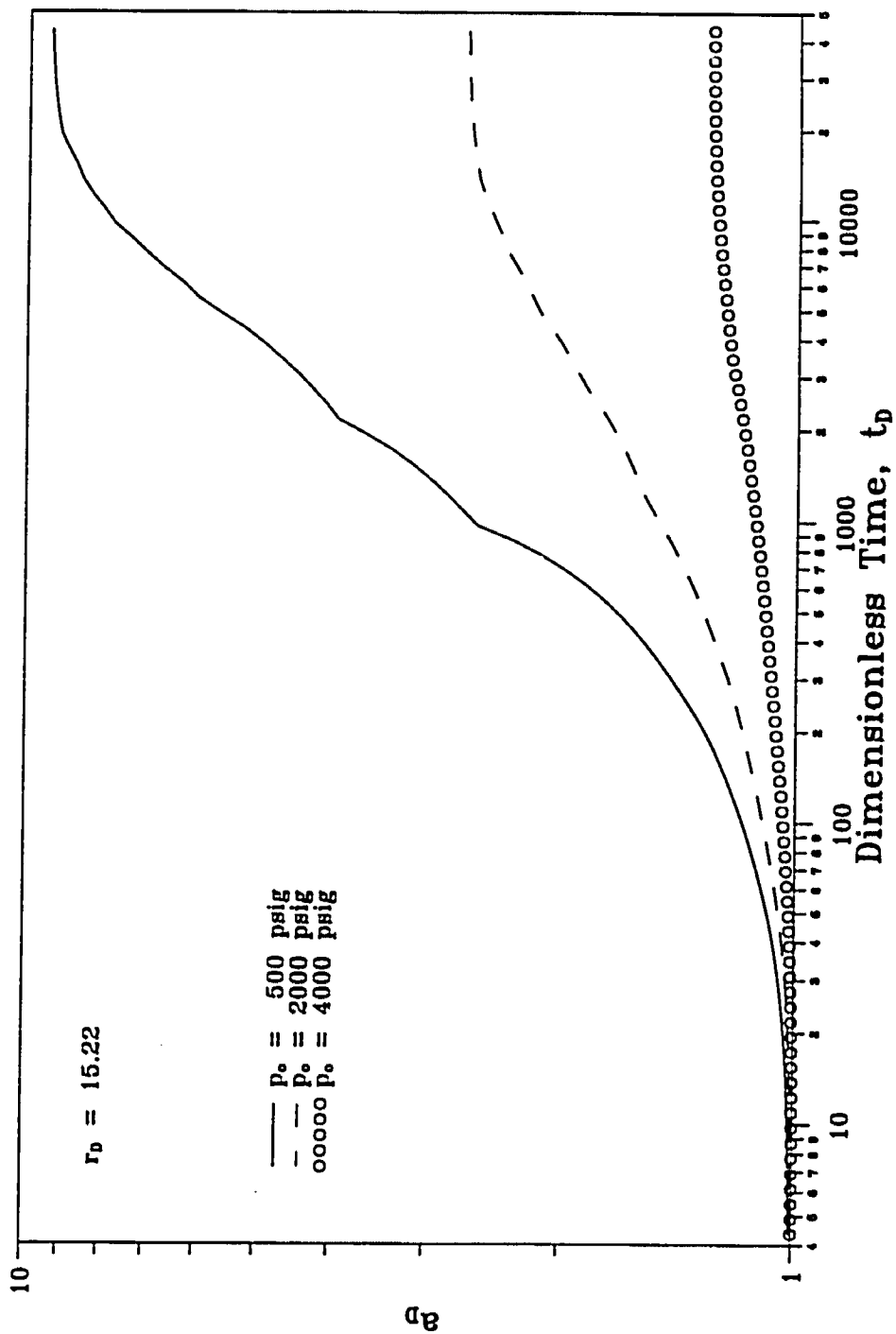


Fig. 3.8 - Effect of Wellbore Initial Pressure on a_p

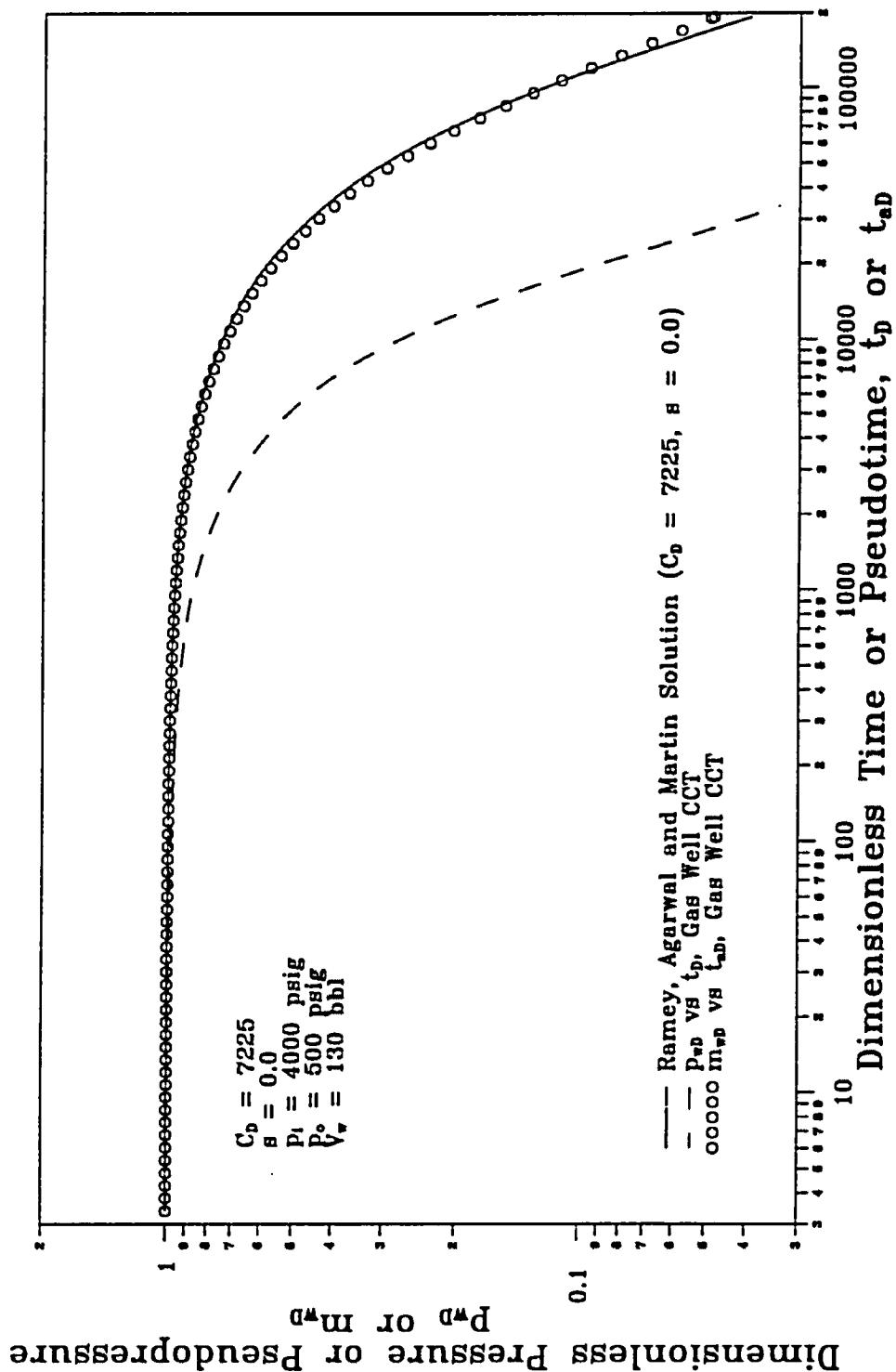


Fig. 3.9 - Effect of Initial Reservoir Pressure on Gas Well CCT ($p_i=4000 \text{ psig}$)

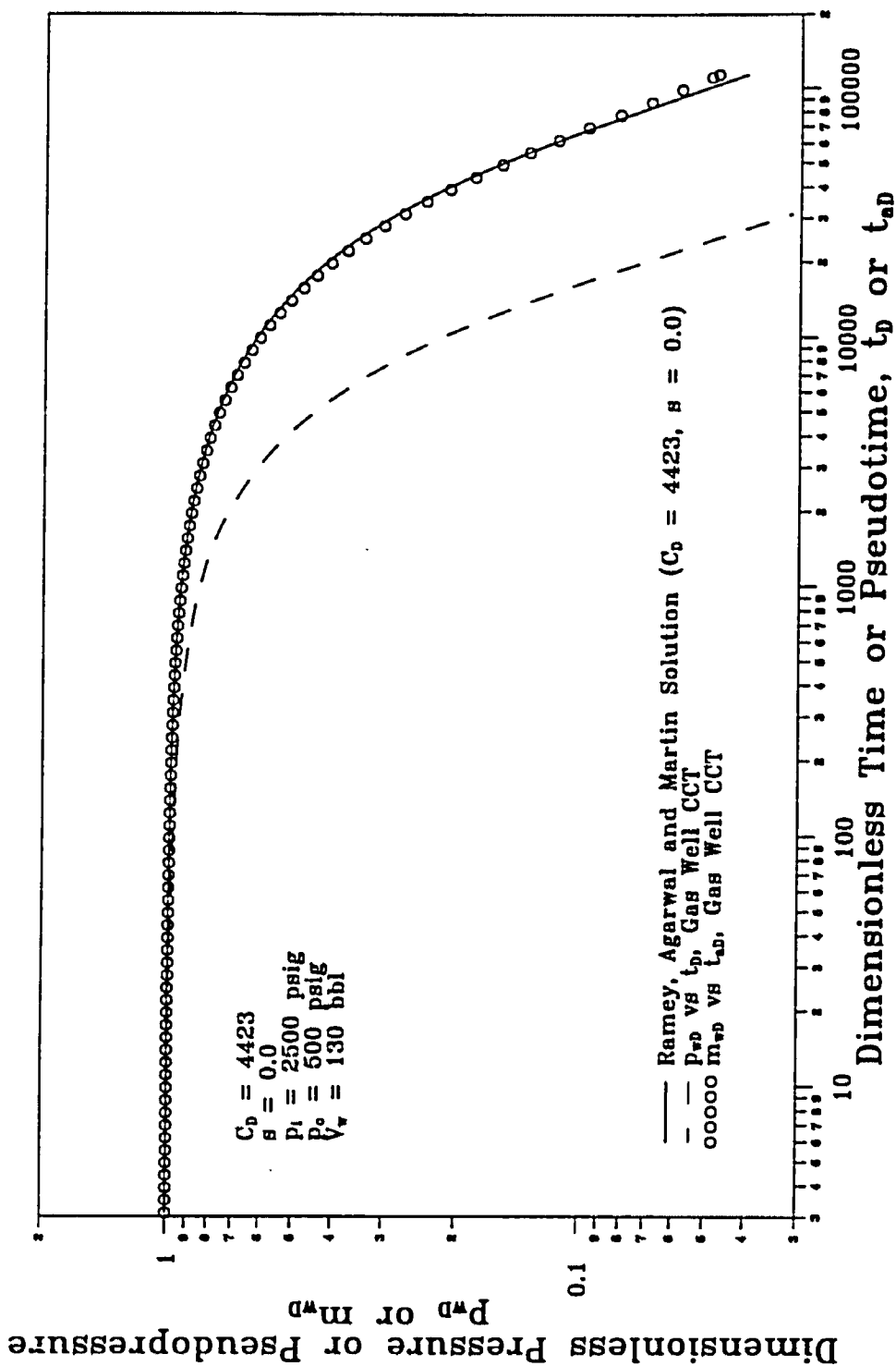


Fig. 3.10 - Effect of Initial Reservoir Pressure on Gas Well CCT ($p_i=2500$ psig)

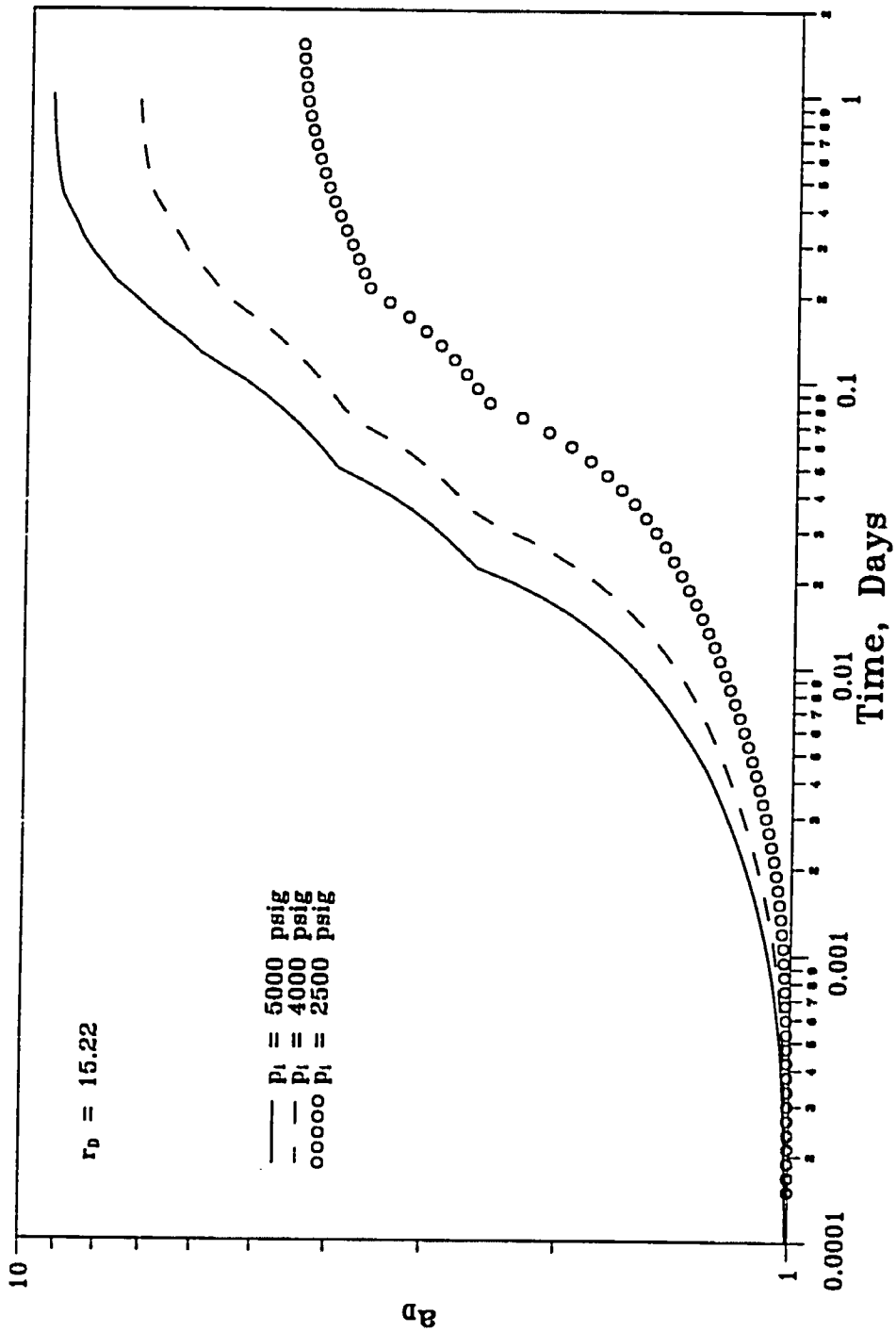


Fig. 3.11 - Effect of Reservoir Initial Pressure on a_D

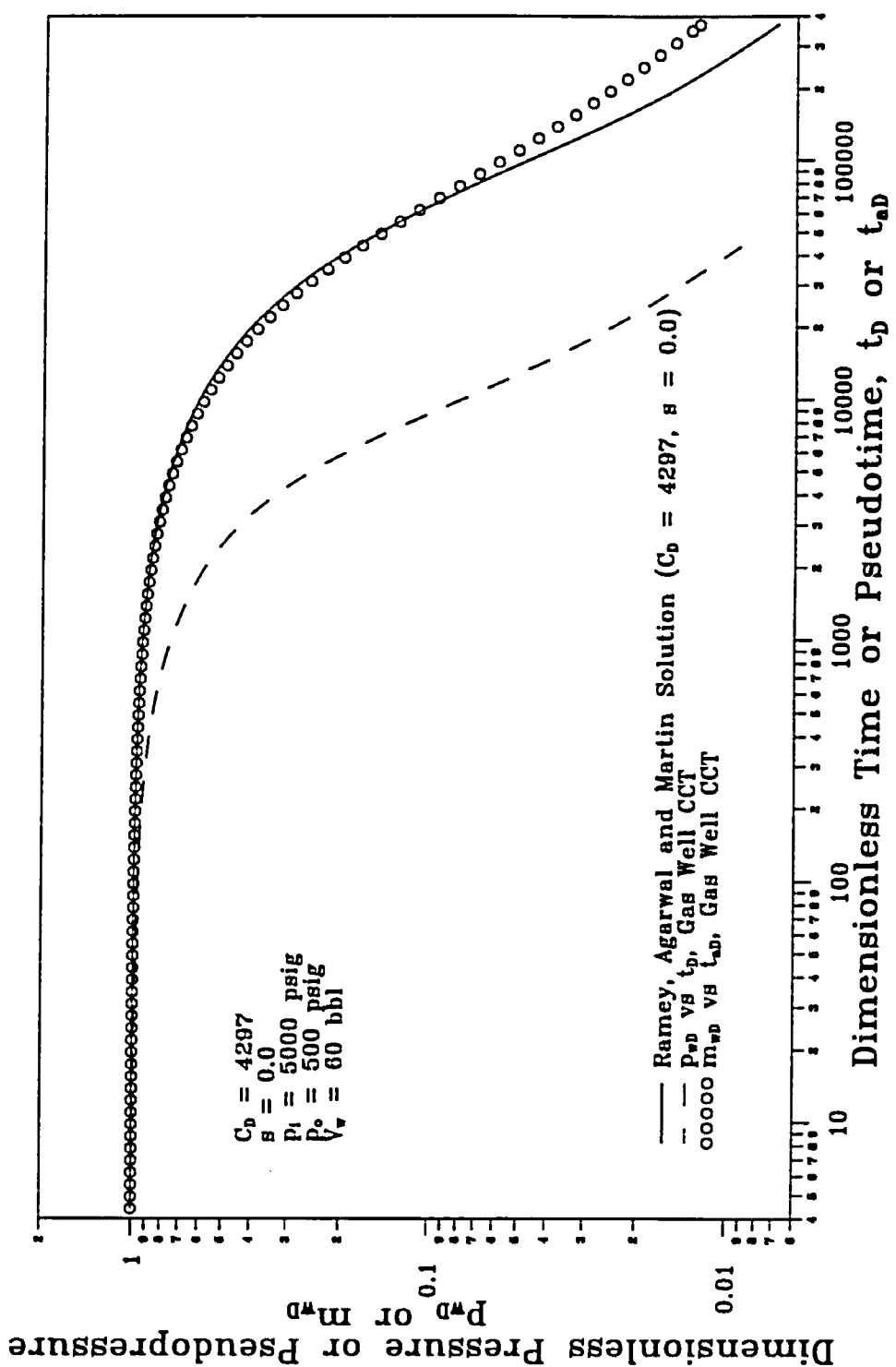


Fig. 3.12 - Effect of Chamber Volume on Gas Well CCT ($V_w = 60 \text{ bbl}$)

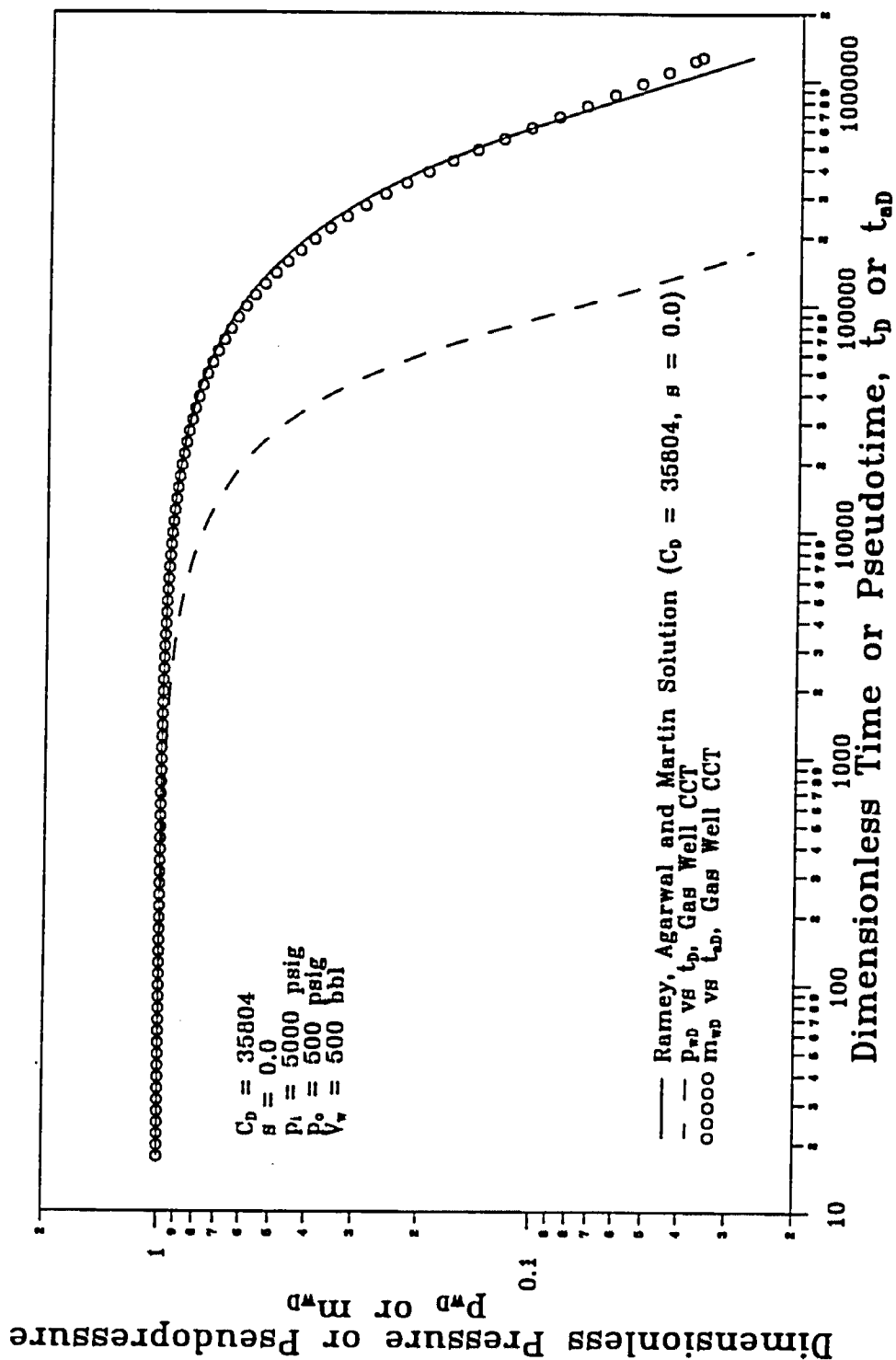


Fig. 3.13 - Effect of Chamber Volume on Gas Well CCT ($V_w = 500 \text{ bbl}$)

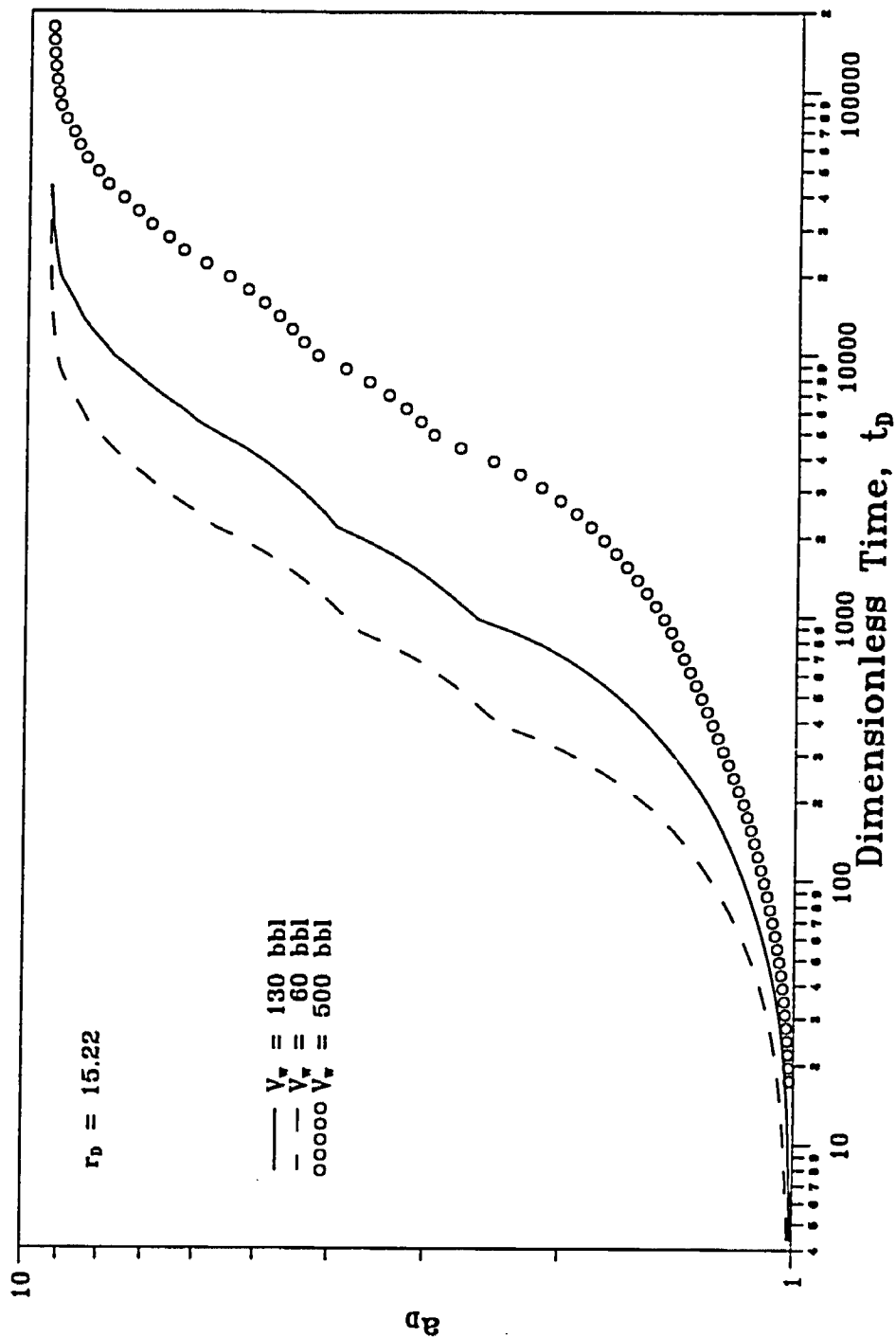


Fig. 3.14 -- Effect of Gas Chamber Volume on a_D

variation in a_D from unity decreases. It is important to point out that a slightly different explanation is plausible, based on the work of Aanonsen²⁵ and of Peres et al.³⁹ who carried out theoretical studies for nonlinear-radial-flow problems. By neglecting wellbore storage effects, Aanonsen was able to construct an accurate approximate analytical solution for single-phase flow of a real gas. Peres et al. used a similar technique to obtain an analytical solution for two-phase flow in a solution-gas-drive reservoir. If the results of Refs. 25 and 39 could be transferred directly to the CCT problem, they would suggest that the accuracy of our pseudopressure-pseudotime transformation is controlled by the magnitude of the change in a_D with respect to m_D at the initial condition, i.e., the magnitude of $[da_D/dm_D]_i$. For our CCT problem, the Boltzmann transform does not apply, and thus we are unable to obtain an approximate analytical solution using the techniques of Refs. 25 and 39. Nevertheless, numerical results given in Figs. 3.5, 3.8, 3.11 and 3.14 support the conjecture that the difference between $m_{wD}(t_{aD})$ and the analogous slug test solution increases as $[da_D/dm_D]_i$ increases.

Peres-Onur-Reynolds (POR) Method: Figs. 3.15 and 3.16 show that one can also use wellbore storage and skin pressure and pressure derivative type curves by converting data using the generalization of the Peres et al.⁴ procedure given by Eqs. 3.12 and 3.13. A unique match should be possible for both cases since the correlation applies well until the pressure derivative has passed its maximum point. Estimates of kh and s obtained from such a type-curve match could be refined using a numerical model such as the one developed by Mfonfu and Grader¹⁰.

3.3.2 Multirate Analysis

Two examples are used to illustrate the convolution analysis technique: the base case, and the case with $s = 5$ and all other parameters the same as in the base case. Sandface flow rates necessary in the convolution analysis are generated from the computer simulator. Calculation results for the two cases are shown in Figs.

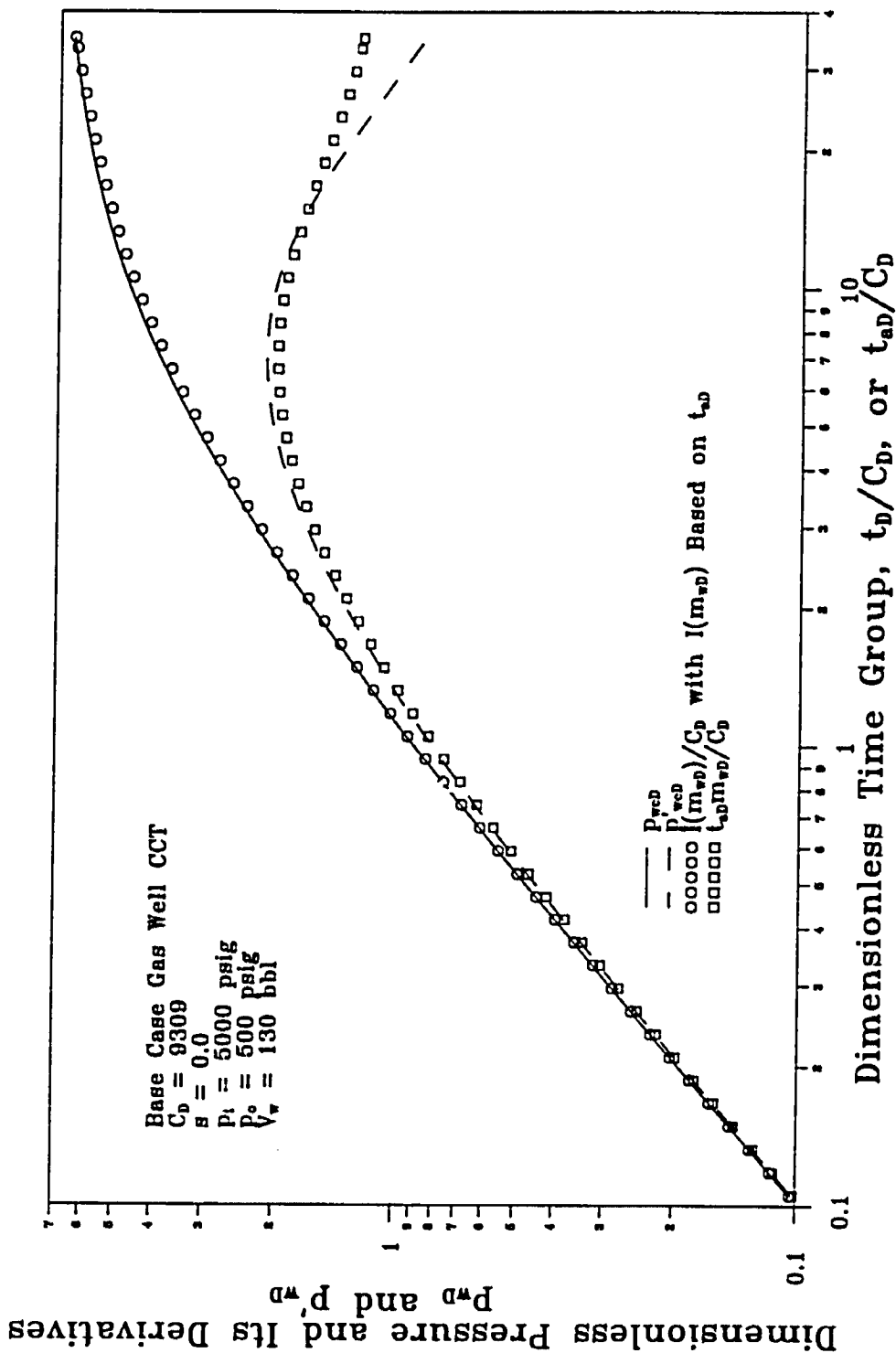


Fig. 3.15 - Comparison of Converted Gas Well CCT Response with Wellbore Storage and Skin Constant Surface Rate Solution, Base Case $s = 0$

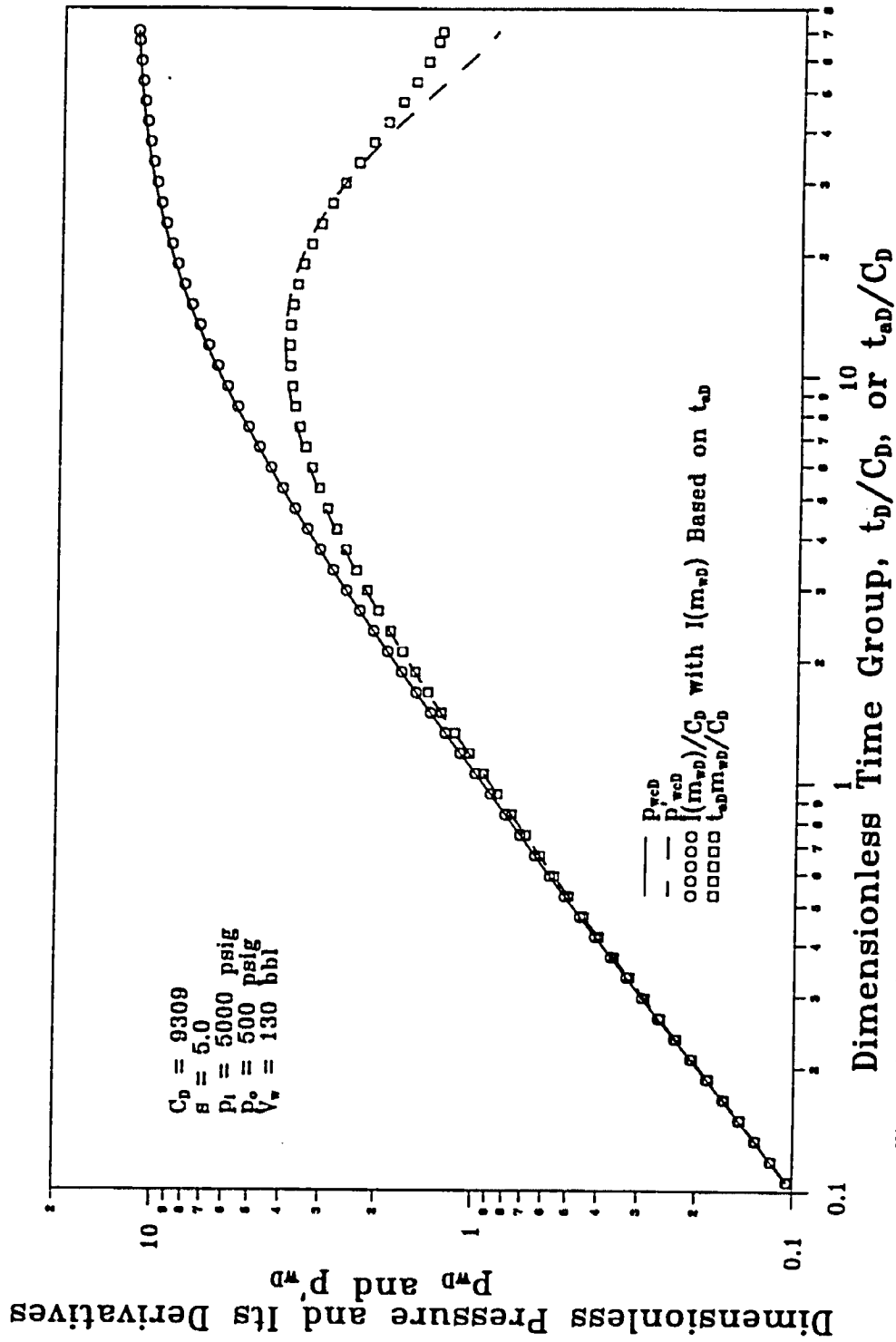


Fig. 3.16 - Comparison of Converted Gas Well CCT Response with Wellbore Storage and Skin Constant Surface Rate Solution, $s = 5$

3.17 and 3.18, respectively. In both Figs. 3.17 and 3.18, the plot shown as circles represents the results generated from pseudopressure versus time data, whereas the plot designated as dots represents the results obtained from pseudopressure versus pseudotime data.

Fig. 3.17 shows that results generated from the pseudopressure versus time data form a perfect straight line with $m' = 1.490$ and $b' = 5.292$. From Eqs. 3.23.2 and 3.23.3, we obtain $kh = 24.64$ and $s = -0.06$. These estimated parameters agree well with the input values of $kh = 25.0$ and $s = 0.0$. The accuracy of these results indicates that Eq. 3.20 is valid, and thus, deconvolution methods can also be used. On the other hand, convolution based on pseudopressure versus pseudotime data gives a straight line with a much higher slope and a lower intercept. As a result, convolution analysis would yield a much lower value for the flow capacity and a much lower value for the skin factor.

In Fig. 3.18, the convolution plot based on pseudopressure versus time data first seems to reflect the skin zone flow capacity and then undergoes a transitional period. After a short period of time, a straight line develops. From the slope and the intercept of the straight line, we obtain $kh = 24.88$ and $s = 5.08$. Again, these values match well with input values of $kh = 25.0$ and $s = 5.0$. Fig. 3.18 also shows that if pseudopressure versus pseudotime data had been used in the analysis, the calculated flow capacity and skin factor would be in significant error.

The results shown in Figs. 3.17 and 3.18 demonstrate our conclusion that in convolution analysis, one should use pseudopressure and time, not pseudopressure and pseudotime.

In the literature, convolution techniques based on a piecewise linear approximation of the flow rate profile have been developed and used for analysis of afterflow data and data from underbalanced perforations⁴⁰⁻⁴². Although not presented here, it was found out that these techniques yield similar results to those given in Figs. 3.17 and 3.18.

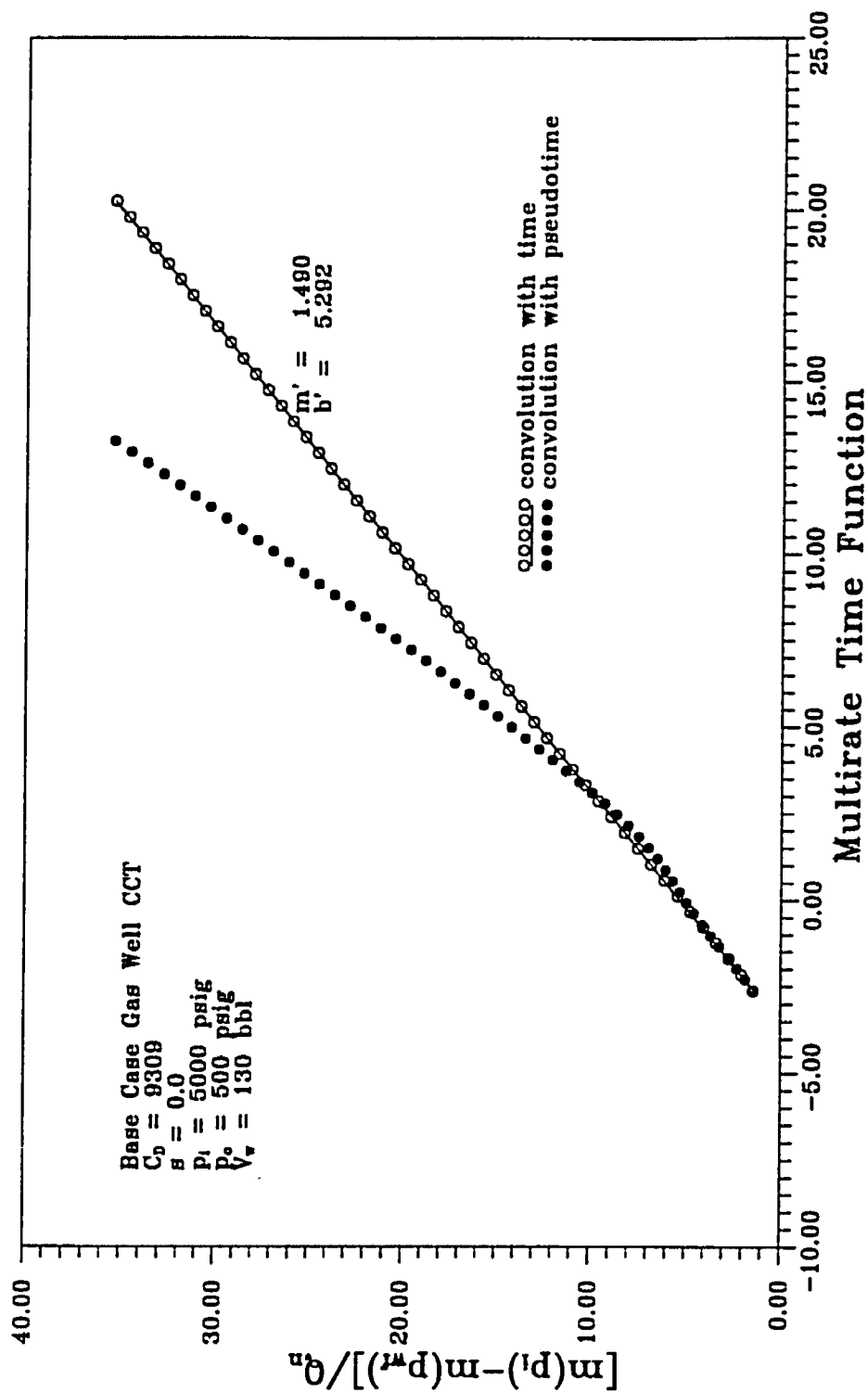


Fig. 3.17 - Comparison of Convolution Analysis for Gas Well CCT in Terms of Time and Pseudotime, Base Case

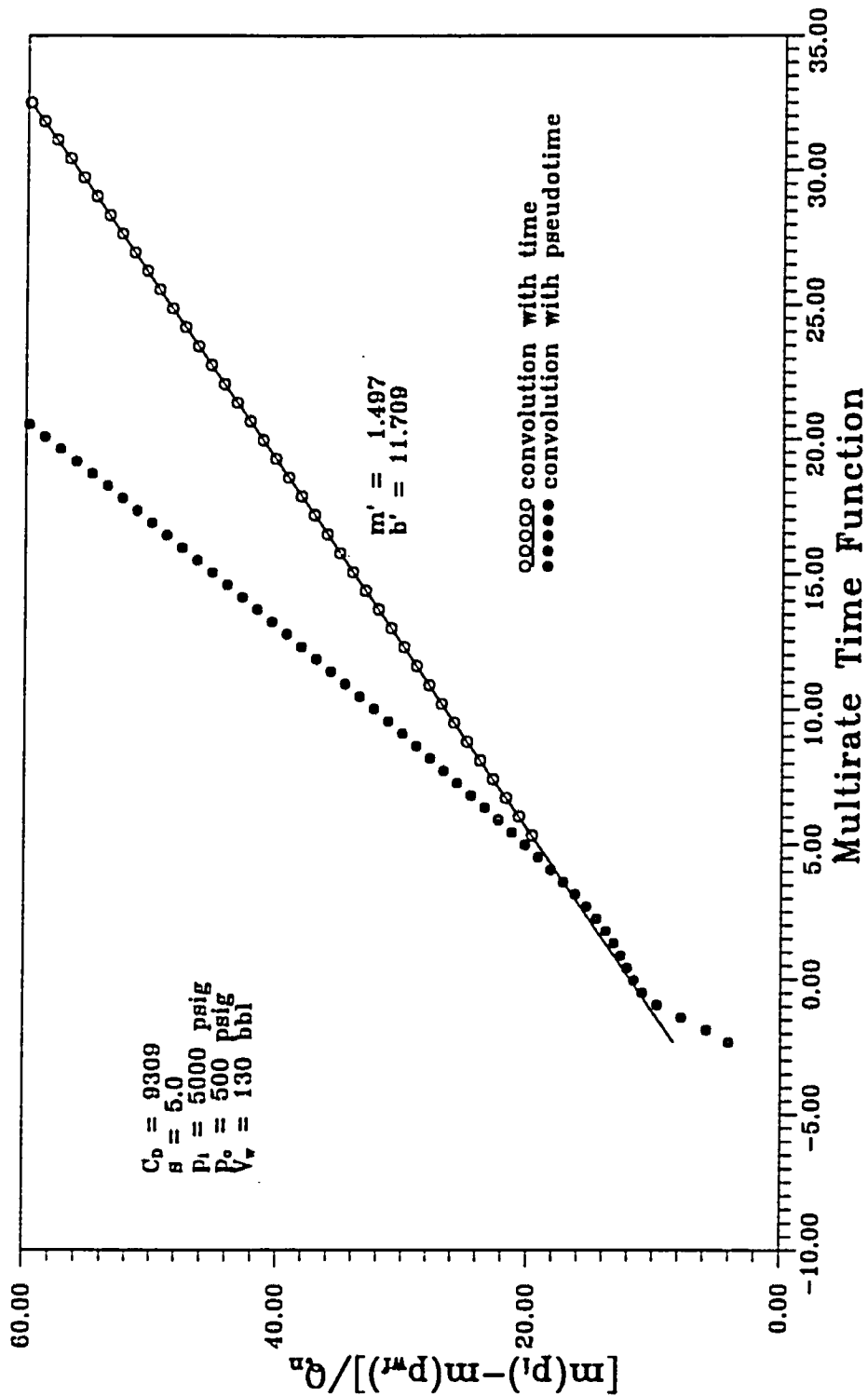


Fig. 3.18 - Convolution Analysis for Gas Well CCT ($s = 5.0$)

CHAPTER IV
MODELING WELLBORE PHASE REDISTRIBUTION
IN PRESSURE BUILDUP TESTS

In the preceding chapters, the wellbore effect on closed chamber tests has been investigated. The focus of this chapter is to study wellbore phase redistribution and its effect on pressure buildup tests.

To understand the phenomenon associated with wellbore phase segregation, one must consider the fundamental laws that govern the motion of fluid particles. In this study, a one-dimensional drift-flux model is used to derive partial differential equations underlying the wellbore transient gas-liquid two-phase flow. The variation of fluid physical properties and the interphase mass transfer as functions of pressure and temperature are considered using the black oil approach, which also takes into account the change of bubble-point pressure along the wellbore caused by the relative motion between the gas and liquid phases. The wellbore flow is coupled with the reservoir flow through the use of Duhamel's principle.

The system of partial differential equations is discretized using standard finite difference methods and the resulting system of nonlinear algebraic equations is solved using a sequential, iterative calculation procedure. The model and the solution algorithm are first verified for a buildup test in a well where single-phase flow exits in the wellbore prior to shut-in. Then, the model is applied to simulate wellbore phase segregation in two pressure buildup tests, a buildup in a naturally flowing well and a buildup in a gas-lift well. These case studies allow us to gain

a better physical understanding about anomalous pressure buildup behaviors observed in the field, and undoubtedly, this will help to develop better interpretation methods in the future.

4.1 Background

Complicated phenomena occur when gas and oil flow simultaneously in the wellbore. One anomalous behavior which occurs in pressure buildup tests is the “pressure hump”, which is characterized by the fact that the bottomhole pressure builds up to a maximum and then falls off⁴³. The pressure hump was first reported in the literature by Stegemeier and Matthews⁴³ in the late 1950’s. It was found that in many cases, this pressure hump behavior was due to the segregation of gas and liquid after the well was shut-in at the wellhead^{43,44}. Due to phase redistribution distortion, the Horner semilog straight line is often delayed or completely suppressed and standard semilog analysis cannot be used.

The work by Fair⁴⁵ is the first attempt to correct wellbore effects caused by phase redistribution in pressure buildup tests. In Fair’s model, phase redistribution was treated as a wellbore storage effect and incorporated into the inner boundary condition for the diffusivity equation. Based on limited experimental data, it was assumed that the phase redistribution pressure function is of an exponential form. New analytical solutions were then obtained and new type curves were developed for the analysis of field data. Fair’s analytical solution shows that, at early times, a well experiencing phase segregation in the wellbore will act like a well with constant storage, but with an apparent storage coefficient, C_{aD} . Then, a transition period will follow during which the wellbore storage coefficient can increase, decrease or even become negative. However, at late times, the well will again act like a well with constant storage, with storage coefficient equal to C_D . Since $C_D > C_{aD}$, Fair’s model has been referred to as an increasing wellbore storage model.

Recently, Hegeman et al.⁴⁶ reported that in some cases, field data indicated that the exponential function used by Fair does not always give a good representation of the phase redistribution pressure rise. Hegeman et al. modified and extended the technique of Fair by using an error function to represent the phase redistribution pressure function. Interestingly, in order to match with some field data, Hegeman et al.⁴⁶ also proposed to assign negative values to the phase redistribution function. This leads to a decreasing wellbore storage coefficient. Assigning negative values to the phase redistribution function means that phase redistribution causes bottom-hole pressure to decrease. This seems to be impossible from a physical point of view. Like Fair's model, the work of Hegeman et al. shows that, at early times, a well will exhibit a constant wellbore storage coefficient C_{aD} , while at late times, the well will exhibit a constant wellbore storage coefficient C_D . Since $C_D < C_{aD}$, the model by Hegeman et al. has been referred to as a decreasing storage model.

Thompson et al.⁴⁷ showed that there exist three different types of pressure responses when phase redistribution occurs and presented conditions under which each of the three types of pressure responses exists. It was also shown that the analysis using Fair's type curves could lead to multiple solutions. They presented correlations to predict the beginning of the semilog straight line for the three types of pressure response when phase redistribution exists.

To overcome the problem of nonuniqueness inherent in the type curve matching process with Fair's type curves, Rushing et al.⁴⁸ proposed an automatic history matching technique to analyze pressure buildup data influenced by wellbore phase redistribution. Analysis of field data was presented to demonstrate the reliability of their methods.

Olarewaju et al.⁴⁹ and Olarewaju⁵⁰ pointed out that when phase redistribution distortion is not severe enough to be easily detected on a log-log plot of pressure change versus shut-in time, pressure derivative plots are necessary to detect the presence of phase segregation distortion and to locate the end of phase redistribution

effects. However, it was found that the derivative of a pressure buildup response influenced by wellbore phase segregation is quite similar to the derivative of the pressure buildup response from a dual porosity reservoir. They discussed methods to distinguish the two types of responses from each other.

The importance of the phase segregation effect on pressure buildup responses and the lack of understanding of the physical process indicate the need to rigorously model multiphase flow in the wellbore. Refs. 51 and 52 developed numerical simulators for multiphase flow in the wellbore. In these simulators, multiphase flow correlations were used. These correlations were developed for steady-state flow, and therefore, it is not clear whether their application for transient flow is appropriate. Recently, Hasan and Kabir⁵³ presented a mechanistic approach to model wellbore phase segregation. However, their coupling of the wellbore and reservoir flow is only approximate. Moreover, to the best of our knowledge, no existing simulator has been able to generate results which confirm the conjectured equations given by Fair⁴⁵ and Hegeman et al.⁴⁶ for the phase redistribution pressure rise.

The objective of this study is to develop computer simulators coupling wellbore multiphase flow with reservoir flow and investigate the effect of wellbore multiphase flow on pressure buildup data. In contrast to the existing work, we wish to (a) develop simplified models for wellbore multiphase flow, which will more closely model the physical process involved in the phase segregation phenomenon, (b) use recent developments in mechanistic modeling of multiphase flow to avoid the use of purely empirical correlations, (c) handle wellbore and reservoir flow interaction more rigorously, (d) include the effect of interphase mass transfer through the black-oil approach and (e) consider the effect of variable-bubble point pressure in fluid physical property calculations.

4.2 Definitions

Investigation of transient gas-liquid two-phase flow in pipes has been pursued following three general approaches^{54–55}: the homogeneous model, the separated model and the drift-flux model. As the simplest model, the homogeneous model assumes no relative motion between the gas and liquid phases. The flow of the two-phase mixture is treated as flow of a pseudo-single phase with physical properties averaged according to the gas void fraction. Because of the inherent assumption, the homogeneous model is not suitable for our problem where a countercurrent flow occurs. The separated model, also called the two-fluid model, takes into account the facts that the two phases have different physical properties and velocities. Generally, separate equations of continuity, momentum and energy are required for each phase, and solutions are obtained by simultaneously solving all of these equations. Usually, a constitutive empirical relation is needed to account for the interphase momentum transfer. Due to the complexity of the model, implementation of the separated model is typically difficult. Unlike the separated model, the drift-flux model is focused on the relative motion between phases rather than the motion of individual phases. This model has been successfully used by a number of investigators in the literature^{56–59}. We have adopted the drift-flux model in our current study.

To accurately simulate the phase segregation process in a pressure buildup test, interphase mass transfer is considered in our study. Since our primary objective is to investigate phase segregation in oil well tests, the black-oil approach commonly used in reservoir simulation⁶⁰ is applied to account for the interphase mass transfer. Application of the black-oil approach assumes that equilibrium between the gas and liquid phases is reached instantaneously. In the course of this study, we found it necessary to incorporate a variable bubble-point pressure calculation procedure in our model. The variation of bubble-point pressure along the wellbore is due to the change of fluid compositions caused by wellbore phase segregation.

In the black-oil model, the flow system is represented by two pseudo components, the oil component and the gas component. The oil component is assumed to be non-volatile and exists only in the liquid phase while the gas component can be present in either the liquid phase or the gas phase. At standard conditions ($p_{sc} = 14.7$ psia and $T_{sc} = 60^\circ F$), all the gas component exits in the gas phase. The following variables are commonly used in the black oil model:

ρ_{os} : density of the oil component at standard conditions, lbm/scf;

ρ_{gs} : density of the gas component at standard conditions, lbm/scf;

R_s : dissolved or solution gas-oil ratio, defined as the volume of gas at standard conditions dissolved at a given pressure and temperature in a unit volume of stock-tank oil, scf/STB;

B_g : gas formation volume factor, defined as the ratio of the volume of free gas (all of which is gas component) at reservoir condition to the volume of the same gas at standard conditions, RB/scf;

B_o : oil formation volume factor, defined as the ratio of the volume of oil plus its dissolved gas at reservoir condition to the volume of the oil component at standard conditions, RB/STB.

R_s , B_g and B_o as functions of pressure and temperature are given as empirical correlations. These variables are used to derive equations of state for the gas and liquid phases. From the definition of B_g , we have

$$\rho_g = \frac{\rho_{gs}}{5.615B_g}, \quad (4.1.1)$$

where ρ_g is the gas phase density, in lbm/ft³. From material balance, we obtain the liquid phase density as

$$\rho_l = \frac{R_s \rho_{gs}}{5.615B_o} + \frac{\rho_{os}}{B_o}. \quad (4.1.2)$$

Let C_{gl} and C_{ol} denote the mass concentration of gas and oil components in the liquid phase, respectively. Then, we have

$$C_{gl} = \frac{R_s \rho_{gs}}{5.615 B_o \rho_l}, \quad (4.2.1)$$

$$C_{ol} = \frac{\rho_{os}}{B_o \rho_l}, \quad (4.2.2)$$

and

$$C_{gl} + C_{ol} = 1. \quad (4.2.3)$$

From the definitions of R_s , C_{gl} and C_{ol} , we obtain

$$R_s = \left(\frac{C_{gl}}{C_{ol}} \right) \left(\frac{5.615 \rho_{os}}{\rho_{gs}} \right). \quad (4.3)$$

Let ρ_{gl} and ρ_{ol} denote the partial densities of the gas and oil components in the liquid phase, respectively, defined by

$$\rho_{gl} = C_{gl} \rho_l, \quad (4.4.1)$$

$$\rho_{ol} = C_{ol} \rho_l, \quad (4.4.2)$$

and

$$\rho_l = \rho_{gl} + \rho_{ol}. \quad (4.4.3)$$

From Eqs. 4.2.1 and 4.4.1, it follows that

$$\rho_{gl} = \frac{R_s \rho_{gs}}{5.615 B_o}. \quad (4.4.4)$$

From Eqs. 4.2.2 and 4.4.2, it is clear that

$$\rho_{ol} = \frac{\rho_{os}}{B_o}. \quad (4.4.5)$$

Let E_g and E_l denote the gas void fraction and liquid holdup, respectively. Then, we have

$$E_g + E_l = 1. \quad (4.5)$$

The density of the gas-liquid two-phase mixture is defined as

$$\rho_m = E_g \rho_g + E_l \rho_l. \quad (4.6)$$

Let C_l and C_g denote the mass concentration of oil and gas components in the two-phase system, respectively. From material balance, we obtain

$$C_l = \frac{E_l \rho_{ol}}{\rho_m}, \quad (4.7.1)$$

$$C_g = \frac{E_l \rho_{gl} + E_g \rho_g}{\rho_m}, \quad (4.7.2)$$

and

$$C_l + C_g = 1. \quad (4.7.3)$$

Let R represent the total gas-oil ratio in a two-phase system, defined as the ratio of the volume of the total gas component, in scf, to the volume of the total oil component, in STB. Then using definitions of R , C_l and C_g , we have

$$R = \left(\frac{C_g}{C_l} \right) \left(\frac{5.615 \rho_{os}}{\rho_{gs}} \right). \quad (4.8)$$

Values of R from Eq. 4.8 will be used to compute the bubble-point pressure at each location along the wellbore by interpolation from the R_s versus p curve. Using Eqs. 4.7.1, 4.7.2, 4.4.1, 4.4.2, 4.1.1, 4.1.2 and 4.3, it can be shown that Eq. 4.8 is equivalent to

$$R = R_s + \left(\frac{B_o}{B_g} \right) \left(\frac{1 - E_l}{E_l} \right). \quad (4.9.1)$$

The above equation can be rearranged to compute liquid holdup as

$$E_l = \frac{B_o}{B_o + B_g(R - R_s)}. \quad (4.9.2)$$

In the multiphase flow literature, superficial gas velocity, v_{sg} , and superficial liquid velocity, v_{sl} , are defined respectively as

$$v_{sg} = \frac{q_g}{A}, \quad (4.10.1)$$

and

$$v_{sl} = \frac{q_l}{A}, \quad (4.10.2)$$

where q_g and q_l are the gas and liquid phase volumetric flow rates in ft³/sec. and A is the pipe cross sectional area. Correspondingly, the gas and liquid phase true velocities are defined as

$$v_g = \frac{q_g}{AE_g}, \quad (4.11.1)$$

and

$$v_l = \frac{q_l}{AE_l}, \quad (4.11.2)$$

where AE_g and AE_l represent the pipe cross sectional area occupied by the gas and liquid phase, respectively. From Eqs. 4.10.1 through 4.11.2, we obtain relationships between the superficial velocity and the true velocity as

$$v_{sg} = E_g v_g, \quad (4.12.1)$$

and

$$v_{sl} = E_l v_l. \quad (4.12.2)$$

The relative velocity between gas and liquid phase is defined as

$$v_r = v_g - v_l. \quad (4.13)$$

In the drift-flux model, we define the two-phase mixture velocity as the density-averaged superficial velocity, i.e.,

$$v_m = \frac{v_{sg}\rho_g + v_{sl}\rho_l}{\rho_m}. \quad (4.14)$$

Note that we have $v_m = v_g$ when $E_g = 1$. Similarly, we have $v_m = v_l$ when $E_l = 1$. From Eq. 4.6 and Eqs. 4.12-4.14, we can derive the following relationships between the true velocity and the mixture velocity:

$$v_l = v_m - \frac{E_g \rho_g v_r}{\rho_m}, \quad (4.15.1)$$

and

$$v_g = v_m + \frac{E_l \rho_l v_r}{\rho_m}. \quad (4.15.2)$$

Eqs. 4.15.1 and 4.15.2 indicate that the flow of each individual phase is a result of a flow due to fluid relative motion superposed on the mixture velocity. Because of these relationships, the drift-flux model is also referred to as the diffusion model.

4.3 Governing Equations

We consider gas-liquid two-phase flow in the wellbore. Two-phase flow could also occur in the reservoir. However, since the anomalous pressure buildup behavior is believed to be caused by phase redistribution in the wellbore, we focus our effort on the analysis of wellbore two-phase flow and consider situations where the bottomhole pressure is still higher than the bubble-point pressure before the well

is shut-in. Furthermore, no attempt is made to solve the flow in the wellbore and the reservoir simultaneously. Rather, we use the superposition principle relating the bottomhole pressure with the sandface flow rate. This relationship provides a boundary condition for the wellbore flow, as shown later. As a result, our study is concentrated on the investigation of wellbore transient two-phase flow during pressure buildup tests.

Throughout, the z coordinate lies along the wellbore which is assumed to be vertical and the positive z direction is upward.

4.3.1 Material Balance Equations

As in reservoir simulation, a standard volume balance for the oil component can be written as:

$$\frac{\partial}{\partial t} \left[\frac{E_l}{B_o} \right] + \frac{\partial}{\partial z} \left[\frac{v_{sl}}{B_o} \right] = 0, \quad (4.16)$$

and the standard volume balance for the gas component is given by

$$\frac{\partial}{\partial t} \left[\frac{E_g}{B_g} + \frac{E_l R_s}{B_o} \right] + \frac{\partial}{\partial z} \left[\frac{v_{sg}}{B_g} + \frac{v_{sl} R_s}{B_o} \right] = 0. \quad (4.17)$$

Similarly, we can rewrite the component mass balance equations as follows:

$$\frac{\partial}{\partial t} \left[\frac{E_l}{B_o} \rho_{os} \right] + \frac{\partial}{\partial z} \left[\frac{v_{sl}}{B_o} \rho_{os} \right] = 0, \quad (4.18)$$

and

$$\frac{\partial}{\partial t} \left[\frac{E_g}{B_g} \rho_{gs} + \frac{E_l R_s}{B_o} \rho_{gs} \right] + \frac{\partial}{\partial z} \left[\frac{v_{sg}}{B_g} \rho_{gs} + \frac{v_{sl} R_s}{B_o} \rho_{gs} \right] = 0. \quad (4.19)$$

Using Eq. 4.4.5 in Eq. 4.18, we find that

$$\frac{\partial}{\partial t} \left[E_l \rho_{ol} \right] + \frac{\partial}{\partial z} \left[v_{sl} \rho_{ol} \right] = 0. \quad (4.20)$$

Using Eqs. 4.1.1 and 4.4.4 in Eq. 4.19 and simplifying gives

$$\frac{\partial}{\partial t} [E_g \rho_g + E_l \rho_{gl}] + \frac{\partial}{\partial z} [v_{sg} \rho_g + v_{sl} \rho_{gl}] = 0. \quad (4.21)$$

In the drift-flux model, it is necessary to write the oil and gas component mass balance equations in terms of v_m and v_r . Using Eqs. 4.12.1, 4.12.2, 4.15.1 and 4.15.2 in Eqs. 4.20 and 4.21, respectively, we obtain

$$\frac{\partial}{\partial t} [E_l \rho_{ol}] + \frac{\partial}{\partial z} [E_l \rho_{ol} v_m] = \frac{\partial}{\partial z} \left[\frac{\rho_{ol} E_l \rho_g E_g v_r}{\rho_m} \right], \quad (4.22)$$

and

$$\frac{\partial}{\partial t} [E_g \rho_g + E_l \rho_{gl}] + \frac{\partial}{\partial z} [(E_g \rho_g + E_l \rho_{gl}) v_m] = -\frac{\partial}{\partial z} \left[\frac{\rho_{ol} E_l \rho_g E_g v_r}{\rho_m} \right]. \quad (4.23)$$

Using Eqs. 4.7.1 and 4.7.2, we can rewrite Eqs. 4.22 and 4.23, respectively, in terms of component concentrations as follows:

$$\frac{\partial}{\partial t} [C_l \rho_m] + \frac{\partial}{\partial z} [C_l \rho_m v_m] = \frac{\partial D_r}{\partial z}, \quad (4.24)$$

and

$$\frac{\partial}{\partial t} [C_g \rho_m] + \frac{\partial}{\partial z} [C_g \rho_m v_m] = -\frac{\partial D_r}{\partial z}, \quad (4.25)$$

Summation of Eqs. 4.24 and 4.25 gives the following overall mass balance equation for the flow system:

$$\frac{\partial}{\partial t} [\rho_m] + \frac{\partial}{\partial z} [\rho_m v_m] = 0. \quad (4.26)$$

In Eqs. 4.24 and 4.25, the parameter D_r , defined by Eq. 4.27, represents diffusion caused by relative motion.

$$D_r = C_l \rho_g E_g v_r. \quad (4.27)$$

Eqs. 4.24, 4.25 and 4.26 are the three basic mass balance equations. In principle, any two of these equations can be used. In our study, we choose to use Eqs. 4.24 and 4.26, i.e., the oil component mass balance equation and the overall mass balance equation.

4.3.2 Simplified Momentum Equation

Phase segregation after the well is shut-in is a slow and gravity dominated process. Therefore, in this study, a complete momentum equation is not considered. It is assumed that for the flow of the gas-liquid mixture, inertia terms are small and neglected and the fluid-wall friction is negligible. Under these assumptions, a simplified mixture momentum equation can be obtained:

$$\frac{\partial p}{\partial z} = -\frac{\rho_m g}{144g_c}. \quad (4.28)$$

Note that in deriving Eq. 4.28, we assume that the upward direction is the positive z -direction. Eqs. 4.24, 4.26 and 4.28 are the three fundamental equations describing transient flow of a gas-liquid mixture in the wellbore. The three primary dependent variables are the oil component concentration, C_l , the mixture velocity, v_m , and the pressure, p . Once the concentration distribution is determined, the total gas-oil ratio, R , can be calculated from Eq. 4.8. Consequently, with known values of R and the pressure distribution, liquid holdup can be obtained through Eq. 4.9.2.

4.3.3 Closure Relationship

A relationship for the relative velocity, v_r , is necessary to close our model. It is known that v_r is a flow pattern dependent variable. Starting with a high flowing bottomhole pressure, only a single phase liquid exists at the bottomhole. As the fluid moves upward in the wellbore, it experiences a pressure decrease, and dissolved gas comes out of solution. As a result, from the bottomhole to the wellhead, the flow pattern may change from single phase liquid flow to bubble flow, slug flow,

churn flow and even annular flow. Since the effect of phase segregation is maximized for bubble and slug flows⁴⁴, in our study, we concentrate on situations where only bubble and slug flows exist in the wellbore. For bubble flow, the well-known Harmathy equation is used⁵⁴:

$$v_r = 1.53 \left[\frac{\sigma g (\rho_l - \rho_g)}{\rho_l^2} \right]^{1/4}, \quad (4.29.1)$$

where σ is the gas-liquid surface tension. Note that all variables in Eq. 4.29.1 are in SI units. In oil field units, Eq. 4.29.1 becomes

$$v_r = 0.79 \left[\frac{\sigma (\rho_l - \rho_g)}{\rho_l^2} \right]^{1/4}. \quad (4.29.2)$$

For slug flow, the relative velocity is given by (see Refs. 54, 59 and 61)

$$v_r = 0.35 \left[\frac{gD(\rho_l - \rho_g)}{\rho_l} \right]^{1/2}, \quad (4.30.1)$$

or in oil field units

$$v_r = 0.61 \left[\frac{D(\rho_l - \rho_g)}{\rho_l} \right]^{1/2}. \quad (4.30.2)$$

In Eqs. 4.30.1 and 4.30.2, D is the diameter of the tubing string. The change of flow pattern from bubble flow to slug flow occurs when the gas void fraction is around 0.20. To avoid numerical oscillation⁶², it is assumed that bubble flow exists for $E_g \leq 0.15$, slug flow exists for $E_g \geq 0.25$ and for $0.15 < E_g < 0.25$, the flow is in the transition zone. The relative velocity in the transition zone is calculated by linear interpolation between values obtained from Eqs. 4.29.2 and 4.30.2.

4.3.4 Initial and Boundary Conditions

Solutions of the partial differential equations governing the phase segregation process in the wellbore require initial distributions of dependent variables along the

wellbore, i.e., the initial condition, and boundary conditions as functions of time. It is assumed that the well produces at a constant rate for a long period of time so that steady-state flow prevails in the wellbore at the instant of shut-in. With a known sandface production rate and producing time, the spatial distributions of the mixture velocity, oil concentration, and pressure are calculated by using a calculation procedure presented in the next section.

We assume that wellhead shut-in occurs instantaneously, and then, the boundary condition at the wellhead is

$$\left[v_m \right]_{wh} = 0, \quad \left[v_r \right]_{wh} = 0, \quad \Delta t > 0, \quad (4.31)$$

where Δt is the shut-in time.

The wellbore is connected with the reservoir at the bottomhole. Immediately after shut-in, fluids may continue to flow into the wellbore, i.e., afterflow occurs. However, at late times, fluids may be injected back into the reservoir due to wellbore phase segregation. The boundary condition at bottomhole for the wellbore two-phase flow is obtained by applying Duhamel's principle which relates the sandface flow rate to the wellbore bottomhole pressure, i.e.,

$$p_{wsD} = \int_0^{t_{pD} + \Delta t_D} q_D(\tau) p'_{cD}(t_{pD} + \Delta t_D - \tau) d\tau + s q_D(t_{pD} + \Delta t_D), \quad (4.32)$$

where t_p is the producing time and t_{pD} is the dimensionless producing time. In Eq. 4.32, p_{wsD} is the dimensionless buildup bottomhole pressure defined as

$$p_{wsD} = \frac{kh(p_i - p_{ws})}{141.2q\mu}, \quad (4.33)$$

where q is the well sandface production rate before the shut-in, in RB/D. The dimensionless flow rate, q_D , is defined as

$$q_D(\tau) = \frac{q_{sf}(\tau)}{q}. \quad (4.34)$$

For $0 < \tau \leq t_p$, $q_{sf} = q$ and $q_D(\tau) = 1$. The dimensionless time, t_D , is defined as

$$t_D = \frac{2.637 \times 10^{-4} kt}{\phi c_l \mu r_w^2}, \quad (4.35)$$

where t is in hours. In Eq. 4.32, t_{pD} is the dimensionless producing time, obtained by replacing t with producing time t_p in Eq. 4.35, and Δt_D in Eq. 4.32 is the dimensionless shut-in time, obtained by replacing t with Δt in Eq. 4.35. In Eq. 4.32, p_{cD} is the dimensionless pressure solution at the sandface for the constant sandface rate production problem with no skin effect, i.e., $s = 0$. Since we assume radial flow, values of p_{cD} can be obtained by numerical inversion of the following Laplace space solution²⁰:

$$\bar{p}_{cD} = \frac{K_0(\sqrt{u})}{u^{3/2} K_1(\sqrt{u})}. \quad (4.36.1)$$

For $t_D > 25$, a semi-log approximation can be used to evaluate p_{cD} , i.e.,

$$p_{cD} = \frac{1}{2} \left[\ln t_D + 0.80907 \right]. \quad (4.36.2)$$

The dimensionless wellbore pressure for the constant sandface rate production problem with an infinitesimally thin skin is

$$p_{wcD} = \frac{kh[p_i - p_{wf}]}{141.2q\mu} = \frac{1}{2} \left[\ln t_D + 0.80907 \right] + s. \quad (4.36.3)$$

Eq. 4.32, which relates sandface flow rate with bottomhole pressure, is the bottomhole boundary condition for the wellbore two-phase flow system. For a given time and flow rate, Eq. 4.32 is numerically integrated to give the bottomhole shut-in pressure, p_{ws} .

4.4 Numerical Solution Method

The system of nonlinear partial differential equations governing the phase segregation process in the wellbore is solved numerically using finite difference methods. The flow field is uniformly divided into small control volumes, as shown in Fig. 4.1. Finite difference equations are derived with a system of staggered grids where dependent variables are defined at different positions in a control volume⁶³. Specifically, oil concentration and all physical properties are defined at the center of each control volume while the mixture velocity is defined at the control volume boundaries or faces. In the conventional application of staggered grids, the pressure is also defined in the center of each control volume. Since we use an approximate momentum equation in our problem, it is convenient to define pressure at the faces of each control volume and estimate the pressure at the center by an arithmetic average, i.e., $p_i = (p_{i+1/2} + p_{i-1/2})/2$.

4.4.1 Finite Difference Equations

Overall Mass Balance Equation: Finite difference equations are obtained by integrating the corresponding partial differential equations over each of the control volumes. Integrating the overall mass balance equation, Eq. 4.26, over the i^{th} control volume, we obtain

$$\frac{(\rho_m)_i^{n+1} - (\rho_m)_i^n}{\Delta t} + \frac{(\rho_m v_m)_{i+\frac{1}{2}}^{n+1} - (\rho_m v_m)_{i-\frac{1}{2}}^{n+1}}{\Delta z} = 0, \quad (4.37)$$

for $i = 1, 2, \dots, N$. (N is the total number of cells in the calculation domain; see Fig. 4.1.) Rearranging Eq. 4.37, we obtain

$$\left[\frac{(\rho_m)_{i+\frac{1}{2}}^{n+1}}{\Delta z} \right] (v_m)_{i+\frac{1}{2}}^{n+1} = \left[\frac{(\rho_m)_{i-\frac{1}{2}}^{n+1}}{\Delta z} \right] (v_m)_{i-\frac{1}{2}}^{n+1} - \frac{(\rho_m)_i^{n+1} - (\rho_m)_i^n}{\Delta t}, \quad (4.38)$$

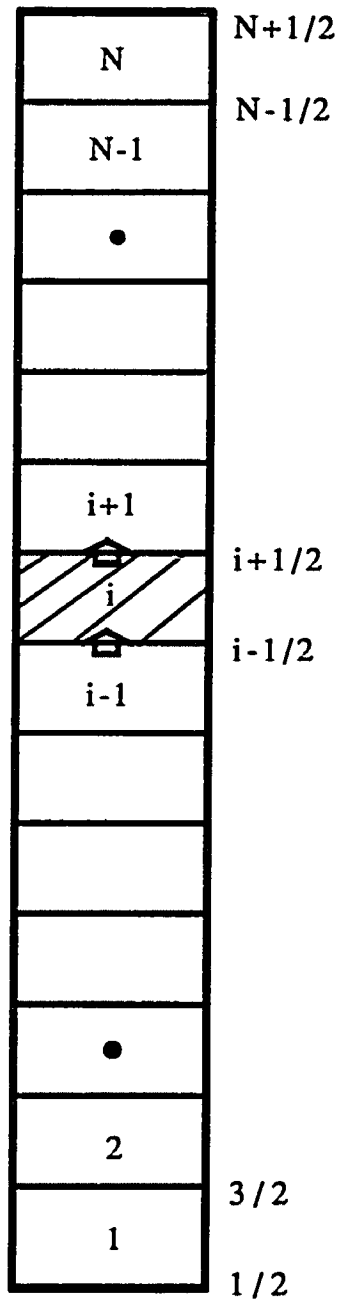


Fig. 4.1 - The Control Volumes and Staggered Grids

for $i = 1, 2, \dots, N$. Summation of Eq. 4.38 over all i and rearranging gives

$$(v_m)_{\frac{1}{2}}^{n+1} = \left(\frac{\Delta z}{\Delta t} \right) \frac{\sum_{i=1}^N [(\rho_m)_i^{n+1} - (\rho_m)_i^n]}{(\rho_m)_{\frac{1}{2}}^{n+1}}. \quad (4.39)$$

Note that Eq. 4.39 is the wellbore mass conservation equation, and in deriving Eq. 4.39, we have used the wellhead boundary condition, Eq. 4.31. In Eqs. 4.37 through 4.39, values of mixture densities at the control volume faces are required. An upstream weighting technique is used to evaluate these variables. For example, for $(\rho_m)_{i+\frac{1}{2}}$, we have

$$(\rho_m)_{i+\frac{1}{2}} = \left[\frac{1 + \beta_{i+\frac{1}{2}}}{2} \right] (\rho_m)_i + \left[\frac{1 - \beta_{i+\frac{1}{2}}}{2} \right] (\rho_m)_{i+1}, \quad (4.40.1)$$

where the coefficient for the upstream weighting is defined as

$$\beta_{i+\frac{1}{2}} = \frac{(v_m)_{i+\frac{1}{2}}}{|(v_m)_{i+\frac{1}{2}}|}. \quad (4.40.2)$$

Once the sandface velocity, $(v_m)_{\frac{1}{2}}^{n+1}$, satisfying both the bottomhole boundary condition, Eq. 4.32 and the wellbore mass conservation equation, Eq. 4.39, is obtained, Eq. 4.38 can be applied recursively to compute velocity from the bottomhole to the wellhead. The details of the computational procedure are discussed later.

Oil Component Concentration Equation: To derive the finite difference equation for the oil component concentration, it is necessary to write the finite difference overall mass balance equation in a different form. Applying the concept of upstream weighting, we have

$$(\rho_m v_m)_{i+\frac{1}{2}}^{n+1} = (\rho_m)_i^{n+1} \max \left[(v_m)_{i+\frac{1}{2}}^{n+1}, 0 \right] - (\rho_m)_{i+1}^{n+1} \max \left[-(v_m)_{i+\frac{1}{2}}^{n+1}, 0 \right]. \quad (4.41)$$

A similar equation can be obtained for $(\rho_m v_m)_{i-\frac{1}{2}}^{n+1}$. Substituting equations for $(\rho_m v_m)_{i+\frac{1}{2}}^{n+1}$ and $(\rho_m v_m)_{i-\frac{1}{2}}^{n+1}$ into Eq. 4.37 and multiplying both sides of the resulting equation by $(C_l)_i^{n+1}$, we obtain

$$\begin{aligned} & \frac{(C_l)_i^{n+1}(\rho_m)_i^{n+1} - (C_l)_i^{n+1}(\rho_m)_i^n}{\Delta t} + \frac{(C_l)_i^{n+1}(\rho_m)_i^{n+1} \max[(v_m)_{i+\frac{1}{2}}^{n+1}, 0]}{\Delta z} \\ & - \frac{(C_l)_i^{n+1}(\rho_m)_{i+1}^{n+1} \max[-(v_m)_{i+\frac{1}{2}}^{n+1}, 0]}{\Delta z} - \frac{(C_l)_i^{n+1}(\rho_m)_{i-1}^{n+1} \max[(v_m)_{i-\frac{1}{2}}^{n+1}, 0]}{\Delta z} \\ & + \frac{(C_l)_i^{n+1}(\rho_m)_i^{n+1} \max[-(v_m)_{i-\frac{1}{2}}^{n+1}, 0]}{\Delta z} = 0. \end{aligned} \quad (4.42)$$

Integrating the oil component mass balance, Eq. 4.24, over the i^{th} control volume, we obtain

$$\frac{(C_l \rho_m)_i^{n+1} - (C_l \rho_m)_i^n}{\Delta t} + \frac{(C_l \rho_m v_m)_{i+\frac{1}{2}}^{n+1} - (C_l \rho_m v_m)_{i-\frac{1}{2}}^{n+1}}{\Delta z} = \frac{(D_r)_{i+\frac{1}{2}}^{n+1} - (D_r)_{i-\frac{1}{2}}^{n+1}}{\Delta z}, \quad (4.43)$$

for $i = 1, 2, \dots, N$. In Eq. 4.43, values of C_l and ρ_m are required at the control volume boundaries. Again, they are evaluated according to the upstream weighting concept. For example, for $(C_l \rho_m v_m)_{i+\frac{1}{2}}^{n+1}$, we have

$$(C_l \rho_m v_m)_{i+\frac{1}{2}}^{n+1} = (C_l \rho_m)_i^{n+1} \max[(v_m)_{i+\frac{1}{2}}^{n+1}, 0] - (C_l \rho_m)_{i+1}^{n+1} \max[-(v_m)_{i+\frac{1}{2}}^{n+1}, 0]. \quad (4.44)$$

A similar equation can be obtained for $(C_l \rho_m v_m)_{i-\frac{1}{2}}^{n+1}$. Substituting these equations into Eq. 4.43, we get

$$\frac{(C_l \rho_m)_i^{n+1} - (C_l \rho_m)_i^n}{\Delta t} + \frac{(C_l \rho_m)_i^{n+1} \max[(v_m)_{i+\frac{1}{2}}^{n+1}, 0]}{\Delta z}$$

$$\begin{aligned} & \frac{(C_l \rho_m)_{i+1}^{n+1} \max \left[-(v_m)_{i+\frac{1}{2}}^{n+1}, 0 \right]}{\Delta z} - \frac{(C_l \rho_m)_{i-1}^{n+1} \max \left[(v_m)_{i-\frac{1}{2}}^{n+1}, 0 \right]}{\Delta z} \\ & + \frac{(C_l \rho_m)_i^{n+1} \max \left[-(v_m)_{i-\frac{1}{2}}^{n+1}, 0 \right]}{\Delta z} = \frac{(D_r)_{i+\frac{1}{2}}^{n+1} - (D_r)_{i-\frac{1}{2}}^{n+1}}{\Delta z}. \end{aligned} \quad (4.45)$$

Subtracting Eq. 4.42 from Eq. 4.45 and rearranging yields

$$-a(C_l)_{i-1}^{n+1} + b(C_l)_i^{n+1} - c(C_l)_{i+1}^{n+1} = d, \quad (4.46.1)$$

where

$$a = \frac{(\rho_m)_{i-1}^{n+1}}{\Delta z} \max \left[(v_m)_{i-\frac{1}{2}}^{n+1}, 0 \right], \quad (4.46.2)$$

$$b = \frac{(\rho_m)_i^n}{\Delta t} + \frac{(\rho_m)_{i-1}^{n+1}}{\Delta z} \max \left[(v_m)_{i-\frac{1}{2}}^{n+1}, 0 \right] + \frac{(\rho_m)_{i+1}^{n+1}}{\Delta z} \max \left[-(v_m)_{i+\frac{1}{2}}^{n+1}, 0 \right], \quad (4.46.3)$$

$$c = \frac{(\rho_m)_{i+1}^{n+1}}{\Delta z} \max \left[-(v_m)_{i+\frac{1}{2}}^{n+1}, 0 \right], \quad (4.46.4)$$

$$d = \frac{(D_r)_{i+\frac{1}{2}}^{n+1} - (D_r)_{i-\frac{1}{2}}^{n+1}}{\Delta z} + \frac{(C_l \rho_m)_i^n}{\Delta t}, \quad (4.46.5)$$

for $i = 1, 2, \dots, N$. Note that if we write Eq. 4.46.1, for all control volumes, in a matrix form, the coefficient matrix will be a tridiagonal matrix. Solution of the system of nonlinear algebraic equations will yield the oil component concentration distribution along the wellbore.

The evaluation of diffusion terms at the control volume boundaries needed in Eq. 4.46.5 deserves special treatment. For situations where both sides of a control volume boundary are in two-phase flow, the diffusion term can be evaluated with any averaging techniques so long as the same value is used for both control volumes to preserve mass balance. However, for situations where either side of a boundary

is in single-phase flow, the diffusion term should be zero. Alhanati⁶⁴ suggested that we chose the minimum value in the two adjacent cells, i.e., for $(D_r)_{i+\frac{1}{2}}$, we have

$$(D_r)_{i+\frac{1}{2}} = \min [(D_r)_i, (D_r)_{i+1}]. \quad (4.47)$$

The use of Eq. 4.47 will automatically take care of situations where either side of the face is in single-phase flow. Note that from the boundary condition at the wellhead, we should have $(D_r)_{N+\frac{1}{2}} = 0$. Since we consider single phase liquid flow in the bottomhole, we should also have $(D_r)_{\frac{1}{2}} = 0$.

It is a common practice to use overrelaxation to accelerate convergence or apply underrelaxation to slow down the changes in a variable to achieve convergence (see Refs. 63-66). Without relaxation, the new value for the oil component concentration from Eq. 4.46.1 is

$$(C_l)_i^{n+1} = \frac{[a(C_l)_{i-1}^{n+1} + c(C_l)_{i+1}^{n+1}] + d}{b}. \quad (4.48)$$

With relaxation, the new value will be computed as

$$(C_l)_i^{n+1} = \Theta \left[\frac{[a(C_l)_{i-1}^{n+1} + c(C_l)_{i+1}^{n+1}] + d}{b} \right] + (1 - \Theta)(C_l^*)_i^{n+1}, \quad (4.49)$$

where Θ is the relaxation factor and $(C_l^*)_i^{n+1}$ is the previous iteration value. Eq. 4.49 can be rearranged to give

$$-a(C_l)_{i-1}^{n+1} + \left(\frac{b}{\Theta}\right)(C_l)_i^{n+1} - c(C_l)_{i+1}^{n+1} = d + (1 - \Theta)\left(\frac{b}{\Theta}\right)(C_l^*)_i^{n+1} \quad (4.50.1)$$

or

$$-a(C_l)_{i-1}^{n+1} + b'(C_l)_i^{n+1} - c(C_l)_{i+1}^{n+1} = d', \quad (4.50.2)$$

where

$$b' = \left(\frac{b}{\Theta}\right), \quad (4.50.3)$$

and

$$d' = d + (1 - \Theta)\left(\frac{b}{\Theta}\right)(C_l^*)_i^{n+1}. \quad (4.50.4)$$

Eq. 4.50.2 indicates that relaxation can be achieved by slightly modifying the original finite difference equation, Eq. 4.46.1. Overrelaxation is achieved when using $1 < \Theta < 2$ and underrelaxation is obtained when setting $0 < \Theta < 1$. In this study, we begin the iteration process by using overrelaxation with $\Theta = 1.5$. If convergence is not achieved after a certain number of iterations, Θ will be subsequently reduced. For all cases presented in this report, convergence is obtained with $\Theta = 1.5$ and the number of iterations generally ranges from 15 to 30.

It should be pointed out that there is no guarantee that C_l obtained from Eq. 4.50.2 always remain in the interval $[0,1]$. If solution of Eq. 4.50.2 returns any values of C_l outside this range, the iteration process will no longer maintain the continuity of each individual fluid⁶⁷. Carver⁶⁷ suggested that since Eq. 4.50.2 is an expression of continuity, it is not sufficient merely to solve Eq. 4.50.2, and then correct stray values back into range. This will detract from continuity, as the remaining variables cannot be adjusted accordingly. Alhanati⁶⁴ and Carver⁶⁷ proposed modifications to Eq. 4.50.2 so that C_l obtained always stays in the desired interval. The idea is to separate the positive and negative components of d' . Let Eq. 4.50.2 be rewritten as

$$b'(C_l)_i^{n+1} = \left[a(C_l)_{i-1}^{n+1} + c(C_l)_{i+1}^{n+1} \right] + d'_1 - d'_2, \quad (4.51)$$

where d'_1 and d'_2 are the positive and negative components of d' , respectively. ($d' = d'_1 - d'_2$, $d'_1 \geq 0$, $d'_2 > 0$). Since all coefficients in Eq. 4.51 are positive, $(C_l)_i^{n+1}$

has chances to become negative only when $d'_1 < d'_2$. Under this condition, Eq. 4.51 is modified to

$$-a(C_l)_{i-1}^{n+1} + \left[b' + \frac{d'_2}{(C_l^*)_i^{n+1}} \right] (C_l)_i^{n+1} - c(C_l)_{i+1}^{n+1} = d'_1, \quad (4.52.1)$$

or

$$-a(C_l)_{i-1}^{n+1} + b''(C_l)_i^{n+1} - c(C_l)_{i+1}^{n+1} = d'', \quad (4.52.2)$$

where

$$b'' = \left[b' + \frac{d'_2}{(C_l^*)_i^{n+1}} \right], \quad (4.52.3)$$

and

$$d'' = d'_1. \quad (4.52.4)$$

Eq. 4.52.2 indicates that by modifying the coefficients of Eq. 4.50.2 the computed concentration is ensured to retain a positive sign, providing the previous iteration value is positive. On the other hand, if $d'_1 > d'_2$ in Eq. 4.51, solution of Eq. 4.51 will be guaranteed to give positive values for all positions. However, under this condition, there are chances for oil component concentrations to be greater than one. To keep the oil component concentration below one is the same as keeping the gas component concentration above zero. Therefore, we transform Eq. 4.51 to

$$b' [1 - (C_l)_i^{n+1}] = \left[\left[a [1 - (C_l)_{i-1}^{n+1}] + c [1 - (C_l)_{i+1}^{n+1}] \right] + [b' + d'_2] \right] - [a + c + d'_1]. \quad (4.53)$$

The strategy to keep $[1 - (C_l)_i^{n+1}]$ positive is the same as to keep $(C_l)_i^{n+1}$ positive. Therefore, proceeding as before, we modify Eq. 4.53 as

$$-a(1 - C_l)_{i-1}^{n+1} + \left[b' + \frac{a + c + d'_1}{1 - (C_l^*)_i^{n+1}} \right] (1 - C_l)_i^{n+1} - c(1 - C_l)_{i+1}^{n+1} = [b' + d'_2]. \quad (4.54)$$

Eq. 4.54 can be rearranged to give

$$-a(C_l)_{i-1}^{n+1} + \left[b' + \frac{a + c + d_1'}{1 - (C_l^*)_i^{n+1}} \right] (C_l)_i^{n+1} - c(C_l)_{i+1}^{n+1} = \frac{(a + c + d_2')(C_l^*)_i^{n+1} + d'}{1 - (C_l^*)_i^{n+1}}, \quad (4.55.1)$$

or

$$-a(C_l)_{i-1}^{n+1} + \hat{b}''(C_l)_i^{n+1} - c(C_l)_{i+1}^{n+1} = \hat{d}'', \quad (4.55.2)$$

where

$$\hat{b}'' = \left[b' + \frac{a + c + d_1'}{1 - (C_l^*)_i^{n+1}} \right], \quad (4.55.3)$$

and

$$\hat{d}'' = \frac{(a + c + d_2')(C_l^*)_i^{n+1} + d'}{1 - (C_l^*)_i^{n+1}}. \quad (4.55.4)$$

From the above derivation, it is clear that the implementation of relaxation and procedures to keep the oil component concentration within the correct range is quite simple. The only changes are in the coefficients of the original system of equations.

Simplified Momentum Equation: Finally, the simplified momentum equation is integrated over the i^{th} control volume. The result is

$$\frac{p_{i+\frac{1}{2}}^{n+1} - p_{i-\frac{1}{2}}^{n+1}}{\Delta z} = -(\rho_m)_i^{n+1} \frac{g}{144g_c}. \quad (4.56)$$

The three governing finite difference equations (Eq. 4.38, Eq. 4.52.2 or Eq. 4.55.2 and Eq. 4.56) are used to solve for the three primary dependent variables, v_m , C_l and p . These equations are not simultaneously solved over the entire flow domain, but rather we propose a sequential, iterative solution procedure as outlined in the next subsection.

4.4.2 Calculation Algorithm

Reading Input Data: Input data are classified into five categories:

1. Production data: sandface production rate, q RB/D, producing time, t_p hours, and gas injection rate, q_{ginj} scf/D, if it is a gas-lift well.
2. Wellbore description data: pipe inside diameter and length.
3. Fluid physical property data: ρ_{os} and ρ_{gs} , oil-gas surface tension, tabulated data for R_s , B_o and B_g as functions of pressure (assuming isothermal flow).
4. Reservoir related data: p_i , k , h , ϕ , c_t , μ , s and r_w .
5. Simulator control data: spatial increment, Δz , time step size, ΔT , total simulation time, T , and convergence tolerances, ϵ .

Note that R_s , B_o and B_g as functions of pressure and temperature are obtained from empirical correlations. In this study, R_s and B_o are calculated from Standing correlation⁶⁸ and B_g is computed from Eq. 4.57 using gas compressibility factor, z , obtained from Standing and Katz⁶⁹ correlation.

$$B_g = 0.0283 \frac{zT_w}{p}, \quad (4.57)$$

where T_w is the wellbore temperature in $^{\circ}R$. Also Note that for simplification, when simulating a buildup test in a gas-lift well, the gas injection point is located at the sandface. Furthermore, we assume no mass transfer between the injection gas and the producing fluid and the producing fluid is incompressible and contains no dissolved gas ($R_s = 0$).

Calculation of Initial Distributions of Dependent Variables: From the production rate, q , and producing time, t_p , we can calculate the bottomhole pressure at the instant of shut-in, $p_{wf,s}$, using the semilog approximation, Eq. 4.36.3. Once $p_{wf,s}$ is determined, values of B_o and R_s are obtained through linear interpolation

from the physical property table. With these parameters, we calculate the oil and gas component flow rate at standard conditions, i.e., $q_{os} = q/B_o$ (STB/D) and $q_{gs} = q_{os}R_s$ (scf/D). Note that for gas-lift wells, we have $q_{gs} = q_{ginj}$, according to our assumptions.

As previously stated, steady-state two-phase flow is assumed to exist in the wellbore prior to shut-in. For steady-state flow, if the pressure at a given position is known, all other variables can be calculated. The procedure is as follows:

- i. From the known pressure, calculate R_s , B_o and B_g through linear interpolation.
- ii. Calculate ρ_l and ρ_g using Eqs. 4.1.1 and 4.1.2.
- iii. From mass balances, calculate in-situ gas and liquid phase volumetric flow rates, q_g and q_l in $\text{ft}^3/\text{sec}.$:

$$q_g = \frac{5.615[q_{gs} - q_{os}R_s]B_g}{86400}, \quad (4.58.1)$$

$$q_l = \frac{5.615q_{os}B_o}{86400}. \quad (4.58.2)$$

- iv. Calculate superficial gas and liquid phase velocities, v_{sg} and v_{sl} , from Eqs. 4.10.1 and 4.10.2.
- v. Calculate relative velocity, v_r , from Eq. 4.29.2 or Eq. 4.30.2, depending on the existing flow pattern.
- vi. Obtain the gas void fraction (liquid holdup) from the following equation:

$$\frac{v_{sg}}{E_g} - \frac{v_{sl}}{1 - E_g} = v_r. \quad (4.59)$$

Note that Eq. 4.59 is obtained from Eqs. 4.12.1, 4.12.2 and 4.13.

- vii. Calculate the mixture density, ρ_m , and velocity, v_m , with Eqs. 4.6 and 4.14. Determine oil component concentration, C_l (Eq. 4.7.1), and total gas-oil ratio, R (Eq. 4.8). Using the value of R , we can obtain the corresponding bubble-point pressure by interpolation from the R_s versus p table.

Note that although in steady state flow the producing GOR (q_{gs}/q_{os}) is a constant along the wellbore, the total gas-oil ratio, R , is changing from the bottom-hole to the wellhead because of the slippage between the gas phase and the liquid phase.

The distributions of the dependent variables along the wellbore at the instant of shut-in are determined according to the following procedure:

1. Beginning at the bottomhole, from $p_{\frac{1}{2}} = p_{wf,s}$, we calculate $(v_m)_{\frac{1}{2}}$ using the procedure described above (Steps i-vii).
2. Guess pressure $p_{1+\frac{1}{2}}^*$.
3. Calculate $p_1 = 0.5[p_{\frac{1}{2}} + p_{1+\frac{1}{2}}^*]$.
4. Using p_1 , we determine $(C_l)_1$, $(\rho_m)_1$ and all other parameters from Steps i-vii.
5. Calculate $p_{1+\frac{1}{2}}$:

$$p_{1+\frac{1}{2}} = p_{\frac{1}{2}} - \frac{(\rho_m)_1 g}{144g_c} \Delta z. \quad (4.60)$$

6. If $|p_{1+\frac{1}{2}} - p_{1+\frac{1}{2}}^*| > \epsilon$, let $p_{1+\frac{1}{2}}^* = p_{1+\frac{1}{2}}$ and go back to step 3.
7. Once calculation converges, calculate $(v_m)_{1+\frac{1}{2}}$ using $p_{1+\frac{1}{2}}$ following Steps i-vii.
8. Repeat Steps 2-7 for all other control volumes until we reach the wellhead.

Calculation at a New Time Step: During pressure buildup, pressure, mixture velocity and oil component mass concentration distributions in the wellbore at a new time step are determined using the following procedure:

1. Guess a new oil component mass concentration profile $(C_i^*)_i^{n+1}$ for $i = 1, \dots, N$.
2. Calculate the distribution of the total gas-oil ratio, R , from Eq. 4.8 and determine the distribution of the bubble-point pressure along the wellbore from linear interpolation with the physical property table.
3. Calculate the sandface velocity, $(v_m)_{\frac{1}{2}}^{n+1}$, that satisfies both the bottomhole boundary condition, Eq. 4.32, and the wellbore mass conservation, Eq. 4.39, by the following procedure:
 - 3.1 Assume a sandface velocity.
 - 3.2 From the bottomhole boundary condition, Eq. 4.32, calculate the bottomhole pressure, $p_{\frac{1}{2}}^{n+1} = p_{ws}^{n+1}$.
 - 3.3 Guess pressure $p_{1+\frac{1}{2}}^*$.
 - 3.4 Calculate $p_1 = 0.5[p_{\frac{1}{2}} + p_{1+\frac{1}{2}}]$.
 - 3.5 Obtain R_s , B_o and B_g from physical property table using p_1 . Calculate ρ_l and ρ_g from Eqs. 4.1.1 and 4.1.2.
 - 3.6 Calculate E_l from Eq. 4.9.2 and calculate ρ_m from Eq. 4.6.
 - 3.7 Calculate $p_{1+\frac{1}{2}}$ from Eq. 4.60.
 - 3.8 If $|p_{1+\frac{1}{2}} - p_{1+\frac{1}{2}}^*| > \epsilon$, let $p_{1+\frac{1}{2}}^* = p_{1+\frac{1}{2}}$ and go back to step 3.4.
 - 3.9 Repeat Steps 3.3-3.8 over all control volumes.
 - 3.10 Calculate a new sandface velocity from Eq. 4.39.
 - 3.11 To accelerate convergence on the sandface velocity from Steps 3.1 to 3.10, the secant method⁷⁰ is applied. Let x_0 and x_1 represent two initial guesses of the sandface velocity, and Δx_0 and Δx_1 denote the corresponding velocity differences between the guessed value and the

one obtained from Steps 3.2-3.10. Based on the secant method, a new velocity should be determined as

$$x_2 = x_1 - \frac{\Delta x_1(x_1 - x_0)}{\Delta x_1 - \Delta x_0}. \quad (4.61)$$

3.12 Upon calculation of x_2 , a check of convergence is made. If convergence is not achieved, use the two latest sandface velocities and repeat Steps 3.2-3.11 until convergence. Note that the mixture velocity at the sandface is also the liquid phase velocity since we consider single flow from the reservoir and, for gas-lift wells, the injection of gas is terminated upon shut-in.

4. Update the mixture velocity distribution from Eq. 4.38 from bottomhole to wellhead applying $(v_m)_{\frac{1}{2}}^{n+1}$ calculated at step 3.
5. Update the oil component mass concentration from Eq. 4.52.2 and/or 4.55.2.
6. Check convergence. If $|(C_l)_i^{n+1} - (C_l^*)_i^{n+1}| < \epsilon$ is not satisfied for any i ($i = 1, 2, \dots, N$), replace $(C_l^*)_i^{n+1}$ by $(C_l)_i^{n+1}$ for $i = 1, 2, \dots, N$ and go back to step 2.
7. Repeat steps 1-6 for all time steps.

4.5 Results and Discussion

A computer simulator has been developed to implement the proposed solution algorithm. In this section, pressure responses generated with the simulator for three pressure buildup tests are presented and analyzed. Case A is a buildup test in a naturally flowing well where only single-phase oil flows in the wellbore prior to shut-in. Case B is also a buildup test in a naturally flowing well, but unlike Case A, the bottomhole flowing pressure in Case B is slightly higher than the reservoir fluid initial bubble-point pressure and as a result, two-phase flow develops in the

wellbore during production. Case C represents a pressure buildup test conducted in a gas-lift well producing only single phase oil from the reservoir.

4.5.1 Case A

For pressure buildup tests conducted in wells having only single phase oil in the wellbore, the wellbore storage is due to wellbore fluid compression. Buildup data acquired in these tests can be analyzed with Horner analysis and type-curve matching with the classical wellbore storage and skin drawdown type curves to yield values of formation flow capacity, skin factor, initial reservoir pressure and the wellbore storage coefficient.

Case A was chosen to verify our simulator under single phase liquid flow conditions in the wellbore. Table 4.1 presents a list of input parameters for Case A. As indicated, we consider a 120-hour flow period followed by a 20-hour (72,000 seconds) buildup test. It should be pointed out that for single-phase flow, there is no separation of gas and oil components; thus, the bubble-point pressure remains constant along the wellbore, and for pressure above the bubble-point pressure, the oil formation volume factor can be computed as

$$B_o = B_{ob} \exp[-c_o(p - p_b)], \quad (4.62)$$

where B_{ob} is the oil formation volume factor at the bubble-point pressure, p_b , and c_o is the oil compressibility, in 1/psi, and is assumed to be a constant.

We now analyze the pressure response generated with the simulator for Case A. A log-log plot of buildup data for Case A is shown in Fig. 4.2. Early time pressure and pressure derivative data form a unit slope straight line, showing the effect of wellbore storage. As shown in Fig. 4.2, nonlinear regression with the classical wellbore storage and skin model yields parameters which are in excellent agreement with their corresponding input values. The input value for the wellbore

Table 4.1
Input Parameters for Case A

Parameter	Value	Unit
Drawdown oil production rate	100.0	RB/D
Total producing time	120.0	Hours
Initial reservoir pressure	5215.0	psia
Initial bubble point pressure	214.7	psia
Oil compressibility ($p > p_b$)	1.0E-5	1/psi
Oil formation volume factor at $p = p_b$	1.06	RB/STB
Oil component API gravity at S.C.	45.0	API
Gas component specific gravity at S.C.	0.70	-
Oil-gas surface tension	4.5	dynes/cm
Wellbore pipe inside diameter	1.80	in.
Formation absolute permeability	25.0	md
Formation thickness	10.0	ft
Formation porosity	0.20	-
Wellbore radius	0.364	ft
System isothermal compressibility	2.0E-5	1/psi
Average oil viscosity	2.0	cp
Skin factor	15.0	-
Wellbore depth	6000.0	ft
Spatial increment	30.0	ft
Buildup simulation time	72000.0	sec.
Time step	4.0	sec.
Convergence tolerance	1.0E-06	-

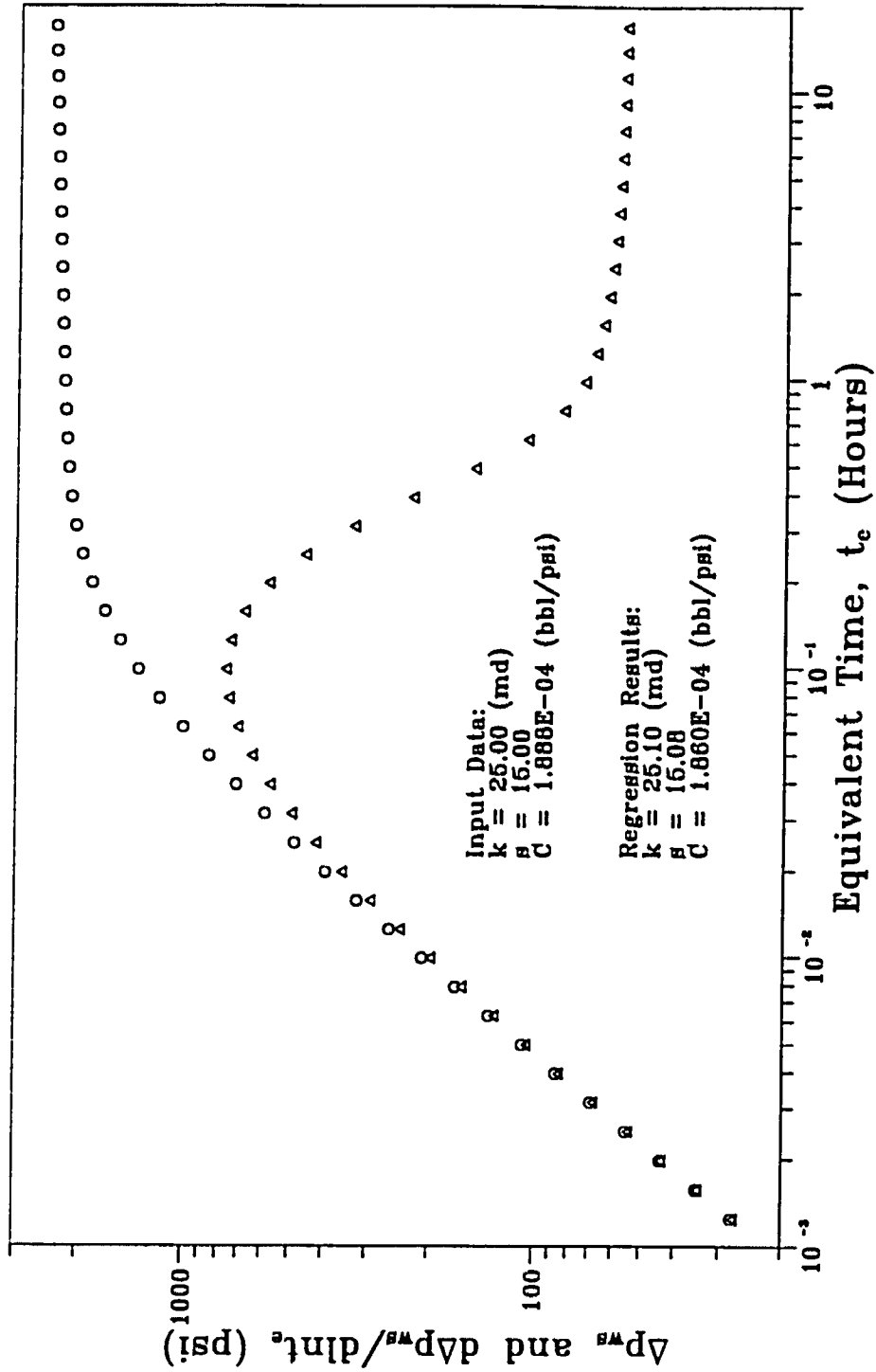


Fig. 4.2 - Type Curve Analysis for Case A, Single Phase Oil Well

storage coefficient shown in Fig. 4.2 is calculated from the input oil compressibility ($c = 1.0 \times 10^{-5}$) and the wellbore volume.

Fig. 4.3 is a Horner plot of pressure buildup data from Case A. As shown, at late times, buildup data exhibits a semilog straight line. Semilog analysis of this data yields estimates of flow capacity, skin factor and the initial reservoir pressure. As presented in Fig. 4.3, all calculated parameters agree very well with their corresponding input values. At early time, pressure data deviate from the straight line; this deviation is attributable to the effect of wellbore storage.

Fig. 4.4 shows the variation of sandface flow rate as a function of shut-in time. Note that the ordinate uses a log scale and the abscissa uses a Cartesian scale. It can be seen that the sandface rate undergoes a significant decline at early shut-in times, i.e., at the beginning of the test, and is approximately a straight line, indicating that rate decline is approximately of an exponential form, as suggested by Van Everdingen and Hurst²⁰.

The bottomhole pressure and sandface flow rate generated with the simulator can be used to calculate the wellbore storage coefficient. The wellbore storage coefficient is defined as the change of total volume of wellbore fluids per unit change in bottomhole pressure²:

$$C = \frac{\Delta V}{\Delta p}, \quad (4.63)$$

where ΔV is the change in volume of fluid in the wellbore at wellbore conditions, bbl, and Δp is the change in bottomhole pressure, psi. For pressure buildup tests, Eq. 4.63 can be written as

$$C = \frac{dV/dt}{dp_{ws}/dt} = \frac{q_{sf}/24}{dp_{ws}/dt}, \quad (4.64)$$

where q_{sf} is in RB/D and p_{ws}/dt is in psi/hour. Applying bottomhole pressure and sandface flow rate data for Case A in Eq. 4.64, a constant wellbore storage

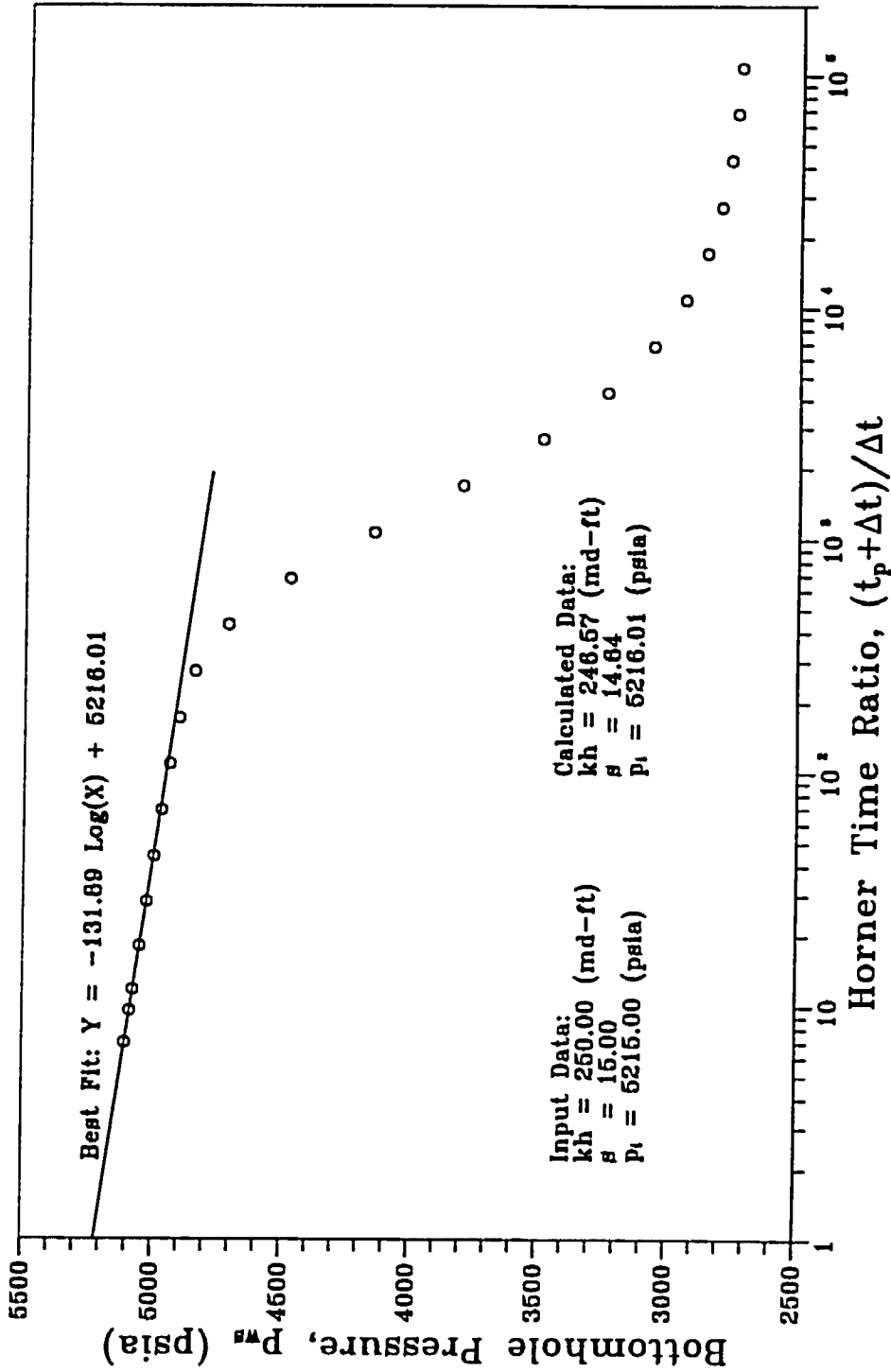


Fig. 4.3 - Horner Plot of Pressure Buildup Data for Case A

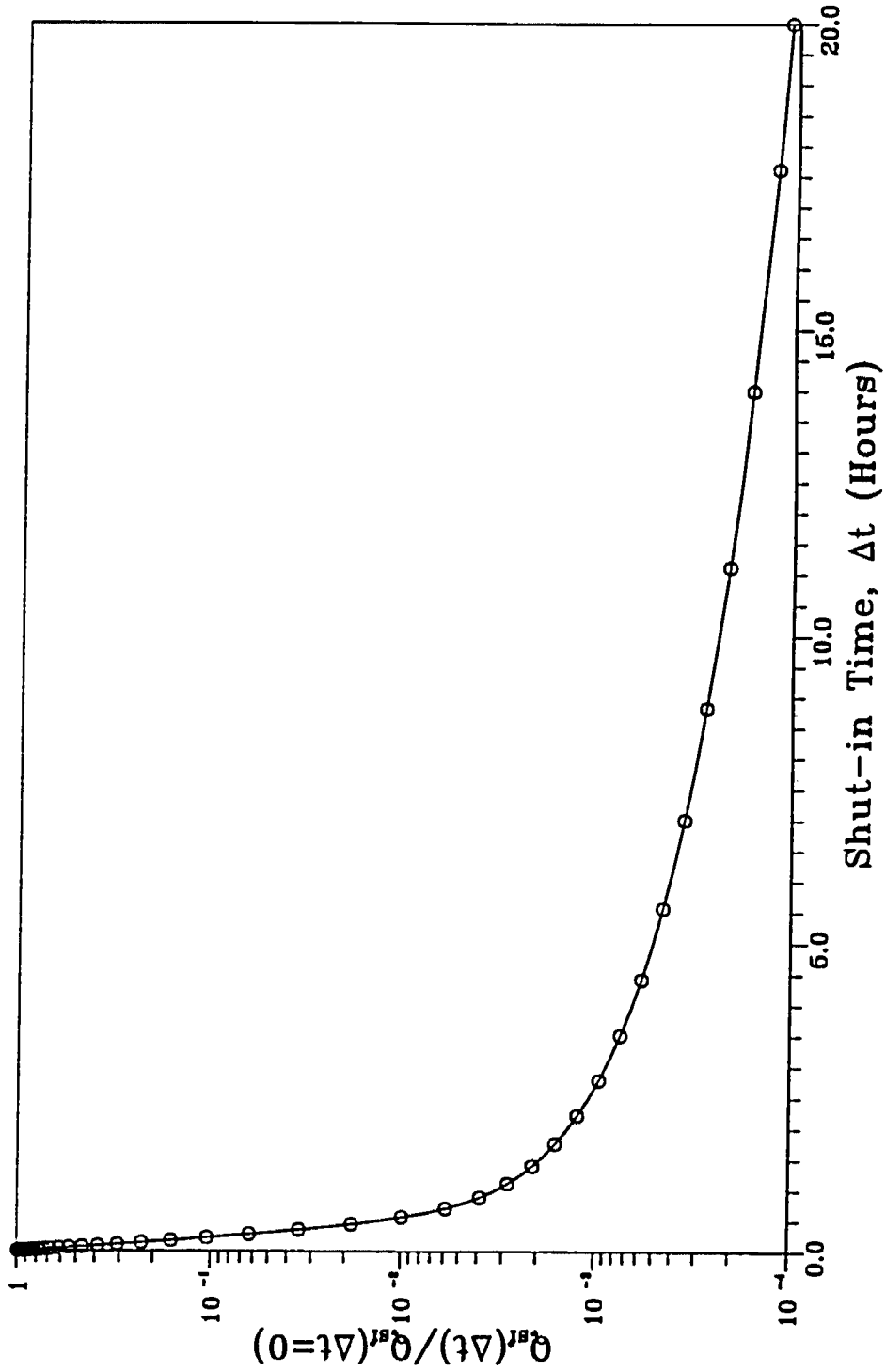


Fig. 4.4 - Sandface Flow Rate Ratio as a Function of Shut-in Time, Case A

coefficient of 1.85×10^{-4} bbl/psi is obtained for the entire duration of the test even though both p_{ws} and q_{sf} are varying. The calculated value for C is in excellent agreement with the input value which is computed from the input oil compressibility and the wellbore volume.

Results shown in Figs. 4.2-4.4 validate our model and solution algorithm, at least for the single-phase flow case.

4.5.2 Case B

Case B is also a pressure buildup test in a well that was flowed at a constant sandface rate for 120 hours prior to conducting a 20-hour pressure buildup test. However, unlike Case A, our objective here is to simulate the transient process of wellbore phase segregation and to examine its effect on pressure buildup data analysis. To that end, input parameters for Case B are chosen such that bottomhole pressure is only a few psi higher than the initial reservoir bubble-point pressure, and consequently, fluids come out of the reservoir as single-phase flow and develop into two-phase flow in the wellbore. Table 4.2.1 gives a list of input parameters used in Case B and Table 4.2.2 tabulates B_o , R_s and B_g as functions of pressure (Wellbore temperature is assumed to be $150^\circ F$).

Fig. 4.5 presents a log-log plot of buildup data generated for Case B. Toward the end of the buildup test, the derivative plot is still slightly decreasing, and therefore, fitting a semilog straight line through the last few data points will yield a low estimate of kh . At early times, Fig. 4.5 shows that both pressure and derivative data form a unit slope line. Although wellbore phase segregation is taking place, this part of the buildup data shows the basic appearance of the classical wellbore storage and skin solution. However, in the transition region, the derivative data plot rises above the pressure data, a characteristic indicative of a decreasing wellbore storage coefficient⁴⁶. The behavior of the buildup data shown in Fig. 4.5 is comparable to the behaviors of field data reported by Hegeman et al.⁴⁶. An explanation for the

Table 4.2.1
Input Parameters for Case B

Parameter	Value	Unit
Drawdown oil production rate	100.0	RB/D
Total producing time	120.0	Hours
Initial reservoir pressure	5215.0	psia
Initial bubble point pressure	2710.0	psia
Oil compressibility ($p > p_b$)	1.0E-5	1/psi
Oil component API gravity at S.C.	45.0	API
Gas component specific gravity at S.C.	0.70	-
Oil-gas surface tension	4.5	dynes/cm
Wellbore pipe inside diameter	1.80	in.
Formation absolute permeability	25.0	md
Formation thickness	10.0	ft
Formation porosity	0.20	-
Wellbore radius	0.364	ft
System isothermal compressibility	2.0E-5	1/psi
Average oil viscosity	2.0	cp
Skin factor	15.0	-
Wellbore depth	9000.0	ft
Spatial increment	30.0	ft
Buildup simulation time	72000.0	sec.
Time step	4.0	sec.
Convergence tolerance	1.0E-06	-

Table 4.2.2
Physical Properties As Functions of Pressure for Case B

p (psia)	B_o (RB/STB)	R_s (scf/STB)	B_g (RB/scf)
214.7	1.059474	45.256641	0.139674E-01
414.7	1.082794	100.044716	0.705830E-02
614.7	1.109518	160.754761	0.464529E-02
814.7	1.139001	225.723618	0.342061E-02
1014.7	1.170882	294.077362	0.268376E-02
1214.7	1.204915	365.266510	0.219513E-02
1414.7	1.240920	438.909729	0.185027E-02
1614.7	1.278753	514.725098	0.159619E-02
1814.7	1.318298	592.494812	0.140309E-02
2014.7	1.359457	672.044739	0.125281E-02
2214.7	1.402147	753.232605	0.113366E-02
2414.7	1.446294	835.939514	0.103775E-02
2614.7	1.491835	920.064026	0.959553E-03
2814.7	1.538714	1005.519287	0.895068E-03
3014.7	1.586879	1092.229370	0.841354E-03
3214.7	1.636284	1180.127563	0.796194E-03
3414.7	1.686889	1269.154541	0.757891E-03
3614.7	1.738654	1359.257568	0.725133E-03
3814.7	1.791545	1450.389038	0.696891E-03
4014.7	1.845530	1542.505493	0.672355E-03
4214.7	1.900579	1635.567871	0.650881E-03
4414.7	1.956664	1729.540405	0.631954E-03
4614.7	2.013758	1824.389648	0.615160E-03
4814.7	2.071839	1920.085938	0.600165E-03
5014.7	2.130883	2016.600464	0.586700E-03
5214.7	2.190870	2113.907959	0.574546E-03
5414.7	2.251778	2211.983643	0.563524E-03
5614.7	2.313589	2310.804688	0.553491E-03
5814.7	2.376285	2410.350342	0.544329E-03
6014.7	2.439848	2510.600098	0.535942E-03

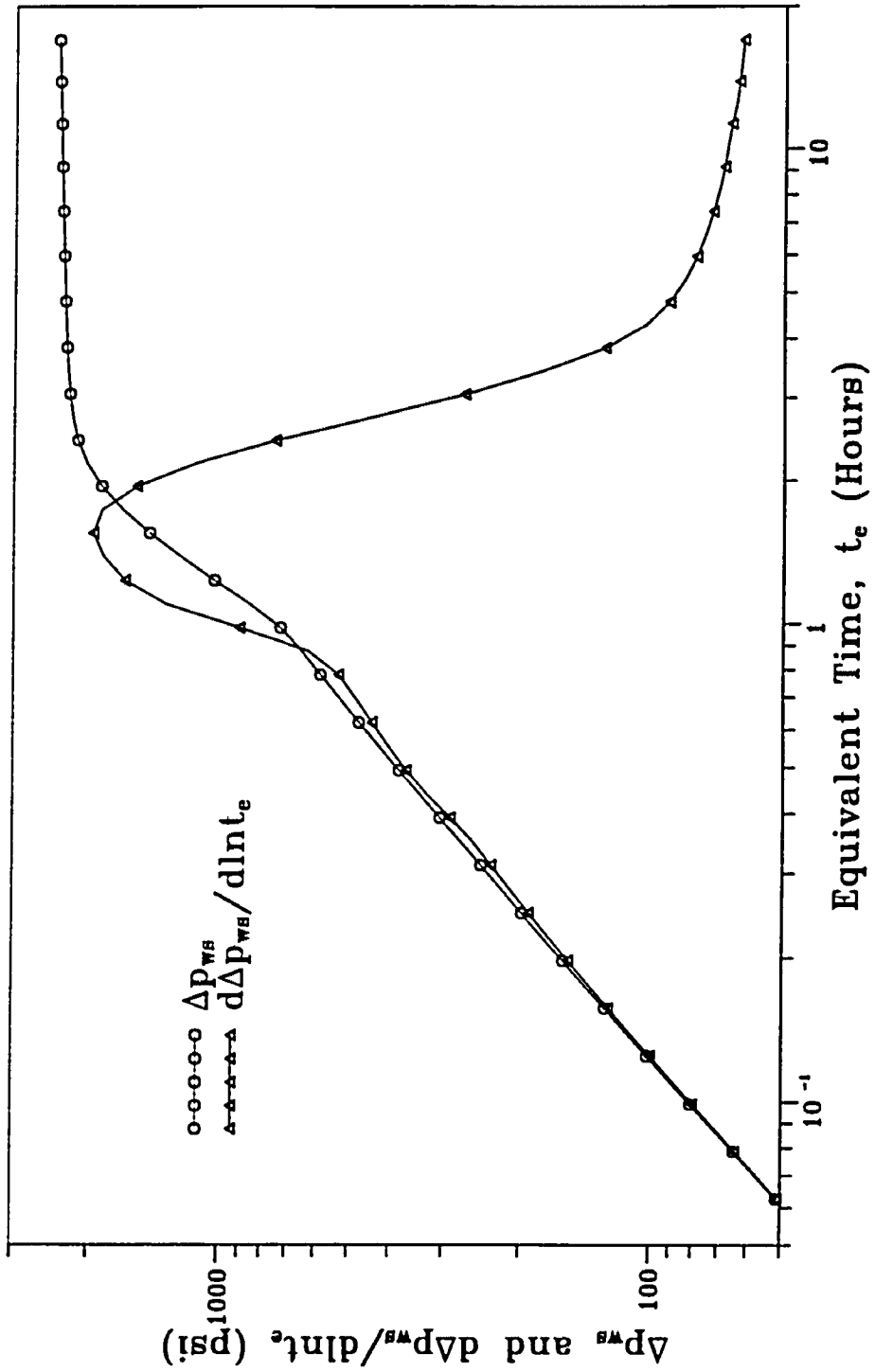


Fig. 4.5 - Type Curve Analysis for Case B, Naturally Flowing Well

decreasing wellbore storage behavior is provided by our analysis of the results of Fig. 4.6.

The distributions of the gas void fraction along the wellbore for several Δt values are shown in Fig. 4.6. Note that the total wellbore depth is 9000 ft, and in Fig. 4.6, distributions in only the top 1000 ft of the wellbore are shown. Comparing the profiles at $\Delta t = 0$ and $\Delta t = 240$ sec., one can see that gas void fraction for the top 200 ft has increased, and at the wellhead, a single-phase gas zone has been formed by $\Delta t = 240$ seconds. For positions below 200 ft, the gas void fraction has decreased slightly during the first 240 seconds of shut-in. This decrease in the gas void fraction is a result of two factors: the decrease in the gas volume due to compression and the decrease in the amount of free gas due to redissolving free gas, both because of increases in wellbore pressure. As the buildup test continues, a single-phase gas zone propagates downward from the wellhead. At the same time, a single-phase liquid zone is propagating upward from the bottomhole. At $\Delta t = 4080$ seconds, the two phases are just about to completely segregate from each other. At this moment, the wellbore contains a single phase gas column of 600 ft at the top with the rest of the wellbore filled with liquid. After $\Delta t = 4080$ seconds, the gas-oil interphase has continuously moved upward. This implies that the gas column has been continuously compressed. Note that $\Delta t = 4080$ seconds corresponds to $t_e = 1.12$ hours which is approximately the time at which the pressure/pressure derivative responses in Fig. 4.5 show an anomalous behavior. In view of the study for closed chamber tests in oil wells in *Chapter II*, it can be concluded that the decreasing wellbore storage behavior in buildup data of Case B is due to the compression of the gas column after wellbore phase segregation has ceased.

Fig. 4.7 is a Horner plot of pressure buildup data for Case B. Based on the results of Fig. 4.5, we fit the last 6 data points with a straight line. Horner analysis yields flow capacity, skin factor and the initial reservoir pressure. As expected

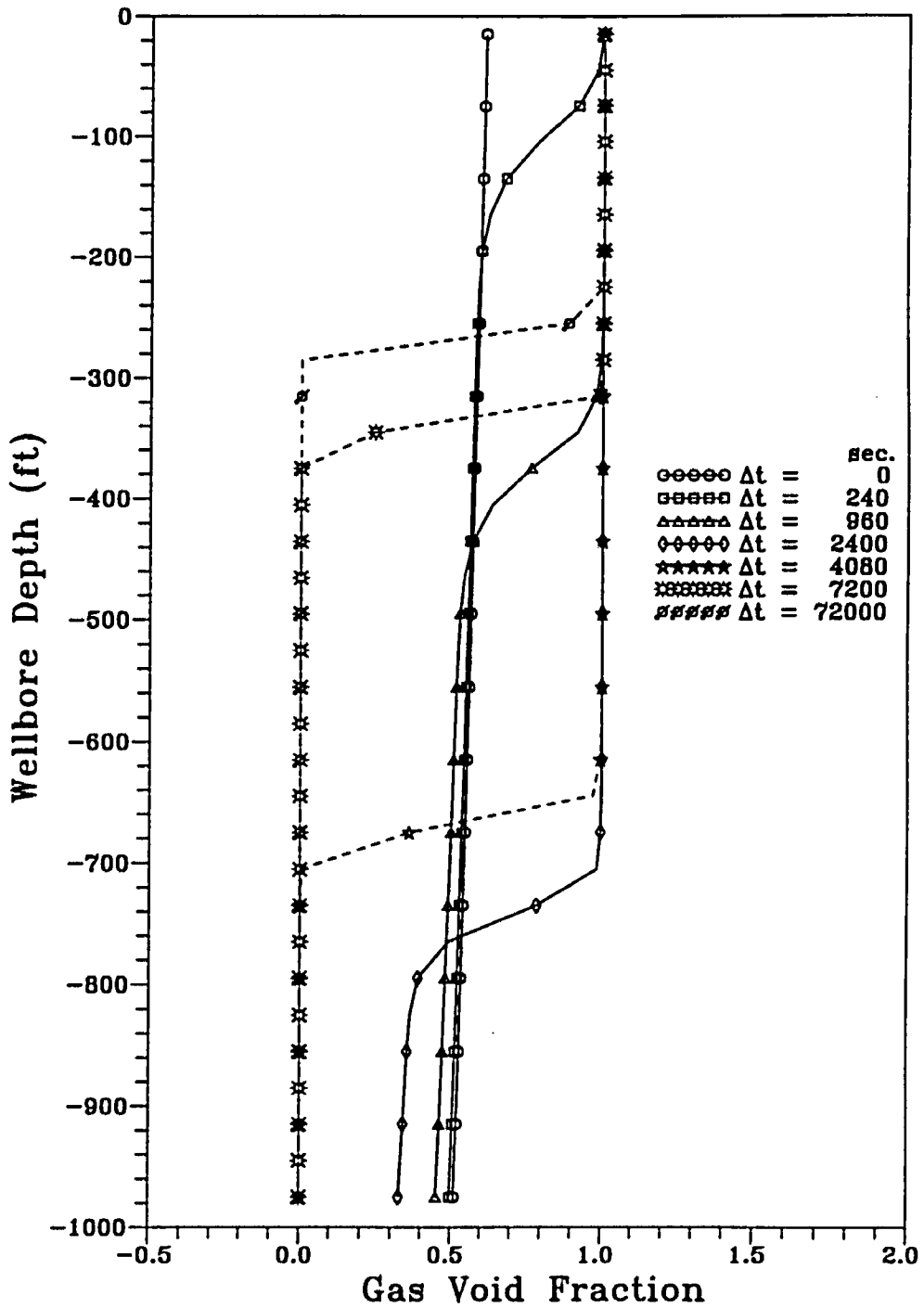


Fig. 4.6 - Gas Void Fraction Distribution, Case B

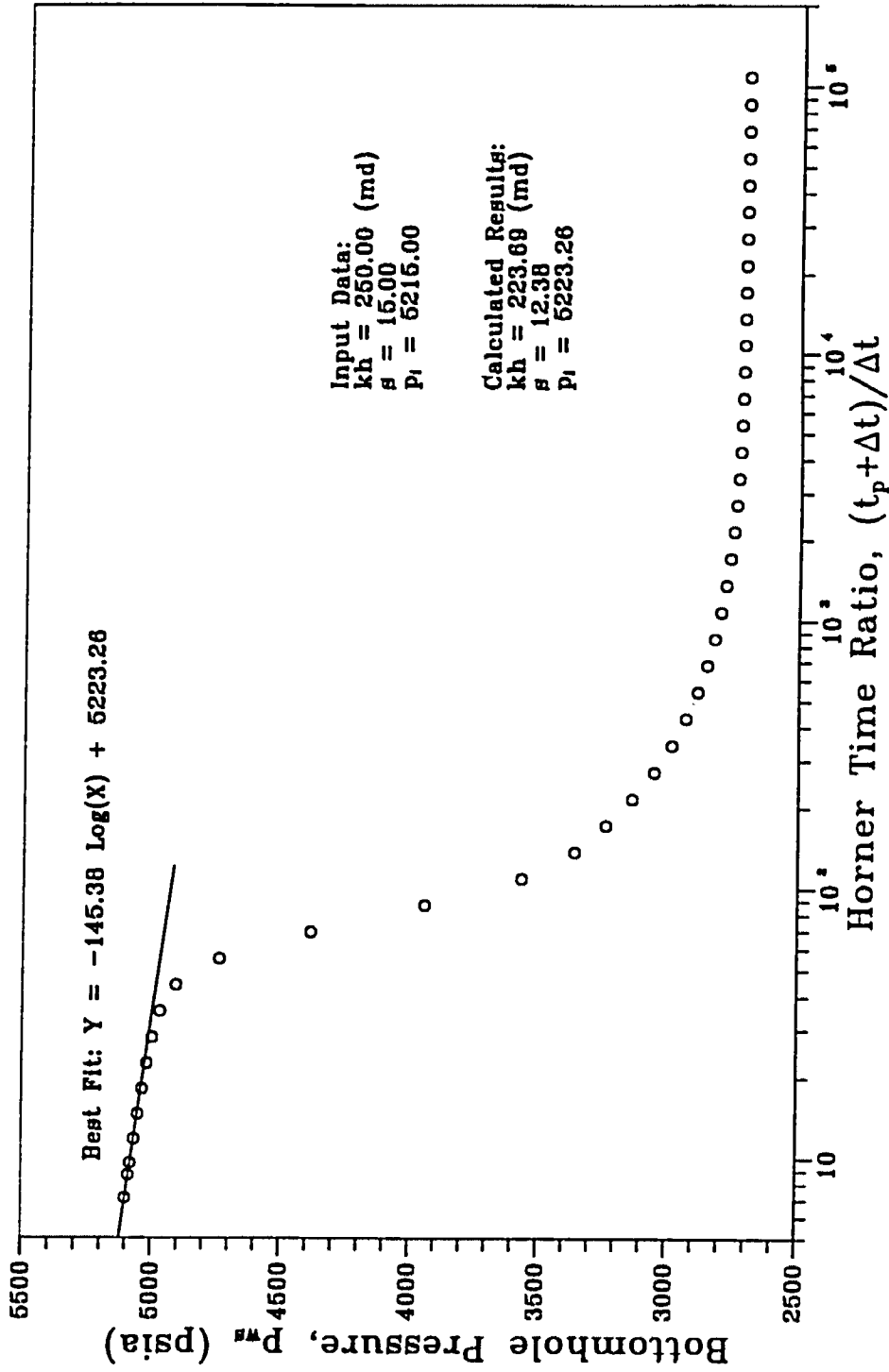


Fig. 4.7 - Horner Plot for Case B, Naturally Flowing well

from the results of Fig. 4.5, our parameter estimates are not highly accurate and specifically, we obtain a low estimate of kh .

Fig. 4.8 presents sandface flow rate as a function of shut-in time. Comparing with Case A, the sandface flow rate for Case B decreases more slowly. Also notice that although phase segregation takes place in the wellbore, the phase segregation pressure rise is not large enough to push wellbore fluids back into the reservoir.

The wellbore storage coefficient calculated from Eq. 4.64 for Case B is presented in Fig. 4.9. As shown in Fig. 4.9, this well experiences an order of magnitude decrease in the wellbore storage coefficient during the 20-hour pressure buildup test. At early times, buildup data show a constant wellbore storage coefficient. The wellbore storage coefficient declines sharply around $\Delta t = 1.0$ hour, which roughly corresponds to the time when the gas column begins to be compressed. At late times, the well again behaves like a well with a constant wellbore storage coefficient.

4.5.3 Case C

Although a additional pressure rise will result whenever phase segregation occurs in the wellbore, not all phase segregation can produce a hump in wellbore pressure. With Case C, we show that our simulator can also used to simulate pressure buildup tests in gas-lift wells. Moreover, unlike Case B, buildup data in Case C shows a substantial pressure hump. To simplify the analysis, for Case C, the following assumptions are made: 1) the injection point is placed at the sandface; 2) nitrogen is used as the injection gas, and hence no mass transfer is considered between the injection gas and the fluid produced from the reservoir; 3) the produced oil is incompressible, i.e., $B_o = 1$, and does not contain solution gas, i.e., $R_s = 0$. All other parameters are listed in Table 4.3. Again we consider a 120-hour flow period followed by a 20-hour buildup test.

Fig. 4.10 shows the changes in bottomhole pressure and wellhead pressure for the Case C buildup test. Also shown in Fig. 4.10 is the difference between

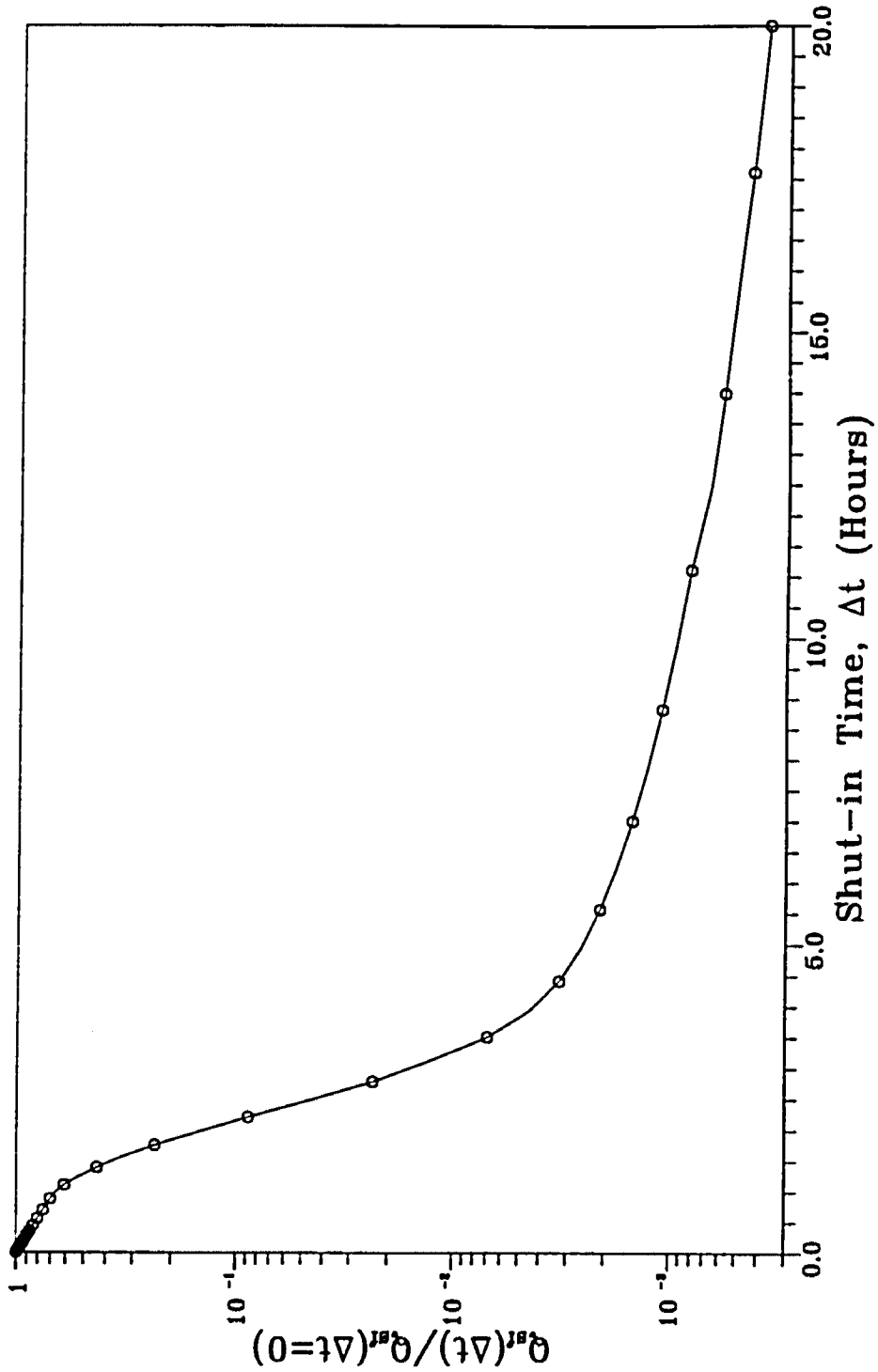


Fig. 4.8 - Sandface Flow Rate Ratio as a Function of Shut-in Time, Case B

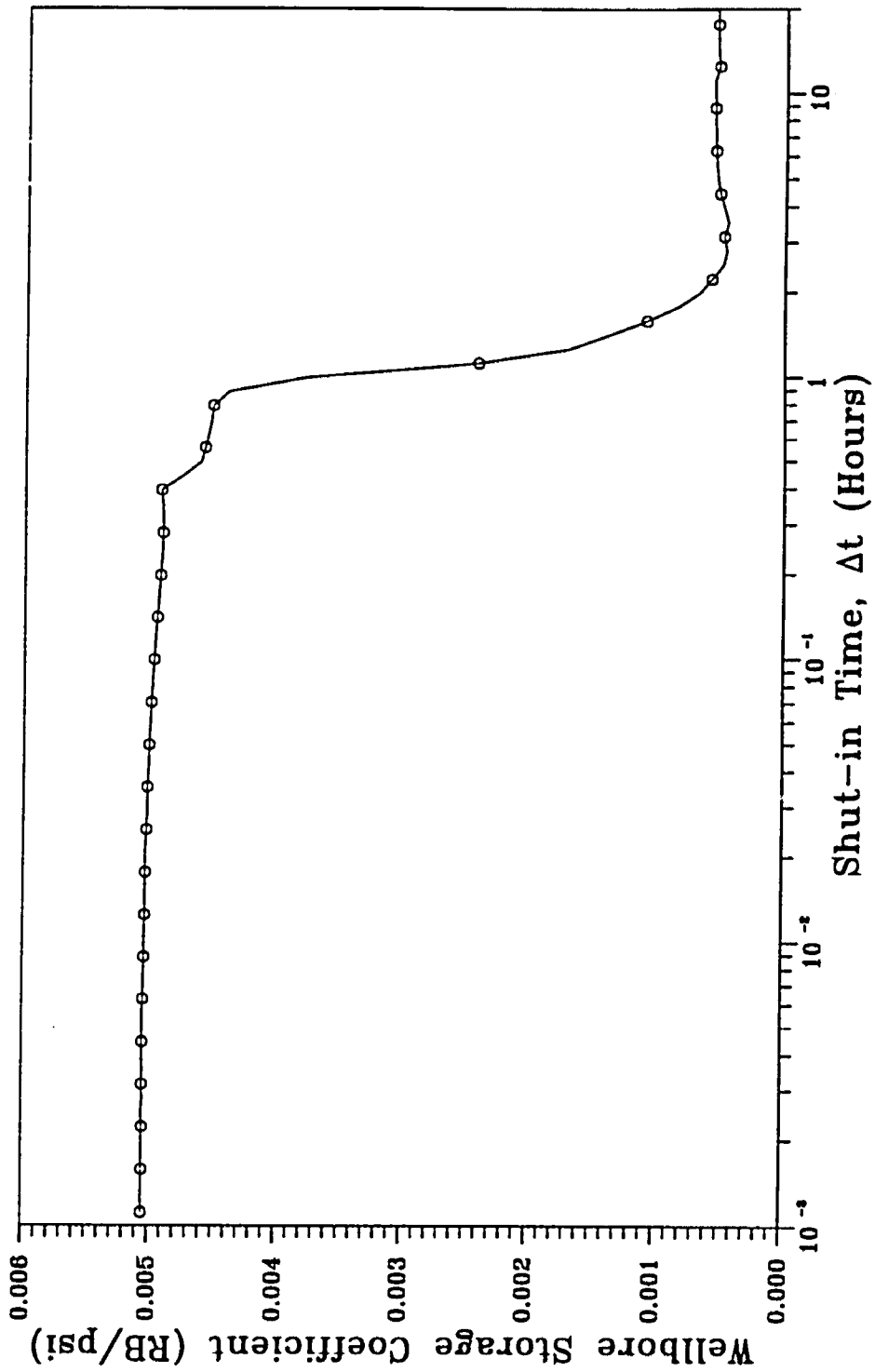


Fig. 4.9 - Change of Wellbore Storage Coefficient for Case B

Table 4.3
Input Parameters for Case C

Parameter	Value	Unit
Drawdown oil production rate	100.0	RB/D
Gas injection rate	200000.0	scf/D
Total producing time	120.0	Hours
Initial reservoir pressure	5215.0	psia
Oil compressibility	0.0	1/psi
Oil component API gravity at S.C.	45.0	API
Gas component specific gravity at S.C.	0.9665	-
Oil-gas surface tension	4.5	dynes/cm
Wellbore pipe inside diameter	1.80	in.
Formation absolute permeability	25.0	md
Formation thickness	75.0	ft
Formation porosity	0.20	-
Wellbore radius	0.364	ft
System isothermal compressibility	2.0E-5	1/psi
Average oil viscosity	2.0	cp
Skin factor	20.0	-
Wellbore depth	9000.0	ft
Spatial increment	30.0	ft
Buildup simulation time	72000.0	sec.
Time step	4.0	sec.
Convergence tolerance	1.0E-06	-

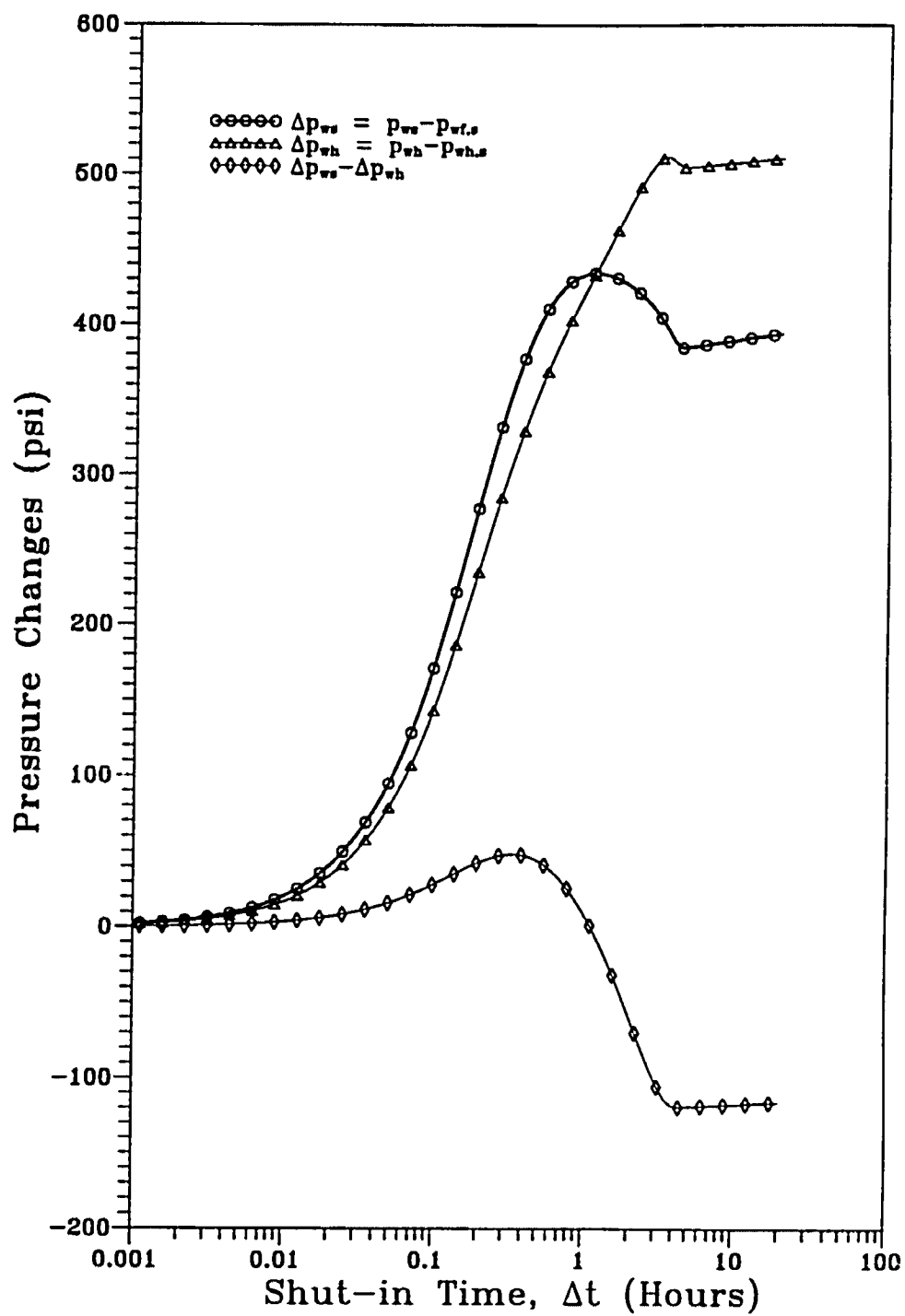


Fig. 4.10 - Pressure Buildup, Case C

the two pressure response curves. Since in our model, frictional pressure drop is neglected, the value of the difference curve is proportional to the amount of fluid which has entered into the wellbore after shut-in, regardless of the wellbore phase redistribution. Any increase in the difference curve represents an increase in mass of material in the wellbore, and, conversely, a decrease in the difference curve implies an outward flow of material from the wellbore. In Fig. 4.10, the difference curve rises in the beginning of the test, indicating a normal afterflow into the wellbore. At $\Delta t = 0.3$ (hours), the difference curve reaches a maximum value. After this time, the wellbore pressure exceeds the adjacent reservoir pressure and an outward flow of fluids from the wellbore begins to take place, even though the wellbore pressure is still below the initial reservoir pressure. As the test continues, the difference curve becomes negative, resembling liquid efflux behaviors reported by Mattar⁷¹. The bottomhole pressure shows a pressure hump of 25 psi, i.e., at its maximum, p_{ws} is approximately 25 psi above $p_i = 5215$ psia. Due to strong backflow, the wellbore pressure decreases below the initial reservoir pressure after it passes the maximum value. It is interesting to note that the wellhead pressure continues to rise after the wellbore pressure begins to decline due to the continuous migration of gas bubbles. After most of the gas has moved to the top, the wellhead pressure begins to decline because of continued backflow. This anomalous wellhead pressure behavior has been reported by Stegemeier and Matthews⁴³ and Kazemi et al.⁷². At late time, all three curves shown in Fig. 4.10 increase slightly because of a slow afterflow.

Fig. 4.11 is a log-log plot of the buildup data. At early times, both pressure and pressure derivative data exhibit a unit slope straight line, despite the effect of wellbore phase segregation. At late times, the derivative data approach a constant, suggesting that the flow is in the infinite acting radial flow region so that Horner analysis should be applicable. The derivative data in the transition period display a

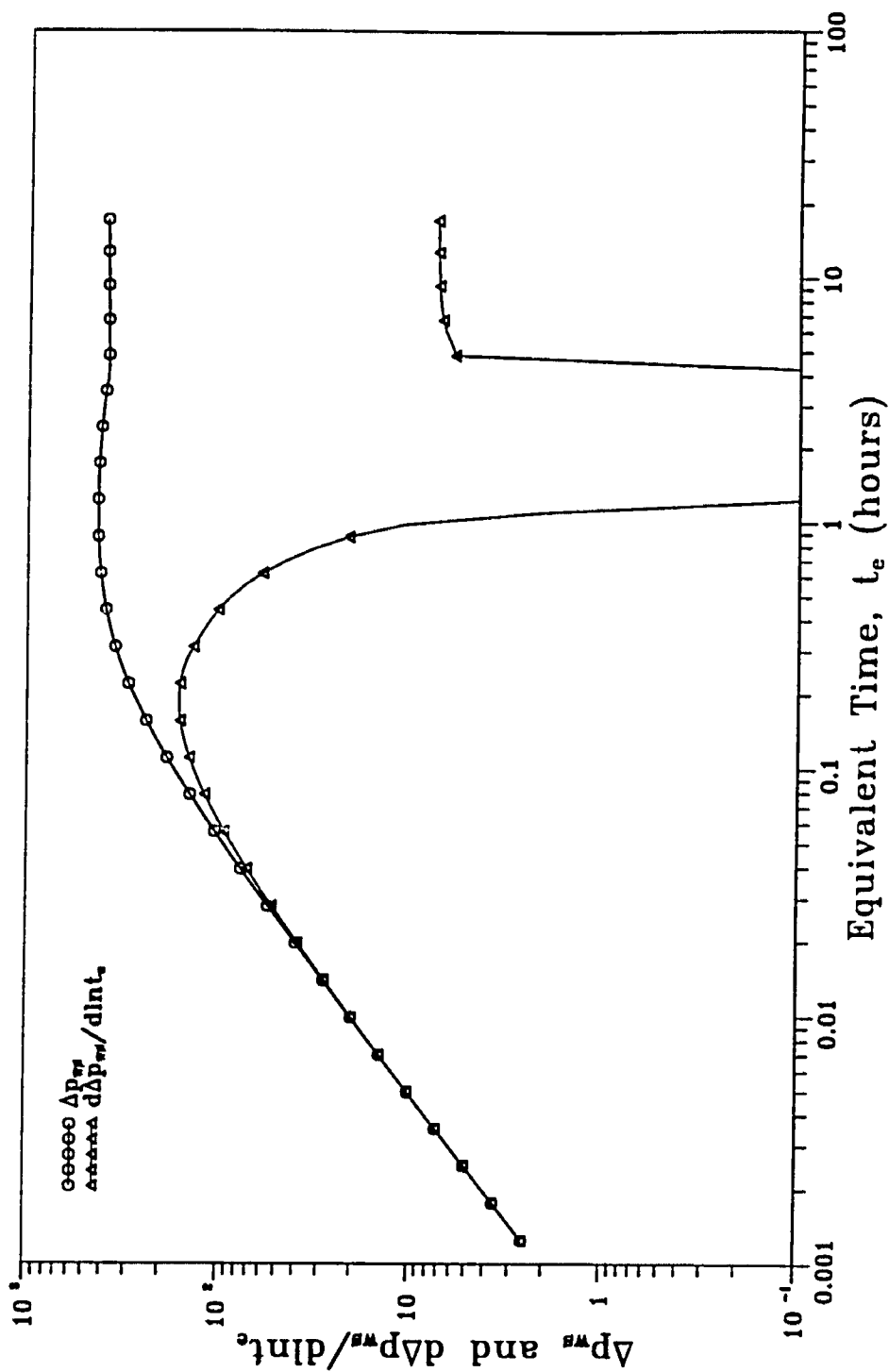


Fig. 4.11 - Type Curve Analysis for Case C, Gas-lift Well

v-shaped depression and even become negative. The pressure and pressure derivative characteristics showing in Fig. 4.11 are comparable to those reported by Fair⁴⁵ and Olarewaju⁸.

The distributions of the gas void fraction along the wellbore for a few Δt values are presented in Fig. 4.12. As shown, as the buildup test progresses, the single-phase zone grows. At $\Delta t = 5$ hours, gas and oil have been completely segregated. Note that from $\Delta t = 5$ hours to the end of the buildup test, i.e., $\Delta t = 20$ hours, the gas-oil contact remains almost unchanged. This implies that after phase segregation is completed afterflow becomes insignificant. Consequently, the effect of gas column compression is negligible.

Horner analysis of the pressure buildup data is performed. Fig. 4.13 shows that early time data are influenced by the effects of wellbore storage and wellbore phase segregation. The wellbore pressure hump can be clearly seen. At late times, a straight line develops, as noted in our discussion of Fig. 4.11. Analysis yields excellent estimates of flow capacity, skin factor and the initial reservoir pressure, as indicated in Fig. 4.13.

Fig. 4.14 shows the change of the wellbore storage coefficient for Case C. At early times, buildup data show a constant wellbore storage coefficient. Then, a transition period follows during which the wellbore storage coefficient decreases and even becomes negative, indicating a reversal in the direction of flow. Once the wellbore pressure passes the maximum hump point, the wellbore storage coefficient becomes a large positive number, but as the test continues, the wellbore storage coefficient decreases. At late times, the well again acts like a well with constant storage. The wellbore storage coefficient at late times is approximately 40% larger than the wellbore storage coefficient at early times.

Buildup data from both Case B and Case C are influenced by wellbore phase segregation. However, buildup data from Case B clearly show a decreasing wellbore

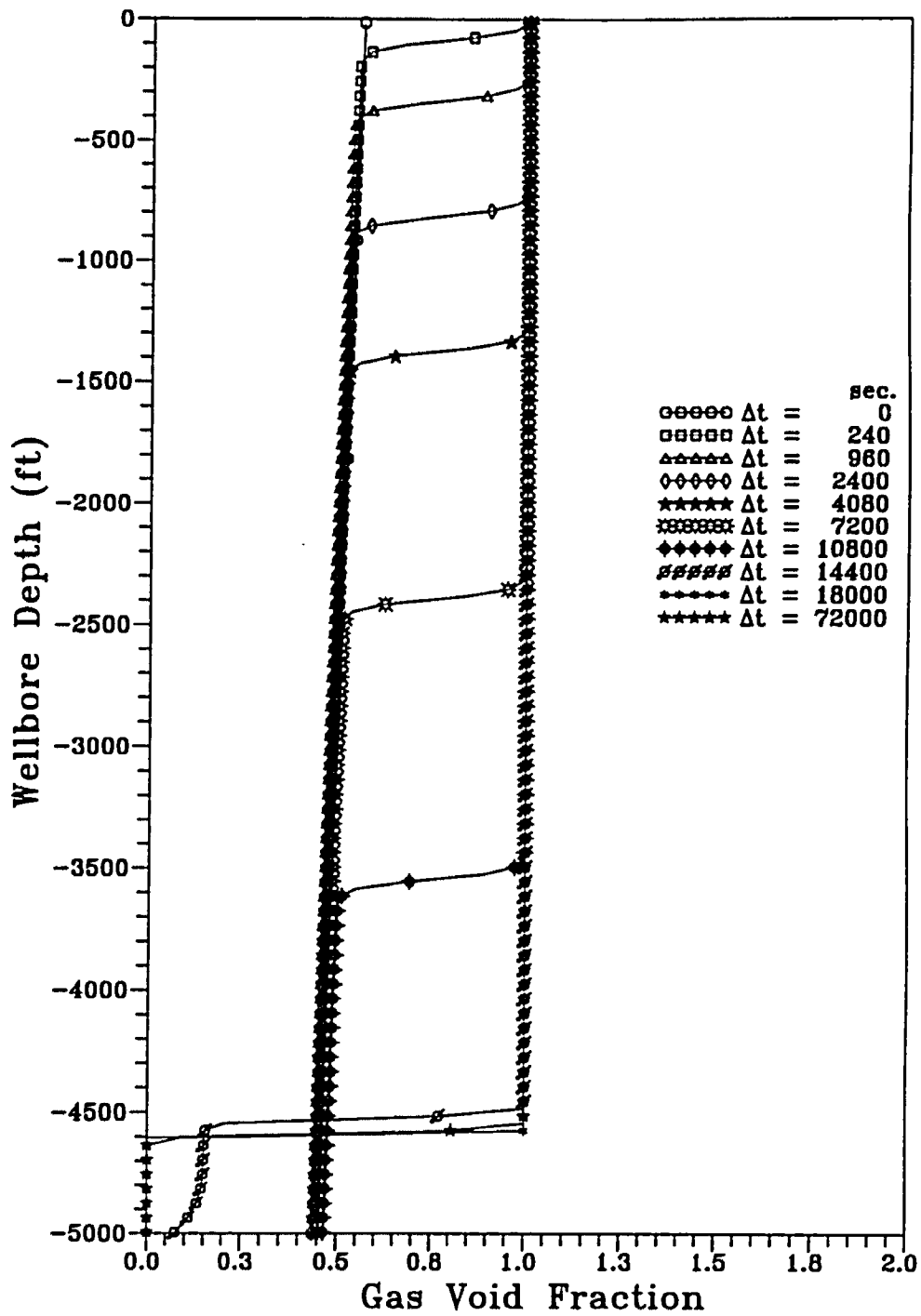


Fig. 4.12 - Gas Void Fraction Distribution, Case C

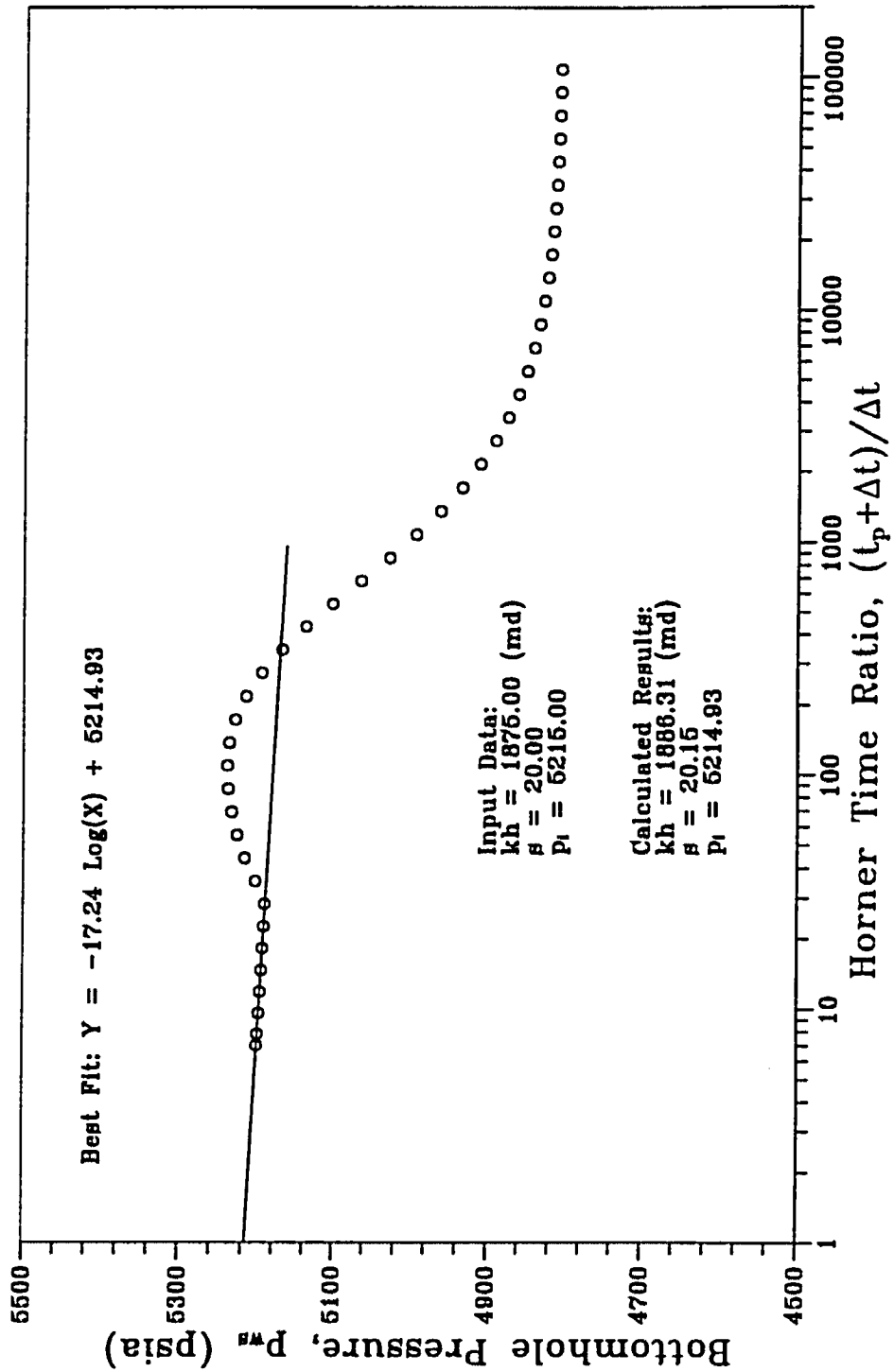


Fig. 4.13 - Horner Plot of Pressure Buildup data for Case C

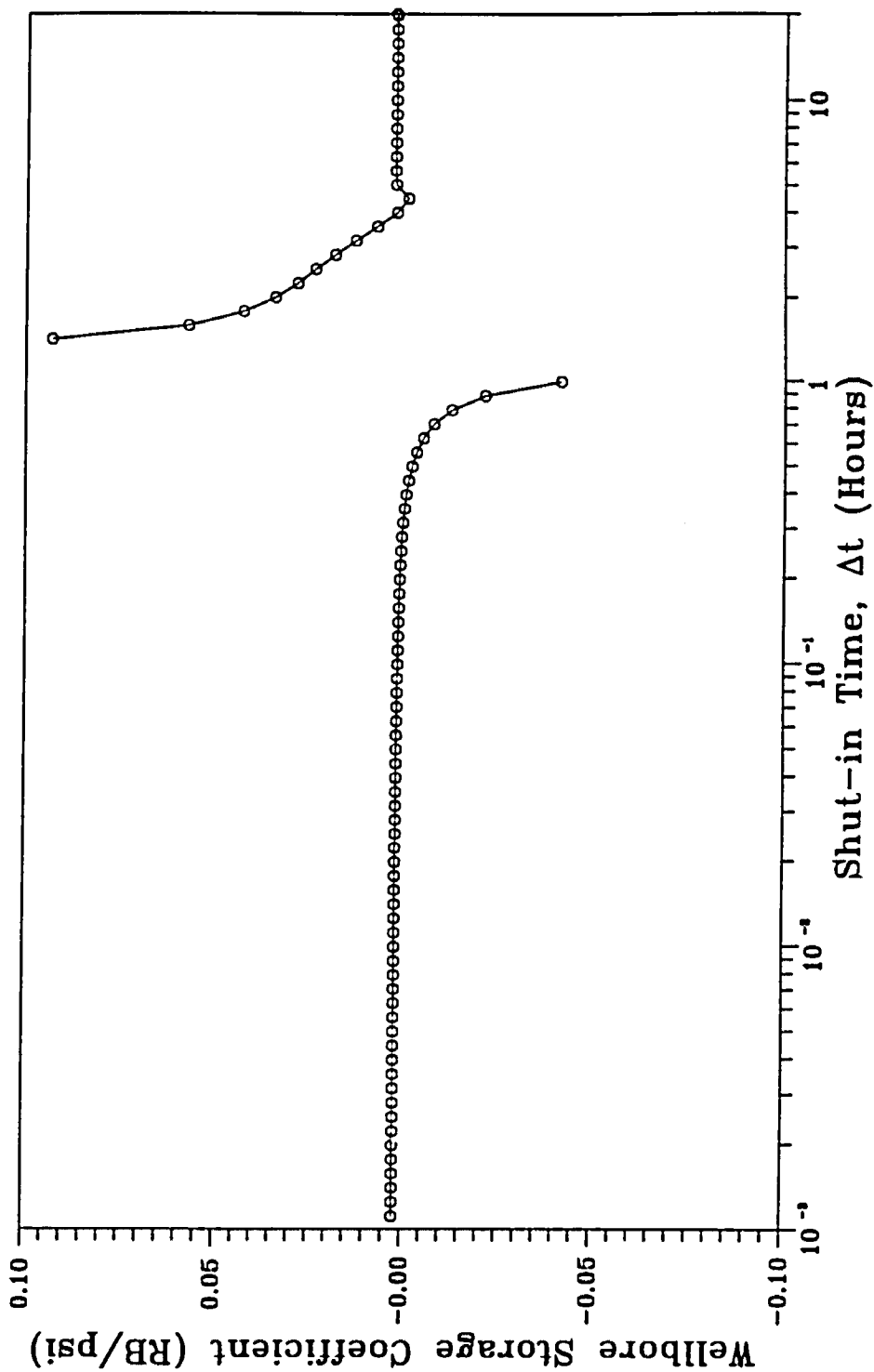


Fig. 4.14 - Change of Wellbore Storage Coefficient for Case C

storage effect while buildup data from Case C show an increasing wellbore storage effect in the end. Comparing the gas void fraction profiles for the two cases, Fig. 4.6 and Fig. 4.12, it can be concluded that the variation of wellbore storage coefficient is affected by both phase segregation and gas compression. If the magnitude of afterflow is small after the end of wellbore phase segregation, the phase segregation will be the dominating factor, and pressure buildup data will eventually show an increasing wellbore storage coefficient. On the other hand, if the afterflow is still large after gas and liquid have completely segregated in the wellbore, the gas column will be compressed due to afterflow and the pressure buildup data will eventually show a decreasing wellbore storage coefficient.

Results from the above case studies have clearly demonstrated the applicability of our numerical simulator. We believe that, with minimum modification, our simulator can also be used to simulate pressure buildup tests in pumping wells.

CHAPTER V

CONCLUSIONS

Most well testing theories are developed under the assumption that the wellbore storage coefficient is a constant throughout a well test. In many situations, however, this is merely a mathematical convenience rather than a true representation of reality. Very often, the wellbore storage coefficient will change during a test. In order to to correctly interpretate well-test data, it is a must to recognize and properly treat the changing wellbore conditions. The current study represents an important step toward the development of better interpretation methods for well tests influenced by a changing wellbore storage coefficient. Specifically, this work has been focused on the investigation of the wellbore effects on closed chamber tests in oil and gas wells as well as the effect of wellbore phase segregation on pressure buildup tests.

Closed chamber tests (CCT) are used in the oil industry as closed chamber drillstem tests, underbalanced perforation and backsurge perforation cleaning. Pressure responses in these tests are governed by a changing wellbore storage coefficient which results in a nonlinear mathematical problem with no known solution. Available methods to analyze data from such a test include history matching through the use of numerical simulators, convolution methods utilizing flow rate directly measured or calculated from the measurement of the chamber gas pressure, and techniques developed from the short producing time concept.

In *Chapter II*, a new inner boundary condition has been derived for a CCT problem, taking into account the changing wellbore storage. The concept of pseudo-time has been applied to improve the correlation between a CCT and a conventional

slug test, and to develop a new analysis procedure for closed chamber tests. Using pseudotime, pressure data from a CCT can be converted into an equivalent slug test response, and then type curve matching techniques can be used to deduce the reservoir flow capacity and well skin factor. A numerical simulator was implemented, based on the superposition principle for constant bottomhole pressure production solutions. The new analysis procedure was then used to analyze simulator generated pressure data. Parameters affecting pressure responses of closed chamber tests have also been studied.

The application of pseudotime concept was extended to slug tests which have a step change in the wellbore storage coefficient due to the change of wellstring diameter as the fluid level rises from the drill collar into the drill pipe during the test. It was shown that application of pseudotime can effectively correlate such a test into a slug test with a constant wellbore storage coefficient, and as a result, data from a slug test with a step change in the wellbore storage coefficient can be easily analyzed using methods developed for slug tests with constant wellbore storage coefficients.

As a result of this study, the following conclusions are warranted.

1. We have derived an equation for the effective wellbore storage coefficient and formulated a new inner boundary condition for a closed chamber test in an oil well.
2. It has been shown that a new version of pseudotime can be applied to correlate CCT data with corresponding slug test data. In general, this correlation applies for a sufficiently long period of time so that slug test analysis techniques can be applied to CCT pressure data.
3. It has been shown that whether pseudotime can be applied to improve the analysis of CCT data largely depends on the magnitude of change in the effective wellbore storage coefficient. Among the various parameters studied,

skin factor, chamber length, initial chamber gas pressure and initial reservoir pressure were found to have the most influence on the length of time for which the correlation based on pseudotime applies. In general, the length of the correlation time period increases as the skin factor increases, the chamber length increases, the initial chamber gas pressure increases or the initial reservoir pressure decreases.

4. Pseudotime can also be used to analyze data from slug tests with a changing wellbore storage coefficient due to the change of wellstring diameter or inclination angle.

The work of *Chapter II* has been extended to closed chamber gas well tests. In *Chapter III*, we formulated the initial boundary value problem (IBVP) for a gas well closed chamber test. The IBVP for a gas well CCT is nonlinear and is solved using a finite difference numerical simulator. We proposed to use pseudopressure and pseudotime transformations to correlate a gas well CCT with an equivalent liquid slug test problem. Various parameters affecting this correlation have also been investigated. Results from this part of the study can be summarized as follows.

1. In many cases, data from gas well closed chamber tests can be correlated with the liquid slug test solutions by using an appropriate pseudopressure and pseudotime transformation. This correlation usually works sufficiently long so that methods developed for slug test analysis, such as type-curve matching, can be applied to gas-well, closed-chamber test data to obtain estimates of the formation flow capacity and skin factor.
2. The proposed correlation applies for a longer period of time, and up to a higher magnitude of pressure recovery, for cases with a larger skin factor, higher initial wellbore pressure, lower initial reservoir pressure and a larger gas chamber.

3. Convolution analysis techniques in terms of pseudopressure and time can always be used for gas-well, closed-chamber tests if an accurate measurement of sandface flow rate is available, or one can accurately determine the sandface flow rate from the measurement of chamber gas pressure. Convolution time should be based on time, not pseudotime.

It is well-known that when wellbore phase segregation occurs during a pressure buildup test, the buildup data may exhibit a characteristic pressure hump. In *Chapter IV*, the effect of transient two-phase gas-oil flow in the wellbore on pressure buildup tests has been investigated. A one-dimensional drift-flux model is used to derive partial differential equations governing the phase segregation process. The black-oil approach, which accounts for a variable bubble-point pressure, is used to account for the effect of interphase mass transfer. After obtaining the corresponding finite-difference equations, solutions are computed with a sequential, iterative calculation procedure.

A computer simulator has been developed to implement the proposed model and the finite-difference solution procedure. For the purpose of verification, the simulator was first used to generate pressure responses from a buildup test in a well where single phase flow exits in the wellbore before shut-in. The analysis of generated pressure buildup data was carried out by type-curve matching with the classical wellbore storage and skin type curves and also by using Horner analysis. These studies yield correct values of permeability, skin factor, initial reservoir pressure and also the wellbore storage coefficient.

After verification, the simulator was then applied to simulate the phase redistribution process occurring in the wellbore during pressure buildup tests in wells shut-in at the surface. Two case studies have been presented in *Chapter IV*: a buildup test in a naturally flowing well and a buildup test in a gas-lift well. These investigations resulted in a better understanding about various anomalous pressure

buildup test behaviors reported in the literature. Based on this study, the following conclusions have been reached:

1. We have developed a mechanistic model to simulate wellbore phase segregation. Our model rigorously treats wellbore and reservoir flow interaction, accurately handles the effect of interphase mass transfer through the black-oil approach incorporating the concept of variable bubble-point pressure.
2. Our model has been implemented, verified and its applicability has been demonstrated through case studies.
3. Our investigation reveals that buildup tests in wells with multiphase flow in the wellbore prior to shut-in can show an increase or a decrease in the wellbore storage coefficient. The variation of wellbore storage coefficient is affected by both phase segregation and gas compression. If the magnitude of afterflow is small after the end of wellbore phase segregation, the phase segregation will be the dominating factor, and pressure buildup data will show an increasing wellbore storage coefficient at the end. On the other hand, if the afterflow is still large after gas and liquid have completely segregated in the wellbore, the gas column will be compressed due to afterflow and the pressure buildup data will show a decreasing wellbore storage coefficient.

In terms of future studies, efforts should be made to develop analytical solutions for closed chamber tests. Also, the simulator developed in *Chapter IV* should be modified to handle multiphase flow within the reservoir.

NOMENCLATURE

Symbol

a	= matrix coefficient.
a_D	= $[(\mu_g c_g)/(\mu_g c_g)_w][(\mu_g c_g)_o/(\mu_g c_g)_i]$.
A, A_{ch}	= cross sectional area of the wellstring, ft ² .
b, b', b''	= matrix coefficients.
B	= formation volume factor, RB/STB.
B_g	= gas formation volume factor, RB/scf.
B_o	= oil formation volume factor, RB/STB.
B_{ob}	= oil formation volume factor at p_b , RB/STB.
c	= matrix coefficient.
c_g	= gas isothermal compressibility, psi ⁻¹ .
c_{gi}	= gas isothermal compressibility evaluated at p_i , psi ⁻¹ .
c_{go}	= gas isothermal compressibility evaluated at p_o , psi ⁻¹ .
c_{gw}	= gas isothermal compressibility evaluated at p_{wf} , psi ⁻¹ .
c_l	= liquid isothermal compressibility, psi ⁻¹ .
c_o	= oil compressibility for $p > p_b$, 1/psi.
c_t	= total system compressibility, psi ⁻¹ .
C	= wellbore storage coefficient, RB/psi.
C_a	= combined wellbore storage coefficient, RB/psi.
C_{ai}	= initial combined wellbore storage coefficient, RB/psi.
C_{aD}	= combined dimensionless wellbore storage coefficient.
C_{aDi}	= initial combined dimensionless wellbore storage coefficient.
C_D	= dimensionless wellbore storage coefficient.

C_g	= wellbore storage coefficient due to gas compression, RB/psi; gas component mass concentration.
C_{gD}	= dimensionless wellbore storage coefficient due to gas compression.
C_{gl}	= gas component mass concentration in liquid phase.
C_l	= wellbore storage coefficient due to rising liquid level, RB/psi; oil component mass concentration.
C_{lD}	= dimensionless wellbore storage coefficient due to rising liquid level.
C_{ol}	= oil component mass concentration in liquid phase.
d_p	= diameter of the drillpipe, ft.
d, d', d''	= matrix coefficient.
D	= pipe diameter, ft.
D_r	= diffusion term.
E_g	= gas void fraction.
E_l	= liquid holdup.
f	= friction factor, dimensionless.
g	= acceleration of gravity, ft/sec ² .
g_c	= unit conversion factor, 32.17 lbf-ft / (lbf-sec ²).
h	= formation thickness, ft.
i	= initial or index.
$I(m_w D)$	= integral of the dimensionless wellbore pseudopressure.
k	= absolute permeability, md or index.
K_1	= modified Bessel function of the second kind of order one.
K_0	= modified Bessel function of the second kind of order zero.
L_c	= total chamber length, ft.
L_i	= initial liquid height, ft.
M	= total time steps.
m_D	= dimensionless real gas pseudopressure.

m_{wD}	= dimensionless wellbore real gas pseudopressure.
$m(p)$	= normalized real gas pseudopressure, psia.
n	= time step.
N	= index for time step or total number of wellbore control volumes.
p	= pressure, psia.
p_b	= bubble point pressure, psia.
p_{cD}	= constant surface rate dimensionless pressure.
\bar{p}_{cD}	= Laplace transform of p_{cD} .
p_{ch}	= chamber gas pressure, psia.
p_{chi}	= initial chamber gas pressure, psia.
p_D	= slug or closed chamber test dimensionless pressure.
p_g	= gas pressure, psia.
p_i	= initial reservoir pressure, psia.
p_o	= initial wellbore pressure, psia.
p_r	= reference pressure, psia.
$p(r, t)$	= pressure at r and t , psia.
p_{sc}	= pressure at standard conditions 14.7 psia.
p_w	= wellbore pressure, psia.
p_{wD}	= dimensionless wellbore pressure.
p_{wcD}	= constant surface rate dimensionless wellbore pressure.
p'_{wcD}	= logarithmic derivative of p_{wcD} .
p_{wcD}^*	= constant sandface rate dimensionless wellbore pressure.
p_{wf}	= flowing wellbore pressure, psia.
$p_{wf,s}$	= wellbore pressure at the instant of shut-in, psia.
p_{wh}	= wellhead pressure, psia.
p_{ws}	= shut-in wellbore pressure, psia.
p_{wsD}	= dimensionless buildup pressure.
q	= constant surface flow rate, STB/D; sandface rate, RB/D.

- q_c = flow rate for constant bottomhole pressure production, RB/D.
 q_{cD} = dimensionless flow rate for constant bottomhole pressure production.
 q_g = in-situ gas flow rate, ft³/sec.
 q_{ginj} = gas injection rate, scf/D.
 q_{gs} = gas component production rate at standard conditions, scf/D.
 q_l = liquid in-situ flow rate, ft³/sec.
 q_{os} = oil component production rate at standard conditions, STB/D.
 q_{sf} = sandface production rate, RB/D.
 q_v = flow rate for variable bottomhole pressure production, RB/D.
 Q = cumulative flow rate, RB/D.
 Q = equivalent sandface flow rate at p_i , RB/D.
 Q_c = cumulative flow rate for constant bottomhole pressure production, RB.
 Q_{cD} = dimensionless cumulative flow rate for constant bottomhole pressure production.
 Q_D = dimensionless converted sandface flow rate.
 Q_{sf} = cumulative sandface flow rate, RB.
 Q_v = cumulative flow rate for variable bottomhole pressure production, RB.
 q_{vD} = dimensionless flow rate for variable bottomhole pressure production.
 Q_{vD} = dimensionless cumulative flow rate for variable bottomhole pressure production.
 r = radial distance, ft.
 r_D = dimensionless radial distance.
 r_p = radius of the drill pipe, ft.

r_w	= wellbore radius, ft.
R	= total gas-oil ratio, scf/STB.
R_s	= solution gas-oil ratio, scf/STB.
s	= skin factor due to damage or stimulation.
t	= time, hours
t_a	= pseudotime, hour.
t_{aD}	= dimensionless pseudotime based on wellbore radius.
t_D	= dimensionless time based on wellbore radius.
t_{max}	= desirable test duration, seconds.
t_N	= time at time step N, seconds.
t_p	= production time, hours.
t_{pD}	= dimensionless production time.
T	= total simulation time.
T_{sc}	= temperature at standard conditions, $60^\circ F$.
T_w	= wellbore temperature, $^\circ R$.
u	= Laplace space variable.
v, V	= volume, RB.
v_g, V_g	= wellbore volume occupied by gas, RB; gas true velocity, ft/sec.
v_l	= liquid true velocity, ft/sec.
v_m	= density averaged mixture velocity, ft/sec.
v_r	= relative velocity, ft/sec.
v_{sg}	= superficial gas velocity, ft/sec.
v_{sl}	= superficial liquid velocity, ft/sec.
V_w	= wellbore volume, RB.
X	= Dynamic liquid level, ft.
z	= coordination or gas compressibility.
$I(p_wD)$	= integral of the dimensionless wellbore pressure.

μ	= viscosity, cp.
μ_g	= gas viscosity, cp.
μ_{gi}	= gas viscosity evaluated at p_i , cp.
μ_{go}	= gas viscosity evaluated at p_o , cp.
ϕ	= porosity, fraction.
ρ	= fluid density, lbm/ft ³ .
ρ_g	= density of gas, lbm/ft ³ .
ρ_{gl}	= partial density of gas component in the liquid phase, lbm/ft ³ .
ρ_{gs}	= gas component density at standard conditions, lbm/ft ³ .
ρ_l	= density of liquid, lbm/ft ³ .
ρ_m	= mixture density, lbm/ft ³ .
ρ_{ol}	= partial density of oil component in the liquid phase, lbm/ft ³ .
ρ_{os}	= oil component density at standard conditions, lbm/ft ³ .
γ	= Euler's constant (0.57722).
τ	= integration variable.
Δ	= difference.
Δp	= pressure drop, psi.
Δp_f	= frictional pressure drop, psi.
Δp_{skin}	= additional pressure drop due to the skin, psi.
Δp_{wf}	= wellbore pressure change, psi.
Δt	= shut-in time or time step, seconds.
Δt_D	= dimensionless shut-in time or dimensionless time step.
ΔT	= time step size, sec.
Δv	= change in volume of the wellbore fluid, RB.
Δz	= length of each control volume, ft.
ϵ	= convergence tolerance.
Θ	= relaxation factor.
σ	= gas-oil surface tension, dynes/cm.

REFERENCES

1. Matthews, C. S. and Russell, D. G.: "*Pressure Buildup And Flow Tests in Wells*," SPE Monograph Volume 1, 1967.
2. Earlougher, R. C. Jr.: "*Advances in Well Test Analysis*," SPE Monograph No. 5, 1977.
3. Ramey, H. J. Jr., Agarwal, R. G. and Martin, I.: "Analysis of 'Slug Test' or DST Flow Period Data," *J. Can. Pet. Tech.*, 14 (July-Sept. 1975) 37-47.
4. Peres, A., Onur, M. and Reynolds, A.: "A New General Pressure Analysis for Slug Tests," paper SPE 18801 presented at the 1989 SPE California Regional meeting, Bakersfield, CA, April 5-7.
5. Alexander, L. G.: "Theory and Practice of the Closed-Chamber Drillstem Test Method," *J. Pet. Tech.*, (December 1977) 1539-1544.
6. Erdle, J. C., Upchurch, J. M. and Warren, D. A.: "Early Fluid Entry Determination; Key to Safe, Optimum Drill Stem Testing," paper SPE 6884 presented at the 52nd Annual Fall Technical Conference and Exhibition of SPE of AIME, Oct. 9-12, 1977, Denver, Colorado.
7. Saldana-C, M. A. and Ramey, H. J. Jr.: "Slug Test and Drillstem Test Flow Phenomena Including Wellbore Inertial and Frictional Effects," paper SPE 15118 presented at the 56th SPE California Regional Meeting, Oakland, CA, April 2-4, 1986.
8. Simmons, J. F. and Grader, A. S.: "Application of Closed-Chamber Theory to Backsurge Completion testing," *SPE Production Engineering*, (November 1988) 527-535.

9. Salas, B. and Sageev, A.: "Closed Chamber Testing: The Effects of Wellbore Friction and Fluids Compression," paper SPE 16800 presented at the 62nd Annual Technical Conference and Exhibition of SPE, Sept. 27-30, 1987, Dallas, Texas.
10. Mfonfu, G. B. S. and Grader, A. S.: "An Implicit Numerical Model for the Closed Chamber Test," paper SPE 19832 presented at the 64th Annual Technical Conference and Exhibition of SPE, Oct. 8-11, 1989, San Antonio, Texas.
11. Petak, K. R., Prasad, R. K. and Coble, L. E.: "Surge Test Simulation," paper SPE 21832 presented at Rocky Mountain Regional Meeting and Low Permeability Reservoir Symposium, April 15-17, 1991, Denver, Colorado.
12. Tariq, S. M. and Ayestaran, L.: "Analyses and Application of Pressure, Flow-rate, and Temperature Measurements During a Perforation Run," paper SPE 15475 presented at the 61st Annual Technical Conference and Exhibition of SPE, Oct. 5-8, 1986, New Orleans, LA.
13. Simmons, J. F.: "Interpretation of Underbalanced Surge Pressure Data by Rate-Time Convolution," paper SPE 15477 presented at the 61st Annual Technical Conference and Exhibition of SPE, Oct. 5-8, 1986, New Orleans, LA.
14. Soliman, M. Y., Petak, K. and Christensen, J.: "Analysis of Sequential Formation Testing and Surge Tests Using New Techniques," paper no. 88-39-53 presented at the 39th Annual Technical Meeting of the Petroleum Society of CIM, June 12-16, 1988, Calgary, Canada.
15. Garrett, J. C., Shealy, R. A., Centanni, R. J., Ruiz, S. J. and Chacon, E. A.: "The Analysis of Pressure Transient Data from Underbalanced Perforating," paper SPE 18878 presented at SPE Production Operation Symposium, March 13-14, 1989, Oklahoma, OK.

16. Ayoub, J. A., Bourdet, D. P. and Chauvel, Y. L.: "Impulse Testing," *SPE Formation Evaluation*, (September 1988) 534-546.
17. Cinco-Ley, H., Kuchuk, F., Ayoub, J., Samaniego-V., F. and Ayestaran, L.: "Analysis of Pressure Tests Through the Use of Instantaneous Source Response Concepts," paper SPE 15476 presented at the 1986 SPE Annual Technical Conference and Exhibition, New Orleans, Oct. 5-8.
18. Manohar, M. M., Morris, C. W., Brunner, S. R. and Hill, D. D.: "Evaluation of Underbalanced Through-Tubing Perforating and Closed Chamber test Interpretation techniques," paper SPE 21657 presented at SPE Production Operation Symposium, April 7-9, 1991, Oklahoma, OK.
19. Ramey, H. J. Jr. and Agarwal, R. G.: "Annulus Unloading Rates as Influenced by Wellbore Storage and Skin Effect," *Trans. AIME*, 253 (1972) 453-463.
20. Everdigen, A. F. V. and Hurst, W.: "The Application of The Laplace Transformation to Flow Problems in Reservoirs," *Petroleum Transactions, AIME*, December 1949, 305-324.
21. Stehfest, H.: "Algorithm 386, Numerical Inversion of Laplace Transforms," *Comm. of the ACM*, 13(1), (1970) 47-49.
22. Agarwal, R.: "'Real Gas Pseudotime' - A New Function for Pressure Buildup Analysis of MHF Gas Wells," paper SPE 8279 presented at the 54th SPE Annual Technical Conference and Exhibition, Las Vegas, Nevada, Sept. 23-26, 1979.
23. Finjord, J.: "A Study of Pseudotime," paper SPE 12577 (1984) SPE Book Order Department.
24. Reynolds, A. C., Bratvold, R. B. and Ding, W.: "Semilog Analysis of Gas Well Drawdown and Buildup Data," *SPE Formation Evaluation* (Dec. 1987) 657-670.

25. Aanonsen, S. I.: "*Nonlinear Effects During Transient Fluid Flow on Reservoir As Encountered in Well-Test Analysis*," Ph.D. Dissertation, University of Bergen, Norway, March 1985.
26. Correa, A. C. and Ramey, H. J. Jr.: "A Method for Pressure Buildup Analysis of Drillstem Tests," paper SPE 16802 presented at the 1987 SPE Annual Technical Conference and Exhibition, Dallas, Sept. 27-30.
27. Dake, I. P.: "*Fundamentals of Reservoir Engineering*," Development in Petroleum Science 8, Elsevier Science Publishing Company, Amsterdam (1978).
28. Stanislav, J. F. and Kabir, C. S.: "*Pressure Transient Analysis*," Prentice-Hall, Inc. (1990).
29. Hagoort, J.: "*Fundamentals of Gas reservoir Engineering*," Development in Petroleum Science 23, Elsevier Science Publishing Company, Amsterdam (1988).
30. Al-Hussainy, R., Ramey, H. J. Jr. and Crawford, P. B.: "The Flow of Real Gases Through Porous Media," *J. Pet. Tech.*, (May 1966) 624-636.
31. Lee, W. J. and Holditch, S. A.: "Application of Pseudotime to Buildup Test Analysis of Low-Permeability Gas Wells With Long-Duration Wellbore Storage Distortion," *J. Pet. Tech.*, (December 1982) 2877-2887.
32. Spivey, J. P. and Lee, W. J.: "The Use of Pseudotime, Wellbore Storage and the Middle Time Region," paper SPE 15229 presented at the SPE Unconventional Gas Technology Symposium, Louisville, KY, May 18-21, 1986.
33. Reid, H. W.: "Evaluation of Low Permeability Gas Reservoirs Utilizing Closed Chamber Drillstem Test Techniques," paper SPE 10184 presented at the 56th Annual Fall Technical Conference and Exhibition of SPE of AIME, Oct. 5-7, 1981, San Antonio, Texas.

34. Weir, G. and Kissling, W. M.: "Scaled Time. A New Pseudotime Function for Approximately Linearizing Gas Reservoir Models," SPE 13418 (1984), SPE Book Order Department.
35. Agarwal, R. G., Al-Hussainy, R. and Ramey, H. J. Jr.: "An Investigation of Wellbore Storage and Skin Effect in Unsteady Liquid Flow: I. Analytical Treatment," *Trans. AIME* (1970) 249, 279-290.
36. Odeh, A. S. and Jones, L. G.: "Pressure Drawdown Analysis, Variable-Rate Case," *J. Pet. Tech.*, (August 1965) 960-964.
37. Hawkins, M. F. Jr.: "A Note on the Skin Effect," *Trans. AIME* (1956) 207, 356-357.
38. Fraim, M. L. and Wattenbarger, R. A.: "Gas Reservoir Decline-Curve Analysis Using Type Curves With Real Gas Pseudopressure and Normalized Time," *SPE Formation Evaluation*, (December 1987) 671-682.
39. Peres, A. M. M., Serra, K. V. and Reynolds, A. C.: "Toward a Unified Theory of Well Testing for Nonlinear-Radial-Flow Problems With Application to Interference Tests," *SPE Formation Evaluation*, June 1990, 151-160.
40. Meunier, D., Wittmann, M. J. and Stewart, G.: "Interpretation of Pressure Build-up Test Using In-Situ Measurement of Afterflow," *J. Pet. Tech.*, (January 1985) 143-152.
41. Tariq, S. M. and Ayestaran, L.: "Analyses and Application of Pressure, Flow Rate, and Temperature Measurements During a Perforation Run," paper SPE 15475 presented at the 61st Annual Technical Conference and Exhibition of SPE, Oct. 5-8, 1986, New Orleans, LA.
42. Ablewhite, P. K.: "Formation Damage and Flow Capacity Estimation Using Pressure Data Recorded While Perforating," paper OSEA 90168 presented at the Eighth Offshore South East Asia Conference in Singapore, 4-7 December 1990.

43. Stegemeier, G. L. and Matthews, C. S.: "A Study of Anomalous Pressure Build-up Behavior," *Trans., AIME*, 213, 44-50 (1958).
44. Pitzer, S. C., Rice, J. D. and Thomas, C. E.: "A Comparison of Theoretical Pressure Build-up Curves with Field Curves Obtained from Bottom-Hole Shut-in Tests," *Trans., AIME*, 216, 416-419 (1959).
45. Fair, W. B.: "Pressure Buildup Analysis with Wellbore Phase Redistribution," *Society of Petroleum Engineers Journal* (April 1981) 259-270; *Trans., AIME*, 271.
46. Hegeman, P. S., Hallford, D. L. and Joseph, J. A.: "Well Test Analysis with Changing Wellbore Storage," paper SPE 21829 presented at the Rocky Mountain Regional Meeting and Low-Permeability Reservoirs Symposium, April 15-17, 1991, Denver, CO.
47. Thompson, L. G., Jones, J. R. and Reynolds, A. C.: "Analysis of Pressure Buildup Data Influenced by Wellbore Phase Redistribution," *SPE Formation Evaluation*, October 1986, 435-452.
48. Rushing, J. A. and Lee, W. J.: "Use of an Automatic History-Matching Technique to Analyze Pressure Buildup Data Affected by Wellbore Phase Segregation: Case Histories," paper SPE 18837 presented at the SPE Production Operation Symposium, March 13-14, 1989, Oklahoma City, OK.
49. Olarewaju, J. S., Holditch, S. A. and Lee, W. J.: "Effects of Phase Segregation on Buildup Test Data from Gas Wells," paper SPE 19100 presented at the SPE Gas Technology Symposium, June 7-9, 1989, Dallas, TX.
50. Olarewaju, J. S.: "Detection and Interpretation of Well Test Data Distorted by Phase Segregation," *Journal of Petroleum Science and Engineering*, 5 (1990) 210-212.
51. Winterfeld, P. H.: "Simulation of Pressure Buildup in a Multiphase Wellbore/Reservoir System," *SPE Formation Evaluation* (June 1989) 247-252.

52. Almehaideb, R. A., Aziz, K. and Pedrosa, O. A.: "A Reservoir/Wellbore Model for Multiphase Injection and Pressure Transient Analysis," paper SPE 17941 presented at the SPE middle East Oil Technical Conference and Exhibition, March 11-14, 1989, Manama, Bahrain.
53. Hasan, A. R. and Kabir, C. S.: "Modeling Changing Storage During a Shut-in Test," paper SPE 24717 presented at the 67th Annual Technical Conference and Exhibition of the Society of Petroleum Engineers, Washington, DC, October 4-7, 1992.
54. Wallis, G. B.: "*One-Dimensional Two-Phase Flow*," McGraw-Hill, Inc., 1969.
55. Ishii, M.: "*Thermo-Fluid Dynamic Theory of Two-Phase Flow*," Eyrolles, 1975.
56. Scoggins, M. W. Jr.: "*A Numerical Simulation Model for Transient Two-Phase Flow in a Pipeline*," Ph.D. Dissertation, University of Tulsa, 1977.
57. Liles, D. R. and Reed, Wm. H.: "A Semi-Implicit Method for Two-Phase Fluid Dynamics," *Journal of Computational Physics*, 26, 390-407 (1978).
58. Sarica, C.: "*Two-Phase Flow in Low Velocity Hilly Terrain Pipelines*," Ph.D. Dissertation, University of Tulsa, 1990.
59. Gokdemir, O. M.: "*Transient Drift Flux Model for Wellbore*," MS Thesis, University of Tulsa, 1992.
60. Peaceman, D. W.: "*Fundamentals of Numerical Reservoir Simulation*," Elsevier Scientific Publishing Company, 1977.
61. Ansari, A. M.: "*A Comprehensive Mechanistic Model for Upward Two-Phase Flow*," MS Thesis, the University of Tulsa, 1988.
62. Capucci, E. C. and Serra, K. V.: "Transient Aspects of Unloading Oil Wells Through Gas-lift Valves," SPE 22791 presented at the 66th SPE Annual Technical Conference and Exhibition, Dallas, TX, Oct. 6-9, 1991.

63. Patanker, S. V.: "*Numerical Heat Transfer and Fluid Flow*," Hemisphere Publishing Corporation, 1980.
64. Alhanati, F.: "*Bottomhole Gas Separation Efficiency in Electrical Submersible Pump Installation*," PhD Dissertation, the University of Tulsa, 1993.
65. Anderson, D. A., Tannehill, J. C. and Pletcher, R. H.: "*Computational Fluid Mechanics and Heat Transfer*," Washington, Hemisphere Pub. Corp.; New York, McGraw-Hill, 1984.
66. Peyret, R. and Taylor, T. D.: "*Computational Methods for Fluid Flow*," Springer-Verlag New York Inc., 1983.
67. Carver, M. B.: "A Method of Limiting Intermediate Values of Volume Fraction in Iterative Two-Fluid Computations," *J. Mechanical Engineering Science*, Vol. 24 No. 4 1982, 221-224.
68. Standing, M. B.: "A Pressure-Volume-Temperature Correlation for Mixtures of California Oils and Gases," *API Drilling and Production Practice* (1947) 275-287.
69. Standing, M. B. and Katz, D. L.: "Density of Natural Gases," *Trans. AIME* (1942), 140.
70. Burden, R. L., Faires. J. D. and Reynolds, A. C.: "*Numerical Analysis*," Prindle, Weber and Schmidt, 1978.
71. Mattar, L.: "Critical Evaluation and Processing of Data Prior to Pressure Transient Analysis," SPE 24729 presented at the 1992 SPE Annual Technical Conference and Exhibition, Washington, Oct. 4-7, 1992.
72. Kazemi, H, et al.: "Complexities of the Analysis of Surface Shut-In Drillstem Tests in an Offshore Volatile Oil Reservoir," *J. of Petroleum Technology*, January 1983, 173-177.
73. Thompson, L. G.: "Computation of Pressure Response for Horizontal Wells in Naturally Fractured Reservoirs," TUPREP Report No. 4, Nov. 13, 1990.

APPENDIX A
DUHAMEL'S PRINCIPLE
FOR
VARIABLE BOTTOMHOLE PRESSURE PRODUCTION

Duhamel's principle for variable bottomhole pressure production was introduced to the petroleum engineering literature by Van Everdingen and Hurst²⁰ and was recently studied by Thompson⁷³. General relationships have been derived, relating the pressure distribution in the reservoir and the sandface flow rate, when a well produces at a variable bottomhole pressure, to corresponding variables when the well produces at a constant bottomhole pressure. In this appendix, as an extension of the previous work, we derive the superposition principle for the cumulative production, from which a numerical scheme used in the present study is constructed. For completeness, some material from Thompson⁷³ is duplicated here.

We consider flow of a slightly compressible fluid of constant viscosity in an arbitrarily shaped reservoir to an arbitrarily shaped wellbore. Without loss of generality, the initial pressure everywhere in the reservoir is assumed to be zero.

Let D denote the region in space occupied by the reservoir, S_w denote the wellbore area contributing to production and S denote the remainder of the reservoir boundary. We use \underline{x} to represent the spatial vector in R^n , $p_v(\underline{x}, t)$ to represent the pressure distribution in the reservoir when the well produces at a variable bottomhole pressure, $p_{wv}(t)$. Throughout, $p_c(\underline{x}, t)$ represent the pressure distribution when the well produces at a constant bottomhole pressure, p_r . With these variables, the initial boundary value problem (IBVP) for production at a variable bottomhole

pressure can be written as

$$\nabla \cdot [k] \nabla p_v(\underline{x}, t) = \mu c_t \frac{\partial p_v(\underline{x}, t)}{\partial t}; t > 0; \underline{x} \in D \quad (A-1-1)$$

$$[p_v(\underline{x}, t = 0)]_{\underline{x} \in D} = 0; \quad (A-1-2)$$

$$[p_v(\underline{x}, t)]_{\underline{x} \in S_w} = p_{wv}(t); \quad (A-1-3)$$

$$[\alpha p_v(\underline{x}, t) + \beta \nabla p_v(\underline{x}, t)]_{\underline{x} \in S} = 0. \quad (A-1-4)$$

The corresponding IBVP for production at a constant bottomhole pressure is

$$\nabla \cdot [k] \nabla p_c(\underline{x}, t) = \mu c_t \frac{\partial p_c(\underline{x}, t)}{\partial t}; t > 0; \underline{x} \in D \quad (A-2-1)$$

$$[p_c(\underline{x}, t = 0)]_{\underline{x} \in D} = 0; \quad (A-2-2)$$

$$[p_c(\underline{x}, t)]_{\underline{x} \in S_w} = p_r; \quad (A-2-3)$$

$$[\alpha p_c(\underline{x}, t) + \beta \nabla p_c(\underline{x}, t)]_{\underline{x} \in S} = 0. \quad (A-2-4)$$

In the above equations, $[k]$ is the permeability tensor and ∇ is the gradient operator. Note that $[k]$, α and β may be functions of position but not functions of time.

Since the two IBVP's under consideration are linear, the Laplace transform can be applied. Let a bar over a variable denote the Laplace transform of that variable, u denote the Laplace variable. Taking the Laplace transform with respect to time of Eqs. (A-1) and (A-2), we obtain

$$\nabla \cdot [k] \nabla \bar{p}_v(\underline{x}, u) = u \mu c_t \bar{p}_v(\underline{x}, u); \underline{x} \in D \quad (A-3-1)$$

$$[\bar{p}_v(\underline{x}, u)]_{\underline{x} \in S_w} = \bar{p}_{wv}(u); \quad (A-3-2)$$

$$[\alpha \bar{p}_v(\underline{x}, u) + \beta \nabla \bar{p}_v(\underline{x}, u)]_{\underline{x} \in S} = 0; \quad (A-3-3)$$

and

$$\nabla \cdot [k] \nabla \bar{p}_c(\underline{x}, u) = u \mu c_l \bar{p}_c(\underline{x}, u); \underline{x} \in D \quad (A-4-1)$$

$$[\bar{p}_c(\underline{x}, u)]_{\underline{x} \in S_w} = \frac{p_r}{u}; \quad (A-4-2)$$

$$[\alpha \bar{p}_c(\underline{x}, u) + \beta \nabla \bar{p}_c(\underline{x}, u)]_{\underline{x} \in S} = 0; \quad (A-4-3)$$

respectively.

Since ∇ is a linear operator, we can multiply Eqs. (A-4-1) - (A-4-3) by $u \bar{p}_{wv}(u)/p_r$ to obtain

$$\nabla \cdot [k] \nabla \left(\frac{u \bar{p}_{wv}(u) \bar{p}_c(\underline{x}, u)}{p_r} \right) = u \mu c_l \left(\frac{u \bar{p}_{wv}(u) \bar{p}_c(\underline{x}, u)}{p_r} \right); \underline{x} \in D \quad (A-5-1)$$

$$\left(\frac{u \bar{p}_{wv}(u) \bar{p}_c(\underline{x}, u)}{p_r} \right)_{\underline{x} \in S_w} = \bar{p}_{wv}(u); \quad (A-5-2)$$

$$\left[\alpha \left(\frac{u \bar{p}_{wv}(u) \bar{p}_c(\underline{x}, u)}{p_r} \right) + \beta \left(\frac{u \bar{p}_{wv}(u) \bar{p}_c(\underline{x}, u)}{p_r} \right) \right]_{\underline{x} \in S} = 0; \quad (A-5-3)$$

Comparing Eqs. (A-3-1) - (A-3-3) and (A-5-1) - (A-5-3), we see that $\bar{p}_v(\underline{x}, u)$ and the group, $u \bar{p}_{wv}(u) \bar{p}_c(\underline{x}, u)/p_r$, satisfy the same boundary value problem; thus, we must have

$$\bar{p}_v(\underline{x}, u) = \left(\frac{u \bar{p}_{wv}(u) \bar{p}_c(\underline{x}, u)}{p_r} \right). \quad (A-6-1)$$

Inverting Eq. (A-6-1), we have

$$p_v(\underline{x}, t) = \frac{1}{p_r} \int_0^t p'_{wv}(\tau) p_c(\underline{x}, t - \tau) d\tau + \frac{p_{wv}(t=0)}{p_r} p_c(\underline{x}, t), \quad (A-6-2)$$

or equivalently,

$$p_v(\underline{x}, t) = \frac{1}{p_r} \int_0^t p'_c(\underline{x}, t - \tau) p_{wv}(\tau) d\tau. \quad (A-6-3)$$

Let q_v denote the wellbore sandface flow rate in RB/D for variable bottom-hole pressure production and q_c denote the wellbore sandface flow rate RB/D for constant bottomhole pressure production. Then, we have

$$q_v(t) = 1.127 \times 10^{-3} \int \int_{S_w} \frac{[k]}{\mu} \nabla p_v(\underline{x}, t) \cdot \vec{n} dS_w, \quad (A-7-1)$$

and

$$q_c(t) = 1.127 \times 10^{-3} \int \int_{S_w} \frac{[k]}{\mu} \nabla p_c(\underline{x}, t) \cdot \vec{n} dS_w, \quad (A-7-2)$$

Taking the Laplace transform of Eqs. (A-7-1) and (A-7-2), we obtain

$$\bar{q}_v = 1.127 \times 10^{-3} \int \int_{S_w} \frac{[k]}{\mu} \nabla \bar{p}_v(\underline{x}, u) \cdot \vec{n} dS_w, \quad (A-8-1)$$

and

$$\bar{q}_c = 1.127 \times 10^{-3} \int \int_{S_w} \frac{[k]}{\mu} \nabla \bar{p}_c(\underline{x}, u) \cdot \vec{n} dS_w. \quad (A-8-2)$$

Substituting Eq. (A-6-1) into Eq. (A-8-1) and using Eq. (A-8-2), we obtain

$$\bar{q}_v = \left(\frac{u \bar{p}_{wv}(u) \bar{q}_c(u)}{p_r} \right). \quad (A-9-1)$$

Inverting Eq. (A-9-1) into real time, we have

$$q_v(t) = \frac{1}{p_r} \int_0^t q_c(t - \tau) p'_{wv}(\tau) d\tau + \frac{p_{wv}(t=0)}{p_r} q_c(t), \quad (A-9-2)$$

or equivalently

$$q_v(t) = \frac{1}{p_r} \int_0^t q'_c(t - \tau) p_{wv}(\tau) d\tau + \frac{p_{wv}(t)}{p_r} q_c(t=0). \quad (A-9-3)$$

Let Q_v denote the cumulative production for variable bottomhole pressure production and Q_c denote the cumulative production for constant bottomhole pressure production. Then, we have

$$Q_v(t) = \int_0^t q_v(\tau) d\tau, \quad (A - 10 - 1)$$

and

$$Q_c(t) = \int_0^t q_c(\tau) d\tau. \quad (A - 10 - 2)$$

Taking the Laplace transform of Eqs. (A - 10 - 1) and (A - 10 - 2), we obtain

$$\bar{Q}_v(u) = \frac{\bar{q}_v(u)}{u}, \quad (A - 11 - 1)$$

and

$$\bar{Q}_c(u) = \frac{\bar{q}_c(u)}{u}. \quad (A - 11 - 2)$$

Using Eqs. (A - 9 - 1), (A - 11 - 1) and (A - 11 - 2), we have

$$\bar{Q}_v = \left(\frac{u \bar{p}_{wv}(u) \bar{Q}_c(u)}{p_r} \right). \quad (A - 12 - 1)$$

Inverting Eq. (A - 12 - 1) into real time, we obtain

$$Q_v(t) = \frac{1}{p_r} \int_0^t Q_c(t - \tau) p'_{wv}(\tau) d\tau + \frac{p_{wv}(t=0)}{p_r} Q_c(t), \quad (A - 12 - 2)$$

or equivalently,

$$Q_v(t) = \frac{1}{p_r} \int_0^t Q'_c(t - \tau) p_{wv}(\tau) d\tau. \quad (A - 12 - 3)$$

Eq. (A - 12 - 1) through (A - 12 - 3) represent the Duhamel's principle relating the cumulative production solution of a variable bottomhole pressure production problem to the cumulative production solution of a constant bottomhole pressure production problem.

In the following, we consider a fully-penetrating well in an infinite, homogeneous and isotropic reservoir of uniform thickness. Initially, the pressure is constant throughout the reservoir and equal to p_i whereas in the wellbore, the pressure is instantaneously set equal to p_o . Using dimensionless variables defined earlier, we obtain the dimensionless form of Eq. (A - 12 - 3)

$$Q_{vD}(t_D) = \int_0^{t_D} Q'_{cD}(t_D - \tau) p_{wvD}(\tau) d\tau. \quad (A - 13)$$

For production at a sequence of constant bottomhole pressures, Eq. (A - 13) becomes

$$\begin{aligned} Q_{vD} &= \sum_{j=1}^N \int_{t_{D,j-1}}^{t_{D,j}} Q'_{cD}(t_D - \tau) p_{wvD}(\tau) d\tau \\ &= \sum_{j=1}^N p_{wvD}(t_{D,j-1}) [Q_{cD}(t_D - t_{D,j-1}) - Q_{cD}(t_D - t_{D,j})] \\ &= p_{wvD}(t_D = 0) Q_{cD}(t_D) \\ &\quad + \sum_{j=1}^{N-1} Q_{cD}(t_D - t_{D,j}) [p_{wvD}(t_{D,j}) - p_{wvD}(t_{D,j-1})]. \end{aligned} \quad (A - 14)$$

Note that in Eq. (A - 14) we used the facts that $t_{D,N} = t_D$ and $Q_{cD}(t_D = 0) = 0$.

Eq. (A - 14) can also be written as

$$\begin{aligned} Q_v &= \beta(p_i - p_o) Q_{cD}(t_D) \\ &\quad - \beta \sum_{j=1}^{N-1} (p_j - p_{j-1}) Q_{cD}(t_D - t_{D,j}) \end{aligned} \quad (A - 15)$$

where $\beta = 2\pi\phi h c_l r_w^2 / 5.615$. Eq. (A - 15) represents the basic equation used in the present study.

APPENDIX B
WELLBORE STORAGE COEFFICIENT
FOR
CCT IN OIL WELLS

Once a closed chamber test is initialized and the reservoir begins to produce, the liquid level moves upward in the wellstring and, as a result, compresses the chamber gas. It is rather obvious that two types of wellbore storage phenomena simultaneously govern the test: one is due to rising liquid level and the other one is due to gas compression. Here, we derive the wellbore storage coefficient for a closed chamber test. This is carried out through the use of the basic definition of the wellbore storage coefficient as a starting point, although a material balance on the wellbore fluid could lead to the same results.

Several assumptions have to be made in order to simplify our analysis. These include the following: 1) The reservoir is assumed to produce a single phase liquid; 2) There is no mass transfer between chamber gas and produced formation fluids; 3) Liquid in the wellstring is incompressible and chamber gas behaves as an ideal gas; 4) There is no temperature and pressure gradients in the gas column; 5) Friction and momentum effects are neglected; and 6) Critical flow is not present. We also consider that the wellstring has a constant inner diameter and inclination angle.

The wellbore storage coefficient is defined as the change of the total volume of wellbore fluids per unit change in bottomhole pressure²,

$$C_a = \frac{\Delta v}{\Delta p_{wf}}, \quad (B - 1)$$

where

C_a = Wellbore storage coefficient, bbl/psi

Δv = Change in volume of fluid in the wellbore at wellbore conditions, bbl

Δp_{wf} = Change in bottomhole pressure, psi.

During a closed chamber test the bottomhole pressure continuously increases until it reaches the reservoir static pressure. Assuming that the liquid level is $h = h(t)$ at some time during the test, the bottomhole pressure is the summation of the chamber gas pressure and the hydrostatic pressure caused by the liquid column, that is,

$$p_{wf} = p_g + \frac{\rho g}{144g_c} h. \quad (B - 2)$$

Therefore, the change in bottomhole pressure can be written as

$$\Delta p_{wf} = \Delta p_g + \frac{\rho g}{144g_c} \Delta h. \quad (B - 3)$$

For an ideal gas under isothermal conditions, the equation of state can be stated as

$$p_g v_g = \text{constant}. \quad (B - 4)$$

From Eq. B-4, the change of $(p_g v_g)$ will be

$$\Delta(p_g v_g) = 0, \quad (B - 5)$$

or

$$(\Delta p_g) v_g + (\Delta v_g) p_g = 0. \quad (B - 6)$$

Note that the change of gas volume is related to the change of liquid volume by

$$\Delta v_g = -\Delta v. \quad (B - 7)$$

Combining Eqs. (B-6) and (B-7) leads to the following expression for the change of chamber gas pressure,

$$\Delta p_g = p_g \frac{\Delta v}{v_g}. \quad (B-8)$$

Substituting Eq. (B-8) into Eq. (B-3), we obtain the change of bottomhole pressure

$$\Delta p_{wf} = p_g \frac{\Delta v}{v_g} + \frac{\rho g}{144g_c} \Delta h. \quad (B-9)$$

Combining Eqs. (B-1) and (B-9) and using $\Delta v = A\Delta h/5.615$, we have

$$\frac{1}{C_a} = \frac{p_g}{v_g} + \frac{5.615\rho g}{144g_c A}. \quad (B-10)$$

Note the isothermal compressibility of an ideal gas is the inverse of its pressure, that is,

$$c_g = \frac{1}{p_g}. \quad (B-11)$$

Substituting Eq. (B-11) into Eq. (B-10) and rearranging, we end up with

$$\frac{1}{C_a} = \frac{1}{C_g} + \frac{1}{C_l}, \quad (B-12)$$

or

$$C_a = \frac{C_g C_l}{C_g + C_l}, \quad (B-13)$$

where C_l denotes the wellbore storage coefficient due to rising liquid level and C_g denotes the wellbore storage coefficient due to gas compression.

Eq. (B-13) suggests that the effective wellbore storage coefficient for a closed chamber test is a combination of wellbore storage due to changing liquid level and gas compression. Note that during the test C_l remains constant while C_g continuously decreases and thus a closed chamber test is controlled by a variable

wellbore storage. Also note that if the gas volume remains relatively large throughout the test the combined wellbore storage given in Eq. (B - 13) approaches C_l , and in this case the closed chamber test becomes a conventional slug test.

With the wellbore storage coefficient derived above, we define the inner boundary condition for closed chamber tests. A material balance yields

$$1.127 \times 10^{-3} (2\pi) \frac{kh}{\mu} \left(r \frac{\partial p}{\partial r} \right)_{r=r_w} = C_a \frac{\partial p_{wf}}{\partial t}. \quad (B - 14)$$

In dimensionless variables, Eq. (B - 14) becomes

$$\left(r_D \frac{\partial p_D}{\partial r_D} \right)_{r_D=1} = C_{aD} \frac{\partial p_{wD}}{\partial t_D}, \quad (B - 15)$$

where C_{aD} is the combined dimensionless wellbore storage coefficient.

Eq. (B - 15) represents the inner boundary condition for a closed chamber test. This equation is similar to the inner boundary condition for conventional slug tests except that the wellbore storage coefficient for a closed chamber test is a function of the bottomhole pressure. Consequently, the inner boundary condition for a closed chamber test is non-linear.

APPENDIX C
LATE TIME ANALYSIS
OF
CCT IN OIL WELLS

For all cases investigated, the converted pressure derivative data using dimensionless time seems to approach a constant at late time, i.e.,

$$p'_{wcD} = \frac{t_D}{C_{aDi}} p_{wD} = \text{constant.} \quad (C - 1)$$

Here, a theoretical derivation is provided for this characteristic behavior.

It has been shown in *Chapter II* that the combined wellbore storage coefficient for a closed chamber test continuously decreases during the test (see, e.g., Fig. 2.5). If we divide the total time span into small time intervals and assume that in each small time interval the combined wellbore storage coefficient remains constant, a CCT will become a slug test with multiple step changes in the wellbore storage coefficient.

Correa and Remy²⁶ derived analytical wellbore pressure solutions for multi-cycle DST problems. In principle, a multi-cycle DST problem is the same as a slug test with multiple step changes in the wellbore storage coefficient. Applying the Correa and Remy²⁶ solution to the current problem, we have

$$p_{wD}(t_D) = [C_{aD,n}] p'_{wcD}(s, C_{aD,n}, t_D) + \sum_{k=1}^{n-1} [C_{aD,n} - C_{aD,k}] \int_{t_{D,k-1}}^{t_{D,k}} p'_{wcD}(s, C_{aD,n}, t_D - \tau_D) p'_{wD}(\tau_D) d\tau_D. \quad (C - 2)$$

where p_{wD} is the wellbore pressure solution for a CCT whereas p'_{wcD} is the regular pressure derivative for the classical wellbore storage and skin problem.

For large values of t_D , i.e., at late time, the following approximation is assumed to hold:

$$p'_{wcD}(s, C_{aD,n}, t_D - \tau_D) = p'_{wcD}(s, C_{aD,n}, t_D). \quad (C - 3)$$

Using this approximation, Eq. C-2 becomes

$$p_{wD}(t_D) = C p'_{wcD}(s, C_{aD,n}, t_D), \quad (C - 4)$$

where

$$C = C_{aD,n} + \sum_{k=1}^{n-1} [C_{aD,n} - C_{aD,k}] [p_{wD}(t_{D,k}) - p_{wD}(t_{D,k-1})]. \quad (C - 5)$$

For large values of t_D , we have

$$p'_{wcD}(s, C_{aD,n}, t_D) = \frac{1}{2t_D}. \quad (C - 6)$$

Substituting Eq. C-6 into Eq. C-4, we obtain

$$p_{wD}(t_D) = \frac{C}{2t_D}. \quad (C - 7)$$

Then, the converted pressure derivative data using dimensionless time will be

$$p'_{wcD} = \frac{1}{2} \left(\frac{C}{C_{aDi}} \right). \quad (C - 8)$$

Since C is a constant, Eq. C-8 indicates that the converted pressure derivative data using dimensionless time will become a constant at late time, and hence, a semilog plot of the converted pressure data using time versus time will be a straight line with a slope of $C/2C_{aDi}$ not $1/2$.